THESE

Présentée pour obtenir

LE TITRE DE DOCTEUR DE L'INSTITUT NATIONAL POLYTECHNIQUE DE TOULOUSE

Spécialité : Chimie Organométallique et de Coordination

Par

Nicolas LASSAUQUE

APPROCHE DU MECANISME DE LA REACTION DE CARBONYLATION DU METHANOL A BASSE TENEUR EN EAU CATALYSEE PAR L'IRIDIUM ET LE RHODIUM

Soutenance prévue le 5 décembre devant le jury composé de :

Président :	Bruno CHAUDRET	Directeur de recherche CNRS, Laboratoire de Catalyse et de Coordination, Toulouse.
Rapporteurs :	Pierre BRAUNSTEIN	Directeur de recherche CNRS, Université de Strasbourg, Strasbourg.
	Cornelis J. ELSEVIER	Professeur, Université d'Amsterdam, Amsterdam.
	Françoise SPIRAU	Professeur, Ecole Nationale Supérieure de Montpellier, Montpellier
Membres :	Philippe KALCK	Professeur, ENSIACET/INP Toulouse.
	Philippe SERP	Professeur, ENSIACET/INP Toulouse.
Membres invités :	Carole LEBERRE	Docteur, Ingénieur de recherche INP Toulouse.
	Samuel GAUTRON	Docteur, Process chemist Celanese. Pardies.
	Paull TORRENCE	Docteur, Research Associate Celanese. Houston.

TABLE OF CONTENTS

TABLE OF CONTENTS

GENERAL INTRODUCTION

GENERAL INTRODUCTION

The catalyzed methanol carbonylation into acetic acid is probably the most successful example of an industrial process homogeneously catalyzed by a metal complex that has yet been realized. For many years, the only source of this acid was the oxidation of ethanol by fermentation and was used as food or as conservative. Today, the production of acetic acid reach 8.10^6 T/year and is used primarily as a raw material for the production of vinyl acetate monomer (VAM), acetic anhydride or as solvent for purified terephthalic acid (PTA) production (Fig 1).

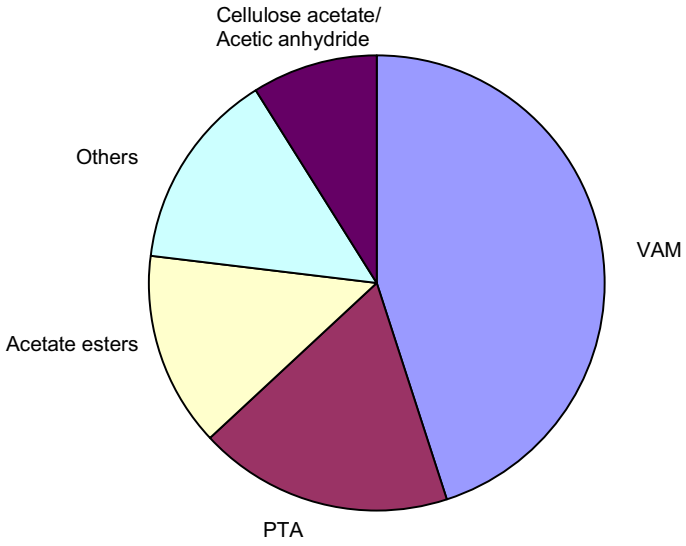

Figure 1 : Use of acetic acid.

It was not until 1920, in the United States, that catalytic production of acetic acid was begun by the oxidation of acetaldehyde in the presence of manganese acetate. From the beginning both the need for improved production methods and the development of these methods grew rapidly. In 1960, BASF introduced the methanol carbonylation to acetic acid using a cobalt catalyst which was more efficient than all previous system involving oxidation of ethanol, acetaldehyde or hydrocarbons to produce acetic acid.

This breakthrough has led many research teams to explore the carbonylation pathway and in the late 1960s the Monsanto Company developed a process for carbonylating methanol in the presence of a rhodium catalyst to produce acetic acid in higher yields and lower pressure than the BASF process. Few years latter, Celanese improved the Monsanto process by introducing iodide salts as lithium iodide. This new process need a water content of only 4 wt% whereas 14 wt% are required for the Monsanto process to obtain same carbonylation rate. This low water concentration decreased significantly the energy cost needed for the separation of water from acetic acid. In 1996, BP Chemical announced a low water new carbonylation process using iridium catalyst and ruthenium as co-catalyst named Cativa process. A plant is today operating in Asia using this technology.

Nowadays, the carbonylation processes using rhodium or iridium catalyst are the most used system for the world acetic acid production.

After a bibliographical part recalling the old and the recent processes for the catalyzed methanol carbonylation to acetic acid, we will study in Schlenck tube both, the rhodium and the iridium catalytic cycle. We will pay particular attention on the methods developed to enhance the rate determining step of the iridium catalytic cycle and we will see in Schlenk tube experiments that a rhodium complex can enhance this step.

We will also study the impact of water and lithium iodide on the rhodium catalytic system under catalytic conditions by performing batch run experiments. Thus we will try to explain the role of water and iodide salt in the rhodium-catalyzed methanol carbonylation reaction.

CHAPTER I :

BIBLIOGRAPHY

CHAPTER I : BIBLIOGRAPHY

The homogeneous methanol carbonylation reaction (scheme 1) is today the most used process for the production of acetic acid and is now practiced commercially by all major acetic acid manufacturers, including BP-Amoco, Celanese and others. Consequently, more than 60% of the world acetic acid production employs the methanol carbonylation methods[1] (Fig. 1).

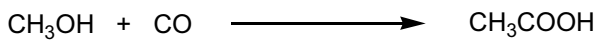

Scheme 1 : Methanol carbonylation into acetic acid

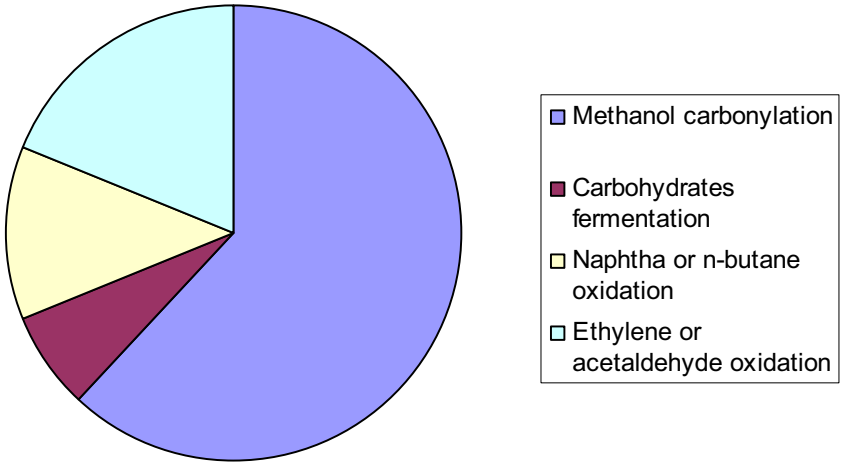

Figure 1 : Acetic acid process routes

This sprightliness for the methanol carbonylation using CO gas is essentially due to the low cost of the raw materials, CO (130 $/T) being synthesized from coal and methanol (160 $/T) being catalytically synthesized from CO and dihydrogene. All others routes to acetic acid are economically obsolete[2].

After the raw materials cost, the main concern of the methanol carbonylation process is the catalyst efficiency. The group VIII metals Co, Ni, Rh, Pd, Ir, and Pt have been demonstrated to be effective carbonylation catalysts, each metal showing a different carbonylation activity. The most important element of the methanol carbonylation process is the ability of the metal to undergo facile oxidative addition of methyl iodide, carbon monoxide insertion into the methyl-metal bond, and reductive elimination of the acetyl group affording acetyl iodide (Sc. 2).

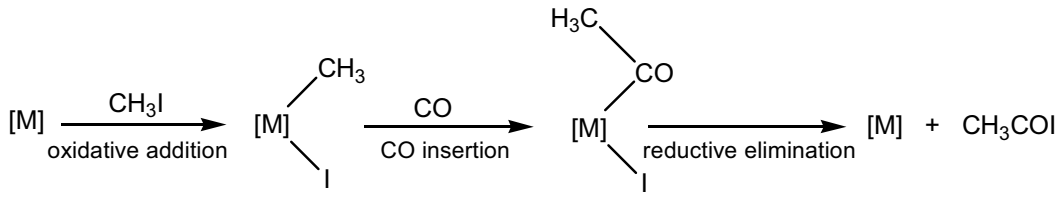

Scheme 2 : Reaction pathway in the methanol carbonylation process.

Today, the most used processes are based on iridium as well as rhodium catalyst, cobalt and nickel being only of historical interest. It is worth to note that all these metals have been tested for the catalytic synthesis of acetic anhydride, which is also a methanol carbonylation process, but only rhodium is today industrially used in this process.

In this first chapter, we will study rapidly these processes using different metals underlining similarities and differences in a mechanistic point of view. We will pay particularly attention on the iridium and the rhodium processes which are today in the research stream for the synthesis of acetic acid and acetic anhydride. Finally, we will study the attempts done to enhance the rate determining step and thus, the total catalytic cycle rate.

I-1. Cobalt-catalyzed methanol carbonylation.

The first catalytic process for the methanol carbonylation to produce acetic acid was commercialized by BASF in 1960 and used cobalt iodide as catalyst[3,4]. This system present weak catalytic activity, therefore, a temperature of 250℃ and a pressure of 700 bars are required to give commercially acceptable reaction rate[5]. Moreover, this cobalt process is very sensitive to hydrogen, which is usually present as impurity in CO gas, giving side products as acetaldehyde and crotonaldehyde[6]. The acetic acid yield is 90% based on methanol and 70% based on carbon monoxide. A catalytic cycle has been proposed[3,7,8] and is depicted in scheme 3.

The first step of this system is the generation of the active nucleophilic complex $[Co(CO)_4]^-$ by a two-step reduction of halide cobalt (II), usually CoI_2, by water and CO pressure[4]. Once the active complex is generated, methyl iodide formed by reaction of methanol with HI undergoes a nucleophilic attack by the coordinatively saturated Co(-I) complex $[Co(CO)_4]^-$ anion to form the neutral Co(I) complex $[Co(CH_3)(CO)_4]$. The methyl-cobalt complex formed is the stable intermediate of the catalytic cycle, thus, the following methyl migration step affording the acetyl complex $[Co(CH_3CO)(CO)_4]$ is the rate determining step of the catalytic cycle. Since the latter acetyl complex does not hold a iodide ligand, a simple reductive elimination can not occur, thus, acetyl iodide is formed by direct reaction of hydrogen iodide on the acetyl complex regenerating the active complex $[Co(CO)_4]^-$.

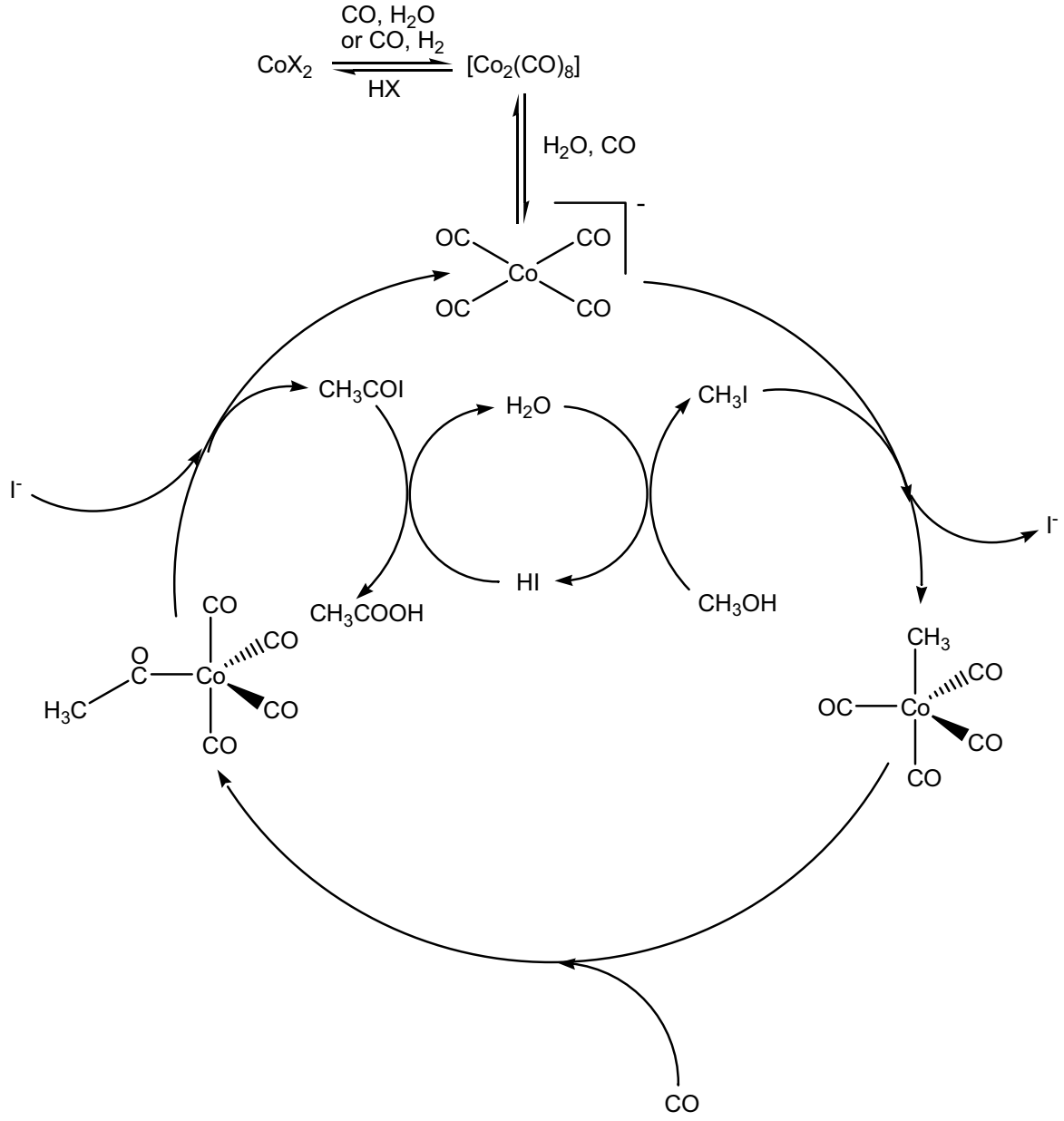

Scheme 3 : Proposed catalytic cycle for the methanol carbonylation with cobalt catalyst.

Due to the severe conditions required and the low selectivity toward methanol and carbon monoxide, the BASF process is today uncompetitive in comparison with the iridium or rhodium processes.

I-2. Nickel-catalyzed methanol carbonylation.

Although the nickel-catalyzed methanol carbonylation process has been deeply studied by Halcon-Rhône Poulenc, leading to numerous patents[9,10,11,12,13] and required milder conditions than the cobalt one (*c.a* 200 bar and a temperature ranged between 250℃ and 300℃), this process has never been commercialized due to the high toxicity and volatility of its active species $[Ni(CO)_4]$.

The stable active species $[Ni(CO)_4]$ is synthesized from nickel iodide salt NiI_2 as shown in scheme 4.

$$NiI_2 + H_2O + 5CO \rightleftharpoons [Ni(CO)_4] + CO_2 + 2HI$$

Scheme 4 : Synthesis of the active species $[Ni(CO)_4]$.

It was found that Ni species can be charged in the reactor in any form and need not be of very high purity[14]. The accepted catalytic cycle for the nickel-catalyzed methanol carbonylation is depicted in scheme 5. Oxidative addition of methyl iodide on the active species give the methyl nickel complex $[Ni(CH_3)I(CO)_2]$, this step appears to be the slower one of the catalytic cycle[15]. Under CO, a *cis*-migration reaction occurs leading to the acetyl complex $[Ni(COCH_3)I(CO)_2]$ which gives, after reductive elimination reaction the starting active complex $[Ni(CO)_4]$ and acetyl iodide. The latter species is hydrolyzed by water to give acetic acid.

One of the advantage of this system is that nickel metal is very cheap in comparison with rhodium or iridium which are the commonly used metal for carbonylation. This reason has led some research group to develop a process using nickel catalyst and to try to reduce the toxic $[Ni(CO)_4]$ in the medium.

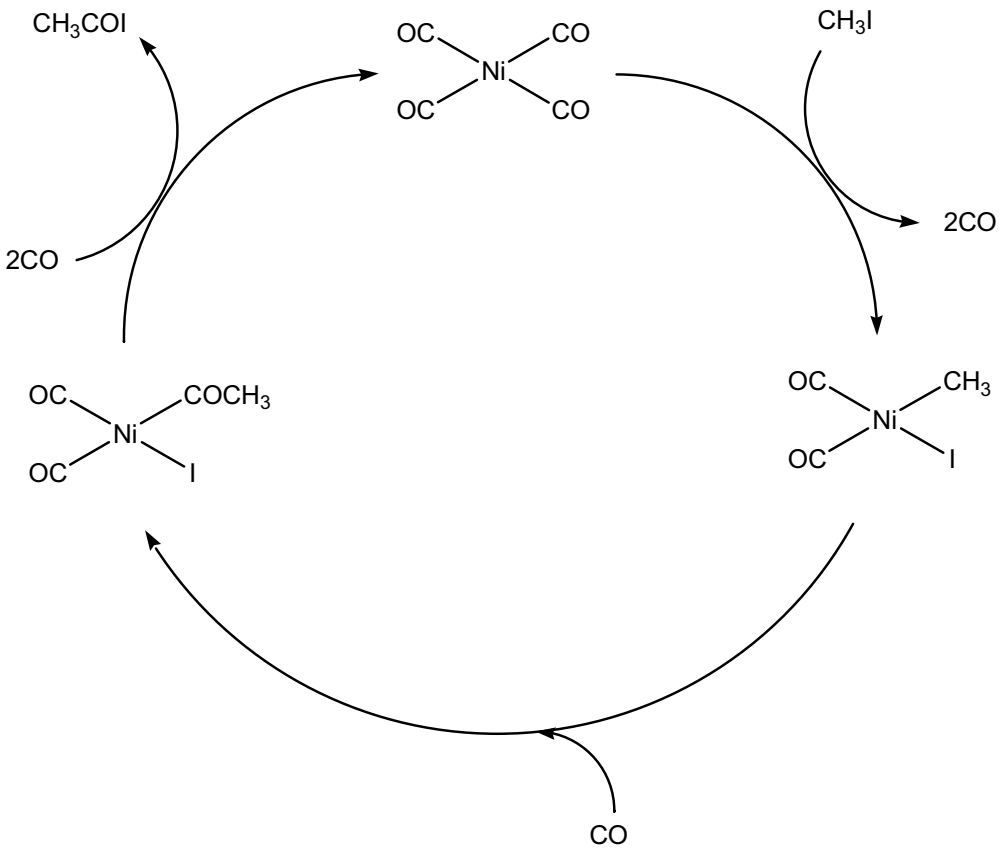

Scheme 5 : Accepted catalytic cycle for the Ni-catalyzed methanol carbonylation.

An answer was given by Moser *et al.*[16] by introducing free phosphonium salt as $[CH_3PPh_3]^+ I^-$ in the catalytic medium and a low H_2 partial pressure. They have observed by high pressure infra-red spectroscopy the reduction of the ν_{CO} stretching bands associated to the toxic complex $[Ni(CO)_4]$ keeping a high carbonylation rate. They proposed a catalytic cycle for this phosphonium-Ni catalytic system (Sc. 6)

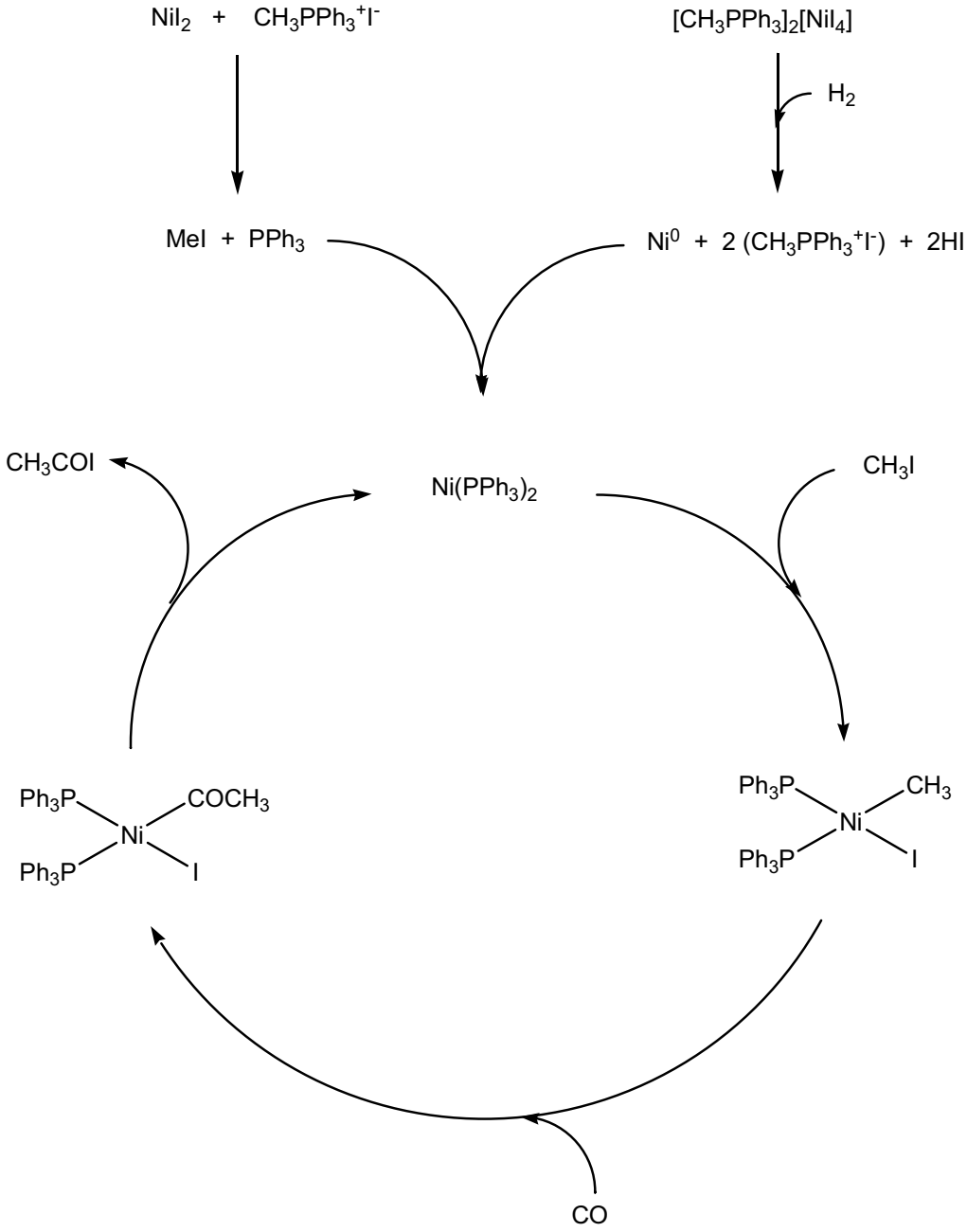

Scheme 6 : Proposed catalytic cycle for the phosphonium-Ni catalyzed methanol carbonylation

This system was patented by Eastman in 1999[17].

It is worth to note that nickel can be use as catalyst in the carbonylation of methyl acetate to acetic anhydride. The proposed catalytic cycle for this reaction is similar to this proposed for the nickel-catalyzed methanol carbonylation, the methyl acetate reacting with acetyl iodide to give acetic anhydride. It has been shown that lithium acetate ions enhanced dramatically the reaction rate[18].

I-3. Palladium-catalyzed methanol carbonylation.

Carbonylation of methanol with palladium catalyst, patented by Shell, used severe operating conditions (182℃, 110 bar of CO) with sulfolane as solvent and nitrogen-containing ligands to avoid catalyst deactivation and thus, to give acceptable carbonylation rate[19]. The proposed active species of this system is $[PdI_3(CO)]^-$ and the proposed catalytic cycle is displayed in scheme 7[20].

As for the nickel-catalyzed system, palladium catalyzed methanol carbonylation reaction involves the methyl iodide oxidative addition reaction followed by the *cis*-migration reaction and the insertion of a CO ligand. Concerning the last step of the catalytic cycle which is usually the reductive elimination of CH_3COI, a direct hydrolysis of the acetyl complex is preferred here, as it is the case for some palladium catalytic reaction as co-polymerization of ethene and carbon monoxide[21].

Recent advances[22] have shown that a iodo-bridged dimer $[Pd_2I_6]^{2-}$ was in equilibrium with the active species $[PdI_3(CO)]^-$ but since this system shows lower activity than the rhodium-catalyzed system, that palladium is an expensive noble metal and that 20% water content is required, leading to a high energy cost for the separation of acetic acid and water, this system has not been commercialized and is today less studied.

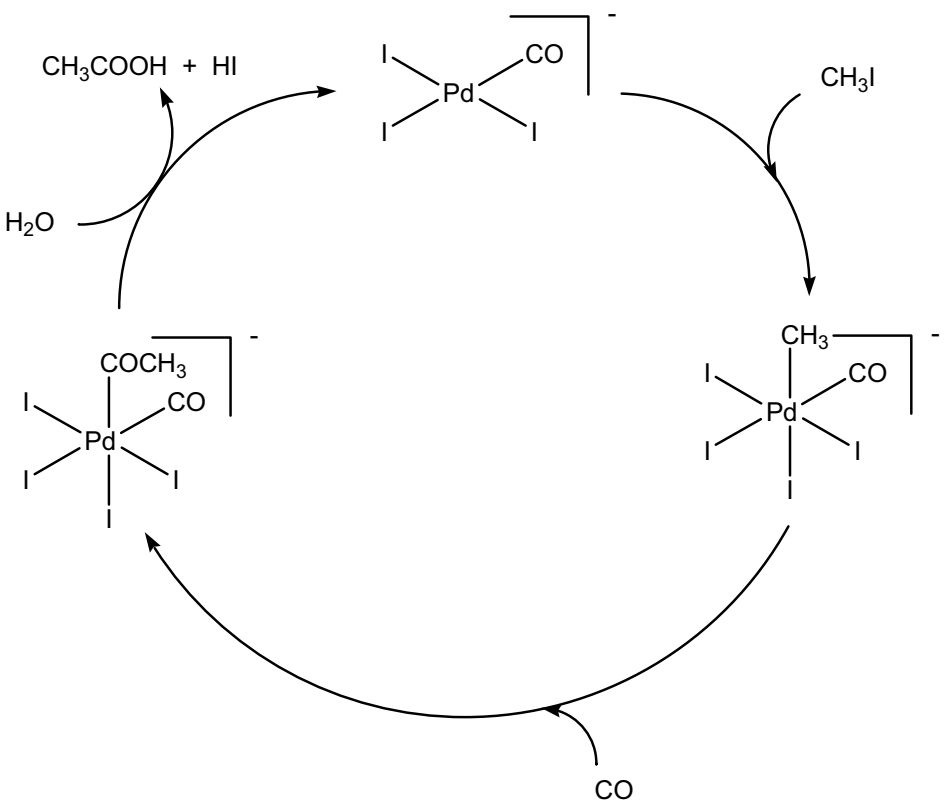

Scheme 7 : Proposed catalytic cycle for the palladium-catalyzed methanol carbonylation.

I-4 Iridium catalyzed methanol carbonylation.

I-4-1 Iridium-catalyzed system without promoters

It has been demonstrated by Paulik and Roth in 1968 that iridium was an excellent homogeneous catalyst for the methanol carbonylation under relatively mild reaction conditions[23]. First mechanistic studies have been reported[24,25] but in a mechanistic investigation performed by Forster in 1979, it became obvious that iridium-catalyzed process was more complex than the first proposed mechanistic pathway[26]. He proposed that two mains cycle are interconnected, one involving neutral iridium complexes and the other anionique iridium complexes, depending on the iodide ions concentration[8] (sc. 8).

When experiments are performed at low ionic iodide concentration, the observed iridium species is $[IrI(CO)_3]$ and the reaction is inhibited by increasing carbon monoxide pressure. This iridium complex present low reactivity toward methyl iodide since it is a poor nucleophile and the complex formed is $[Ir(CH_3)I_2(CO)_2]$ rather than $[Ir(CH_3)I_2(CO)_3]$, that explain the inhibition of CO pressure. Without removal of a CO ligand from complex $[IrI(CO)_3]$, no oxidative addition occurs. Under these conditions, oxidative addition of methyl iodide is the determining step. Under CO, the complex $[Ir(CH_3)I_2(CO)_2]$ affords easily the acetyl complex $[Ir(CH_3CO)I_2(CO)_2]$.

By increasing ionic iodide level, there is a change in the predominant form of iridium to $[Ir(CH_3)I_3(CO)_2]^-$ and the reaction rate is increased by increasing the carbon monoxide pressure. In this system, the active species which prime the catalytic cycle is the anionic complex $[IrI_2(CO)_2]^{-1}$. This species appears more nucleophile than $[IrI(CO)_3]$ and thus, the oxidative addition of methyl iodide on $[IrI_2(CO)_2]^-$ is rapid. It has been demonstrated that the oxidative addition of methyl iodide on iridium complex (as on rhodium complex) is a nucleophilic attack of the metal center on the electrophile carbon atom of the methyl iodide via a S_{N2} reaction[27] (scheme 9). Methyl-iridium complex appears to be the resting state of this system since an iodide ligand need to be removed to give the neutral complex $[Ir(CH_3)I_2(CO)_3]$ which

allows the formation of the acetyl complex. This reaction occurs at 80℃ under 5 bar of CO for several hours.

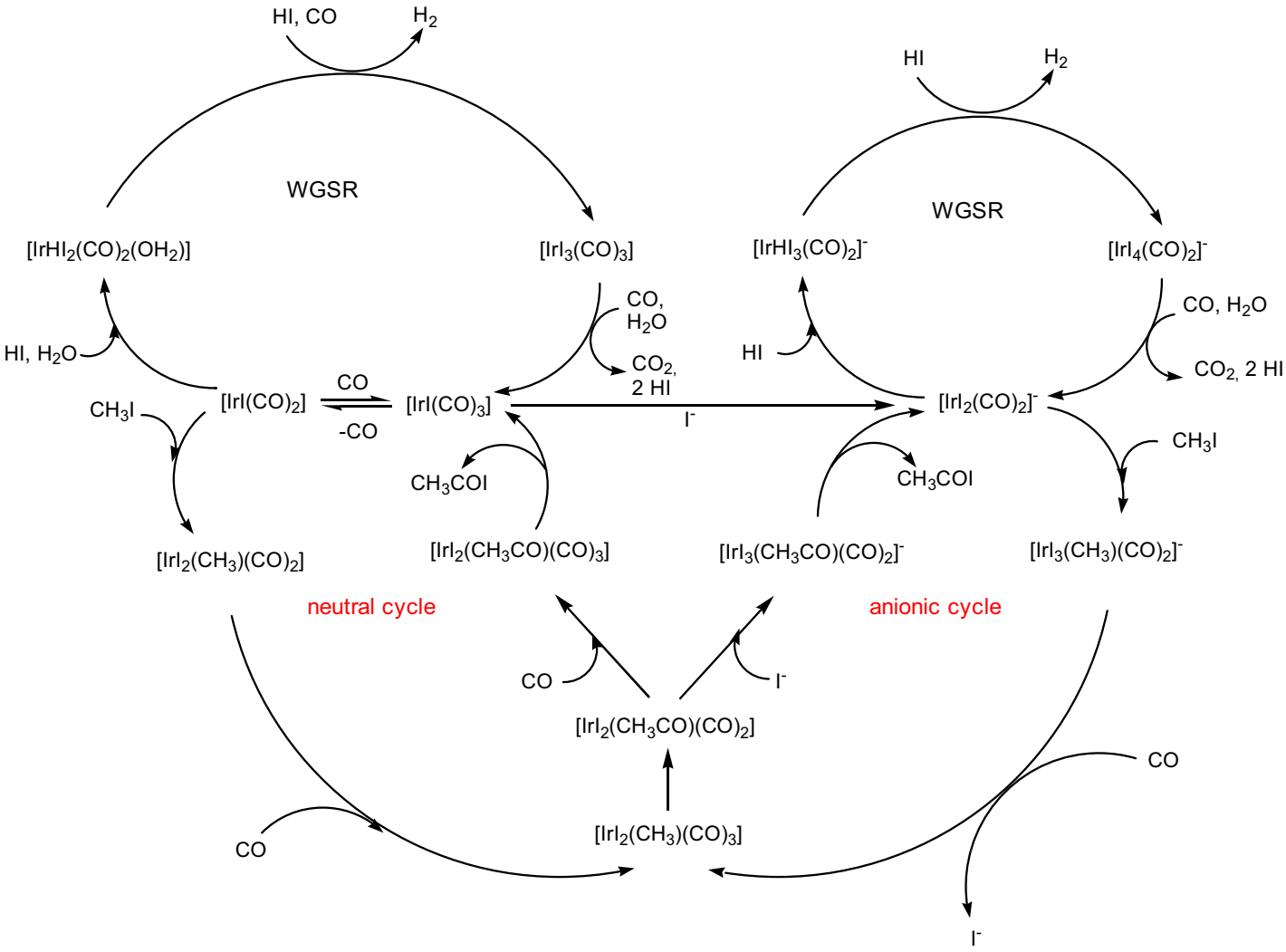

Scheme 8 : Iridium-catalyzed methanol carbonylation

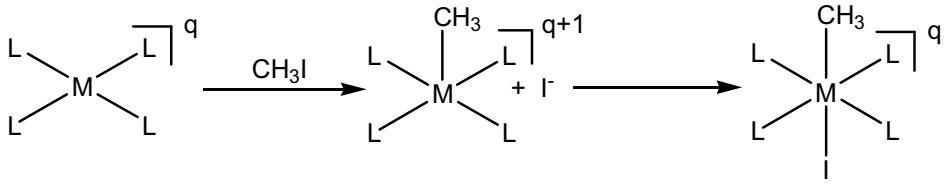

Scheme 9 : Oxidative addition mechanism

However, the overall catalytic reaction is only slightly faster, because the generation of the iridium acetyl species from the iridium methyl species is more difficult with the anionic system than the neutral system but this anionic cycle is preferred for the methanol carbonylation. Forster has also shown than a too high ionic iodide level in the medium inhibited the acetyl iridium formation[8]. This iodide effect has been well explained by *Maitlis et al*[28].

The great advantage of the iridium system is that the maximal carbonylation reaction rate was founded for a 4-6 wt% water content whereas 14 wt% water content are needed for optimal carbonylation rate with rhodium catalyst. It has been shown[8] that increasing water concentration decreased the carbonylation rate. This phenomenon was explain by the formation of the hydride complex $[IrHI_3(CO)_2]^-$ due to the formation of larger quantities of HI at higher water concentration. Under catalytic conditions, the formation of this hydride complex induces the Water Gas Shift Reaction (WGSR) which is a side reaction since it consumes CO gas without forming acetic acid (see sc. 8).

Although iridium-catalyzed methanol carbonylation process shows slower carbonylation rate than the rhodium-catalyzed one, the low water level used is of industrial interest since a high energetic cost is needed for the separation of water from acetic acid in the distillation column. Thus, many research groups have focus their attention to try to enhance the rate determining step, the methyl migration step, in order to obtain a iridium-catalyzed system suitable for industrial application.

I-4-2 Iridium-catalyzed system using promoters.

As it has been explained above (section I-4-1), the determining step of the iridium-catalyzed methanol carbonylation is the methyl *cis*-migration from methyl iridium complex $[Ir(CH_3)I_3(CO)_2]^-$ to produce the acetyl iridium complex $[Ir(CH_3CO)I_3(CO)_2]^-$ via the neutral complex $[Ir(CH_3)I_2(CO)_3]$. To obtain this neutral complex, on which the methyl *cis*-migration reaction occurs rapidly due to the lower electron density on the metal center in comparison with the anionic methyl iridium species, an iodide ligand has to be removed from complex $[Ir(CH_3)I_3(CO)_2]^-$. This explain why too high iodide concentration in the medium reduces the iridium catalyst activity.

Maitlis *et al.* noticed that addition of methanol in the medium to performed the methyl *cis*-migratory reaction accelerated dramatically the reaction rate[29]. Some thermodynamic data were reported for this reaction using chlorobenzene and chlorobenzene/methanol (3/1) solvent mixture (table. 1)

$[Ir(CH_3)I_3(CO)_2]^- + CO \longrightarrow [Ir(COCH_3)I_3(CO)_2]^-$

Solvent		$\Delta H^{\#}$/kJ mol^{-1}	$\Delta S^{\#}$/kJ mol^{-1}
Ph-Cl		155	91
Ph-Cl/MeOH		33	-197

Table 1 : Thermodynamic data for the methyl *cis*-migration reaction

This accelerating effect was explained by the ability of methanol to remove an iodide ligand from complex $[Ir(CH_3)I_3(CO)_2]^-$ via H-bonds and then, facilitate the CO insertion affording the neutral complex $[Ir(CH_3)I_2(CO)_3]$.

Taking into account the dramatic acceleration of migratory insertion induced by methanol or by Lewis acids that Shriver *et al.* have reported[30,31], further metal iodides as SnI_2 or InI_3 were introduced as promoters in this reaction. These investigations led BP chemical to announce and patent in 1996 a new process named Cativa for the iridium-catalyzed methanol carbonylation into acetic acid using a ruthenium promoter[32,33,34]. It was demonstrated that ruthenium promoter as $[RuI_2(CO)_4]$ interact with the methyl iridium resting state $[Ir(CH_3)I_3(CO)_2]^-$ by abstracting an iodide ligand and thus accelerating the methyl migratory insertion[35]. Regarding the lone reaction of methyl iridium complex with ruthenium promoter, a heterobimetallic complex has been observed[36]. Mechanistic details are displayed in section II.

For our part, we have developed in the LCCFP in collaboration with Acetex Chimie and patented a iridium-catalyzed methanol carbonylation system using platinum $[PtI(CO)_2]$ as promoter [37]. As for the Cativa process, the platinum promoter acts on the methyl iridium resting state unbolting the slow methyl migratory insertion and a heterobimetallic complex has been detected[38,39,40,41]. In this thesis we will present in section II the results of a mechanistic studies based on the enhancement of the rate determining step of the iridium catalytic cycle by the use of a rhodium complex as promoter.

It is interesting to note that recently, mechanistic studies on the iridium-catalyzed methanol carbonylation has been carried out using photochemical reaction and time resolved spectroscopic analyses[43]. Thus, the resting state methyl-iridium complex $[Ir(CH_3)I_3(CO)_2]^-$ was placed in dichloromethane under one atmosphere of CO and at room temperature. The solution was subjected to bulk photolysis and the complete formation of the acetyl-iridium complex $[Ir(CH_3CO)I_3(CO)_2]^-$ has been observed within only two hours. This reaction time is short in comparison with the required conditions for this reaction without any promoters meaning that photolysis accelerates the *cis*-migration reaction rate.

I-5 Rhodium-catalyzed methanol carbonylation

Just few years after BASF commercialized the cobalt-catalyzed process, Monsanto developed a low pressure process with a rhodium iodide promoted catalyst system that demonstrated significantly higher activity and selectivity to produce acetic acid than the cobalt process[43]. Indeed methanol can be converted even at atmospheric pressure with yields of 99% and 90% with respect to methanol and carbon monoxide, respectively[44,45,7]. This system require mild conditions as 30 bar of CO and 190℃ and is not as sensitive to hydrogen as the BASF process, and therefore the amounts of reduction products such as methane and propionic acid are comparatively low[5].

All these advantages have conducted the Monsanto process to be the most used catalytic way to produce acetic acid for 30 years. Its catalytic cycle was well studied by several research group[46,47,48] and a catalytic cycle was proposed (Sc. 10).

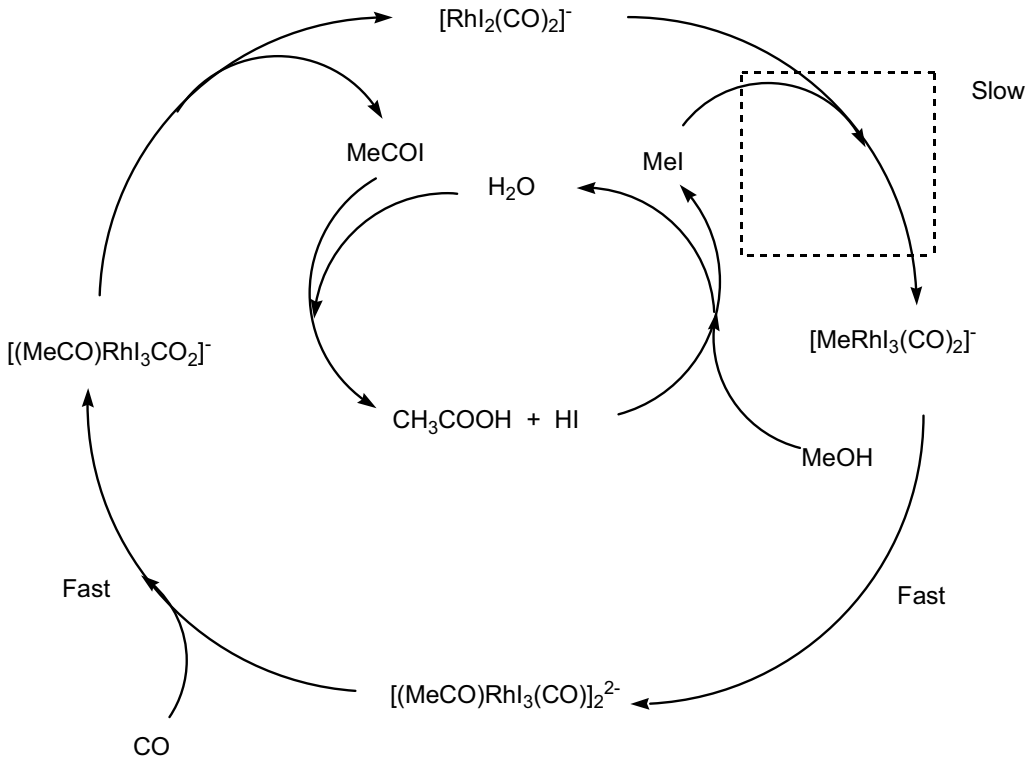

Scheme 10 : Proposed rhodium-catalyzed methanol carbonylation catalytic cycle.

The active species which primes the catalytic cycle is the 16e$^-$ complex $[RhI_2(CO)_2]^-$. This complex can be generated from rhodium salt RhI_3, $RhCl_3$ or $Rh(OAc)_3$ in an acetic acid/water mixture with a small quantity of HI under CO pressure. The different steps of this catalytic cycle are the same than those of the anionic iridium catalytic cycle. The first reaction is the oxidative addition of methyl iodide on $[RhI_2(CO)_2]^-$ giving the methyl-rhodium complex $[RhI_3(CH_3)(CO)_2]^-$ followed by a rapid *cis*-migration affording the acetyl complex $[RhI_3(COCH_3)(CO)]_2^{2-}$. This latter complex was isolated and its structure was determined by X-ray crystallography[49]. Under CO, this complex gives the di-carbonyl acetyl complex $[RhI_3(COCH_3)(CO)_2]^-$ which leads after reductive elimination, as for its iridium homologue, to the active complex and acetyl iodide.

The main drawback of the Monsanto process is that a water content of 14% is required to have hight carbonylation rate and to avoid black rhodium precipitation. This high water content needed, in comparison with the iridium-catalyzed methanol carbonylation system, leads to a high energy cost for the separation of water from acetic acid. Furthermore, it has been shown that under these conditions, the Water Gas Shift Reaction (WGSR) occurs, consuming CO without production of acetic acid[50]. The WGSR will be detailed later.

In 1980, Celanese improved the Monsanto process with the Low-Water Acid Optimisation (AO) Technology, adding large quantities of iodide salt as lithium iodide, potassium iodide or sodium iodide in the medium[51]. Thus, methanol carbonylation reaction proceed at only 4% water content at hight carbonylation rate without rhodium loss. The Monsanto catalytic cycle is still operating in the low-water process. Industrial application of the Low-Water AO Technology led Celanese Company to be the first acetic acid producer in the world.

I-5-1 Mechanistic approach

In this section, we will study step by step the rhodium catalytic cycle and describe advance in its comprehension and its improvement.

The oxidative addition

As for the nickel-, palladium- and iridium-catalyzed methanol carbonylation, the first step is the oxidative addition of methyl iodide to the active complex $[RhI_2(CO)_2]^-$. Kinetic data presented in 1971 show that the reaction is first order in both rhodium and methyl iodide concentration, strongly suggesting that the methyl iodide addition step is rate determining[44]. Few years later, in 1979, Forster performed batch reactions using a high pressure, high temperature infrared cell and obtained, starting from $RhCl_3$, heptanoic acid, methanol, methyl iodide and water, at 100℃ and 6 bar of CO, spectra containing two strong bands at 1996 cm^{-1} and 2067 cm^{-1} characteristic of the complex $[RhI_2(CO)_2]^-$. He analyzed the solution by gas chromatography and observed the presence of acetic acid and methyl acetate showing that the carbonylation reaction occured[46]. Although the conditions used by Forster in 1979 are far from the real catalytic conditions used in the industry, these results, together with the results obtained by Paulik et Roth in 1971 indicate that the oxidative addition is the rate determining step of the rhodium-catalyzed methanol carbonylation catalytic cycle following the general rate law: $-d[CH_3OH]/dt = k.[Rh].[CH_3I]$.

Since it was evidenced that oxidative addition is the rate determining step of the rhodium system, several studies aiming to enhance the rate of this reaction were performed. In 1975, Forster has shown that the anionic complex $[RhI_2(PPh_3)(CO)]^-$ was a much better nucleophile towards methyl iodide than the neutral $[RhI(PPh_3)(CO)]$[52]. In 1984 Maitlis *et al.* studied this reaction in Schlenk tubes starting from the complex $[Ph_4As][RhI_2(CO)_2]$ were the bulky counter ion $[Ph_4As]^+$ stabilizes the complex[53]. At first, they measured the rate of the oxidative addition at room temperature using different solvent. The results are reported in table 2. They observed that the activation $\Delta G^{\#}$ is smaller in polar solvent like methanol than in non polar solvent as methyl acetate and evaluated a difference of 3.5 in the rates between these two

solvents. This observation is similar to that reported for the oxidative addition of methyl iodide to $[IrCl(PPH_3)_2(CO)]$ in polar and non polar solvent[54].

Solvent	$\Delta G^{\#}$ (298 K) /kJ mol^{-1}	$\Delta H^{\#}$/kJ mol^{-1}	$\Delta S^{\#}$/kJ mol^{-1}
Methanol	96.4	69	-92
Chloroform	97.3	53	-152
Tetrahydrofuran	98.8	52	-154
Methyl acetate	99.4	47	-176

Table 2: Activation parameters for the oxidative addition of CH_3I to $[Ph_4As][RhI_2(CO)_2]$ in different solvents.

Second, they have studied the effect of additives on the oxidative addition. They observed that the presence of halogen salts in the medium enhanced the rate. Results are summarized in Figure 2. They proposed as explanation that this phenomenon appears to arise from a general salt effect.

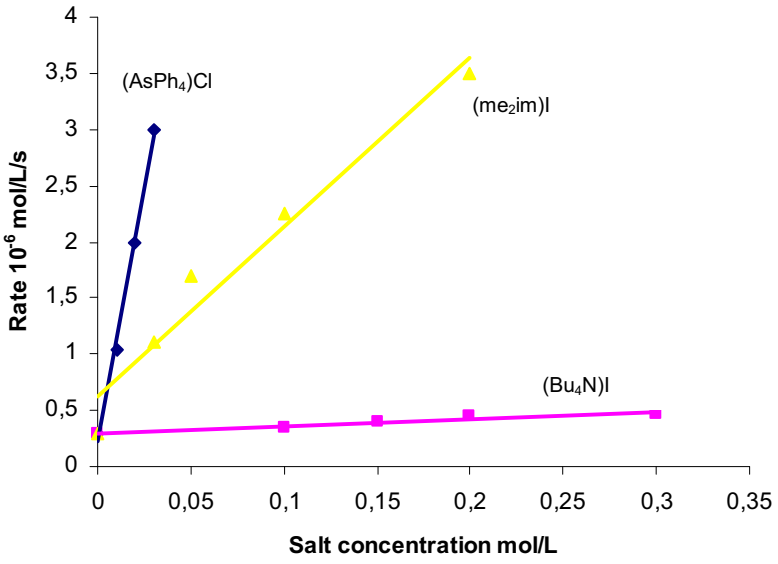

Figure 2 : Variation of rates of oxidative addition of CH_3I to $[AsPh_4][RhI_2(CO)_2]$ (5.10-3 mol. L^{-1}) in dichloromethane in the presence of various salts.

The general mechanism of the oxidative addition is a S_N2 reaction as it has been theoretically proved[27]. As explained in scheme 9, the nucleophilic metal center attack the electrophilic carbon of the methyl iodide forming at first a five coordinated methyl complex which evolves rapidly to the six coordinated methyl complex containing three iodide ligands. The experimental evidence of this pathway was held by Salzer *et al*. in 2004 starting from a neutral rhodium complex (sc. 11).

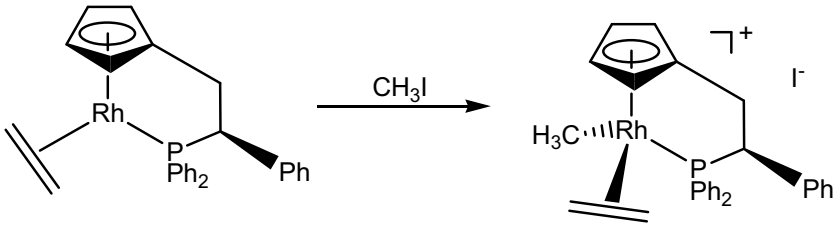

Scheme 11 : Oxidative addition of MeI to the neutral rhodium complex.

The cationic methyl complex has been isolated, crystallized and its structure determined by X-ray analysis[55]. This reaction can continue leading to the expected methyl-iodide complex.

Since it was proved that oxidative addition reaction was a nucleophilic attack of the metal center, it was proposed that in the case of the Celanese low-water AO process that the high lithium iodide content involved two competitive pathway between four-coordinated and five coordinated nucleophilic intermediates (sc. 12). The formation of a dianionic complex $[RhI_2L(CO)_2]^{2-}$, where L could be an iodide ligand or an acetate ligand according to the equilibrium displayed in scheme 13, is more nucleophilic than the classical $[RhI_2(CO)_2]^-$ and thus can react more rapidly with methyl iodide[5,56].

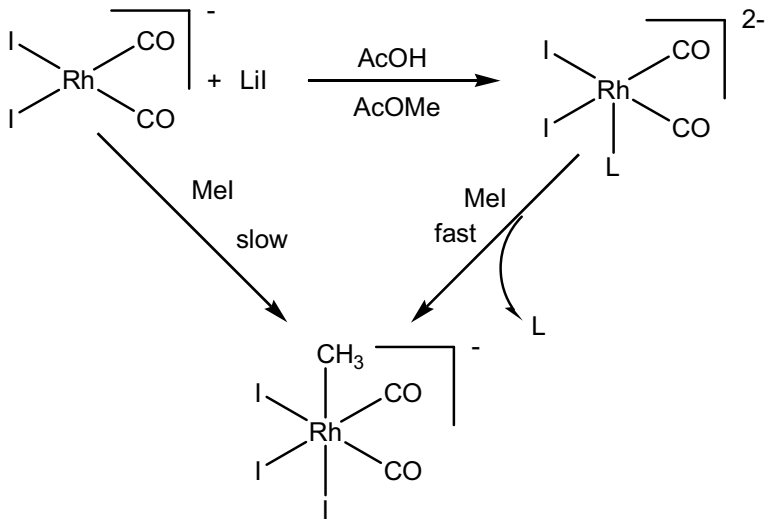

Scheme 12 : Different pathways for the oxidative reaction in the low-water AO process. L = I^- or AcO^-

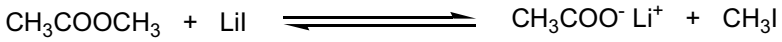

Scheme 13 : Formation of acetate ions from methyl acetate and LiI

It has also been proposed that the enhancement of the rate for the low water process could be due to the formation of additional methyl iodide by the reaction of LiI with methyl acetate (Sc. 13)[57]. However, the increase of CH_3I concentration in the medium appears to be not sufficient[2] and moreover, in continuous carbonylation experiments under commercial reactions conditions, the CH_3I concentration in the solution is kept constant[58].

On the basis that the rate-determining step for rhodium-catalyzed methanol carbonylation is the oxidative addition of CH_3I to Rh(I), numerous attempt have been made to improve catalytic activity by introduction of strongly donating ligands that increase the nucleophilicity of the rhodium centre.

A class of rhodium complexes containing mono-phosphine ligands as $P(Et)_3$ of di-phosphine ligands as PPh_2-CH_2-CH_2-PPh_2 have been developped[59,60]. For example, oxidative addition of CH_3I on *trans*-$[RhI(CO)(PEt_3)_2]$ occurs 57 times faster than on $[RhI_2(CO)_2]$ at 25°C [61]. Cole-Hamilton *et al.* observed ν_{CO} stretching band at 1960 cm^{-1} for complex *trans*-$[RhI(CO)(PEt_3)_2]$ whereas bands at 1988 cm^{-1} and 2059 cm^{-1} are observed for complex $[RhI_2(CO)_2]^-$ suggesting that the rhodium center is more electron-rich in the triethylphosphine complex[60].

The methyl rhodium complex $[Rh(CH_3)I_2(CO)(PEt_3)_2]$ obtained after oxidative addition of CH_3I is stable enough to be isolated in contrast with the very reactive $[Rh(CH_3)I_3(CO)_2]^-$. Since the metal centre is electron-rich in the methyl triethylphosphine rhodium complex, the next step of *cis*-migration is slow, due to the increased back-donation from rhodium to CO. Thus, carbonylation of $[Rh(CH_3)I_2(CO)(PEt_3)_2]$ to give $[Rh(COCH_3)I_2(CO)(PEt_3)_2]$ is 38 times slower than methyl migration in $[Rh(CH_3)I_3(CO)_2]^-$. The catalytic cycle of the methanol carbonylation catalyzed by the neutral complex $[RhI(PEt_3)_2(CO)]$ is shown on scheme 14.

This system shows high carbonylation rate at high water content but present a loss of activity with the time. This phenomenon is explain by the catalyst degradation via the loss of phosphine ligand (to give Et_3PI^+) under the harsh conditions used. Kinetic studies performed with this phosphine-rhodium system show that the oxidative addition remains the rate determining step of the catalytic cycle. It is worth noting that no appreciable benefit is obtained with this system at low water content in comparison with the "classical" system using the $[RhI_2(CO)_2]^-$ catalyst.

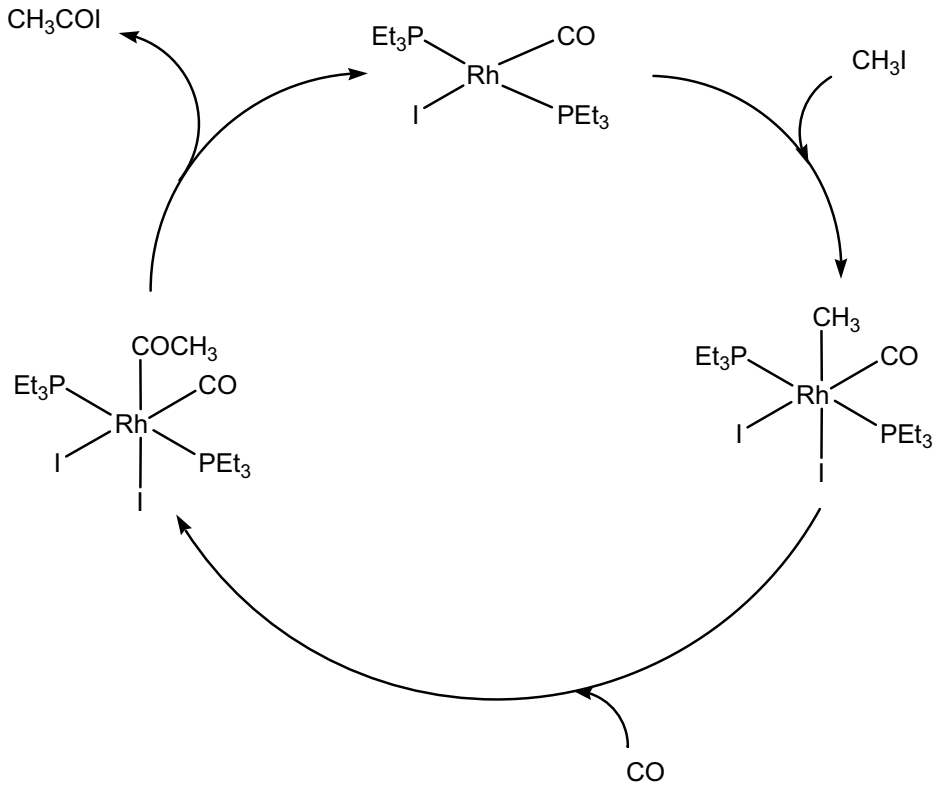

Scheme 14 : Catalytic cycle of the methanol carbonylation catalyzed by the neutral complex $[RhI(PEt_3)_2(CO)]$

In order to avoid catalyst degradation, several studies using ligand chelate effect have been made in attempts to stabilize the ligand-metal interaction. Wegman et al. show that mixed bidentate as PPh_2-CH_2-$P(O)Ph_2$ (dppmo) have a high activity in rhodium-catalyzed carbonylation of methanol[62]. Mechanistic studies indicated that complex *cis*-[RhCl(dppeo)(CO)] presents a hemi-labile behaviour under CO as shown in scheme 15. High pressure infrared spectroscopy studies indicates that under 80℃ and 3.5 bar of CO, only *cis*-[RhCl(η^1-dppeo)$(CO)_2$] is present in the medium. Reaction of *cis*-[RhCl(η^1-dppeo)$(CO)_2$] with methyl iodide was found to lead rapidly to the corresponding acetyl complex. Moreover, no trace of $[RhI_2(CO)_2]^-$ has been detected.

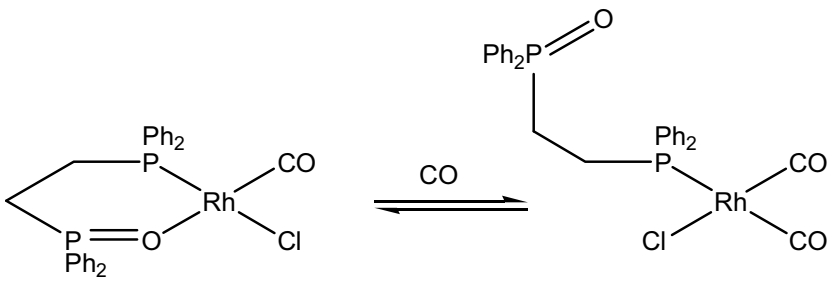

Scheme 15: Equilibrium between [RhCl(η^2-dppeo)(CO)] and [RhCl(η^1-dppeo)$(CO)_2$]

BP researchers have found that the use of P-S ligands as $Ph_2PCH_2P(S)Ph_2$ (dppms) as a promoter for rhodium catalyzed methanol carbonylation gave a substantial acceleration of the rate in comparison with the "classical" rhodium system and even with the use of dppeo[63]. The results they obtained at 185℃ under 70 bar of CO without iodide promoter are reported in table 3.

run	ligand	ligand/Rh ratio	rate mol/L/h
1	dppms	4	14.2
2	none		2.3
3	PPh_3	4	2.6
4	dppeo	4	2.7
5	dppms	1	19.6

Table 3 : Carbonylation rates using different bidentate ligands for the rhodium-catalyzed methanol carbonylation

Entries 1 and 5 in table 3 indicate that the higher carbonylation rates are obtained for a ligand/Rh molar ratio of 1. High pressure infrared spectroscopy studies identified [RhI(CO)(dppms)] as the only detectable complex under the catalytic conditions and mechanistic studies showed that [RhI(CO)(dppms)] react readily with methyl iodide giving directly the acetyl complex [$RhI_2(COCH_3)$(dppms)], the methyl complex being not observed. Under CO, [$RhI_2(COCH_3)$(dppms)] leads to the carbonyl acetyl rhodium complex [$RhI_2(COCH_3)$(CO)(dppms)] which can reductively eliminate acetyl iodide to complete the cycle depicted in scheme 16. This system has been patented by B.P. Chemical in 1994[64].

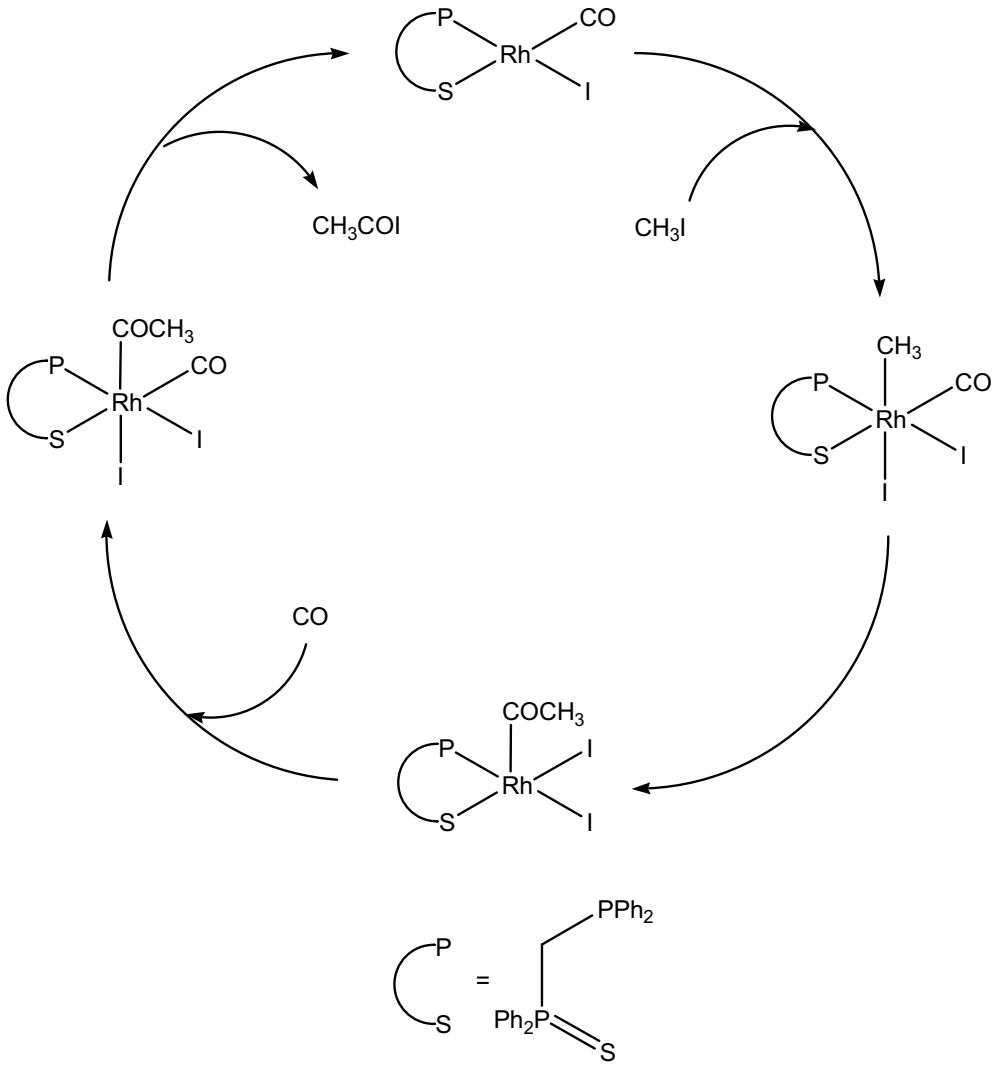

Scheme 16 : [RhI(CO)(dppms)]-catalyzed carbonylation cycle

On the basis of the same kind of ligands, Dilworth *et al*. have developed P-S molecules giving a rate enhancement in the rhodium-catalyzed methanol carbonylation (Sc. 17)[65]. They observed a maximum carbonylation rate four times higher than when starting from $[RhI_2(CO)_2]^-$. The catalytic cycle appears to be the same than the one displayed in scheme 16, the methyl intermediate hasn't being observed.

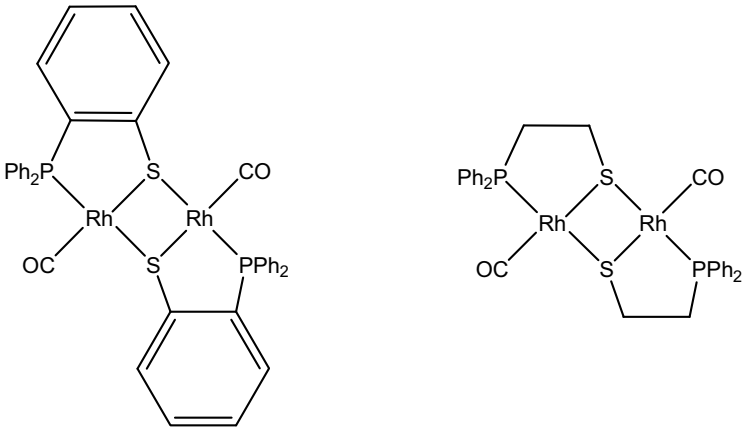

Scheme 17 : P-S-rhodium catalyst used for methanol carbonylation

Some unsymmetrical ethylene diphosphines (Sc. 18) were reported as more efficient ligands than symmetrical diphosphine for rhodium catalyzed methanol carbonylation and are longer-lived under industrial conditions. In situ infrared spectroscopy only shows the diphosphine rhodium complex without traces of $[RhI_2(CO)_2]^-$. But all these diphosphine-rhodium catalysts are less active than the $[RhI_2(CO)_2]^-$ system[66].

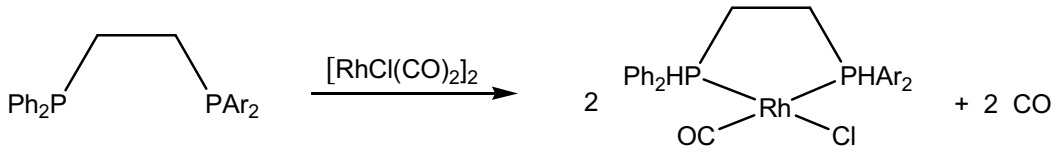

Ar = 4-$C_6H_4OCH_3$ or 3,5-$C_6H_3F_2$ or 3,4,5-$C_6H_2F_3$

Scheme 18 : Unsymmetrical rhodium catalysts for methanol carbonylation reaction

Süss-Fink *et al*. have recently developed a class of *trans*-chelating ligands containing phosphorus or nitrogen atom (Sc. 19)[67,68,69]. These catalysts show higher activities than the $[RhI_2(CO)_2]^-$ system.

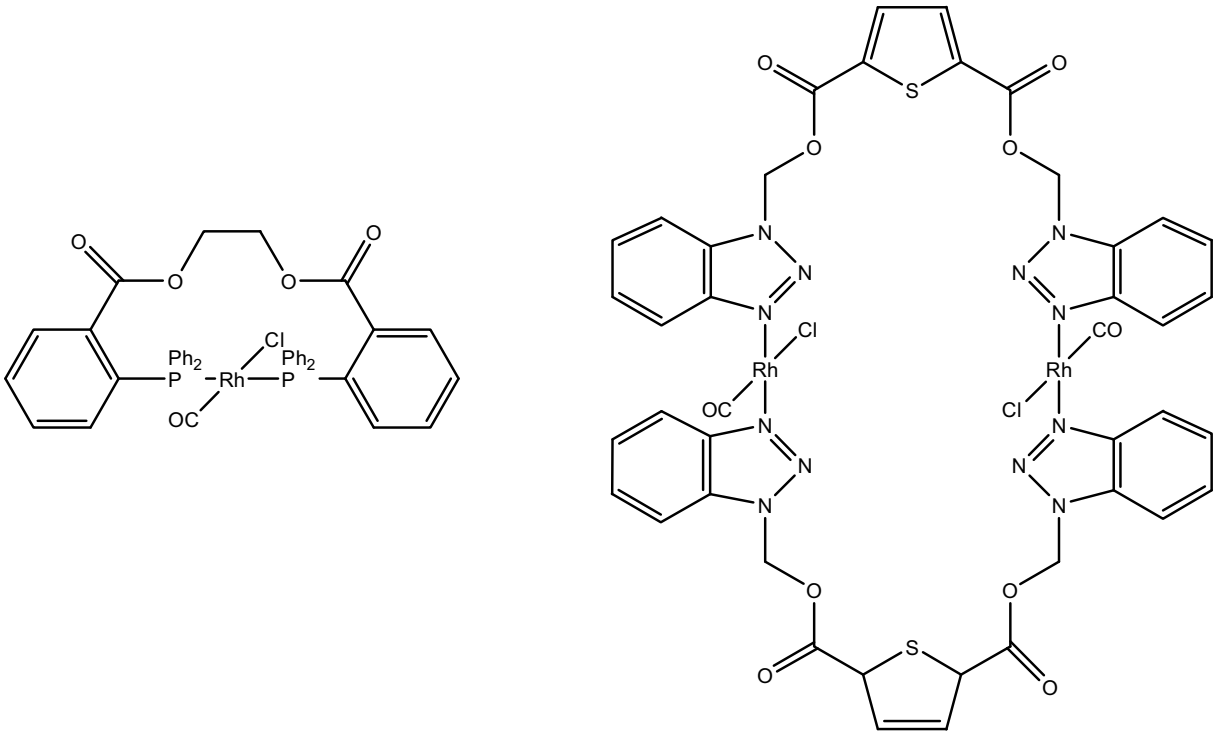

Scheme 19 : Example of trans-chelating ligands rhodium complex for methanol carbonylation

Some other *trans*-chelating diphosphine ligands were reported very recently by van Leeuwen *et al*.[70]. As the latter *trans*-chelate displayed in scheme 19, these ligands show higher activities than the $[RhI_2(CO)_2]^-$ system for methanol carbonylation, the aim being to increase the electron density on the metal center in order to accelerate the methyl iodide oxidative addition determining step.

Most of these new rhodium-catalysts containing chelating ligands mentioned above are presented in the literature as new systems having higher carbonylation rates than the “classical” system using $[RhI_2(CO)_2]^-$ catalyst. Some of these new catalysts were been patented for an industrial application[64,71]. One of the first patent concerning methanol carbonylation and using additional ligands as amines or phophines was published in 1981 by the Monsanto Company[72] but to our knowledge, after around 25 years of research, no company uses today these new catalysts for acetic acid production.

One reason that can explain the preference for the Monsanto, Celanese or Cativa process for industrial acetic acid production is that the published catalytic tests using new rhodium catalysts were performed in batch run under conditions far from the real industrial conditions. Indeed, the reported batch runs using these new catalysts were performed at low water content (less than 8%) or even with no water or no acetic acid as solvent and no iodide salts as lithium iodide are introduced in the reactor. For example, one of the best reported Turn Over Frequency (TOF) for the use of *trans*-chelating ligands is around 2400 h^{-1} and only $h^{-1}.mol^{-1}$ for the “classical” system under the same conditions but reach 2200 h^{-1} under Monsanto conditions (test performed in our laboratory). Thus, the use of phosphine, amine or mixed chelating ligands in the rhodium catalyzed methanol carbonylation presents only a low improvement of the TOF values in comparison with the Monsanto process. Moreover, there are no information concerning the behavior of these new catalyst in continue experiments since all the reported runs were performed in batch conditions.

Thus, the advantage of these σ-donor ligands is that they increase the electron density on the rhodium metal center, accelerating by this way the oxidative addition of methyl iodide. But by giving a metal center more electron rich, the rate of next step, the migratory insertion of a CO ligand into the Rh-CH_3 bond, is decreased so that the overall rate is not substantially enhanced. In comparison with the iridium system which is more electron rich than rhodium, the oxidative addition is fast whereas the *cis*-migration is the rate determining step of the catalytic cycle.

The migratory insertion, CO insertion and the reductive elimination

The next step of the rhodium-catalyzed methanol carbonylation is the migratory insertion[75] of a CO ligand from the $18e^-$ complex $[RhI_3(CH_3)(CO)_2]^-$ to the $16e^-$ acetyl complex $[RhI_3(COCH_3)(CO)]^-$ (Sc. 20).

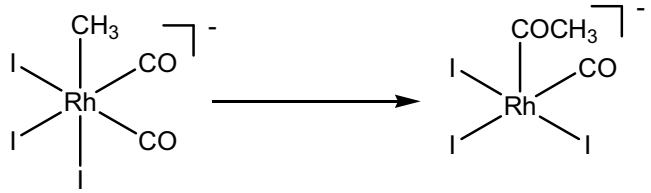

Scheme 20 : *Cis*-migration reaction.

This reaction is fast[45] so that the methyl rhodium complex was only detected recently[56,74]. Indeed, an unknown infrared band at 2104 cm^{-1} was detected using a computer subtraction technique. By comparison with the infrared spectra of the stable complex $[IrI_3(CH_3)(CO)_2]^-$ (2098 cm^{-1} 2045 cm^{-1}), the authors assigned of the band at 2104 cm^{-1} to the high frequency ν_{CO} mode of the *cis*-$[RhI_3(CH_3)(CO)_2]^-$ complex. ^{13}C NMR observations of a new doublet at δ = 175.9 (d, $^1J_{Rh-C}$ = 59.9 Hz) when reacting $[RhI_2(^{13}CO)_2]^-$ in neat CH_3I at low temperature confirm the latter infrared observation. Density functional calculations[75] indicates that the methyl rhodium complex with the CO in *trans* position is energetically favored to the proposed methyl rhodium complex with the CO in *cis* position but this *trans* complex can only arise from the oxidative addition of methyl iodide to the complex *trans*-$[RhI_2(CO)_2]^-$ which is largely energetically disfavoured to the complex *cis*-$[RhI_2(CO)_2]^-$ and furthermore, was not detected in the catalytic medium.

The CO migratory insertion reaction appears to be exothermic with a calculated energy of –32 kJ/mol and involves a transition state having a trigonal bipyramidal structure with a partially formed CH_3CO fragment as one of the ligands in the equatorial plane (Sc. 21)[75].

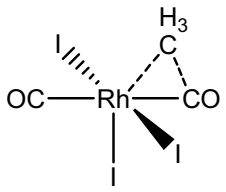

Scheme 21 : Proposed transition state for the migratory insertion reaction

The resulting acetyl complex is five coordinated. A X-ray crystal structure of this intermediates has been obtained[49] as a dianionic dimer (Sc. 22) but NMR spectra of this complex (Chap. II sec. 3) in solution shows two different isomers. We can suppose that in solution, one molecule of coordinative solvent can be coordinated to the metal center.

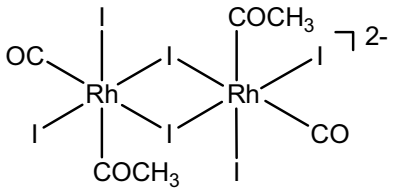

Scheme 22 : Acetyl rhodium dianionic dimer.

Under one atmosphere of CO, this dimer leads rapidly to the 18e$^-$ complex $[RhI_3(COCH_3)(CO)_2]^-$ where a CO ligand is weakly coordinated to the metal centre since this complex give back complex $[RhI_3(COCH_3)(CO)]_2^{2-}$ in the absence of CO[44]. Infrared and NMR data[76] of the dicarbonyl acetyl rhodium complex suggest that its structure is a trigonal bipyramide with the two CO ligands in trans position that is in accordance with the X-ray absorption analysis[77].

Complex *cis*-$[RhI_3(COCH_3)(CO)_2]^-$ has been observed by ^{13}C NMR at –120℃ by direct reaction of acetyl iodide with $[RhI_2(CO)_2]^-$ but it isomerizes at –60℃ to form the *trans*-acetyl complex (Sc. 23)[78].

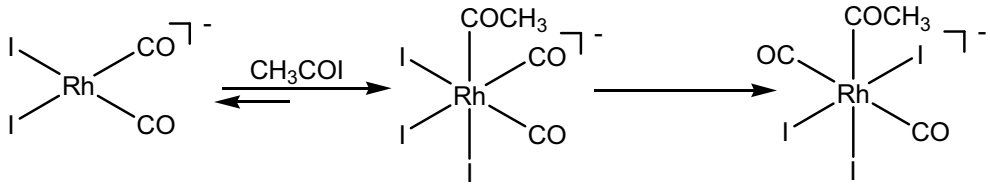

Scheme 23 : Cis-trans isomerization of $[RhI_3(COCH_3)(CO)_2]^-$.

Complex $[RhI_3(COCH_3)(CO)_2]^-$ can eliminate reductively acetyl iodide to give the starting active species $[RhI_2(CO)_2]^-$ and thus, complete the catalytic cycle. It has been reported that decomposition of $[RhI_3(COCH_3)(CO)_2]^-$ occurs slowly under ambient conditions ($t_{1/2}$ = 12 h at 25℃)[46,56]. Forster has proposed two pathways for the reductive elimination reaction (Sc. 24)[46].

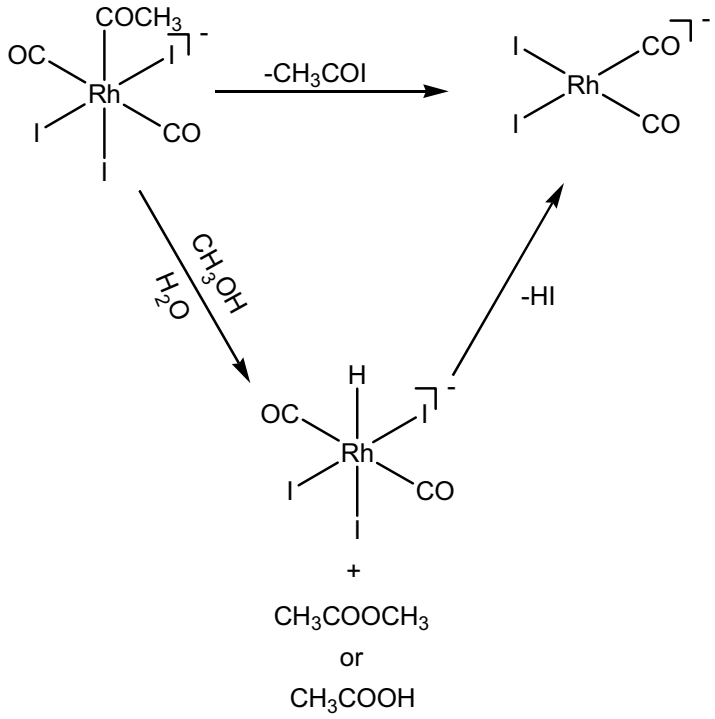

Scheme 24 : Different pathways for the reductive elimination step.

The first way is the direct reductive elimination of acetyl iodide mentioned above and the second involves the intervention of methanol or water in a solvolytic mechanism giving a hydride rhodium complex which eliminates HI to complete the catalytic cycle. Forster indicated that the acetyl iodide elimination is preferred since evidence of this pathway has been reported with rhodium phosphine complexes[79]. Kilner *et al*. proposed also that water can react directly with the acetyl complex via a hydrolysis reaction to give acetic acid and the starting complex and noted that addition of acetic acid increases the rate of the elimination reaction[80].

This solvolysis reaction can be linked on the reaction of methanol with cationic acetyl palladium complexes. Recently, van Leeuwen et al. proposed different mechanistic pathways for the formation of methyl acetate from acetyl palladium complexes in presence of methanol[21]. They reported that methanol can attack the acetyl part or can be coordinated to the metal centre and underwent a reductive elimination (Sc. 25).

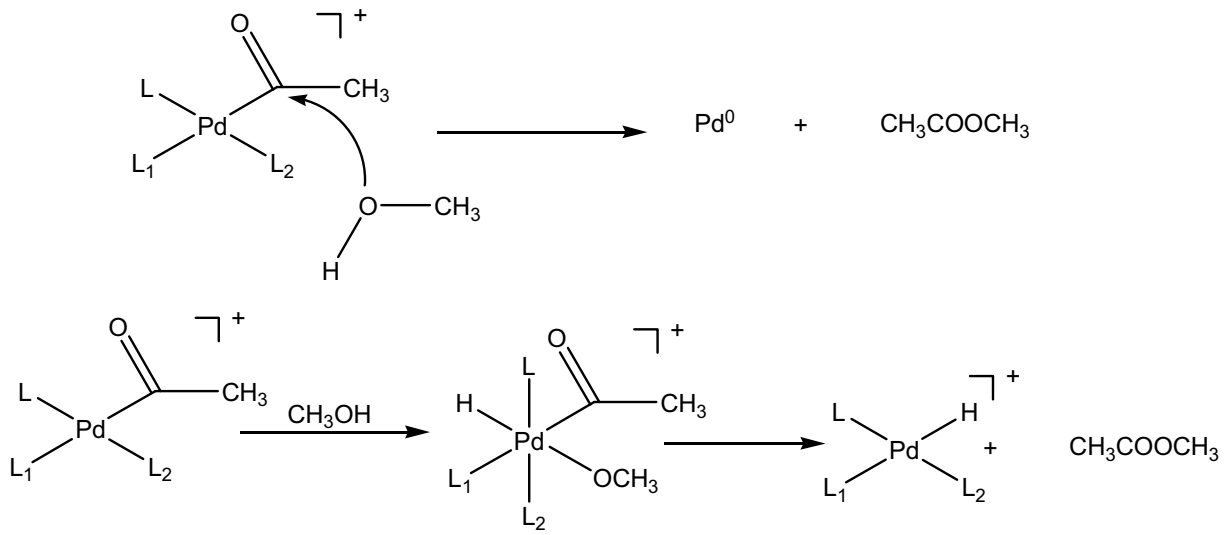

Scheme 25 : Proposed pathways for methanolysis reaction.

Maitlis *et al*. have observed that addition of amines to the acetyl rhodium complex enhanced dramatically the elimination step giving an amide and the starting complex. Preliminary kinetic studies on this reaction with *N*-methyl-aniline suggested a nucleophilic attack of the amine on the acetyl complex (Sc. 26)[56].

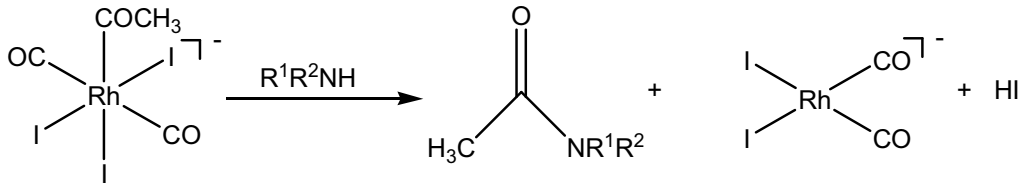

Scheme 26 : Reaction of acetyl rhodium complex with amines.

To the best of our knowledge, no kinetic data were given in the literature concerning the reductive elimination reaction. Only density functional studies have been reported[81]. Nevertheless, this reaction appears to be very important since Jones reported that it is presumably the rate determining step of the rhodium catalytic cycle for a water content below 8% wt[82].

Thus although the direct reductive elimination pathway is largely accepted, other pathway can be proposed.

The Water Gas Shift Reaction (WGSR) in the rhodium catalyzed methanol carbonylation.

The catalysis of the WGSR by a rhodium iodide system has been noted to occur as a side reaction in the rhodium catalyzed methanol carbonylation at elevated temperatures and pressures [44]. The proposed catalytic cycle of the WGSR is depicted in scheme 27.

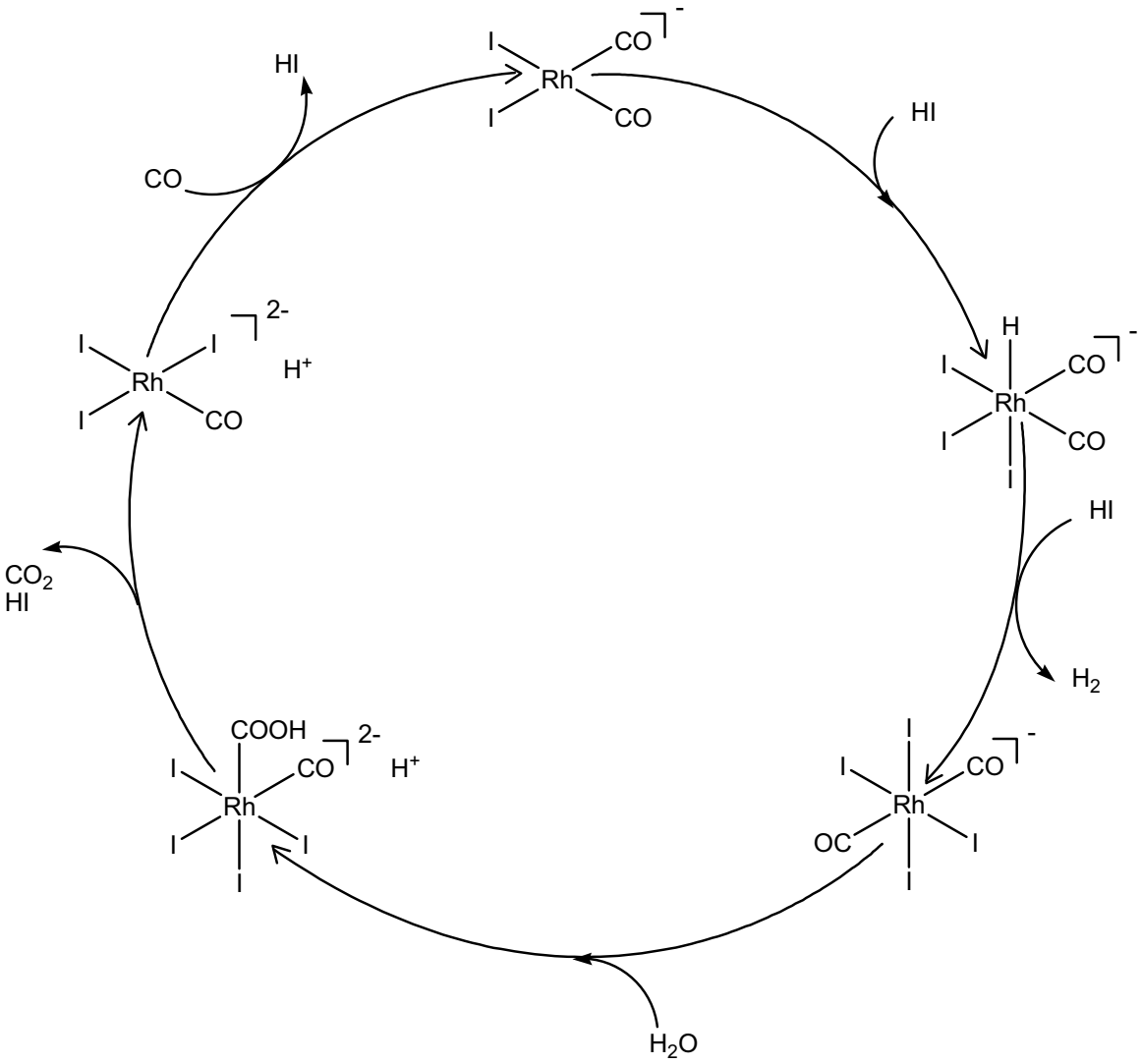

Scheme 27 : Proposed catalytic cycle for the rhodium catalyze WGSR.

The rhodium-catalyzed WGSR starts with the oxidative addition of one molecule of HI on the $[RhI_2(CO)_2]^-$ complex. As its methyl complex homologue $[RhCH_3I_3(CO)_2]^-$, the resulting hydride complex $[RhHI_3(CO)_2]^-$ is not stable at ambient temperature and have only been detected by ^{13}C NMR and infrared spectroscopy by reacting complex $[AsPh_4][RhI_2(CO)_2]$ with one equivalent of HI at –20℃ [83]. This hydride rhodium complex is stable at low temperature (-30℃ or below) but disproportionates at higher temperature ($t_{1/2}$ = 7 h at –20℃) to the starting complex $[AsPh_4][RhI_2(CO)_2]$, the tetra-iodo complex $[AsPh_4][RhI_4(CO)_2]$ and dihydrogen (Sc. 28).

$$2\ [H\text{-}RhI_3(CO)_2][AsPh_4] \longrightarrow [RhI_2(CO)_2][AsPh_4] + [RhI_4(CO)_2][AsPh_4] + H_2$$

Scheme 28 : Disproportionation of complex $[Rh(H)I_3(CO)_2][AsPh_4]$.

This HI oxidative addition reaction monitored by ^{13}C NMR at –100℃ indicates the formation of an unknown hydride-rhodium complex suggesting that this reaction occurs in two steps via the neutral complex $[H\text{-}RhI_2(CO)_2]$ (Sc. 29) that is consistent with the observations made for the methyl iodide oxidative addition on a rhodium complex[55].

$$[RhI_2(CO)_2][AsPh_4] + HI \longrightarrow [H\text{-}RhI_2(CO)_2] + [AsPh_4]I$$

Scheme 29 : Formation of a neutral hydride-rhodium intermediate in the HI oxidative addition reaction.

The next step of the WGSR is the rapid addition of another molecule HI on the hydride-rhodium complex forming the stable tetra-iodo complex $[RhI_4(CO)_2]^-$ and liberating one molecule of dihydrogen.

The structure of this tetra-iodo complex has been determined by X-ray analysis as a bipyramid with the two CO ligands in *trans* position[84]. Infrared in situ studies on the WGSR have shown that this complex is predominant in the medium together with complex $[RhI_2(CO)_2]^-$[85]. Thus, $[RhI_4(CO)_2]^-$ has been proposed as the complex which can decompose to form RhI_3 black rhodium precipitation (Sc. 30)[2].

$$[RhI_4(CO)_2]^- \longrightarrow RhI_3 + 2\,CO + I^-$$

Scheme 30 : Decomposition of $[RhI_4(CO)_2]^-$.

To complete the WGSR catalytic cycle, it has been proposed that complex $[RhI_4(CO)_2]^-$ reacts with water to give back the starting complex $[RhI_2(CO)_2]^-$ via two dianionic intermediates since production of CO_2 and consumption of CO were observed[2,85] but these intermediates have not been observed. Another pathway has been proposed via the neutral complex $[RhI_3(CO)_3]$ formed from $[RhI_4(CO)_2]^-$ complex by insertion of a CO ligand taking the place of an iodide ligand (Sc. 31)[85].

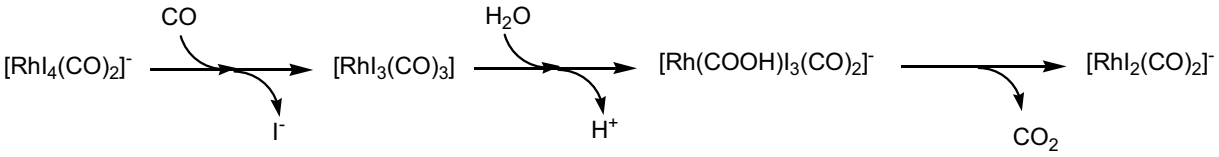

Scheme 31 : Another pathway for the rhodium-catalyzed WGSR.

Kinetic measurements based on the production of CO_2 in a medium containing rhodium catalyst, acetic acid, water and HI under CO for a total pressure of 28 bar at 185°C have been performed in orde r to evaluate the effect of water and HI on the WGSR rate[50]. Results are displayed in figure 3.

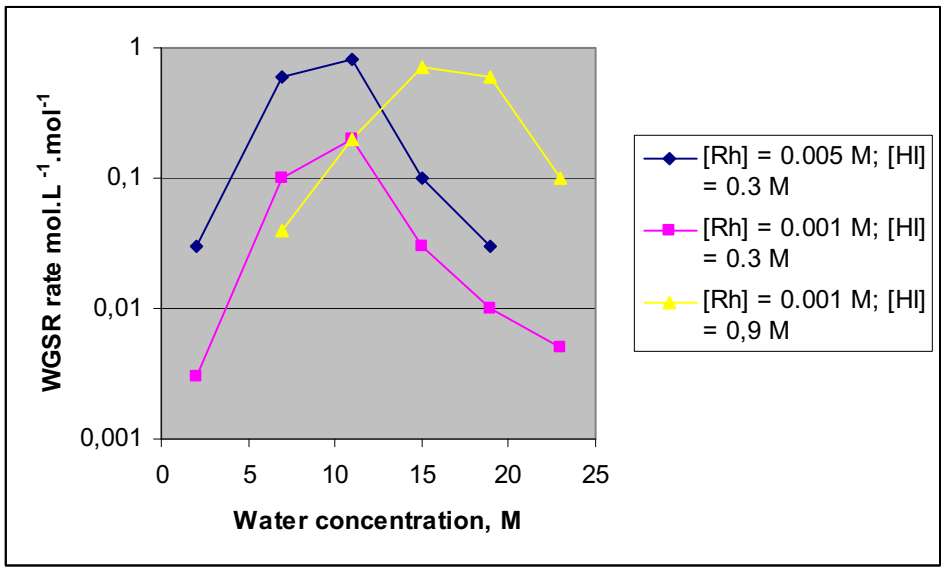

Figure 3 : Variation of the WGSR rate with water and HI concentration.

Figure 3 shows that water, HI and rhodium concentration play an important role in the WGSR rate. The three curves present the same Gaussian type shape. The WGSR rate increases with the increase in water concentration to reach a maximum and then, decreases for higher water concentration. Higher concentrations of HI lead to a shift of the maximum of the curve towards high water concentrations. As, it can be expected, the increase of rhodium concentration increases the WGSR rate. These results have been connected to the total acidity level of the medium, depending on water and HI concentration, indicating that the WGSR rate increases to a maximum when the acidity level increases and then decreases whereas the acidity level continues to increase[50,85].

Other mechanistic studies on the rhodium-catalyzed WGSR based on the temperature influence have been performed[86]. At temperatures above 80℃, the major species obs erved in the catalytic medium is $[RhI_4(CO)_2]^-$ and the catalytic reaction shows first-order dependence on the partial pressure of CO. However, below 65℃ the reaction is independent of CO pressure, and exhibits a second-order dependence on HI concentration. The major species observed is now the Rh(I) complex $[RhI_2(CO)_2]^-$. These observations mean that at high temperature, the determining step of the WGSR reaction is the reaction of CO with the tetra-iodo complex $[RhI_4(CO)_2]^-$ or with $[RhI_3(CO)]^{2-}$ affording complex $[RhI_2(CO)_2]^-$ and at lower temperature, the determining step becomes the oxidative addition of 2 moles of HI on the Rh(I) complex.

Moreover, it has been shown that the WGSR is also dependent on the dihydrogene partial pressure. In situ infrared investigations indicated that complex $[RhI_4(CO)_2]^-$ can be converted into complex $[RhI_2(CO)_2]^-$ by addition of dihydrogen in the catalytic medium meaning that the addition of 2 moles of HI on complex $[RhI_2(CO)_2]^-$ and the resulting liberation of dihydrogen can be reversible (Sc. 32)[87].

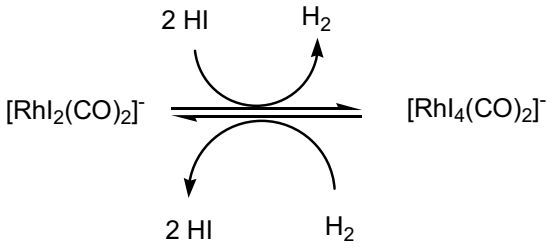

Scheme 32 : reversible reaction between $[RhI_2(CO)_2]^-$ and $[RhI_4(CO)_2]^-$.

Supported rhodium-catalyzed methanol carbonylation.

Another main draw-back of the homogeneous catalytic process is the loss of the catalyst. Thus, for the rhodium-catalyzed methanol carbonylation reaction, some expensive rhodium catalyst can be lost either 1) by precipitation of black rhodium, 2) by the formation of volatile rhodium species when separating catalytic mixture from acetic acid or 3) by degradation of phosphine-rhodium ligands in drastic conditions used as mentioned above. Thus, immobilisation of rhodium catalyst on resins or zeolytes is an economical challenge for industrial applications[62].

An answer has been held in the Acetica process by the use of polyvinypyridine resin tolerant of elevated temperature[88-90]. The catalytically active complex $[RhI_2(CO)_2]^-$ was supported on a ion exchange resin in which the pendant pyridyl groups had been quaternized by reaction with CH_3I (Sc. 33).

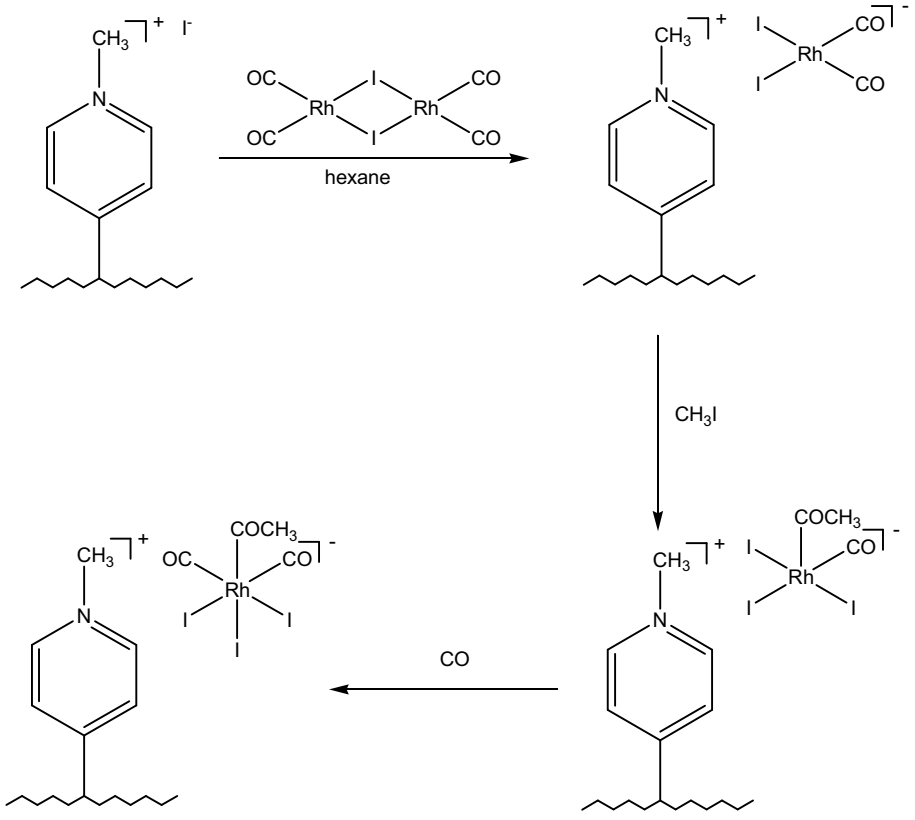

Scheme 33 : Supported rhodium-catalyzed methanol carbonylation.

This process shows increased carbonylation rates for batch experiments at low water content (3-7 wt%) in comparison with the catalytic process using $[RhI_2(CO)_2]^-$ and shows an extremely effective ionic attachment with a very low rhodium concentration in the effluent from the reactor.

Rhodium/iodide catalyzed methanol carbonylation.

In spite of all recent research made to find higher efficiency rhodium process, the two most largely used process in the methanol carbonylation are the Eastman process for the production of acetic anhydride and the Celanese process for the production of acetic acid. In both processes, large amounts of lithium iodide are introduced.

Concerning the production of acetic anhydride from methyl acetate, Monsanto has discovered first the powerful iodide promoted rhodium carbonylation system[44]. Although other systems were considered, the rhodium catalyzed methyl acetate carbonylation was the method of choice. In 1976, Halcon patented a process based on rhodium/LiI catalyst[91]. The Eastman Company entered a technology exchange agreement with Halcon and a plant for acetic anhydride production was achieved in 1983[92].

The development of the rhodium based catalyst for carbonylation of methyl acetate to acetic anhydride would be expected to be similar to the methanol carbonylation described by Monsanto. However, application of the rhodium-catalyzed methanol carbonylation for methyl acetate carbonylation shows very slow carbonylation rate, Addition of lithium iodide in the reactor and dihydrogen in the feed enhance significantly the carbonylation rate[93]. In situ infrared investigations[87,92] have shown that addition of dihydrogene reduced the WGSR steady state $[RhI_4(CO)_2]^-$ to the active species $[RhI_2(CO)_2]^-$. A catalytic cycle for the rhodium-catalyzed methyl acetate carbonylation has been proposed (Sc.34).

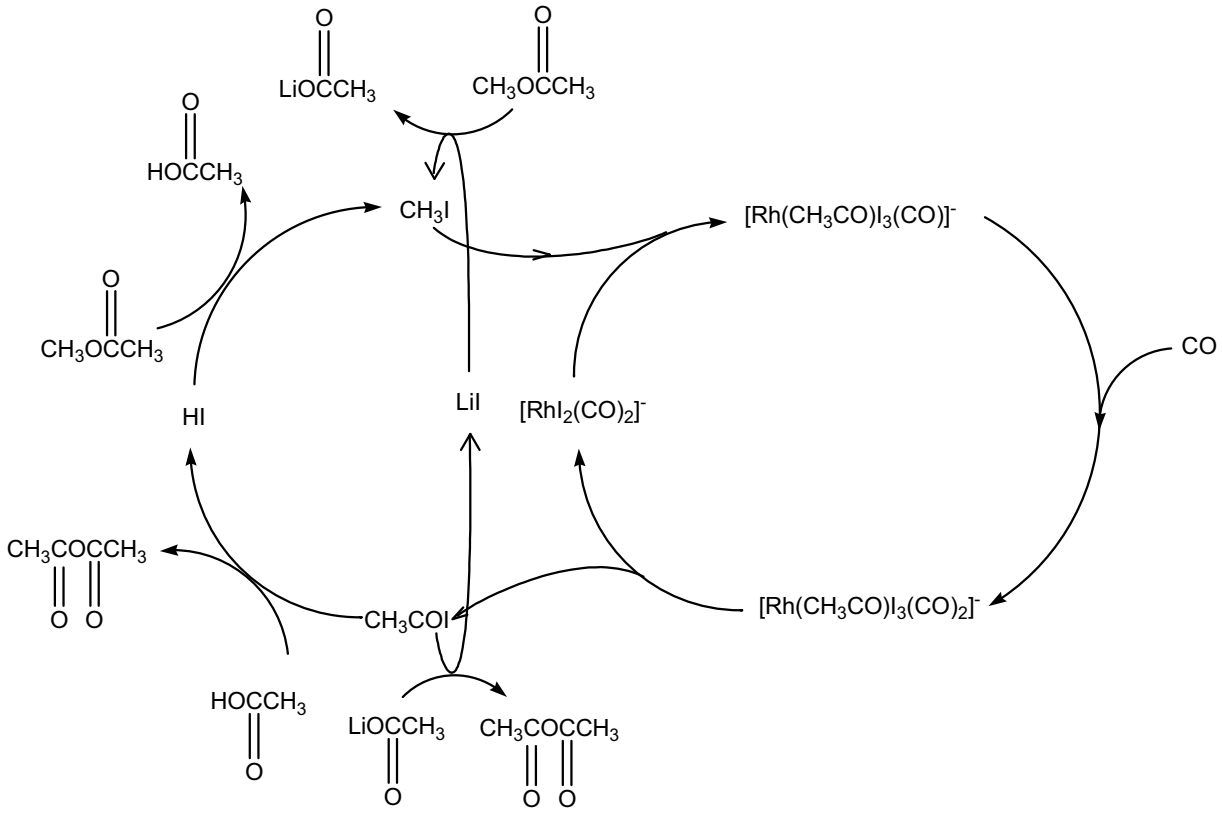

Scheme 34 : Proposed catalytic cycle for the rhodium-catalyzed methyl acetate carbonylation.

The proposed catalytic cycle involves the same rhodium species than the rhodium-catalyzed methanol carbonylation cycle with oxidative addition of methyl iodide on $[RhI_2(CO)_2]^-$ leading to the five coordinated acetyl rhodium complex which gives under CO the dicarbonyl acetyl rhodium complex where reductive elimination of acetyl iodide occurs. In this cycle, lithium iodide plays a prominent role reacting with methyl acetate giving methyl iodide and lithium acetate ions, the latter giving acetic anhydride by reaction with acetyl iodide. Acetyl iodide can also react with acetic acid giving acetic anhydride and HI which reproduces acetic acid and methyl iodide by reaction with methyl acetate.

In 1991, Celanese patented a process for the production of acetic acid based on a rhodium/lithium iodide system[51]. After preliminary investigations Torrence *et al.* showed that addition of lithium iodide or lithium acetate to a solution of methyl iodide/acetic acid and $[RhI_2(CO)_2]^-$ enhances the oxidative addition reaction[94], they optimized water, methyl acetate and lithium iodide concentrations giving a process suitable for industrial application. The main parameters are as follows.

Water effect:

By increasing the water concentration in the reaction medium containing rhodium catalyst, methyl acetate (4-6 wt%), LiI (18-20 wt%), CH_3I (14 wt%) and acetic acid, the carbonylation rate increases rapidly between a water concentration of 0-4 wt% and stabilizes whereas water concentration continues to increase. High water contents (20 wt%) under these conditions do not show significant enhancement of the carbonylation rate.

Lithium iodide effect:

The increase of LiI concentration in the medium increases linearly the carbonylation rate. This enhancement is very effective for low water contents. Furthermore, gas analysis shows that the CO_2 production, due to the WGSR, is significantly reduced for lithium iodide concentration ranging between 10-20 wt%. Rhodium loss is also reduced when using significant quantities of LiI.

Methyl acetate effect:

Methyl acetate concentration effect exhibits almost the same behavior than the water concentration effect with a dramatic enhancement of the carbonylation rate when methyl acetate content increases from 0 to 8 wt% and a plateau is observed with no significant carbonylation rate enhancement for high methyl acetate concentrations. The CO_2 production is also reduced when methyl acetate content increases.

The reduction of the WGSR has been explained by the reduction of the HI concentration in the medium, this latter reacting with the acetate ions formed by reaction of methyl acetate with lithium iodide (Sc. 13).

Thus, the Celanese process present numerous advantages with the reduction of water content, the reduction of rhodium loss and reduction of the WGS reaction. Altought several new rhodium complexes were developed and showed high activity for methanol carbonylation, the most part of acetic acid is produced by the Celanese process. Indeed, these new catalysts may be show high carbonylation activity in batch experiments but their behaviors and especially their stabilities in a continue unit could be very different, batch experiments being limited to the reactor part.

I-6 Context of the present work

Our PhD work was essentially devoted to study the mechanism of the catalytic system in the carbonylation reaction of methanol at low water content. During this work, we performed numerous batch experiments in order to study the catalyst activity for the methanol carbonylation in conditions close to industrial ones. But the behavior of the catalytic system in batch experiments present several differences in comparison with the behavior of the same catalytic system under industrial conditions in a continue plant. In this part, we will describe the conditions used in an industrial plant and the major differences that exist in comparison with batch experiments. We will explain also how to mimic the catalytic conditions used in an industrial plant by changing the catalytic medium for batch experiments.

Description of an industrial plant:

A simplified flow sheet describing the commercial unit used for industrial production of acetic acid for the Celanese process or the Cativa process is displayed in scheme 35.

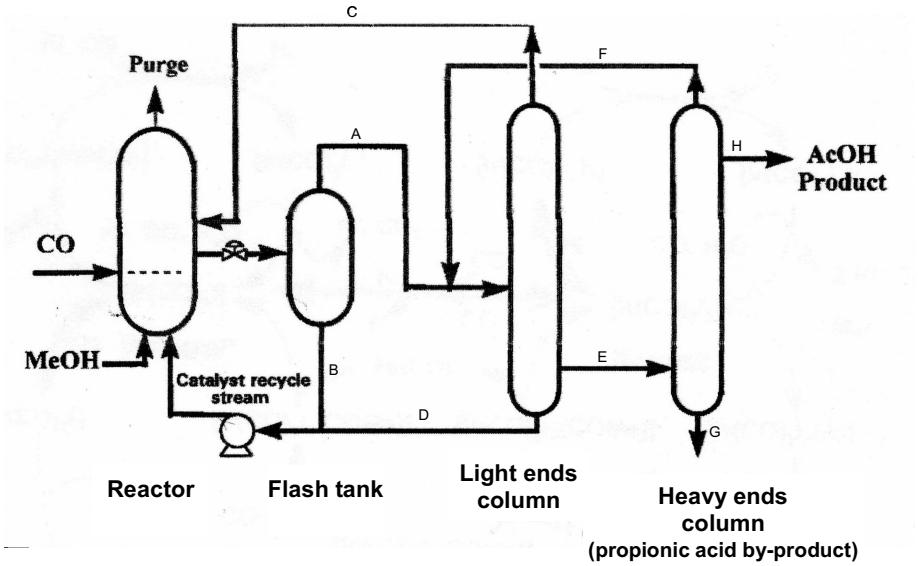

Scheme 35 : Simplified flow sheet for an industrial acetic acid plant

Once the plant is started, the reactor, where the carbonylation reaction occurs, is only fed with methanol and CO gas. The CO partial pressure in the reactor is around 10 bar whereas the total pressure is around 30 bar due to the volatile organic compounds as methyl iodide and methyl acetate present in the reactor and the temperature is set to 190℃. Even if the reactor is fed with methanol, analysis of its composition does not show its presence since it is directly transformed to methyl iodide by reaction with HI produced from the hydrolysis of acetyl iodide, coming from the reductive elimination reaction of the acetyl rhodium complex, and water.

The catalytic mixture is then transferred to the flash tank, its main role being to separate the catalyst from the catalytic solution. Thus, the flash tank cool down the catalytic mixture to 150℃ and depressors it, the total pressure being around 2 bar, essentially due to the volatile compounds. This difference of pressure and temperature separate the catalytic mixture in two parts:

-The residue containing the catalyst and a large part of acetic acid and water is fed back to the reactor (B).

-The over head containing water, acetic acid, methyl acetate, methyl iodide and a small quantity of catalyst is sent to the light ends column (A).

It is worth noting that the loss of catalyst due to its precipitation is observed in the flash tank and not in the reactor. Thus, stabilization of the catalyst in the flash tank is an important feature since rhodium is very expensive.

The light end column: the over head of the light ends column containing methyl iodide, methyl acetate and water is fed back to the reactor (C). The side stream containing the acetic acid and water is sent to a second column (E). The residue containing remaining catalyst and acetic acid is sent back to the reactor.

The over head of the heavy ends column containing essentially water is sent back to the side stream of the flash tank (F). The residue containing heavy propionic acid by-product is exited (G) and the pure acetic acid is collected by the side stream (H).

We can note that for the high water content Monsanto process, a third distillation column is needed to remove the water in order to obtain pure acetic acid, generating higher energy cost.

By feeding back the water, methyl acetate, methyl iodide and some acetic acid in different parts of the unit, their concentrations are kept constant in the reactor. Table 4 summarizes the optimized concentrations in the reactor used for the different processes, acetic acid content being the balance.

	catalyst (ppm)	water wt%	methyl acetate wt%	methyl iodide wt%	temperature ℃	CO partial pressure (bar)
Monsanto	600	14	2	10	190	10
Cativa	1200 (Ir) 800 (Ru)	6	10	10	190	10
Celanese	700 (Rh) 10 wt% (LiI)	4	2	10	190	10

Table 4 : Product concentrations in the reactor for the different processes.

We can notice that for each process, the methyl iodide concentration, the temperature and the CO partial pressure are the same, the differences arising from the methyl acetate concentration, the water content and the nature of the catalyst. For the Monsanto process, a water content of 14 wt% is required to have a good stability in the flash tank whereas the Cativa process using a [Ir/Ru] catalyst shows good stability as well as high activity at 6 wt% and concerning the Celanese process, a good stability of the rhodium catalyst at 4 wt% of water is observed when lithium iodide is introduced in the medium. The catalyst concentration as well the methyl acetate content are optimized for a good compromise between both activity and stability.

Thus, in a industrial plant, two main factors are important, the activity of the catalyst in the reactor but also its stability in the flash tank.

Batch experiments

Batch experiments are usually performed in order to evaluate the activity of a catalyst system before any eventual industrial application. In our case, this technique presents major differences in comparison with a continue unit:

First, batch experiments are performed in a closed reactor meaning that the behavior of the catalytic system in the flasher tank, particularly the stability of the catalyst, cannot be evaluated.

Second, the batch reactor is only fed by gas during the experiment, thus, the concentration of the introduced compounds evolve along the duration of the experiment that it is not the case in a continue plant where all the concentration are kept constant in the reactor.

Taking into account these two comments, we performed batch experiments following the general procedure described below:

First, the active catalyst species is preformed in the reactor by introducing the desired metal salt (RhI_3 or $IrI_{3,4}$) with an acetic acid/water mixture of 10/1 wt%. The reactor is sealed and flushed three times with CO. Then, the CO pressure is adjusted at 5 bar and the temperature at 190℃. We checked by HP-IR experiments that, under these conditions, a preformation time of 25 min. is required to observe a maximum intensity of the active species CO bands.

Second, we introduced the rest of the catalytic medium via an additional over-pressurized tank and the CO pressure is adjusted to 30 bar:

- Methyl iodide: 10 wt%. Same concentration than that used in an industrial plant.

- Methyl acetate: 27 wt%. We introduced higher concentration of methyl acetate in comparison with that present in the reactor of a continue plant in order to keep constant the concentration of methyl iodide in the reactor. Indeed, we consider that for one molecule of methyl iodide consumed in the oxidative addition reaction, one molecule of HI is released by the reaction of acetyl iodide with water, which can react with one molecule of methyl acetate giving back a molecule of methyl iodide and acetic acid (Sc. 36). *Thus, the high concentration role of methyl acetate is to mimic the continue feed of methanol in a continue unit and its concentration decreases during the batch experiment*.

  -Water to the desired starting concentration. In order to study the water effect on the activity of a catalytic system, we introduced various water concentrations via the additional tank, taking into account the water introduced for the preformation reaction and considering that its concentration does not changed during the preformation of the active catalyst. According to the equations displayed in scheme 36, we note that water is consumed during the carbonylation reaction and no water is added during the experiment. *Thus the water concentration decrease during the experiment*.

- Acetic acid as the balance. Acetic acid is introduced as the balance taking into account the different product introduced for the experiment. According to scheme 36, we note that two molecules of acetic acid are produced, one arising from the real carbonylation reaction and one arising from the reaction of methyl acetate with HI. *Thus, the acetic acid concentration increase during the experiment*.

- CO pressure is kept constant at 30 bar during the batch experiment via an over-pressurized ballast where the CO consumption is measured. According to scheme 36, one molecule of CO is consumed whereas two molecules of acetic acid are produced.

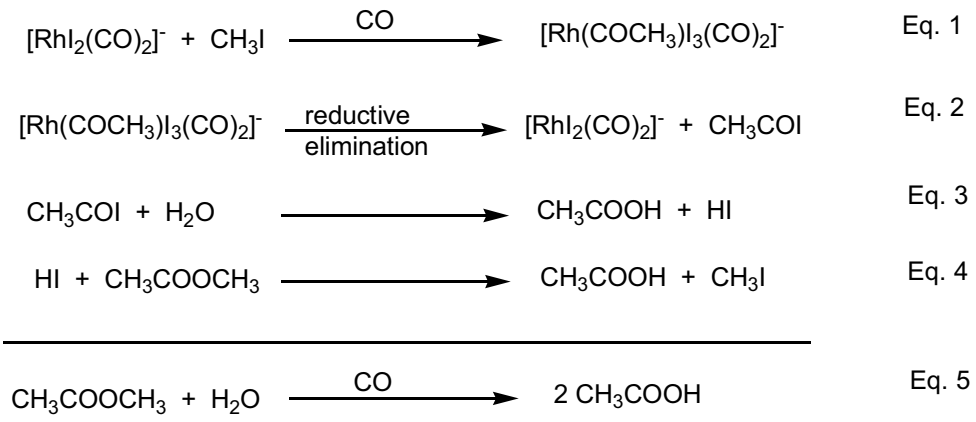

Scheme 36 : Consumption and production of the different products during a batch experiment

Determination of the carbonylation rate:

The carbonylation rate is given in moles of acetic acid produced per liter of the catalytic medium per hour (mol/L/h). According to the equations depicted in scheme 36, we consider that one molecule of acetic acid is produced from the carbonylation reaction (Eq.: 1, 2, 3) and one molecule of acetic is produced from organic reaction (Eq.: 4).

Thus, regarding equation 5, the carbonylation rate can be calculated from the consumption of methyl acetate, the consumption of water, the consumption of CO but half the production of acetic acid.

For our part, carbonylation rates were determined at 20 wt% and 15 wt% of remaining methyl acetate, starting from 27 wt% initial concentration of methyl acetate as explained above. We chose these values to evaluate the catalytic system activity which is not to its maximum when the carbonylation reaction starts and to have a remaining water concentration in the medium close to its initial concentration since water is consumed during the experiment.

To evaluate the carbonylation rate at 20 wt% and 15 wt% of remaining methyl acetate, we consider, regarding the equation 5 (Sc. 36), that one molecule of CO is consumed for one molecule of methyl acetate consumed. Thus, taking into account the temperature and the volume of our gas ballast, we calculate the consumption of CO required, considering CO as a perfect gas.

Once all the catalytic medium is introduced in the reactor and the CO pressure adjusted to 30 bar, a chronometer is started when the ballast pressure, measured with a digital equipment, starts to decrease. At the calculated CO consumption for 20 wt% and 15 wt% of remaining methyl acetate, the time is noted and a sample is taking out from the reactor for chromatography analysis. Thus, concentration of acetic acid, methyl acetate, water and methyl iodide are calculated.

Batch experiments were performed starting from the same weight of catalytic solution (60g), the density of its solution being measured. For the determination of the carbonylation rate, this weight was corrected taking into account the CO introduction in the solution for the formation of acetic acid and considering that the density of the solution at 20 wt% and 15 wt% of remaining methyl acetate is the same than the initial solution.

Thus, regarding the consumption of methyl acetate, the comsuption of CO, the consumption of water and the half production of acetic acid, we calculated for each product, with the reaction time and the calculated volume of the solution, the carbonylation rate and we obtained in each case similar values.

For the batch run experiments performed with lithium iodide, we not take into account its wt% in the balance of acetic acid introduced in order to have similar acetic acid concentration in the batch runs performed without lithium iodide. It is worth noting that by introducing LiI in the reactor, we change slightly the catalyst concentration.

Thus, batch run experiments can be a good technique to evaluate the activity of a catalytic system considering the carbonylation rate and the behavior of the catalyst in reactor conditions. But we have to keep in mind that the reactor is one part of a continue unit and that both, behavior and stability of a catalyst in the flash tank can't be evaluated using this technique.

I-7 References

[1] N. Yoneda, S. Kusano, M. Yasui, P. Pujado, S. Wilcher, *Appl. Catal. A: General* **2001**, *221*, 253.

[2] P. Torrence, in *Applied Homogeneous Catalysis with Organometallics Compounds, Vol. 1*, 2nd ed. (Eds.: B. Cornils, W. A. Herrmann), Wiley-VCH, p. 104.

[3] N. Kutenpov, W. Himmele, H. Hohenshutz, *Hydrocarbon process* **1966**, *45*, 141.

[4] N. Kutenpov, W. Himmele, H. Hohenshutz, *Chem. Ing. Tech* **1965**, *37*, 383.

[5] H. Cheung, R. S. Tank, G. P. Torrence, *Ullmann's Encyclopedia of Industrial Chemistry* **2000**.

[6] W. Reppe, H. Friederich, in *BASF, De Offen*, **1951**.

[7] T. W. Dekleva, D. Forster, *Adv. Catal.* **1986**, *34*, 81.

[8] D. Forster, T. C. Singleton, *J. Mol. Catal.* **1982**, *17*, 299.

[9] T. Isshiki, Y. Kijimi, Y. Miyauchi, T. Kondo, to Mitsubishi Gas Chemical Co., Inc., European Patent 65,817, **1982**.

[10] A. Naglieri, N. Rizkalla, to Halcon SD Group, Inc., U. S. Patent 4,356,320 A, **1982**.

[11] A. Naglieri, N. Rizkalla, to Halcon international, Inc., U. S. Patent 4,134,912, **1979**.

[12] N. Rizkalla, to Halcon SD Group, Inc., French Patent 2,496,643 A1, **1982**.

[13] N. Rizkalla, to Halcon International, Inc., British Patent 2,128,609, **1984**.

[14] W. R. Moser, J. E. Cnossen, A. W. Wang, S. A. Krouse, *J. Catal.* **1985**, *95*, 21.

[15] W. R. Moser, B. J. Marshik-Guerts, S. J. Okrasinski, *J. Mol. Catal.* **1999**, *143*, 57.

[16] W. R. Moser, B. J. Marshik-Guerts, S. J. Okrasinski, *J. Mol. Catal.* **1999**, *143*, 71.

[17] J. S. Kanel, S. J. Okrasinski, for Eastman Chemical Compagny, U.S Patent 5,900,504, **1999**.

[18] J. Gong, Q. Fan, D. Jiang, *J. Mol. Catal.* **1999**, *147*, 113.

[19] P. W. N. Van Leeuwen, for Shell Compagny, European Patent 0090443, **1983**.

[20] J. Yang, A. Haynes, P. M. Maitlis, *Chem. Comm.* **1999**, 179.

[21] P. W. N. Van Leeuwen, M. A. Zuideveld, B. H. G. Swennenhuis, Z. Freixa, P. C. J. Kamer, K. Goubitz, J. Fraanje, M. Lutz, A. L. Spek, *J. Am. Chem. Soc.* **2003**, *125*, 5523.

[22] S. S. Tonde, A. A. Kelkar, M. M. Bhadbhade, R. V. Chaudhari, *J. Organomet. Chem.* **2005**, *690*,

1677.

[23] F. E. Paulik, J. F. Roth, *Chem. Commun.* **1968**, 1578.

[24] D. Brodzki, B. Denise, G. Pannetier, *J. Mol. Catal.* **1977**, *2*, 149.

[25] T. Mizoroki, T. Matsumoto, A. Ozaki, *J. Catal.* **1978**, *51*, 96.

[26] D. Forster, *J. Chem. Soc., Dalton Trans.* **1979**, 1639.

[27] T. R. Griffin, D. B. Cook, A. Haynes, J. M. Pearson, D. Monti, G. E. Morris, *J. Am. Chem. Soc.* **1996**, *118*, 3029.

[28] P. M. Maitlis, A. Haynes, B. R. James, M. Catellani, G. P. Chiusoli, *Dalton Trans.* **2004**, 3409.

[29] J. M. Pearson, A. Haynes, G. E. Morris, G. J. Sunley, P. M. Maitlis, *J. Chem. Soc., Chem Commun.* **1995**, 1045.

[30] S. B. Butts, S. H. Straus, E. M. Holt, R. E. Stimson, N. W. Alcock, D. F. Shriver, *J. Am. Chem. Soc.* **1980**, *102*, 5093.

[31] T. G. Richmond, F. Basolo, D. F. Shriver, *Inorg. Chem.* **1982**, *21*, 1272.

[32] G. J. Sunley, D. J. Watson, *Catal. Today* **2000**, *58*, 293.

[33] K. E. Clode, D. J. Watson, European Patent 616,997, **1994**.

[34] M. J. Muskett, World Patent 03097567 A1, **2003**.

[35] A. Haynes, P. M. Maitlis, G. E. Morris, G. J. Sunley, H. Adams, P. W. Badger, C. M. Bowers, D. B. Cook, P. I. P. Elliott, T. Ghaffar, H. Green, T. R. Griffin, M. Payne, J. M. Pearson, M. J. Taylor, P. W. Vickers, R. J. Watt, *J. Am. Chem. Soc.* **2004**, *126*, 2847.

[36] R. Whyman, A. P. Wright, J. A. Iggo, B. T. Heaton, *J. Chem. Soc., Dalton Trans.* **2002**, 771.

[37] C. Le Berre, P. Serp, P. Kalck, L. Layeillon, D. Thiebault, to Acetex chimie, French Patent 9813954, **1998**.

[38] S. Gautron, PhD thesis thesis, Université Paul Sabatier (Toulouse), **2003**.

[39] S. Gautron, N. Lassauque, C. Le Berre, P. Serp, L. Azam, R. Giordano, G. Laurenczy, D. Thiebault, P. Kalck, *Eur. J. Inorg. Chem.* **2006**, *6*, 1121.

[40] S. Gautron, N. Lassauque, C. Le Berre, P. Serp, L. Azam, R. Giordano, G. Laurenczy, D. Thiebault, P. Kalck, *Topics in Catalysis, in press*.

[41] S. Gautron, N. Lassauque, C. Le Berre, L. Azam, R. Giordano, P. Serp, G. Laurenczy, J. C.

Daran, C. Duhayon, D. Thiebault, P. Kalck, *Organometallics, in press*.

[42] M. Volpe, G. Wu, A. Iretskii, P. C. Ford, *Inorg. Chem.* **2006**, *45*, 1861.

[43] F. E. Paulik, A. Hershman, W. R. Knox, J. F. Roth, for Monsanto company, US Patent 3,769,329, **1973**.

[44] J. F. Roth, J. H. Craddock, A. Hershman, F. E. Paulik, *Chem. Tech.* **1971**, 600.

[45] F. E. Paulik, J. F. Roth, *Chem. Commun.* **1968**, 1578.

[46] D. Forster, *J. Am. Chem. Soc.* **1976**, *98*, 846.

[47] C. E. Hickey, P. M. Maitlis, *J. Chem. Soc., Chem Commun.* **1984**, 1609.

[48] A. Haynes, B. E. Mann, D. J. Gulliver, G. E. Morris, P. M. Maitlis, *J. Am. Chem. Soc.* **1991**, *113*, 8567.

[49] G. W. Adamson, J. J. Daly, D. Forster, *J. Organomet. Chem.* **1974**, *71*, C17.

[50] T. C. Singleton, L. J. Park, J. L. Price, D. Forster, *Preprints-ACS. Division of Petroleum Chemistry* **1979**.

[51] B. L. Smith, G. P. Torrence, A. Aguilo, S. Alder, for Hoechst Celanese Corp., U.S Patent 5,001,259, **1991**.

[52] D. Forster, *J. Am. Chem. Soc.* **1975**, *97*, 951.

[53] C. E. Hickey, P. M. Maitlis, *J. Chem. Soc., Chem Commun.* **1984**, 1609.

[54] P. B. Chock, J. Halpern, *J. Am. Chem. Soc.* **1966**, *88*, 3511.

[55] A. Doppiu, U. Englert, A. Salzer, *Chem. Commun.* **2004**, 2166.

[56] P. M. Maitlis, A. Haynes, G. J. Sunley, M. Howard, J., *J. Chem. Soc., Dalton Trans.* **1996**, 2187.

[57] A. Fulford, C. E. Hickey, P. M. Maitlis, *J. Organomet. Chem* **1990**, *398*, 311.

[58] B. L. Smith, M. A. Murphy, G. P. Torrence, *J. Mol. Catal.* **1987**, *39*, 115.

[59] K. G. Moloy, R. W. Wegman, *Organometallics* **1989**, *8*, 2883.

[60] J. Rankin, A. D. Poole, A. C. Benyei, D. J. Cole-Hamilton, *J. Chem. Soc., Dalton Trans* **1999**, 3771.

[61] A. Haynes, *Top. Organomet. Chem., Vol. 18*, Springer-Verlag, Berlin, **2006**.

[62] R. W. Wegman, A. G. Abatjoglou, A. M. Harrison, *J. Chem. Soc., Chem Commun.* **1987**, 1891.

[63] M. J. Baker, M. F. Giles, A. G. Orpen, M. J. Taylor, R. J. Watt, *J. Chem. Soc., Chem Commun.*

1995, 197.

[64] M. J. Baker, J. R. Dilworth, G. J. Sunley, N. Wheatley, for B.P. Chemicals, European Patent 0631006 A1, **1994**.

[65] J. R. Dilworth, J. R. Miller, N. Wheatley, M. J. Baker, G. J. Sunley, *J. Chem. Soc., Chem Commun.* **1995**, 1579.

[66] C. P. Carraz, E. J. Ditzel, A. G. Orpen, D. D. Ellis, P. G. Pringle, G. J. Sunley, *Chem. Commun.* **2000**, 1277.

[67] C. M. Thomas, G. Süss-Fink, *Coord. Chem. Rev* **2003**, *243*, 125.

[68] C. M. Thomas, R. Mafua, B. Therrien, E. Rusanov, H. Stoeckli-Evans, G. Süss-Fink, *Chem. Eur. J.* **2002**, *8*, 3343.

[69] C. M. Thomas, PhD thesis thesis, University of Neuchatel, **2003**.

[70] Z. Freixa, P. C. J. Kamer, M. Lutz, A. L. Spek, P. W. N. Van Leeuwen, *Angew. Chem. Int. Ed.* **2005**, *44*, 4385.

[71] D. J. Ray, A. J. Stringer, for B. P. Chemicals, World Patent 8,503,703, **1984**.

[72] T. C. Singleton, W. H. Urry, F. E. Paulik, P. McLean, to Monsanto Company, European Patent 0,055,618 A1, **1981**.

[73] A. Wojcicki, *Adv. Organometal. Chem.* **1973**, *11*, 87.

[74] A. Haynes, B. E. Mann, D. J. Gulliver, G. E. Morris, P. M. Maitlis, *J. Am. Chem. Soc.* **1991**, *113*, 8567.

[75] E. I. Ivanova, P. Gisdakis, V. A. Nasluzov, A. I. Rubailo, N. Rösch, *Organometallics* **2001**, *20*, 1161.

[76] A. G. Kent, B. E. Mann, C. P. Manuel, *J. Chem. Soc., Chem Commun.* **1985**, 728.

[77] N. A. Cruise, J. Evans, *J. Chem. Soc., Dalton Trans.* **1995**, 3089.

[78] L. A. Howe, E. E. Brunel, *Polyhedron* **1995**, *14*, 167.

[79] M. C. Baird, J. T. Mague, J. A. Osborn, G. Wilkinson, *J. Chem. Soc.* **1967**, 1347.

[80] M. Kilner, N. J. Winter, *J. Mol. Catal.* **1996**, *112*, 327.

[81] T. Kinnunen, K. Laasonen, *J. Organomet. Chem.* **2001**, *628*, 222.

[82] J. H. Jones, *Platinum Metals Rev.* **2000**, *44*, 94.

[83] D. C. Roe, R. E. Sheridan, E. E. Brunel, *J. Am. Chem. Soc.* **1994**, *116*, 1163.

[84] J. J. Daly, F. Sanz, D. Forster, *J. Am. Chem. Soc.* **1975**, *97*, 2551.

[85] R. T. Eby, T. C. Singleton, *Appl. Ind. Catal.* **1983**, *1*, 275.

[86] E. C. Baker, D. E. Hendriksen, R. Eisenberg, *J. Am. Chem. Soc.* **1980**, *102*, 1020.

[87] S. W. Polichnowski, *J. Chem. Edu.* **1986**, *63*, 206.

[88] U.S Patent 5,334,755, to Chiyoda, **1994**.

[89] U.S patent 5,364,963, to Chiyoda, **1994**.

[90] U.S. Patent 5,576,458, to Chiyoda, **1996**.

[91] German Patent, DOS 2,610,036, to Halcon international, **1976**.

[92] J. R. Zoeller, V. H. Agreda, S. L. Cook, N. L. Lafferty, S. W. Polichnowski, D. M. Pond, *Catal. Today* **1992**, *13*, 73.

[93] T. H. Larkins, S. W. Polichnowski, G. Tustin, D. A. Young, to Eastman Chemical Company, U.S. Patent 4,374,070, **1983**.

[94] M. A. Murphy, B. L. Smith, G. P. Torrence, A. Aguilo, *J. Organomet. Chem.* **1986**, *303*, 257.

CHAPTER II :

FROM THE ACTIVE COMPLEX $[MI_2(CO)_2]^-$

TO THE ACETYL COMPLEX

$[MI_3(COMe)(CO)_2]^-$

CHAPTER II : FROM THE ACTIVE COMPLEX $[MI_2(CO)_2]^-$ TO THE ACETYL COMPLEX $[MI_3(COMe)(CO)_2]^-$

Nowadays the most largely used processes for methanol carbonylation to acetic acid are the low-water-content systems using a rhodium catalyst and an iodide salt (LiI, NaI...) as co-catalyst, patented by Celanese[1] in 1991, and the Cativa process[2], which employs an iridium catalyst and ruthenium as co-catalyst, patented by BP Chemical in 1996. Although the two iridium and rhodium catalytic cycles show some differences related to the nature of the intermediates[3,4], several complexes present the same structures, especially the stable active and acetyl species (scheme 1).

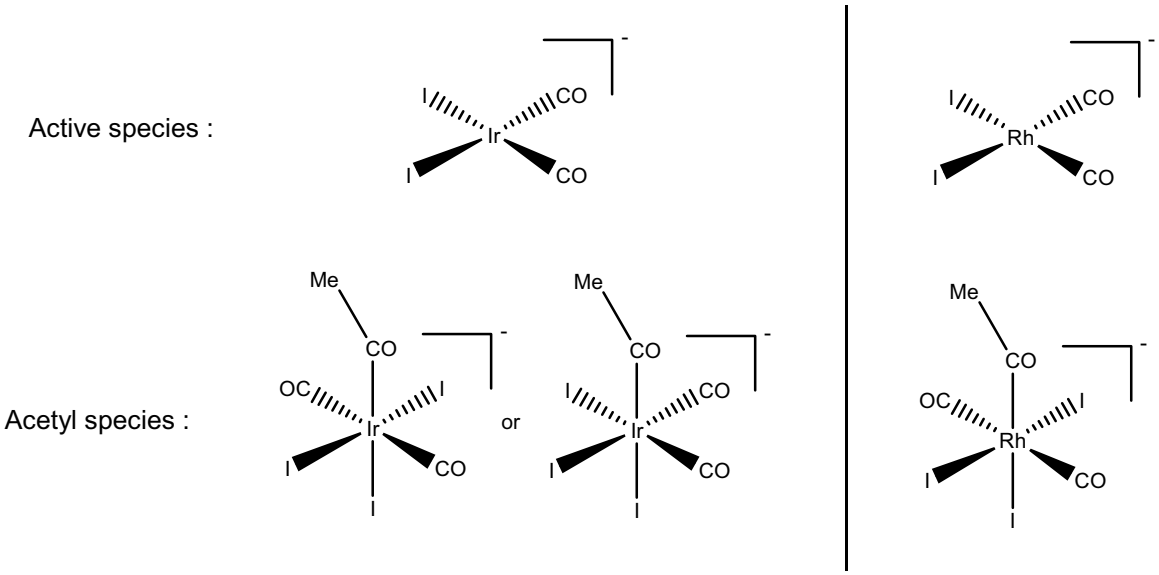

Scheme 1 : Active and acetyl species involved in the iridium and rhodium catalytic cycles

The active species results from the preformation step that we will describe later. In both cases, it is a square planar complex containing two carbonyl ligands in a cis-arrangement and two iodide ligands linked to the metal center. It starts the catalytic cycle leading, after further steps, to the acetyl species. The acetyl complex has two CO ligands, three iodide ligands and the acetyl group coordinated to the metal center, showing a pseudo-octahedral geometry. It is worth noting that two iridium acetyl isomers have been observed at ambient temperature, the *cis*-$[IrI_3(COMe)(CO)_2]^-$, which was crystallized[5], and the *trans*-$[IrI_3(COMe)(CO)_2]^-$; by contrast only the *trans*-$[RhI_3(COMe)(CO)_2]^-$ was observed under the same conditions. The *cis*-rhodium acetyl isomer was detected by ^{13}C NMR at –30℃ [6]. These acetyl compounds are key intermediates of the two catalytic cycles since they provide, after reductive elimination, acetyl iodide that gives acetic acid by immediate reaction with water giving back the active species $[MI_2(CO)_2]^-$.

In this chapter, at first we studied the rhodium catalytic cycle from the active species $[RhI_2(CO)_2]^-$ to the acetyl species $[Rh(COCH_3)I_3(CO)_2]^-$ by synthesizing the different intermediates in the cycle stabilized with the bulk counter ion PPN^+ ($Ph_3P=N=PPh_3^+$), using Schlenk techniques. These complexes were characterized by various techniques in order to collect their spectral data and to have the possibility of identifying them in other experiments. Hence, we did not study these species under catalytic conditions.

Secondly, we also synthesized the intermediates involved in the iridium catalytic cycle with the same aim as for the rhodium catalytic cycle. These iridium complexes show different reactivities than their homologue rhodium complexes. Then, we compared their behavior and their reactivity.

Thirdly, we tried to promote the rate determining step in the iridium catalytic cycle by adding a metal co-catalyst. We know that ruthenium is a good co-catalyst in the Cativa process, and studies performed in our laboratory[7,8,9] by introducing a platinum co-catalyst have also shown also good carbonylation rates. Thus, we tried to determine if any rhodium and iridium complexes are able to exent a positive synergetic effect and, considering that at low-water-content rhodium alone is unstable and shows low carbonylation rates, if rhodium can behave as a co-catalyst in the iridium-catalyzed methanol carbonylation.

II-1. Study of the rhodium catalytic cycle.

The rhodium catalytic process for the carbonylation of methanol to acetic acid was described in detail since it was patented by Monsanto Company in 1973[10]. Since then, reactivity of rhodium was studied and in 1976 Forster proposed a first catalytic cycle described in scheme 2[11]

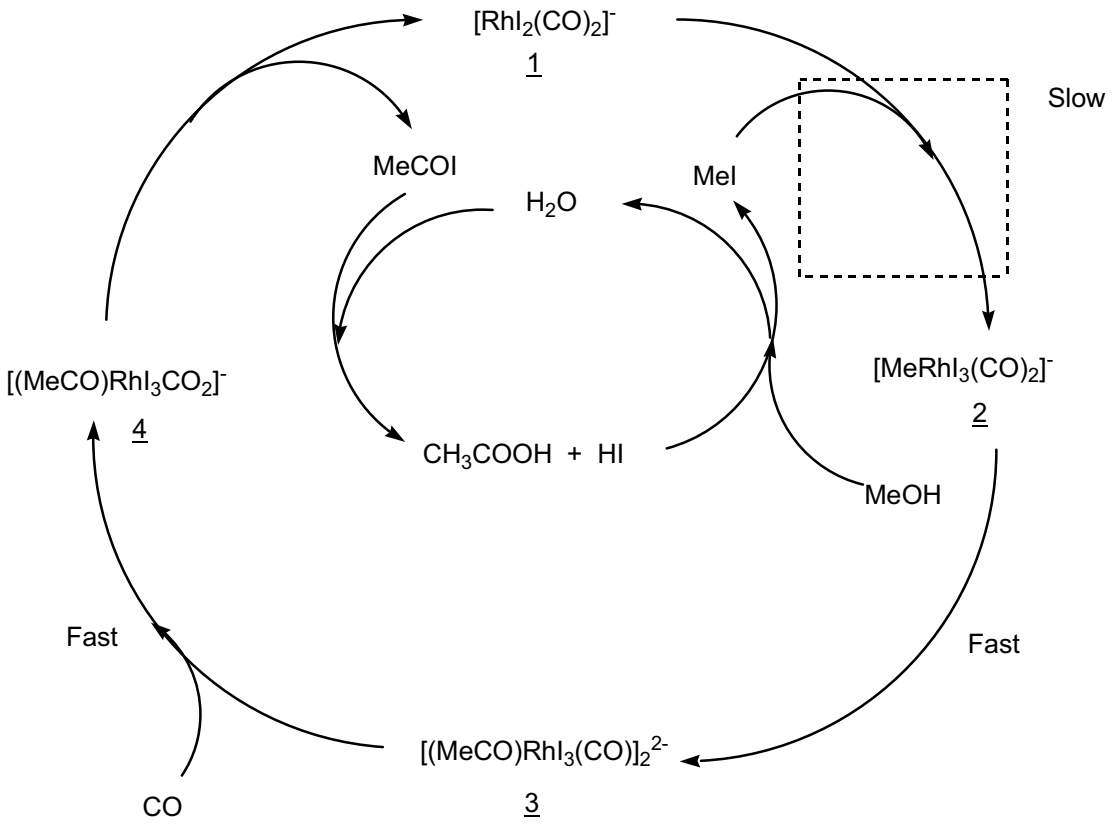

Scheme 2 : Proposed catalytic cycle for methanol carbonylation to acetic acid catalyzed by rhodium.

In order to collect spectroscopic data of the rhodium complexes, we first synthesized complex [PPN][$RhI_2(CO)_2$] 1 by adding a RhI_3 salt to a DMF/water mixture and, by heating the solution under CO bubbling, we obtained the complex [$NH_2(CH_3)_2$][$RhI_2(CO)_2$]. Then, one equivalent of [PPN]Cl was added to give [PPN][$RhI_2(CO)_2$] 1 in a 80% yield. Details of the synthesis are given in the experimental section. Complex 1 was crystallized from a bilayered solution of CH_2Cl_2/hexane at -18°C, and its X-ray structure was solved (Fig. 1).

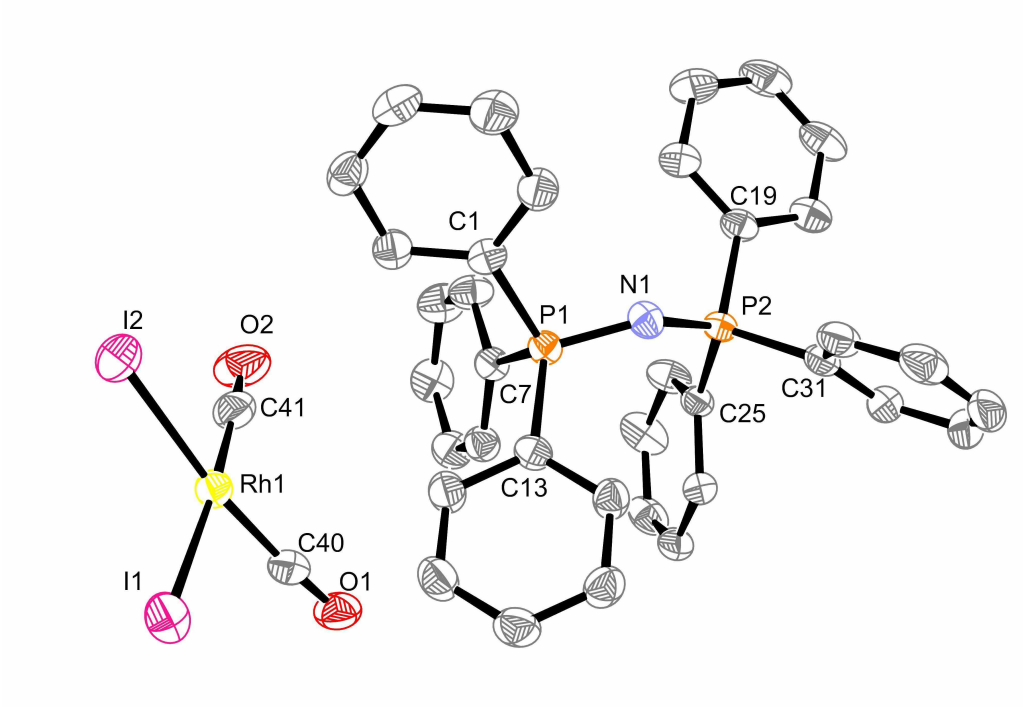

Figure 1 : X-ray structure of [PPN][$RhI_2(CO)_2$] 1.

The geometry of [$RhI_2(CO)_2$]$^-$ 1 is square planar, the crystal lattice is triclinic and its space group is P1. The relevant data of the bond length (Á) and angles (deg) are shown below:

Bond length: C40—O1 = 1.140 (4), C40—Rh1 = 1.844 (4), C41—O2 = 1.140 (5), C41—Rh1 = 1.840 (4), Rh1—I2 = 2.6515 (11), Rh1—I1 = 2.6725 (7)

Angles: C35—C36—H36 = 120, O1—C40—Rh1 = 176.0 (3), O2—C41—Rh1 = 175.6 (4), C41—Rh1—C40 = 92.09 (16), C41—Rh1—I2 = 85.56 (12), C40—Rh1—I2 = 172.99 (11), C41—Rh1—I1 = 174.56 (13), C40—Rh1—I1 = 88.49 (10), I2—Rh1—I1 = 94.48 (3)

The infrared spectrum of $[RhI_2(CO)_2]$ 1 (Fig. 2 top) show two ν_{CO} stretching bands at 2057.8 cm^{-1} for the symmetric vibration, and at 1987 cm^{-1} for the antisymmetric vibration. Complex 1 has been labeled and the IR spectrum of $[PPN][RhI_2(^{13}CO)_2]$ shows bands shifted down to lower frequencies due to the increase of the reduced mass of the CO ligands (Fig. 2 bottom). The ^{13}C NMR spectrum (Fig. 3) shows a doublet at δ = 183.96 ppm (d, $^1J_{C\text{-}Rh}$ = 71.17 Hz).

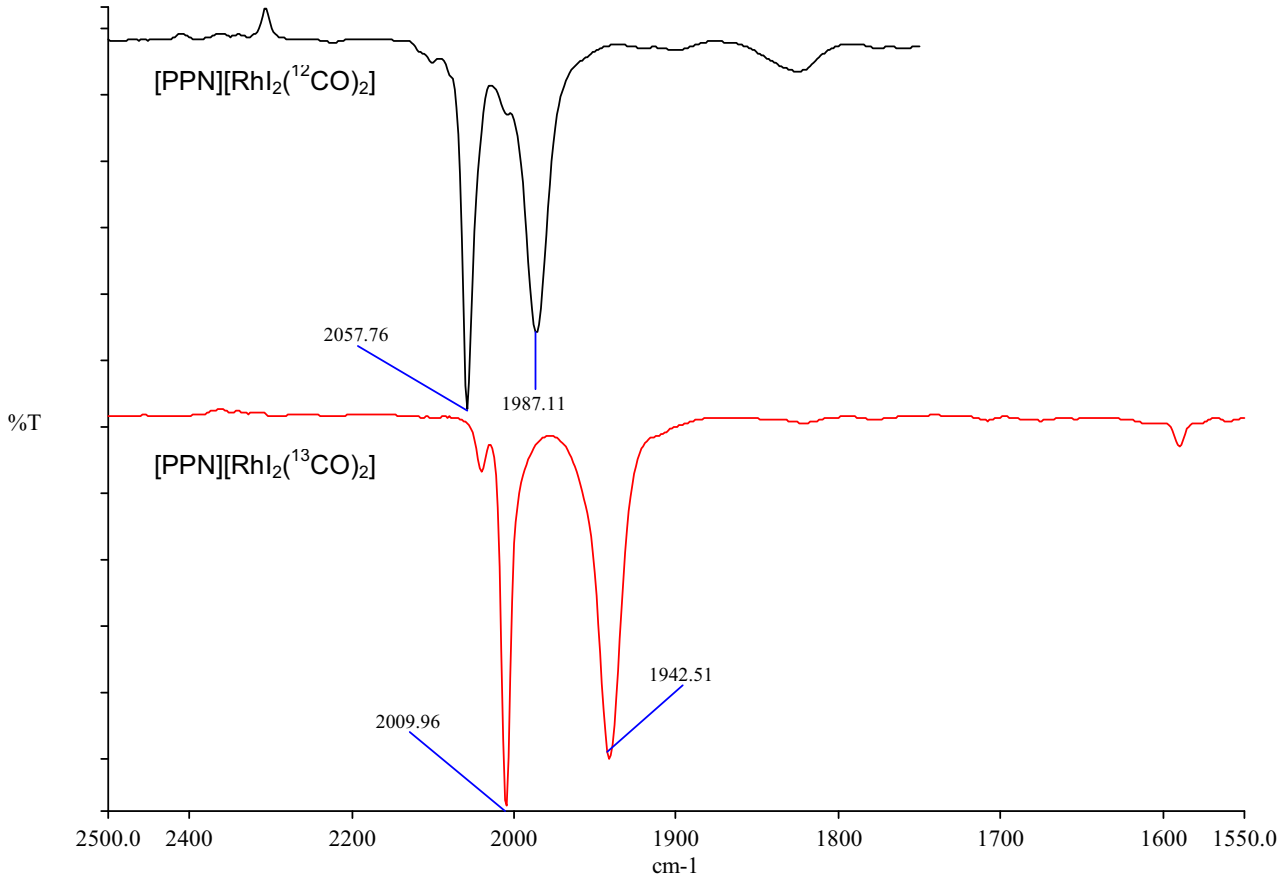

Figure 2 : Infrared spectra of $[PPN][RhI_2(CO)_2]$ 1 (top) and $[PPN][RhI_2{}^{13}(CO)_2]$ 1 (bottom).

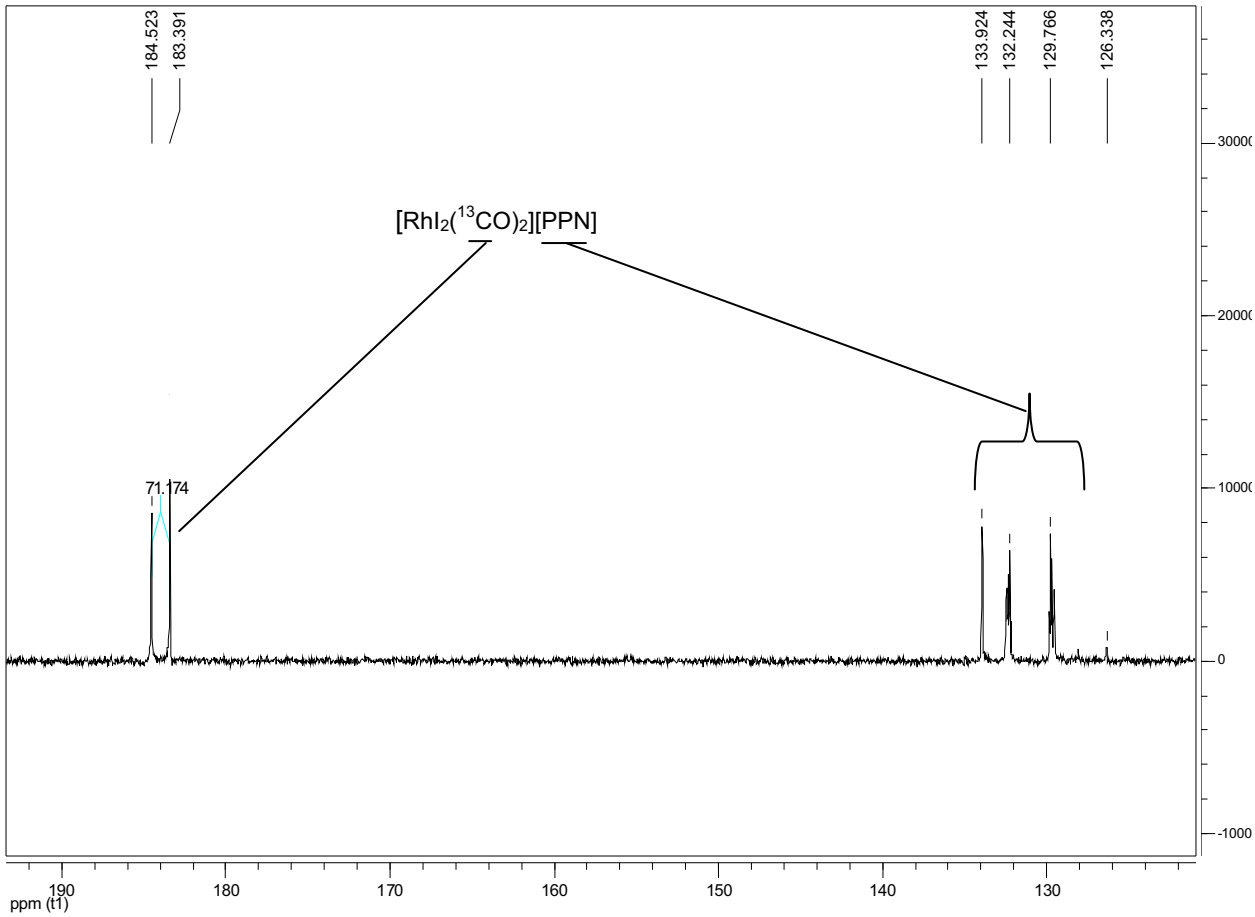

Figure 3 : ^{13}C NMR spectrum of [PPN][$RhI_2(^{13}CO)_2$] 1 in CD_2Cl_2, r. t.

The first step in this catalytic cycle is the oxidative addition of methyl iodide to $[RhI_2(CO)_2]^-$ 1 giving $[RhI_3(CH_3)(CO)_2]^-$ 2. This is the rate determining step of the Monsanto catalytic system at high water content, since it was demonstrated by Paulik *et al.*[12] that this reaction corresponds to a nucleophilic attack of the rhodium metal center at the methyl iodide carbon atom. A kinetic study performed by Roth *et al.*[13] has shown that this reaction is first order with respect to methyl iodide and rhodium catalyst and zero order with respect to CO pressure. This reaction is very slow if compared to the same reaction with the iridium system. This is due to the higher electron density on the iridium atom, giving to iridium a higher nucleophilic nature. As the oxidative addition is very slow for the rhodium system, the next step, the CO *cis*-migration is very fast as shown by the fact that complex 2 was not isolated up to now. Thus, reaction of $[RhI_2(CO)_2]^-$ 1 with methyl iodide gives directly complex $[RhI_3(COCH_3)(CO)]_2^{2-}$ 3. This complex was isolated and crystallized by Forster[14]. Its X-ray structure

shows a dianionic diiodo-bridged dimer $[RhI_2(COCH_3)(CO)(\mu\text{-}I)_2RhI_2(COCH_3)(CO)]^{2-}$. We have monitored this reaction by IR (Fig. 4) after dissolution of $[PPN][RhI_2(CO)_2]$ 1 in methyl iodide.

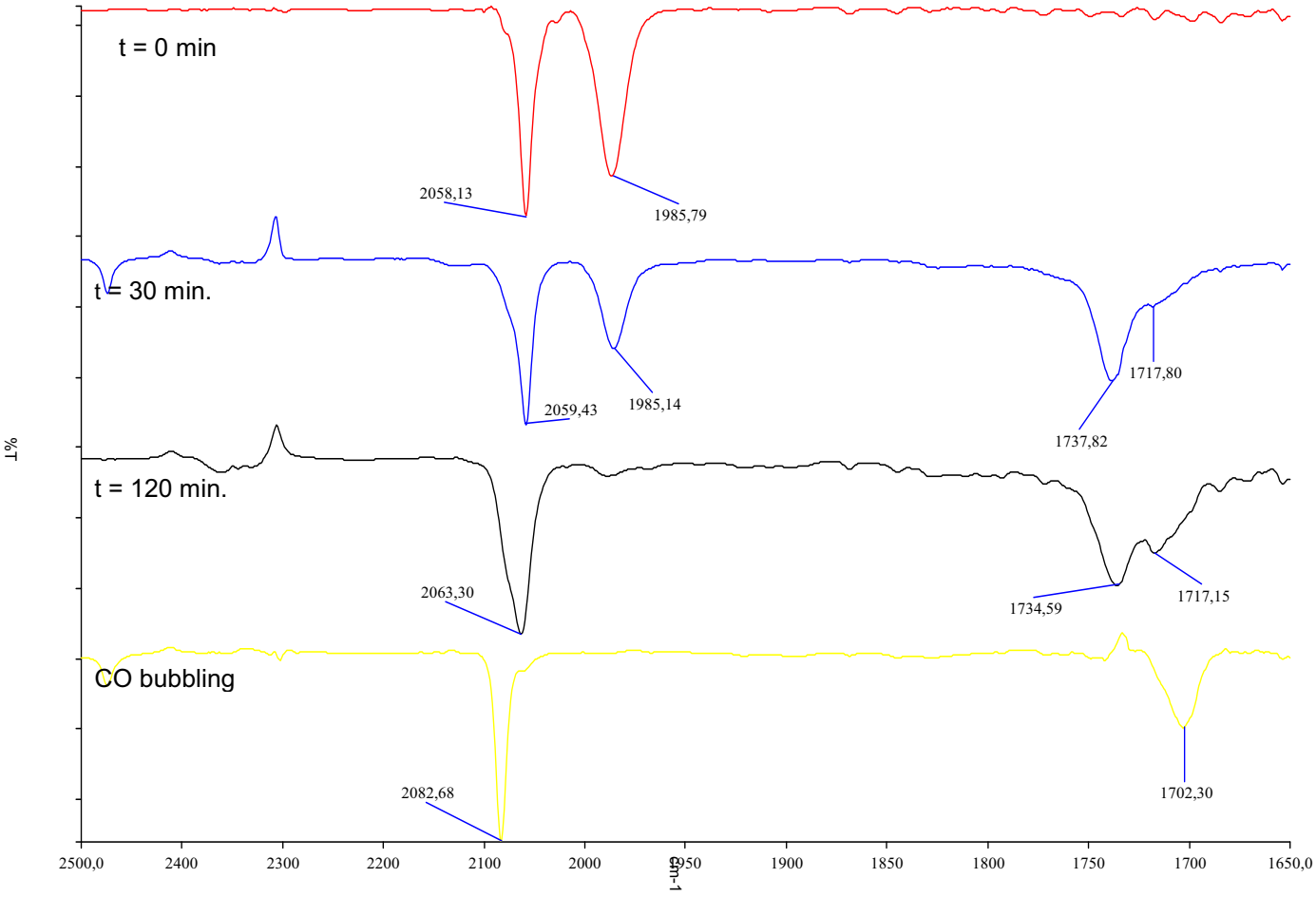

Figure 4 : Reaction of $[RhI_2(CO)_2]^-$ 1 with methyl iodide monitored by IR.

We can observe from these spectra the slow formation of complex 3. The ν_{CO} stretching bands (red spectrum) at 1986 cm^{-1} and 2058 cm^{-1} correspond to the starting complex 1. After 30 min., we note that the intensity of the band at 1986 cm^{-1} has decreased whereas the band at 2058 cm^{-1} is shifted to higher frequencies. We also observe the appearance of ν_{CO} stretching bands in the acetyl area at 1737 cm^{-1} and 1717 cm^{-1}. After a 2 h reaction time (black spectrum), we only observe a shouldered wide band at 2063 cm^{-1} and two acetyls bands at 1737 cm^{-1} and 1717 cm^{-1}. This could mean that we have two isomers of complex 3 in solution. By bubbling CO through the solution for 5 sec., we observe (spectrum in yellow) the total disappearance of the former bands assigned to

complex 3 and the appearance of two new ν_{CO} stretching bands at 2083 cm^{-1} and 1702 cm^{-1} assigned to complex [PPN][$RhI_3(COCH_3)(CO)_2$] 4. The single band corresponding to the terminal CO ligands leads us to believe that the CO ligands are in trans position since we only observe the antisymmetrical infrared vibration. We have isolated complex 3 and labeled it (Fig. 5). We can see that some unlabelled complex 3 (bands at 2056 cm^{-1} and 1734 cm^{-1}) is still present.

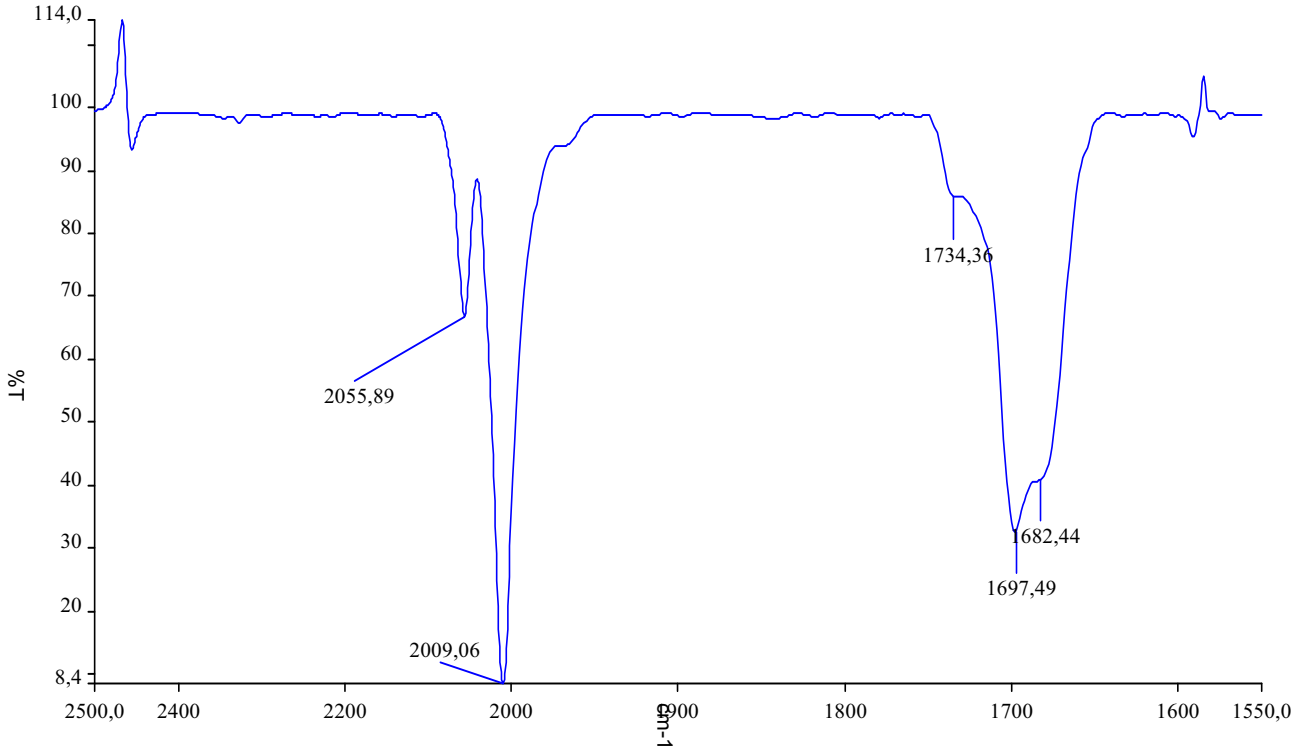

Figure 5 : IR spectrum of $[RhI_3(^{13}COCH_3)(^{13}CO)]_2^{2-}$ 3 in CD_2Cl_2, r.t.

The ^{13}C NMR spectrum of labeled complex 3 (Fig 6) shows two doublets at δ = 182.03 ppm (d, $^1J_{C\text{-}Rh}$ = 66.72 Hz) and δ = 182.37 ppm (d, $^1J_{C\text{-}Rh}$ = 70.95 Hz) in the region of terminal CO ligands, and two others doublets at δ = 204.14 ppm (d, $^1J_{C\text{-}Rh}$ = 18.85 Hz) and δ = 211.35 ppm (d, $^1J_{C\text{-}Rh}$ = 19.82 Hz) corresponding to two acetyl ligands.

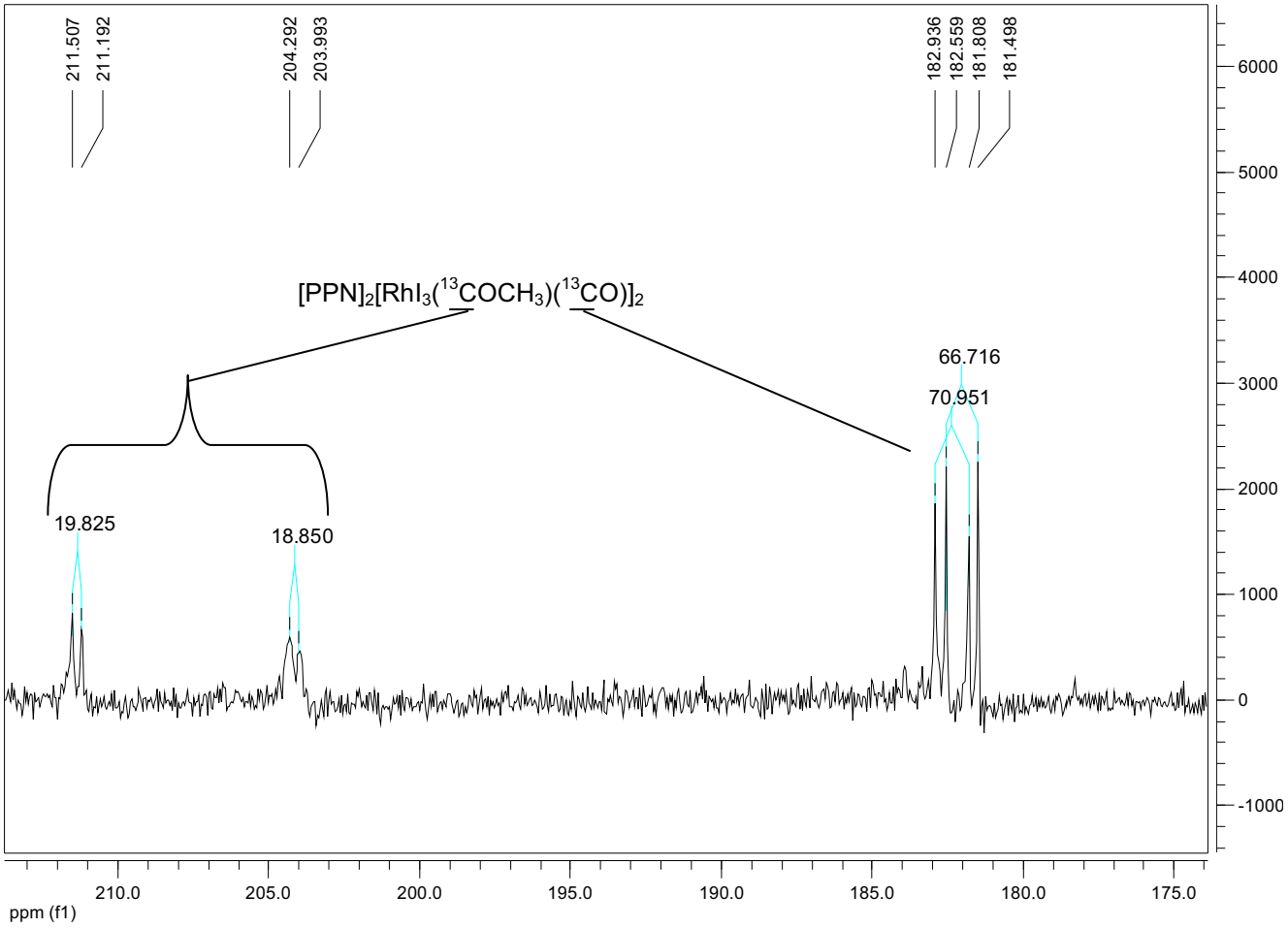

Figure 6 : ^{13}C NMR of $[PPN]_2[RhI_3(^{13}COCH_3)(^{13}CO)]_2$ 3 in CD2Cl2, r.t.

The presence of these features, terminal CO ligands/acetyl CO ligands, shows that we have two isomers in solution, according to the infrared spectrum (Fig. 5, black spectrum) that showed two acetyl vibration bands. ^{1}H NMR of unlabeled complex 3 (Fig. 7) shows two signals at δ = 3.15 ppm and at δ = 3.13 ppm, which confirms the presence of two isomers. We might assume that a molecule of solvent could be coordinated to complex 3 in two different sites in solution.

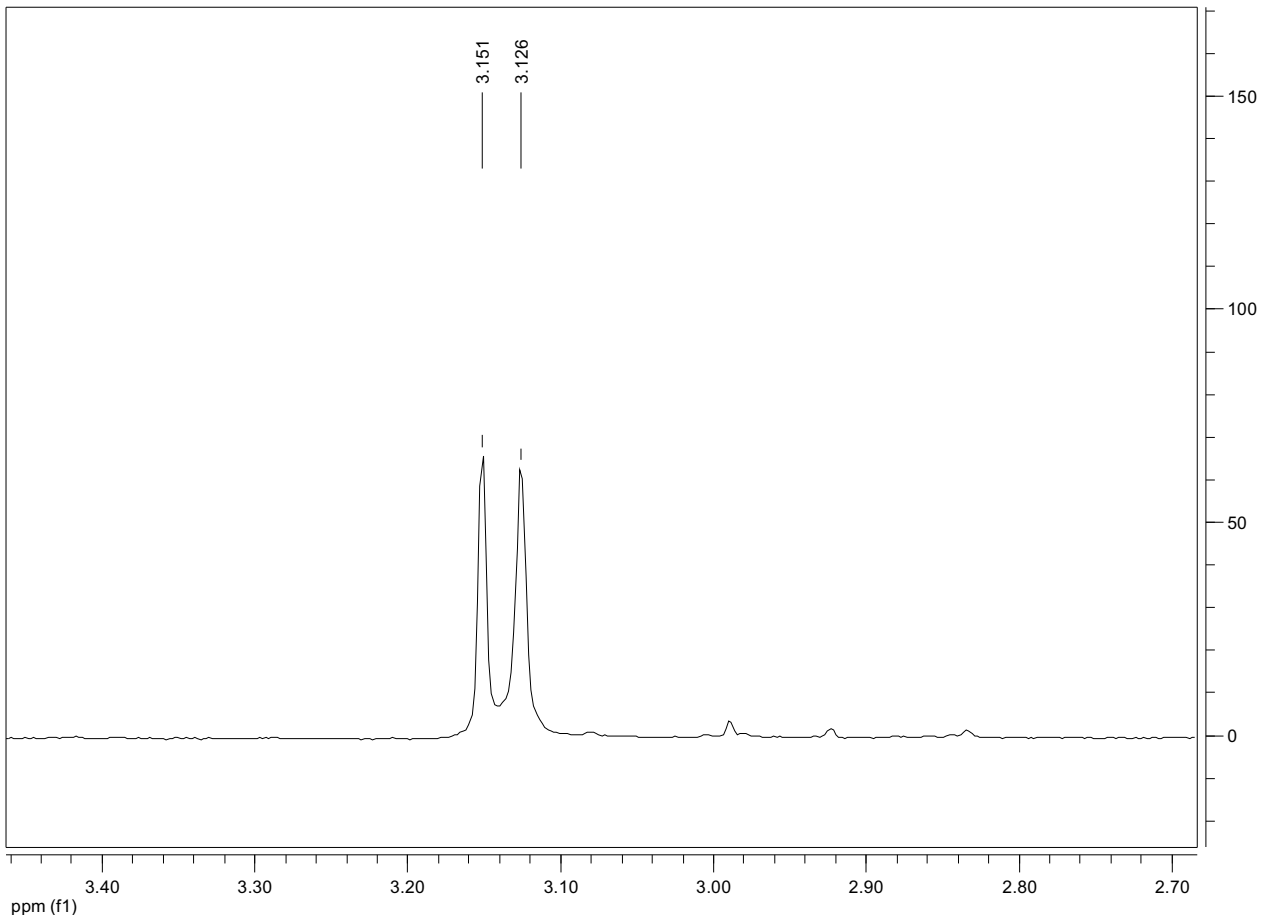

Figure 7 : ^{1}H NMR of $[PPN]_2[RhI_3(COCH_3)(CO)]_2$ 3 in CD2Cl2, r.t.

Then, we tried to isolate the complex $[PPN][RhI_3(COCH_3)(CO)_2]$ 4. After CO bubbling through the solution of complex 3, we removed dichloromethane under reduced pressure, and obtained a red powder. When analyzing this powder by IR, we observed the very bands corresponding to complex 3, which means that under reduced pressure complex 4 loses a CO ligand giving back complex 3. Thus, we dissolved $[PPN]_2[RhI_3(^{13}COCH_3)(^{13}CO)]_2$ 3 in CD_2Cl_2 and stirred it under one atmosphere of ^{13}CO. After 10 min., the infrared spectrum (Fig 8) shows ν_{CO} stretching bands at 2015 cm^{-1} and 1675 cm^{-1} corresponding to $[PPN][RhI_3(^{13}COCH_3)(^{13}CO)_2]$ 4. We could attribute the band at 1697 cm^{-1}, some unaltered $[RhI_3(^{13}COCH_3)(^{13}CO)]^-$ 3 still present in the solution.

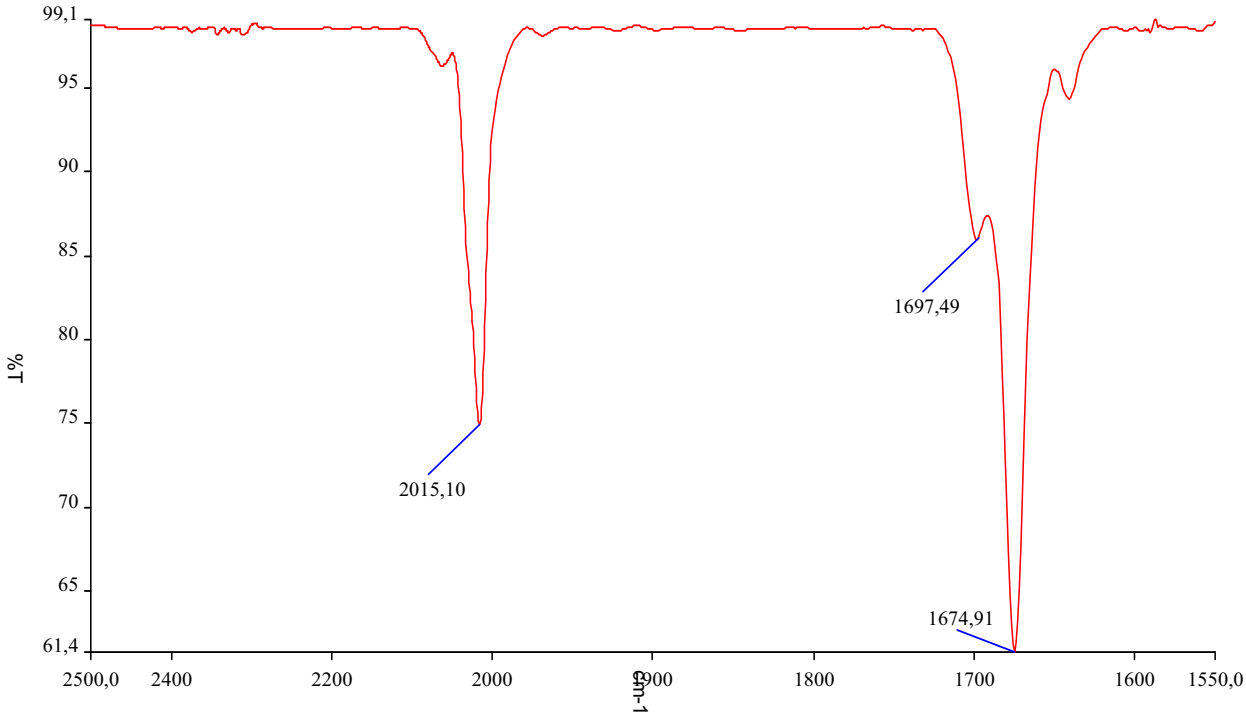

Figure 8 : Infrared spectrum of [PPN][$RhI_3(^{13}COCH_3)(^{13}CO)_2$] 4 in CH_2Cl_2, r.t.

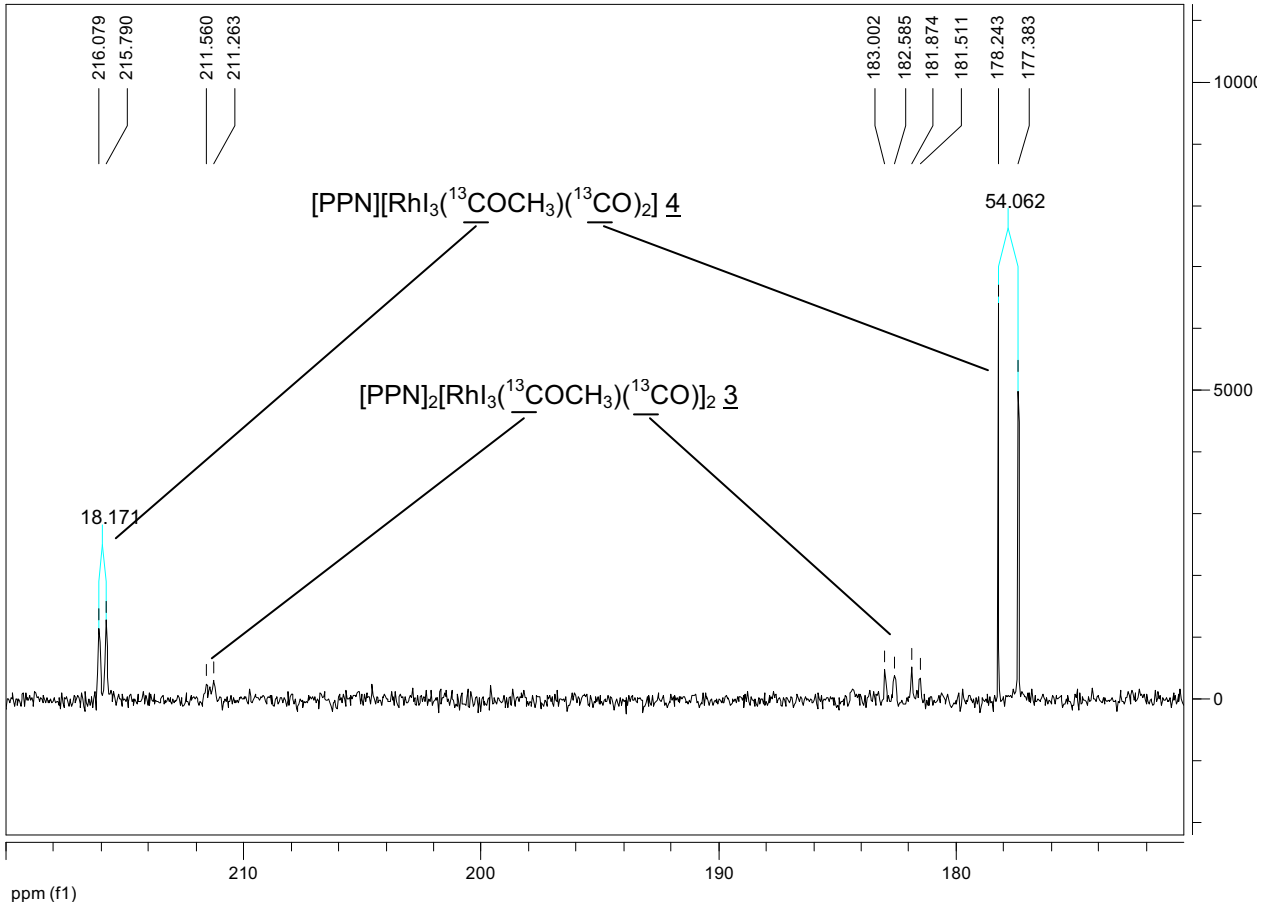

Figure 9 : ^{13}C NMR spectrum of [PPN][$RhI_3(^{13}COCH_3)(^{13}CO)_2$] 4 in CD_2Cl_2, r.t.

The ^{13}C NMR spectrum in figure 9 shows two doublets at δ = 177.81 ppm (d, $^{1}J_{C\text{-}Rh}$ = 54.06 Hz), attributed to the carbon atoms of the terminal CO ligands of complex 4, and at δ = 215.93 ppm (d, $^{1}J_{C\text{-}Rh}$ = 18.17 Hz), attributed to the carbon atom of the acetyl group in complex 4. We can note that a small quantity of complex 3, signals at δ = 182.05 ppm and δ = 182.44 ppm is still present. Since the methyl group of the acetyl ligand was not labeled (in 3 and 4), we didn't observe ^{13}C signals due to methyl carbon during ^{13}C NMR experiments.

After getting [PPN][$RhI_3(COCH_3)(CO)_2$] 4 in dichloromethane, we left the solution under dinitrogen to see by IR if the reductive elimination occurrs under these conditions. Surprisingly, we didn't observe the expected reductive elimination but the formation of complex 3 after 10 min., meaning that a CO ligand of complex 4 is very labile and can dissociate under ambient conditions giving back complex 3. By bubbling again CO through the solution, we observed in the formation of complex 4 (Sc. 3). At 0°C, this phenomenon is not observed a nd complex 4 lives in solution for more than one hour.

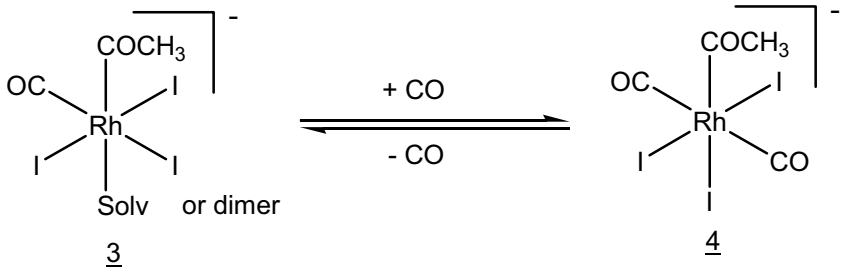

Scheme 3 : Reversibility of the CO coordination on complex 3.

Therefore, we synthesized complex 4 in dichloromethane at 0°C, then added hexane in or der to form a bilayered mixture, and freezed the Schlenk tube to –18°C. After 3 days, we obtained crystals of [PPN][$RhI_3(COCH_3)(CO)_2$] 4. A crystal was selected and its X-ray structure determined (Fig. 10). The crystal system is monoclinic, the space group is P $2_{1/c}$ and the geometry is pseudo-octahedral.

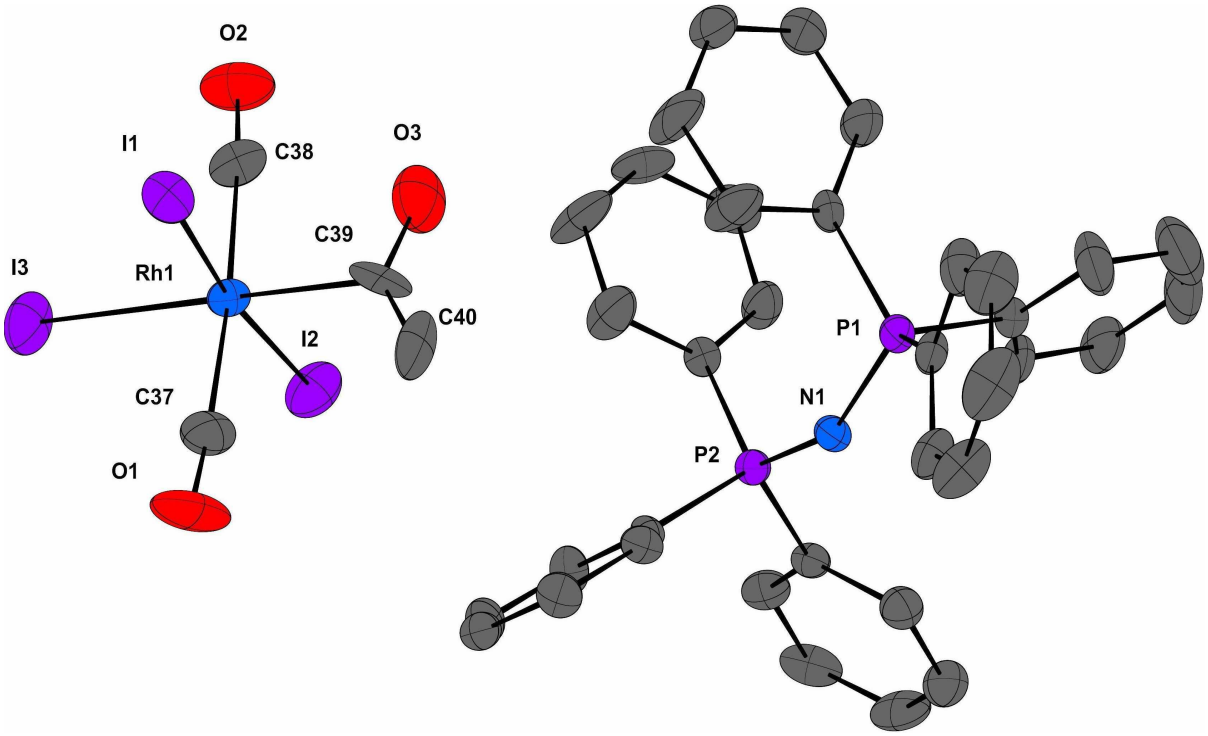

Figure 10 : X-ray structure of [PPN][$RhI_3(COCH_3)(CO)_2$] 4

Bond lengths: C(37)-O(1) = 1.092(6), C(37)-Rh(1) = 1.945(7), C(38)-O(2) = 1.108(6), C(38)-Rh(1) = 1.926(7), C(39)-O(3) = 1.201(6), C(39)-C(40) = 1.234(8), C(39)-Rh(1) = 2.152(7), C(40)-H(40A) = 0.9600, C(40)-H(40B) = 0.9600, C(40)-H(40C) = 0.9600, Rh(1)-I(1) = 2.6602(9), Rh(1)-I(3) = 2.6702(9), Rh(1)-I(2) = 2.8137(11)

AnglesO(1)-C(37)-Rh(1) = 176.3(6), O(2)-C(38)-Rh(1) = 175.6(6), O(3)-C(39)-C(40) = 128.5(7), O(3)-C(39)-Rh(1) = 110.8(5), C(40)-C(39)-Rh(1) = 120.5(5), C(39)-C(40)-H(40A) = 109.5, C(39)-C(40)-H(40B) = 109.4, H(40A)-C(40)-H(40B) = 109.5, C(39)-C(40)-H(40C) = 109.5, H(40A)-C(40)-H(40C) = 109.5, H(40B)-C(40)-H(40C) = 109.5, C(38)-Rh(1)-C(37) = 174.7(2), C(38)-Rh(1)-C(39) = 93.6(3), C(37)-Rh(1)-C(39) = 91.5(3), C(38)-Rh(1)-I(1) = 91.28(19), C(37)-Rh(1)-I(1) = 90.08(16), C(39)-Rh(1)-I(1) = 86.52(15), C(38)-Rh(1)-I(3) = 91.02(19), C(37)-Rh(1)-I(3) = 88.25(16), C(39)-Rh(1)-I(3) = 86.38(15), I(1)-Rh(1)-I(3) = 172.66(2), C(38)-Rh(1)-I(2) = 84.94(17), C(37)-Rh(1)-I(2) = 89.90(18), C(39)-Rh(1)-I(2) = 178.31(19), I(1)-Rh(1)-I(2) = 92.59(2), I(3)-Rh(1)-I(2) = 94.56(2).

This componud is the *mer-trans* isomeric form of complex 4. The trans CO position of the ligands inferred from the IR spectrum (Fig. 4) of complex 4, is thus confirmed by its X-ray structure.

II-2: Study of the iridium catalytic cycle.

The iridium catalytic cycle was first described by Forster in 1979[15] and is depicted in scheme 4. In order to start this cycle, one must form the active species $[IrI_2(CO)_2]^-$. A synthetic procedure was previously described by our laboratory staff[16], starting from the commercial salt $IrI_{3,4}$ which is a mixture of IrI_3 and IrI_4. The procedure to obtain $[PPN][IrI_2(CO)_2]$ 5 is the same that we used for the preparation of $[PPN][RhI_2(CO)_2]$ 1 (see Experimental Section). A single crystal of this compound was obtained and its x-ray structure solved[16].

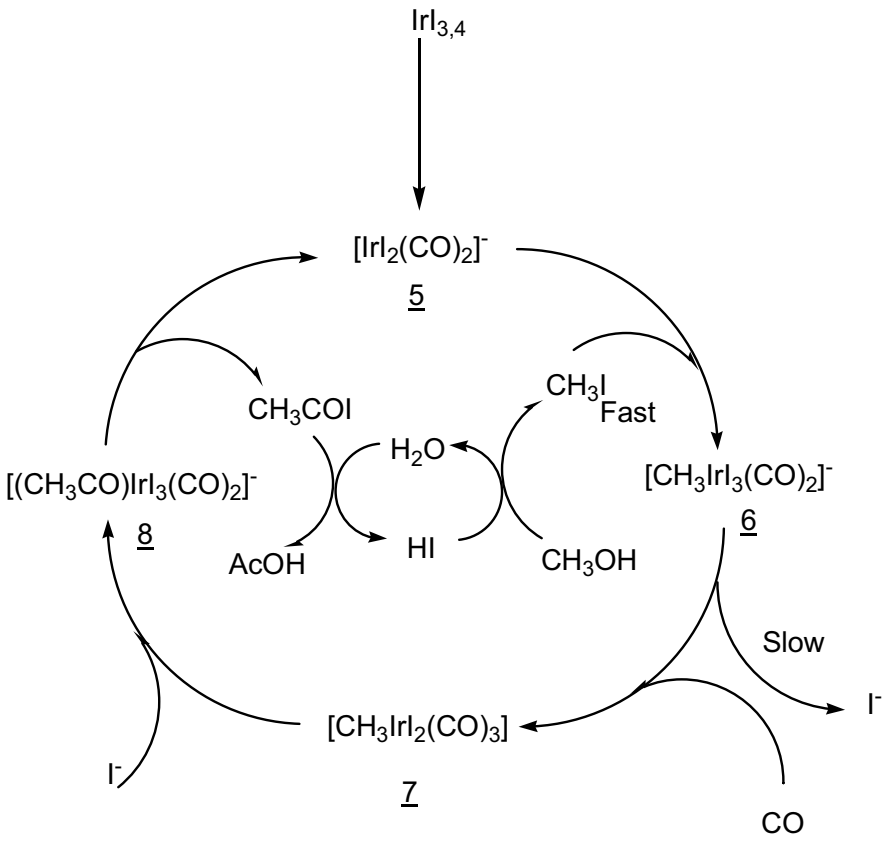

Scheme 4 : Iridium catalytic cycle for methanol carbonylation

The IR spectrum of complex [PPN][$IrI_2(CO)_2$] 5 in dichloromethane shows two stretching bands at ν_{co}= 2046 cm^{-1} for the symmetric vibration and ν_{co}= 1968 cm^{-1} for the antisymmetric vibration (Fig 11). These two ν_{co} bands are characteristic of a *cis*-isomer, in a with its X-ray structure.

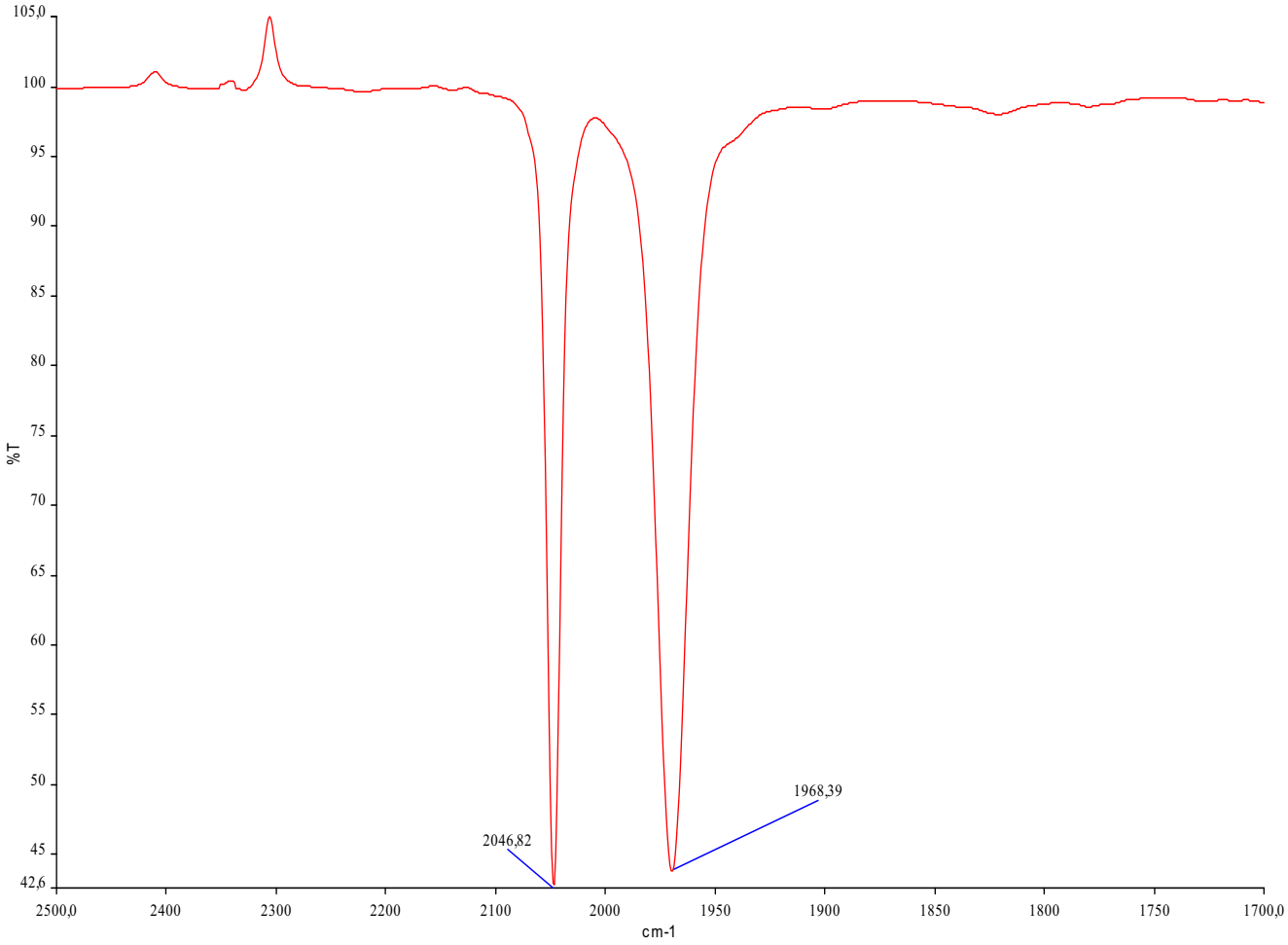

Figure 11 : IR spectrum of [PPN][$IrI_2(CO)_2$] 5 in dichloromethane.

The next step in the iridium catalytic cycle is the oxidative addition of methyl iodide, which is produced in the catalytic medium by reaction of HI with methanol, to the active species $[IrI_2(CO)_2]^-$ 5 giving the Ir(III) complex $[Ir(CH_3)I_3(CO)_2]^-$ 6. This reaction is fast[17], and appears to be a S_N2 type oxidative addition which proceed via a nucleophilic attack of the metal center at the carbon atom of CH_3I[18,19]. 6 is known to be the resting state in the catalytic cycle[17].

In order to synthesize compound 6, $[PPN][IrI_2(CO)_2]$ 5 is dissolved in CH_3I. After 10 min. under ambiant conditions, the solution turns to orange. Two IR stretching bands are observed at ν_{sym}= 2098 cm^{-1} and ν_{asym}= 2046 cm^{-1} (Fig 12). The shift to higher frequencies of the CO bands corresponding to compound 6 with respect to those corresponding to $[PPN][IrI_2(CO)_2]$ 5 is due to the reduced electron density on the metal center. Indeed, the lower electron density on the metal center decreases the back-bonding effect on the anti bonding π^* orbitals of the carbon CO ligand and thus stabilizes the C=O bond. The presence of these two bands is characteristic of a *cis*-complex, which was confirmed by a X-ray crystal structure[16].

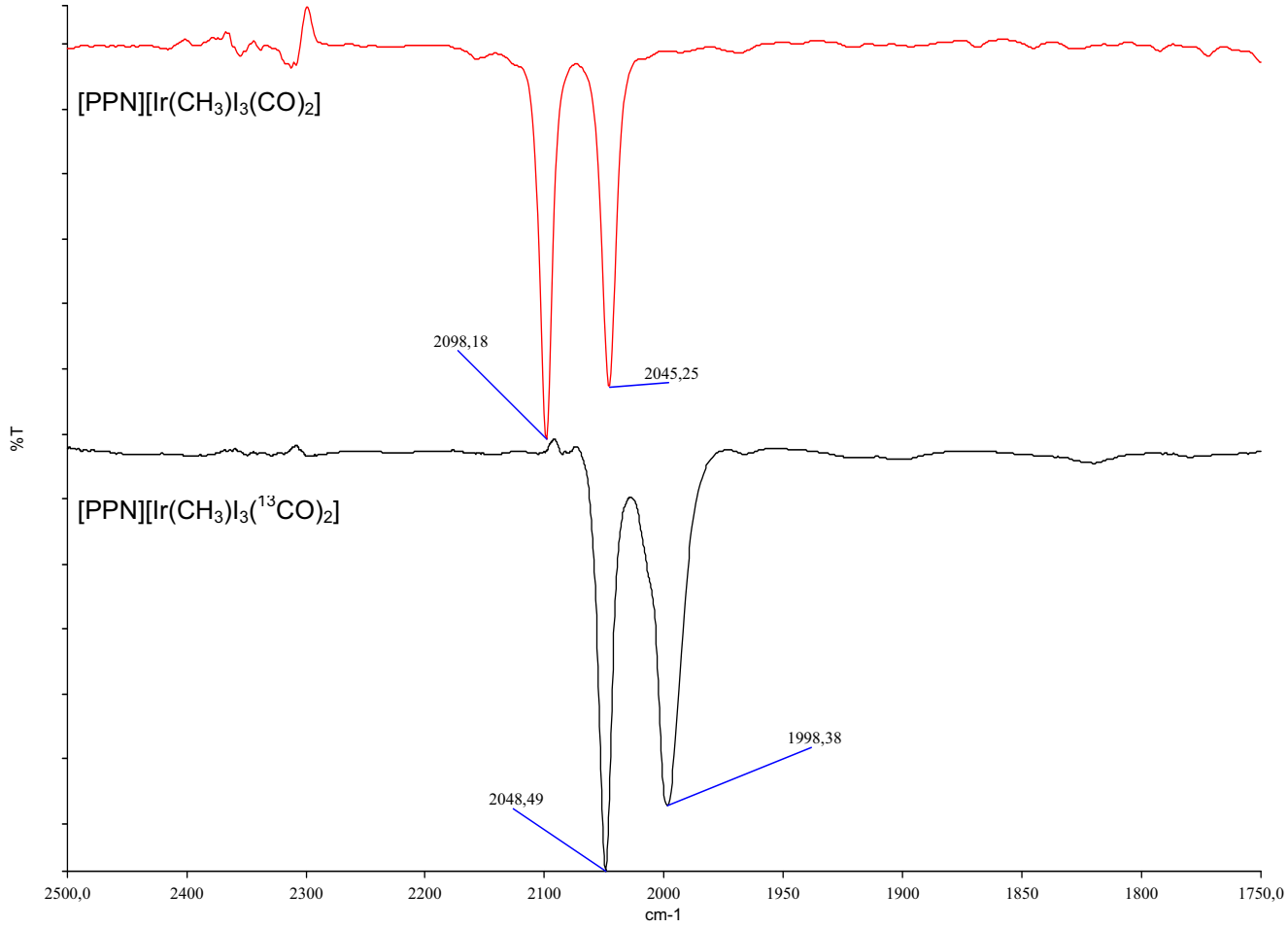

Figure 12 : Infra-red spectra of $[PPN][Ir(CH_3)I_3(CO)_2]$ and $[PPN][Ir(CH_3)I_3(^{13}CO)_2]$ in dichloromethane.

The ^{13}C NMR spectrum of compound 6 (Fig.13) shows a singlet at δ = 156 ppm corresponding to the two carbon atoms of the CO ligands and other peaks around δ= 130 ppm corresponding to the carbon atoms of the [PPN] counter-ion.

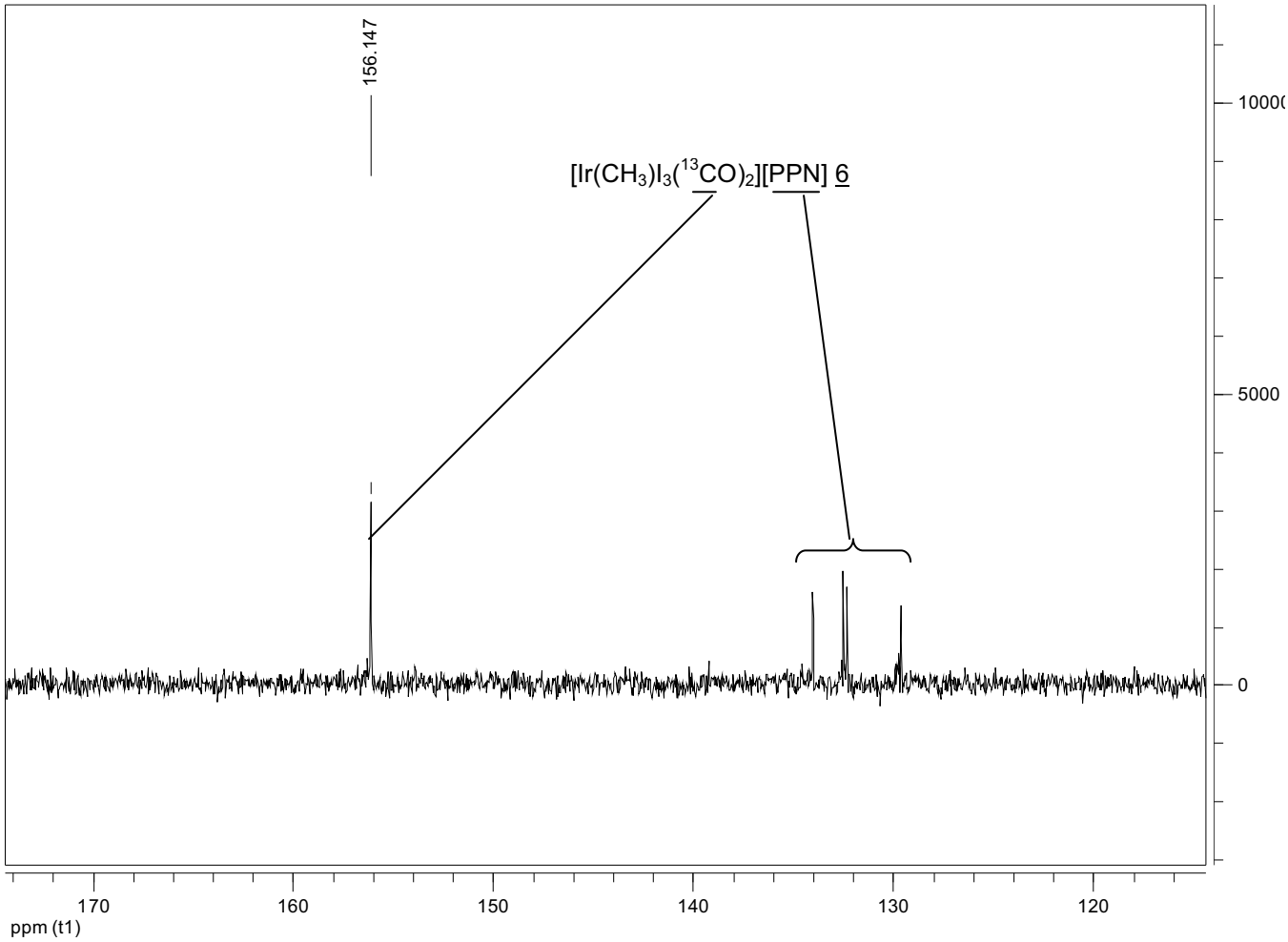

Figure 13 : ^{13}C NMR of [PPN][Ir(CH$_3$)I$_3$(^{13}CO)$_2$] 6 in CD_2Cl_2, r.t.

In a glass reactor under 5 bar of CO, compound 6 dissolved in dichloromethane gives slowly, after 2 h, the iridium acetyl complex 8. Maitlis *et al.*[20] showed that addition of a protic solvent such as methanol to the reaction mixture, increases dramatically the CO cis-migration reaction rate, and the authors proposed the mechanistic pathway depicted in scheme 5.

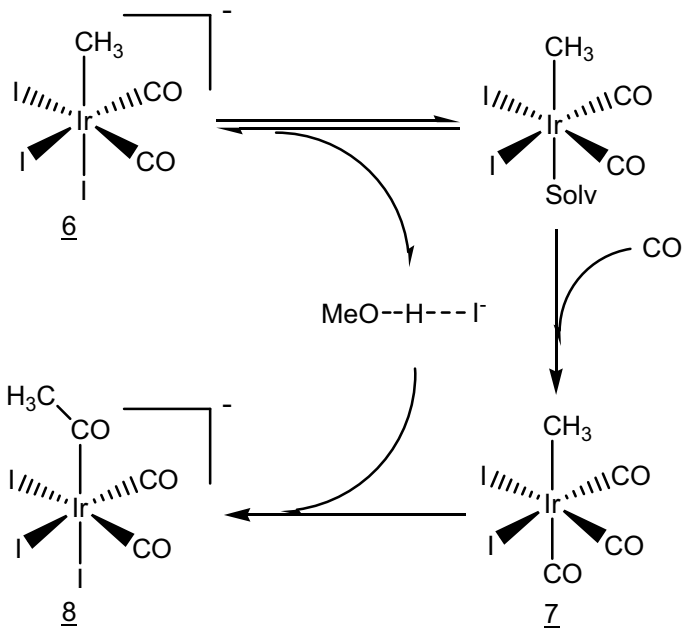

Scheme 5 : Proposed mechanistic pathway for the formation of [PPN][Ir(CH_3CO)I_3(CO)$_2$] 8 from [PPN][Ir(CH_3)I_3(CO)$_2$] 6.

This accelerating effect could be explained by the ability of methanol to coordinate an iodide ligand linked to the iridium, center giving under CO the neutral tricarbonyl complex 7. Thus, the electron density on the metal center is reduced and the CO migratory insertion can occur more rapidly. Since methanol is not present in batch experiments or even in industrial plants (see preliminary information), this accelerating effect was only observed in Schlenk tube experiments but provides an insight into the reaction mechanism. Thus, action of methanol could be mimicked by the use of others

co-catalysts able to abstract an iodide ligand, which could also be introduced in a reactor industrial plant.

On our part, we tried to synthesize compound 8 using a glass reactor (see Experimental Section). We dissolved [PPN][Ir(CH_3)I_3($CO)_2$] 6 in a mixture of CH_2Cl_2/MeOH 20mL/10mL. After 1 hour under 5 bar of CO and at ambient temperature, the initial orange solution turns yellow. The solvent is removed under reduced pressure affording an orange-yellow powder. The infrared spectrum of the resulting solid (Fig. 14) shows three CO bands at ν_{CO} = 2110 cm^{-1} and at 2069 cm^{-1} with a shoulder, corresponding to the terminal CO ligands linked to the metal center, and a band at 1657 cm^{-1} characteristic of the CO acetyl stretching mode. This system of two CO terminal bands could correspond to a cis isomer, but the intensities of the two bands are expected to be the same, that is not the case, thus we think that a mixture of at least two isomers is present in the medium.

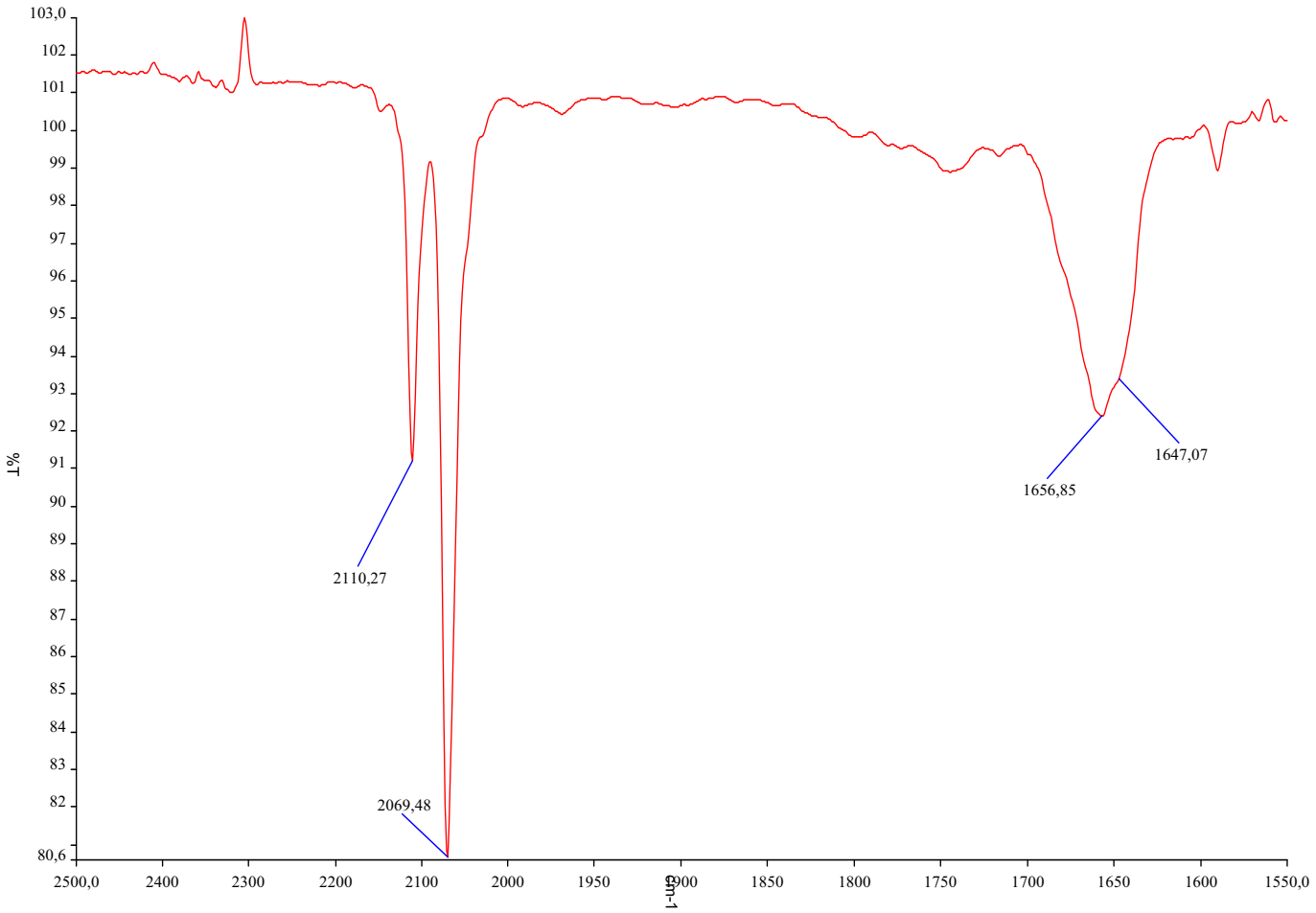

Figure 14 : Infra-red spectrum in CH_2Cl_2 of the product of the reaction of [PPN][Ir(CH_3)I_3($CO)_2$] 6 in CH_2Cl_2/MeOH 20mL/10mL under 5 bar of CO.

Since the effect of methanol on this *cis*-migration reaction was previously established, we tried to determine the influence of methanol concentration on this reaction by performing further reactions under the same conditions (1 hour, 5 bar of CO, 500 mg of [PPN][$Ir(CH_3)I_3(CO)_2$], ambient temperature) except for methanol concentration. By this way, we studied the effect of the polarity and the protic nature of the solvent on the *cis*-migration reaction. Figure 15 shows the infra-red spectra of the product obtained witth three of these reaction mixtures.

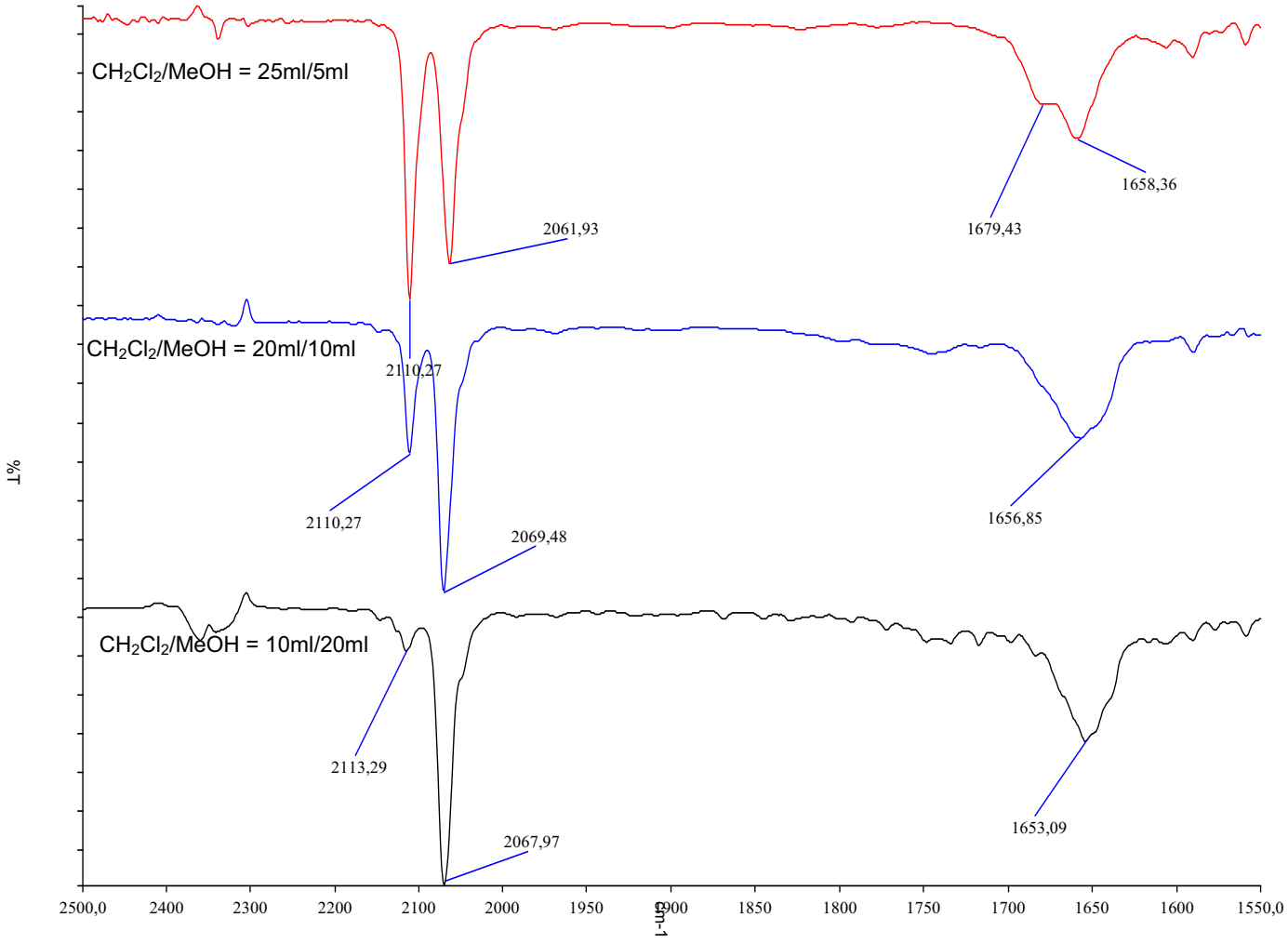

Figure 15 : Infra-red spectra of the CO migratory insertion reaction varying methanol concentration.

We could observe that methanol concentration exerts a strong influence on the cis-migration reaction, and not only on the rate of this reaction as it was published[20] but also on the nature of the species formed.

At low methanol concentration (spectrum in red), we can see two terminal CO bands at ν_{CO} = 2110 cm^{-1} and 2061 cm^{-1} with a shoulder. These two vibrations are due to the *cis*-isomer complex : *cis*-[PPN][$IrI_3(COMe)(CO)_2$] *cis*-8. Examination of the acetyl region reveals two bands at 1679 cm^{-1} and 1658 cm^{-1}. These two acetyl bands and the shoulder on the low frequency terminal CO band make us think that two different isomers are present. Maitlis *et al* observed the same phenomenon[5].

At a higher methanol concentration (spectrum in blue), we observe the decrease of the terminal CO band at 2110 cm^{-1} and the increase of the terminal CO band at 2061 cm^{-1} which is shifted to 2070 cm^{-1}. The acetyl region bands show a large band at 1657 cm^{-1} that might hide two acetyl bands. It is worth noting that the acetyl band at 1680 cm^{-1} has disappeared or is very weak. We believe that, under these conditions, two isomers are formed, *cis*-[PPN][$IrI_3(COMe)(CO)_2$] *cis*-8 and *trans*-[PPN][$IrI_3(COMe)(CO)_2$] *trans*-8 which possesser only one terminal CO band.

The last spectrum, at high methanol concentration, shows mainly one terminal CO band at 2070 cm^{-1}, and an acetyl band at 1653 cm^{-1}, which is sharper than that observed in the second experiment. A single terminal CO band is characteristic of a *trans* complex, that is to say *trans*-[PPN][$IrI_3(COMe)(CO)_2$], *trans*-8.

We monitored the same reactions under the same conditions by ^1H NMR. The different experiments were conducted according to the synthetic method depicted above. The solvent was removed under reduced atmosphere, and the resulting powder analyzed by ^1H NMR in CD_2Cl_2 at ambient temperature (Fig. 16). We can observe in spectrum a) at low methanol concentration, a major peak at δ = 3.12 ppm that can be assigned to compound *cis*-8. The signal at δ = 2.18 ppm corresponds to unreacted complex 6, which is observed (Fig. 15, red spectrum) as a shoulder on the main bands. At higher methanol concentration, spectrum b) shows three mains peaks. The first at δ = 3.12 ppm corresponds to compound *cis*-8. The second at δ = 2.77 ppm is attributed, according to the

literature[5], to *trans*-8 and the third one at δ = 3.60 ppm that has not been identified yet. It could correspond to a third acetyl compound that may be the neutral iodo bridged dimer $[Ir_2I_4(COMe)_2(CO)_4]$ or trace of methanol in the coordinating sphere of *trans*-8. At higher methanol concentration, spectrum c), we observe two major signals at δ = 2.77 ppm and δ = 3.60 ppm corresponding to *trans*-8, and to the hypothetical neutral acetyl dimer or methanol and a weak signal at δ = 3.12 ppm due to *cis*-8.

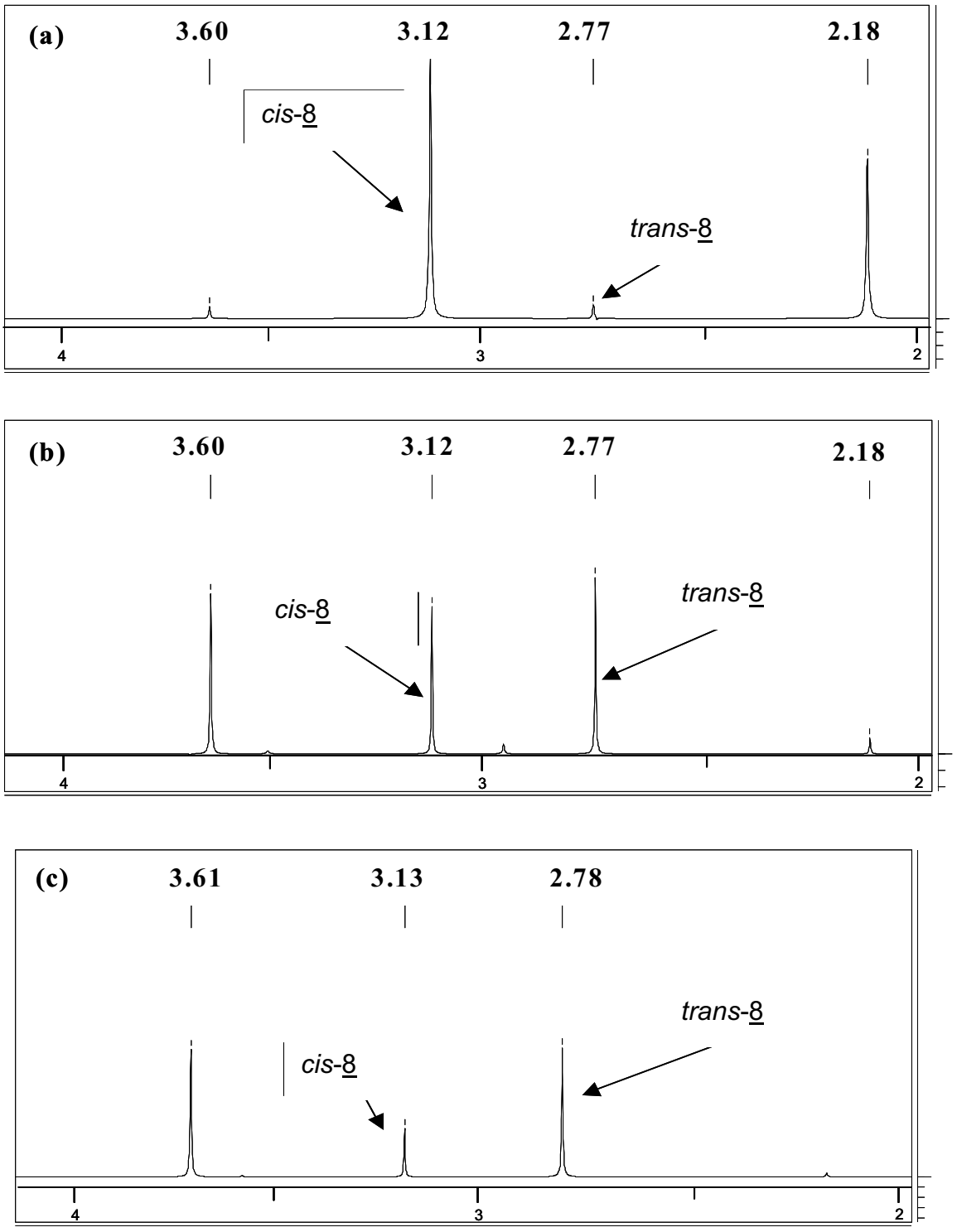

Figure 16 : ^{1}H NMR spectra of the CO migratory insertion reaction at different methanol concentration : a) CH_2Cl_2/MeOH = 25mL/5mL, b) CH_2Cl_2/MeOH = 20mL/10mL; c) CH_2Cl_2/MeOH = 5mL/25mL, CD2Cl2, r.t.

It comes out that the infrared spectra in the figure 15 and the ^{1}H NMR spectra in the figure 16 are in good agreement with each other.

Thus, from these observations we can conclude that by increasing the concentration of methanol, i. e. the protic character and the polarity of the medium as well, the ratio trans-[PPN][IrI$_3$(COMe)(CO)$_2$]/cis-[PPN][IrI$_3$(COMe)(CO)$_2$] does increases. We can also observe that in the two last ^{1}H NMR spectra b) and c), the signal corresponding to [PPN][Ir(CH$_3$)I$_3$(CO)$_2$] 6 is weak, which leads us to propose that the reaction route from compound 6 to compound trans-8 may involve compound cis-8, followed by a cis/trans isomerisation. Theoretical studies on these two isomers have shown that the trans-isomer has a lower energy than the cis one[21], meaning that cis-8 could be the kinetic product and trans-8 the thermodynamic one.

We have encountered some difficulties in labeling these two isomers with ^{13}CO under the above reaction conditions due to the high cost of this gas and the required conditions for the synthesis (5 bar of CO). In order to collect ^{13}C NMR data we synthesized the two isomers, *cis*-8 and *trans*-8, according to the aformentioned procedure using a glass reactor and a solvent mixture of CH_2Cl_2/MeOH = 25mL/5mL to obtain the *cis* isomer (sample 1, Fig. 17) and of CH_2Cl_2/MeOH = 10mL/20mL to obtain the *trans* isomer (sample 2, Fig.18). We analyzed these two samples by ^{13}C NMR spectroscopy in CD_2Cl_2 at ambient temperature over night.

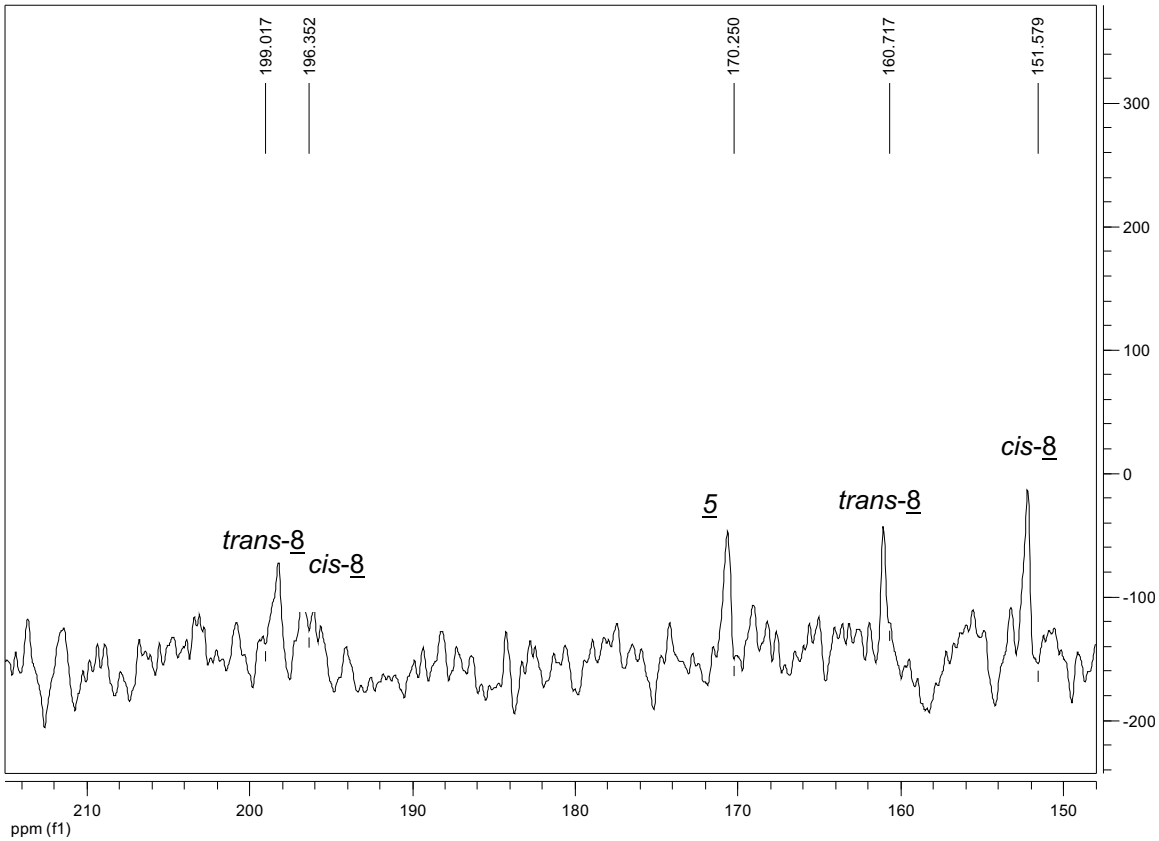

Figure 17 : ^{13}C NMR spectrum in CD_2Cl_2, r.t. of the products coming from reaction of 2 in CH_2Cl_2/MeOH : 25mL/5mL under 5 bar of CO.

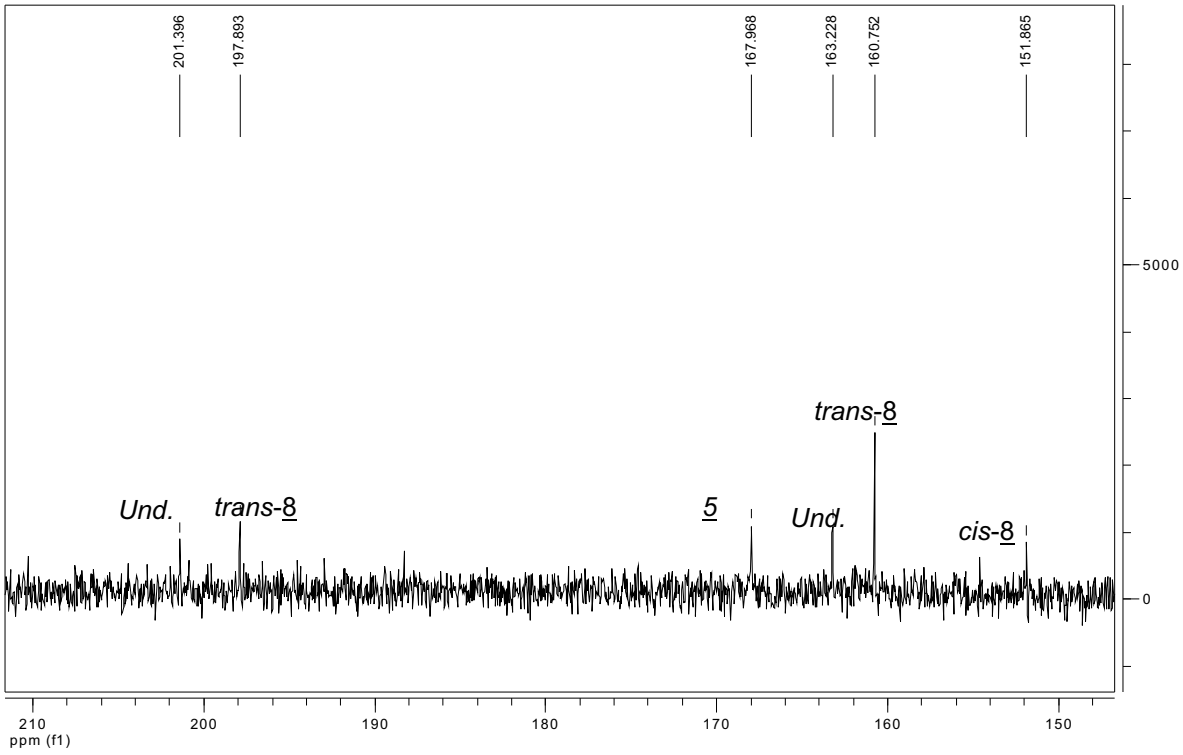

Figure 18 : ^{13}C NMR spectrum of the products coming from reaction of 2 in CH_2Cl_2/MeOH : 10ml/20ml under 5 bar of CO.

Although the infrared spectra of these two samples present the expected CO bands relevant to *cis*-8 for sample 1 and to *trans*-8 for sample 2, the ^{13}C NMR present many peaks (Fig.17 and 18). In the case of the first sample (Fig. 17), we observe signals at δ = 151.58 ppm, δ = 160.72 ppm, δ = 170.25 ppm, δ = 196.35 ppm and at δ = 199.02 ppm, all not well defined. According to the literature[5], we can attribute the signal at δ = 151.58 ppm to the carbon atoms of the terminal CO ligands and that at δ = 196.35 ppm to the carbon atom of the acetyl group in the complex *cis*-8. The signal at δ = 160.72 ppm could correspond to the carbon atoms of terminal CO ligands in complex *trans*-8 and signal at δ = 199.02 ppm to the carbon atom of the acetyl group; the signal at δ = 170.25 ppm corresponds to compound 5 resulting from the reductive elimination from the acetyl complexes. The presence of complex *trans*-8 might be due to a *cis*/*trans* isomerisation occurred overnight. In the case of the second sample (Fig. 18), we observe signals at δ = 160.75 ppm and at δ = 197.9, corresponding to the carbon atoms of complex *trans*-8, the signal at δ = 167.97 ppm attributed to complex 5, and a small signal at δ = 151.86 ppm, which corresponds to complex *cis*-8. We also observe two new signals at δ = 163.23 ppm and δ = 201.4 ppm which could be attributed to the hypothetical neutral acetyl dimer observed previously in ^{1}H NMR. In these two spectra (Fig. 17 and18), we also observe signals at δ = 50.04 ppm and at δ = 51.05 ppm in figure 17 corresponding to the carbon atoms of the methyl group of *cis*-8 and *trans*-8, respectively. In figure 18, these two later signals are still present and we observe a new signal at δ = 51.47 ppm which could correspond to the neutral dimer. We have not shown these signals for the clarity purporse.

These ^{13}C NMR experiments confirm the results observed previously by infrared and ^{1}H NMR spectroscopy concerning the protic solvent effect and the cis/trans isomerisation reaction.

In order to study the *cis*/*trans* isomerisation of compound 8, we monitored the *cis*-migration reaction using our high-pressure infrared (HP-IR) reactor (see Experimental Section). We introduced [PPN][$Ir(CH_3)I_3(CO)_2$] 6 and a CH_2Cl_2/MeOH solvent mixture into the HP-IR reactor. To have a good signal/noise ratio, we have to introduce at least 0.700 g of compound 6 into the reactor for a maximum volume of 25 mL. To dissolve all of the solid, 10 mL of CH_2Cl_2 are needed, since compound 6 is not

soluble in methanol. In a first run, we chose to use a CH_2Cl_2/MeOH = 15 mL/10 mL solvent mixture, a pressure 5 bar of CO and a temperature of 40°C. The spectra obtained by this experiment are shown in figure 19. After 5 min (black spectrum) we can observe the growth of the two CO vibration bands at ν_{CO} = 2110 cm^{-1} and 2063 cm^{-1} characteristic of the *cis*-[PPN][IrI_3(COMe)$(CO)_2$] *cis*-8 complex and of the two bands at 2098 cm^{-1} and 2046 cm^{-1}, corresponding to [PPN][$Ir(CH_3)I_3(CO)_2$] 6. After 30 min, we can neathly observe the CO vibration bands of the two complexes 6 and *cis*-8. 50 min are needed to observe the CO bands of complex *cis*-8. After 2h30 no major change was noted, except for the loss of the signal which is due to the loss of the adjustement between the reactor and the IR beam. The reactor is then depressurized and the red solution placed in a Shlenck tube, the solvent being removed in vacuo. A red-orange solid was obtained. The IR spectrum of this solid (Fig. 20) shows the CO bands of compound *cis*-6 and two additional CO bands corresponding to [PPN][$IrI_2(CO)_2$] 5 which is fromed by the reductive elimination from complex 8. Indeed, under these conditions, we don't observe the *cis*/*trans* isomerisation of complex 8.

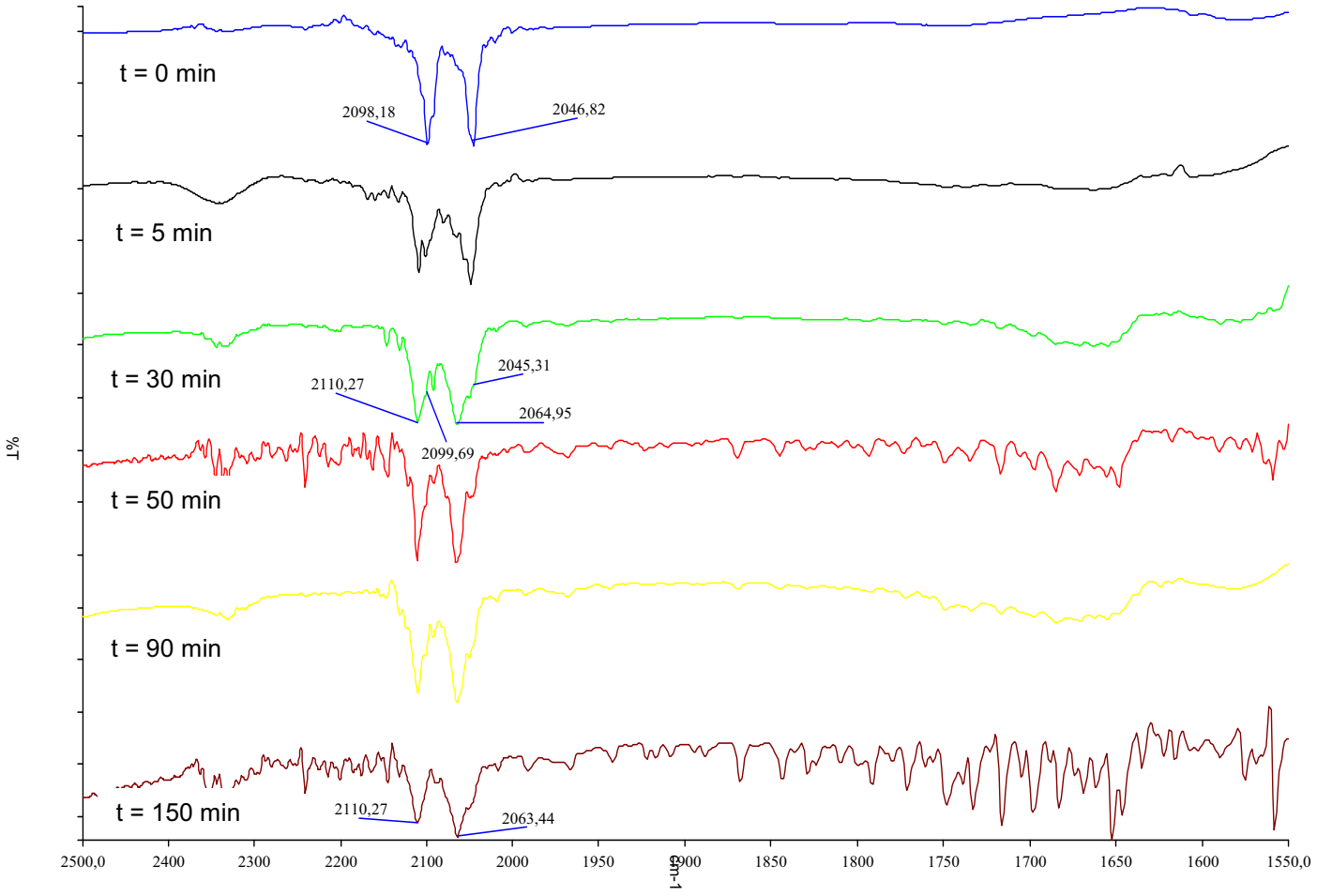

Figure 19 : HP-IR spectra of the cis-migration reaction using CH_2Cl_2/MeOH = 15 mL/10 mL solvent mixture

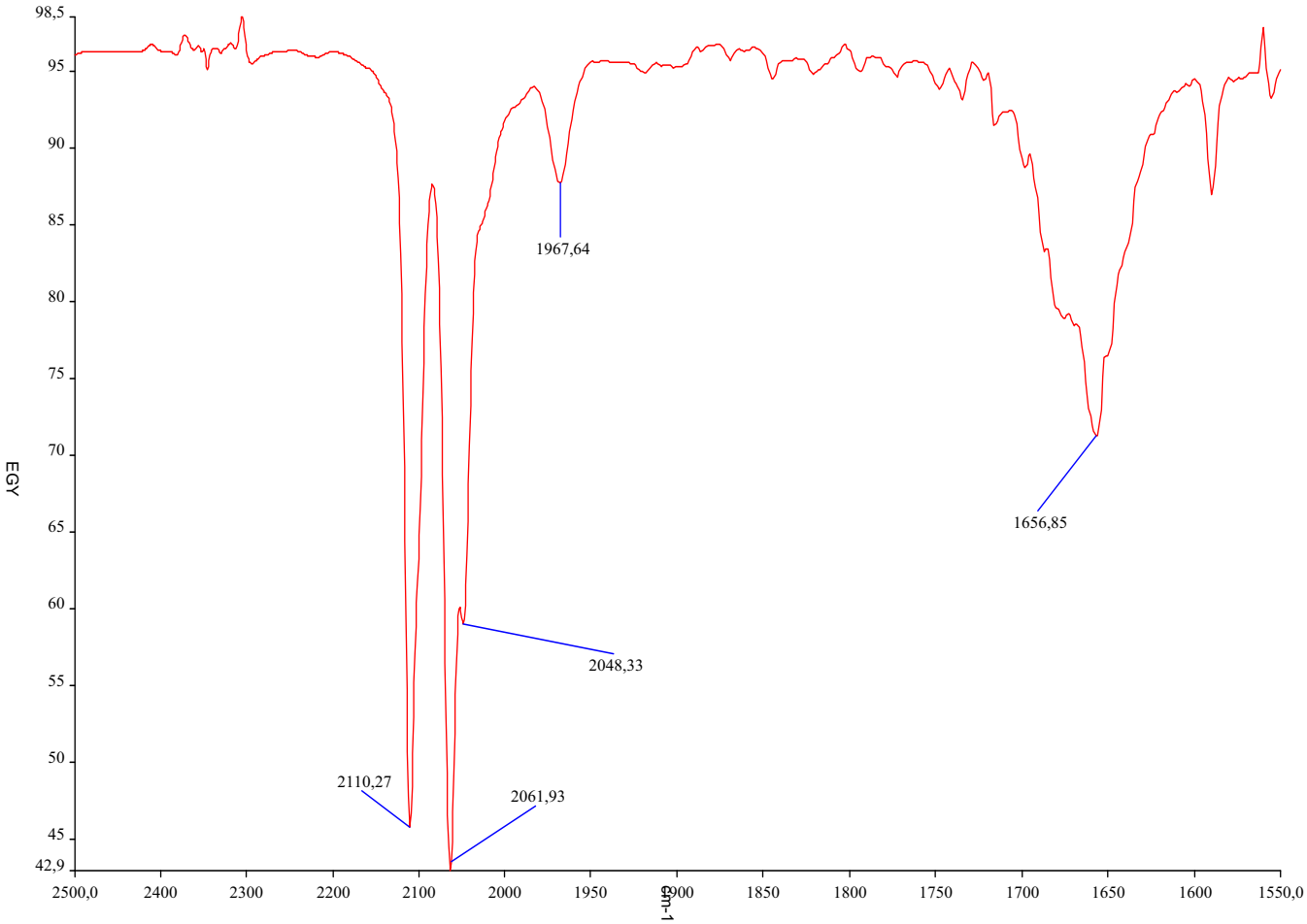

Figure 20. IR spectrum of the product remaining after HP-IR experiment.

Additionally, we monitored by HP-IR another experiment using a CH_2Cl_2/MeOH = 10 mL/15 mL solvent mixture, but we observed the same series of spectra than those shown in figure 19 with a signal loss due to the weak solubility of complexes in this medium. Hence, we chose to follow this type of experiments by High Pressure NMR (HP-NMR), using a sapphire tube (see Experimental Section). We introduced 50 mg of [PPN][$Ir(CH_3)I_3(CO)_2$] 6, 1 mL of CD_2Cl_2 and 2 mL of CD_3OD into the tube which is then filled with 5 bar of ^{13}CO and placed in the NMR probe at 40°C. We collecte d spectra every 10 min. for a total time of 90 min. The most representative spectra are shown in figure 21, 22 and 23.

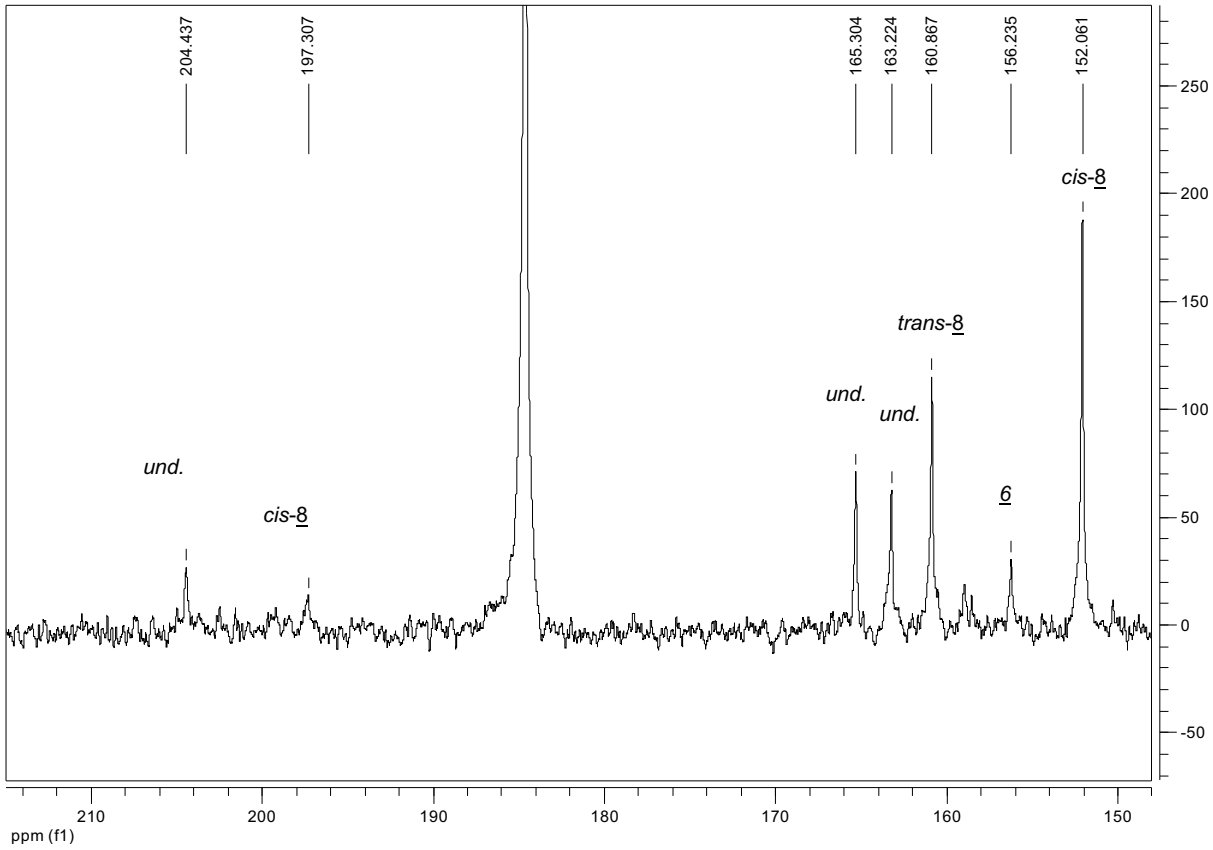

Figure 21 : ^{13}C HP-NMR spectra of the reaction of complex 6 in CD_2Cl_2/CD_3OD = 1mL/2mL at 40℃ under 5 bar of ^{13}CO for **10 min**. reaction.

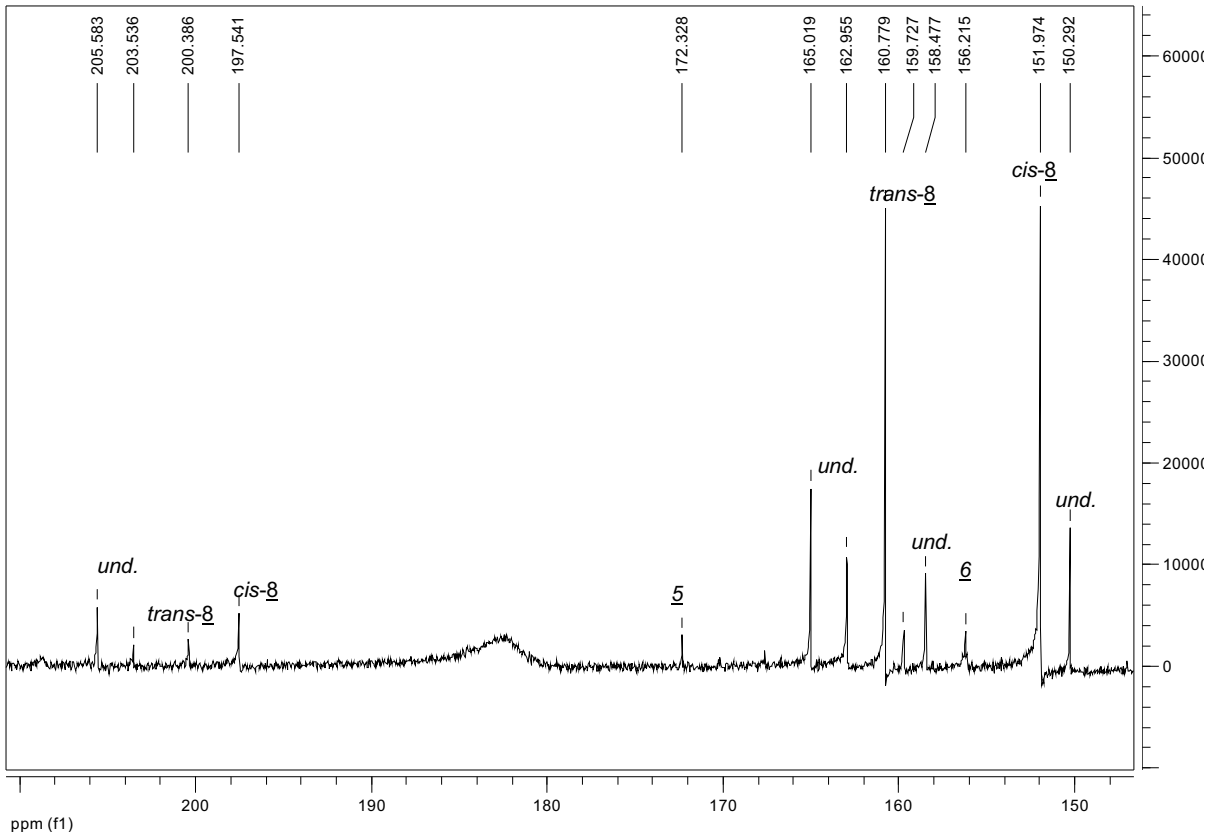

Figure 22 : ^{13}C HP-NMR spectra of the reaction of complex 6 in CD_2Cl_2/CD_3OD = 1mL/2mL at 40℃ under 5 bar of ^{13}CO for **40 min**. reaction.

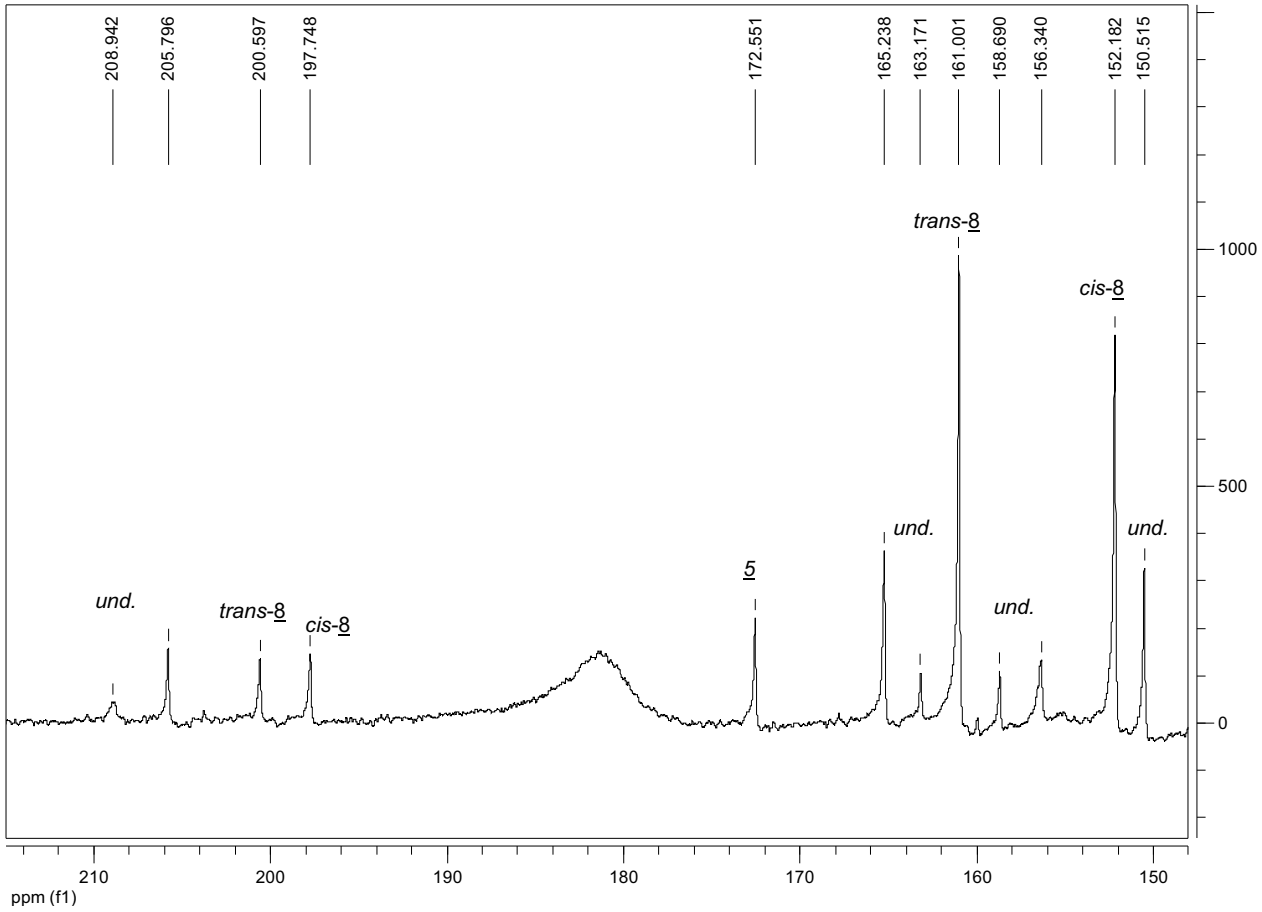

Figure 23 : ^{13}C HP-NMR spectra of the reaction of complex 6 in CD_2Cl_2/CD_3OD = 1mL/2mL at 40°C under 5 bar of ^{13}CO for **90 min**. reaction.

After 10 min., we observe essentially a signal at δ = 152.06 ppm attributed, together with the signal at δ = 197.3 ppm, to the complex *cis*-[PPN][IrI_3(COMe)$(CO)_2$] *cis*-8. We also note the presence of *trans*-[PPN][IrI_3(COMe)$(CO)_2$] *trans*-8 characterized by the signal at δ = 160.87 ppm (the signal corresponding to the acetyl group may be hidden by the noise), of [PPN][$Ir(CH_3)I_3(CO)_2$] 6, characterized by the signal at δ = 156.23 ppm and three other signals at δ = 163.22 ppm , δ = 204.44 ppm, which could be assigned to the neutral dimeric acetyl species, and at δ = 165.30 ppm which was not identified. After 40 min., we observe in figure 22 we observe a change in the relative intensities of the signals corresponding to *cis*-[PPN][IrI_3(COMe)$(CO)_2$] *cis*-8, δ = 151.97 ppm, δ = 197.54 ppm, and *trans*-[PPN][IrI_3(COMe)$(CO)_2$] *trans*-8, δ = 161.00 ppm, δ = 200,38 ppm. We note the presence of the signals at δ = 156.21 ppm corresponding to unreacted complex 6, at δ = 162.95 ppm and δ = 203.54 ppm for the hypothetical neutral dimer and at δ = 165.02 ppm for unidentified species. We also note the appearance of a signal at δ = 172.33 ppm, which could correspond to complex 5 but also of

additional signals at δ = 150.29 ppm, δ = 158.48 and δ = 159.73 ppm, corresponding to carbon atom of the CO ligands on terminal position, and signal at δ = 205.58 ppm corresponding to the carbon atom the acetyl group, which have not been identified. By carrying out the reaction during 90 min., we see that the change in the relative intensities of the signals corresponding to *cis*-[PPN][$IrI_3(COMe)(CO)_2$] *cis*-8 and *trans*-[PPN][$IrI_3(COMe)(CO)_2$] *trans*-8 is more pronounced. The peak corresponding to complex 5 at δ = 172.55 ppm is more intense, meaning that the reductive elimination reaction has occured. The observed unidentified signals are still present, together with an additional peak at δ = 208.94 ppm.

From these ^{13}C NMR experiments, we can confirm that an isomerisation occurs from complex cis-[PPN][$IrI_3(COMe)(CO)_2$] cis-8 to complex trans-[PPN][$IrI_3(COMe)(CO)_2$] trans-8. This cis/trans isomerisation could occur via unidentified intermediates which could correspond to the unidentified signals. On one hand, methanol accelerates the cis-migration reaction from complex 6 to complex 8, and on the other hand the increase in methanol concentration favor the cis/trans isomerisation. We can note that the signal at δ = 185 ppm corresponding to free ^{13}CO dissolved in the reaction mixture decreases significantly after some time since it passes from the liquid phase to the gas phase. That could explain why some complex 6 is found at the end of the reaction. Moreover, under these conditions, the reductive elimination step is likely to be very slow since after 90 min., we only observed a small signal corresponding to the starting complex 5 whereas large signals corresponding to the acetyl species cis-8 and trans-8 are still observed.

In order to increase the rate of the CO migratory insertion step, we increased the polarity and the protic character of the medium, by adding a small quantity of water. Since water is not soluble in dichloromethane, we were obliged to add a small amount of methanol to obtain a homogeneous solution. By reacting the methyl iridium complex 6 in CH_2Cl_2/MeOH/H_2O = 20 mL/5 mL/5 mL under 5 bar of CO and at ambient temperature, we only observed, after 30 min., the CO stretching bands corresponding to *trans*-8, meaning that water is much more effective than methanol for the *cis*-migration reaction and the *cis/trans* isomerisation. Moreover, water is used in the industrial plant

reactor. Therefore, we can believe, regarding the former result, that the increase in water content in batch or continuous experiments could increase the carbonylation rate as it was observed for the Monsanto process using a rhodium catalyst. We will see that it is not the case for iridium-catalyzed batch experiments, where a maximum activity is observed at about 4 wt% water concentration and a decrease in activity is observed for higher water concentrations (Fig. 25). We can correlate these pieces of information to the observations made by Forster[22] for the rhodium-catalyzed water gas shift reaction (WGSR), where the rate of the WGSR increases to a maximum when the water content increase, to about 10 wt% and then decreases, whereas the water concentration continues to increase. Moreover, a too high water content involves high energy costs to separate acetic acid from water.

The X-ray structure of *cis*-[PPN][$IrI_3(COMe)(CO)_2$] *cis*-8 was reported in 2004 by Maitlis *et al.*[5] On our part, following the synthetic procedure using water and after many crystallization attempts, we obtained, from a hexane/dichloromethane bilayered mixture in a Schlenk tube at –18°C, crystals of compound *trans*-[PPN][$IrI_3(COMe)(CO)_2$] *trans*-8. A crystal was selected and analyzed by X-ray crystallography. The octahedral structure of *trans*-8 is shown in figure 24. The crystal lattice is monoclinic and the space group is P $2_{1/C}$.

By comparing the Ir-I bond length, we can note that the Ir – I(2) bond is longer than the two other Ir-I bonds, due to the trans-effect exerted by the acetyl ligand. Volpe *et al* [23] have recently synthesized compound *trans*-$[IrI_3(COMe)(CO)_2]^-$ by photolysis of $[IrI_3(CH_3)(CO)_2]^-$ under CO. They obtained crystals of this complex and published its structure with $AsPh_4^+$ as counter-ion. The bond distances are in good agrement with those we obtained for compound *trans*-8. A density functional study concerning this complex was published in 2001[19], and calculated data for *trans*-$[IrI_3(COMe)(CO)_2]^-$ fit well with those we have observed. It's worth noting that this trans effect is not observed in the rhodium homologue complex shown in figure 10.

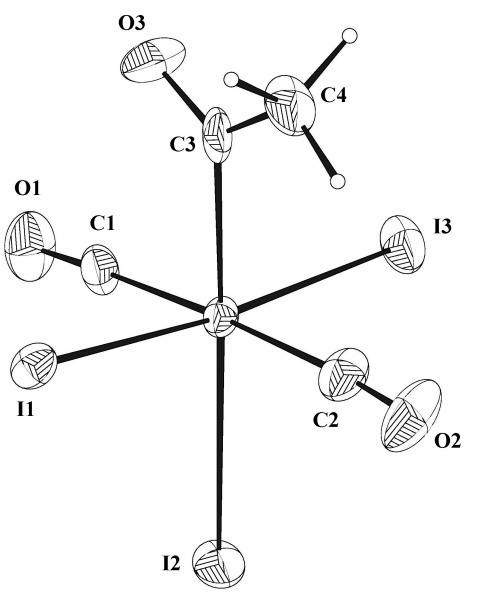

Figure 24 : X-ray crystal structure of *trans*-[PPN][$IrI_3(COMe)(CO)_2$] *trans*-4 (counterion omitted for clarity purposes

Bond length: Ir(1) - I(1) = 2.6849(8), Ir(1) - I(2) = 2.8147(8), Ir(1) - I(3) = 2.6984(9), Ir(1) - C(1) = 1.929(11), Ir(1) - C(2) = 1.915(13), Ir(1) - C(3) = 2.058(12), C(1) - O(1) = 1.116(13), C(2) - O(2) = 1.104(14), C(3) - C(4) = 1.487(18), C(3) - O(3) = 1.183(14).

Angles: I(1) - Ir(1) - I(2) = 91.85(3), I(1) - Ir(1) - I(3) = 174.65(3), I(2) - Ir(1) - I(3) = 93.07(3), I(1) - Ir(1) - C(1) = 89.8(3), I(2) - Ir(1) - C(1) = 89.8(3), I(3) - Ir(1) - C(1) = 88.1(3), I(1) - Ir(1) - C(2) = 91.6(4), I(2) - Ir(1) - C(2) = 86.1(3), I(3) - Ir(1) - C(2) = 90.8(4), C(1) - Ir(1) - C(2) = 175.7(5), I(1) - Ir(1) - C(3) = 87.4(3), I(2) - Ir(1) - C(3) = 178.3(3), I(3) - Ir(1) - C(3) = 87.7(3), C(1) - Ir(1) - C(3) = 88.7(5), C(2) - Ir(1) - C(3) = 95.5(5), Ir(1) - C(1) - O(1) = 177.8(11), Ir(1) - C(2) - O(2) = 175.4(12) Ir(1) - C(3) - C(4) = 117.9(9), Ir(1) - C(3) - O(3)= 119.9(9), C(4) - C(3) - O(3) = 122.0(12).

II-3 Acceleration of the *cis*-migration reaction rate from $[IrI_3(CH_3)(CO)_2]^-$ to $[IrI_3(COMe)(CO)_2]^-$ by addition of a metal co-catalyst.

In section II-2 we studied the effect of a polar protic solvent, such as methanol or water, on the *cis*-migration reaction that transforms complex [PPN][$IrI_3(CH_3)(CO)_2$] 6 into the complex [PPN][$IrI_3(COMe)(CO)_2$] 8 and, we found that this kind of solvent exert a role, first on the *cis*-migration reaction rate, but also on the formation of two isomers, *cis*-[PPN][$IrI_3(COMe)(CO)_2$] *cis*-8 and *trans*-[PPN][$IrI_3(COMe)(CO)_2$] *trans*-8. We could explain this phenomenon by the ability of such solvent to interact with an iodide ligand, which decreases the electron density on the iridium metal center and then facilitates the *cis*-migration reaction.

In this context, some research groups introduced into the iridium catalytic system another metal co-catalyst in order to promote the slowest step and accelerate the carbonylation rate of the process. That is the case of the BP-chemical group who found that addition of a ruthenium complex to the iridium catalytic system enhances dramatically the carbonylation rate, leading to a new process suitable for industrial use named Cativa[2].

On our part a few years ago, we found that addition of a platinum co-catalyst also could enhance the carbonylation rate of the iridium catalytic system. Mechanistic studies were previously performed to understand the role of the platinum in this system[7,8,9], and continuous catalytic experiments showed good activity for this bi-metallic system at low water content in comparison with the iridium system alone. In addition we tried to establish via Schlenk tube experiments if a rhodium complex could promote the *cis*-migration reaction slow step in the iridium catalytic cycle.

In this section, we will describe the [Ir/Ru] and [Ir/Pt] systems and the action of the $[RhI(CO)_2]_2$ complex on the rate determining step in the iridium-catalyzed methanol carbonylation cycle.

II-3-1 The Cativa process

In the first part, we will briefly describe the basics of the Cativa process. The addition of a ruthenium promoter, such as $[RuI_2(CO)_4]$, to the iridium catalytic system, accelerates the carbonylation rate. This effect is explained by the ability of $[RuI_2(CO)_4]$ to loose a CO ligand and to abstract an iodide from $[IrI_3(CH_3)(CO)_2]^-$, via the intermediate formation of an [Ir-Ru] bi-metallic complex, giving $[RuI_3(CO)_3]^-$ and, under CO, the neutral tricarbonyl complex $[IrI_2(CH_3)(CO)_3]$ 7, within which the *cis*-migration reaction occurs more rapidly[5]. The proposed catalytic cycle for this system is depicted in scheme 6[24]

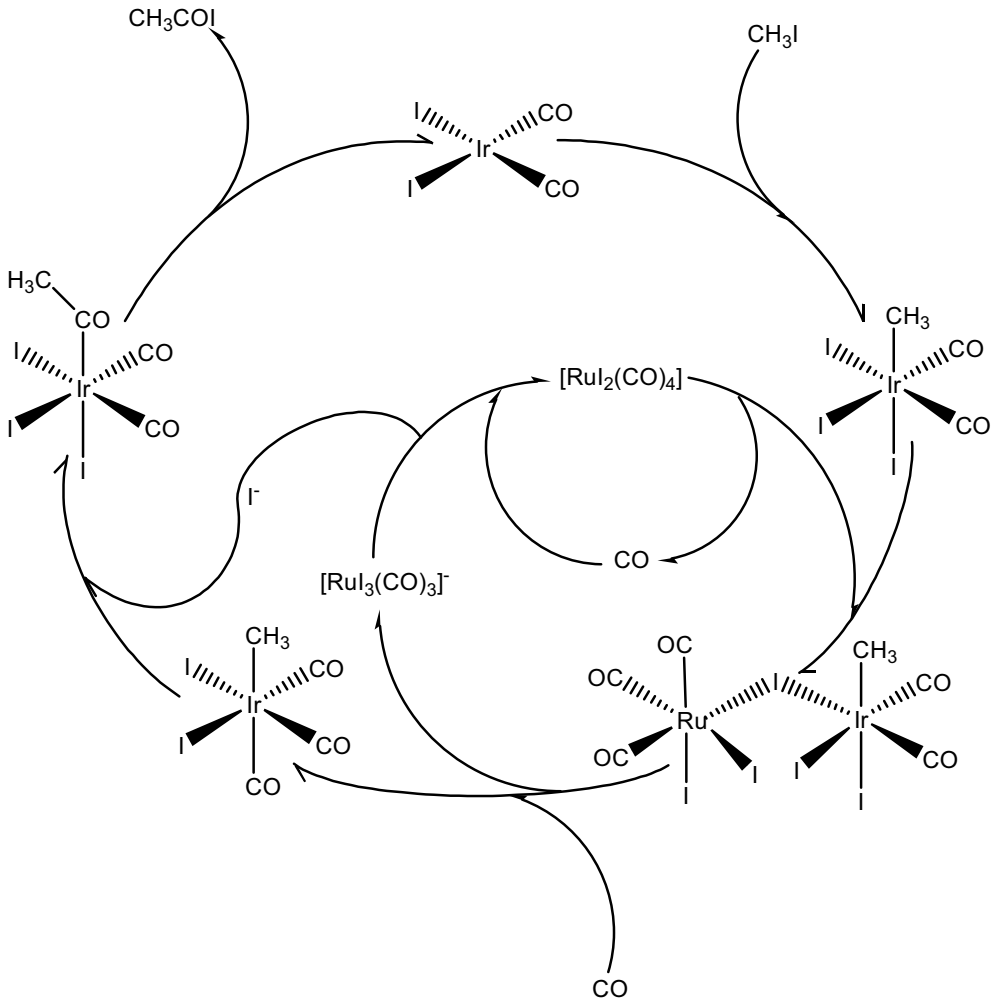

Scheme 6 : Proposed reaction mechanism for the Cativa process.

No direct proof of the formation of the [Ir-Ru] bimetallic intermediate could be got until Whyman *et al.*[24] observed by ^{13}C NMR the appearence of new CO signals after the addition of $[RuI_2(CO)_4]$ to the reaction mixture containing $[IrI_3(CH_3)(CO)_2]^-$. These CO signals were very close to those observed for the anionic methyl iridium species and to those corresponding to $[RuI_3(CO)_3]^-$. These observations could be consistent with the formation of the iodide bridged [Ir-Ru] bimetallic intermediate shown in scheme 6. Moreover, they observed the cleavage of this species under CO and the formation of the neutral tricarbonyliridium complex $[IrI2(CH_3)(CO)_3]$.

II-3-2 The iridium-platinum system.

In our laboratory, we developed and patented[25] a new catalytic process for methanol carbonylation to acetic acid. Previous studied were performed during the PhD of Dr. S. Gautron and by Dr. C. Leberre and are described below. Based on the same principle as the Cativa process, a platinum co-catalyst, namely $[PtI(CO)_2]_2$, was added to the iridium catalytic system. We performed batch experiments (see Experimental Section) in order to determine the platinum/iridium best ratio leading to the highest carbonylation rate. The iridium active species $H[IrI_2(CO)_2]$ is formed first by introducing in a batch hastelloy reactor the commercial $IrI_{3,4}$ salt and a mixture of acetic acid and water. The reactor is then sealed, flushed three times with CO, pressurized to 6 bar of CO and heated at 190° C. After 25 minutes, we introduced, via an additional tank, the remaining part of the catalytic mixture so as to have in the reactor the following wt% proportions: 27% methyl acetate, 11% methyl iodide, 6.4% water, and 55.6% acetic acid (balance). The total platinum/iridium metal content is 3250 ppm. The results of these experiments are summarized in Table 1. The carbonylation rates are measured at 20% of methyl acetate remaining in the reactor based on the CO consumption, and corrected by gas chromatography analysis. It comes out that the best platinum/iridium molar ratio for the highest carbonylation rate is Pt/Ir = 3/7. We can also see that platinum alone has no activity at all for the carbonylation reaction, and that iridium alone has a moderate activity (16 mol/L/h).

We performed a second set of experiments in order to determine the desired water percentage to obtain the maximum activity. These batch runs were based on the same conditions as the former, except for the platinum/iridium molar ratio maintained at Pt/Ir = 3/7 and the variation of water percentage between 2% and 8%. Results are shown in figure 25.

RUN	Pt/Ir (mol/mol)	Carb. Rate* at 20% [AcOMe] (mol. L^{-1}. h^{-1})
1	100/0 %	0
2	0/100 %	16
3	19/81%	31
4	33/67 %	35
5	47/53 %	33
6	67/33 %	24

* Carbonylation rate expressed in mol of AcOH formed per liter of solution per hour.

Table 1 : Carbonylation rate by varying the Pt/Ir ratio

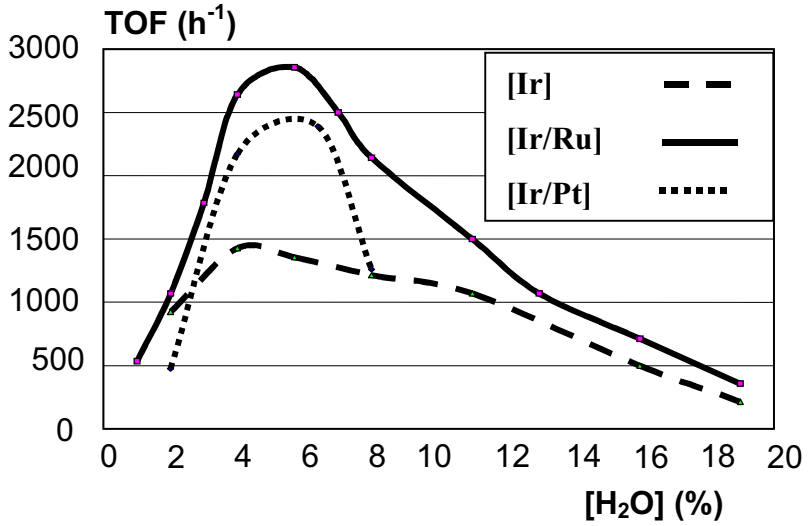

Figure 25 : Influence of water content on the turnover frequency.

The curve representing the activity of the iridium-platinum system as a function of water content presents the shape of a gaussian curve with a maximum for a water content of 5-6 wt%. We chose to express the activity in terms of turnover frequency (TOF), based on metal concentration, to compare our results with those published for the Cativa process[26]. One can see that the TOF reached with the Cativa system are slightly higher than those obtained with the iridium-platinum system. Both of them have their maximum for a water content around 6%, the [Ir-Ru] system being a little bit more active than the [Ir-Pt] system.

In order to get mechanistic information on the [Ir-Pt] system, Schlenk tube experiments were performed under nitrogen using the stabilizing counter ion PPN^+. $[PPN][IrI_3(CH_3)(CO)_2]$ 6 was prepared as described in section II-2. $[PtI_2(CO)]_2$ 9 was synthesized[27] introducing the PtI_2 salt to n-hexane in a reactor. The reactor was pressurized to 12 bar, stirred and heated at 75° C for 1h. The reactor was then cooled down to ambient temperature and a red solid corresponding to the $[PtI_2(CO)]_2$ dimer was obtained. Complex 9 was labeled with ^{13}CO and its ^{13}C NMR spectra show a signal at δ = 154.5 ppm with two satellites ($^1J_{13C\text{-}195Pt}$ = 1843 Hz) due to the coupling with ^{195}Pt (I=1/2, abundance = 33.7%) and the ^{195}Pt NMR spectrum shows a signal at δ = -5328 ppm with two satellites ($^1J_{13C\text{-}195Pt}$ = 1843 Hz).

Then, 0.3 equivalent of complex $[PtI_2(^{13}CO)]_2$ 9 were added into a solution of $[PPN][IrI_3(CH_3)(^{13}CO)_2]$ 6 in dichloromethane. ^{195}Pt NMR spectra performed at –30° C (Fig. 26) show the disappearance of the signals corresponding to complex 9 and the appearance of two news signals. The one at δ = -5460 ppm ($^1J_{13C\text{-}195Pt}$ = 1759 Hz), corresponds to $[PPN][PtI_3(CO)]$, which was previously fully characterized[8] and the other at δ = -5462 ppm ($^1J_{13C\text{-}195Pt}$ = 1650 Hz), corresponds to a novel platinum species. Also the corresponding ^1H NMR spectra at –30° C on this reaction (Fig. 27) also show the presence of new proton signals. Those at δ = 1.9 ppm and 1.85 ppm correspond to the neutral dimer $[IrI_2(CH_3)(CO)_2]_2$, which was previously fully characterized[16], a weak one at δ = 2.13 ppm corresponds to unreacted compound 6, and two new signals at δ = 2.37 ppm and at δ = 2.28 ppm are observed.

The FAB mass spectrum (in negative mode) on this solution (Fig 28) shows two peaks at m/z = 1121 and m/z = 1161 corresponding to two negatives species, and others fragmentation peaks that correspond to the loss of CO ligand. We could propose the following formula: $[IrI_2(CH_3)(CO)_2(\mu\text{-}I)PtI_2(CO)]^-$ for m/z = 1121 and $[IrI_2(CH_3)(CO)_2(\mu\text{-}I)IrI_2(CH_3)(CO)_2]^-$ for m/z = 1161. Hence, we can envisage the mechanistic route described in scheme 7.

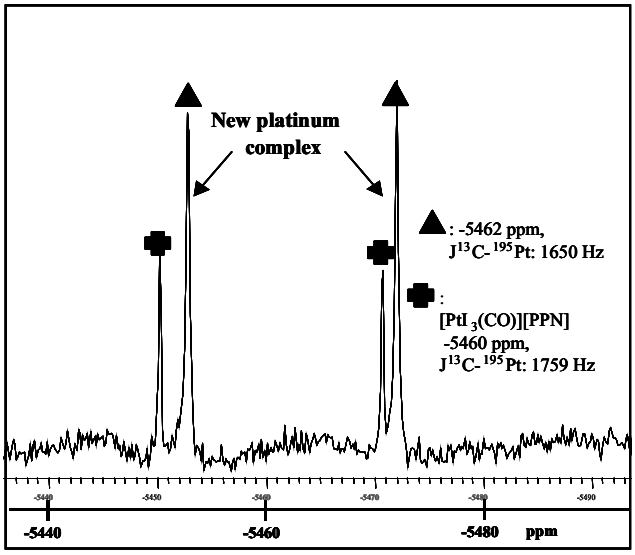

Figure 26 : ^{195}Pt NMR spectra at –30°C on the products from the reaction of $[PPN][IrI_3(CH_3)(^{13}CO)_2]$ 6 with 0.3 eq of $[PtI_2(CO)]_2$.

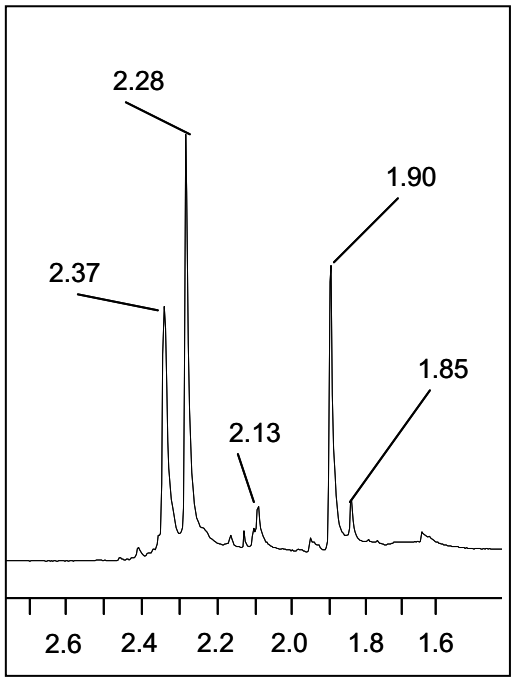

Figure 27 : ^1H NMR spectra at –30°C on the products from the re action between $[PPN][IrI_3(CH_3)(^{13}CO)_2]$ 6 and 0.3 eq of $[PtI_2(CO)]_2$.

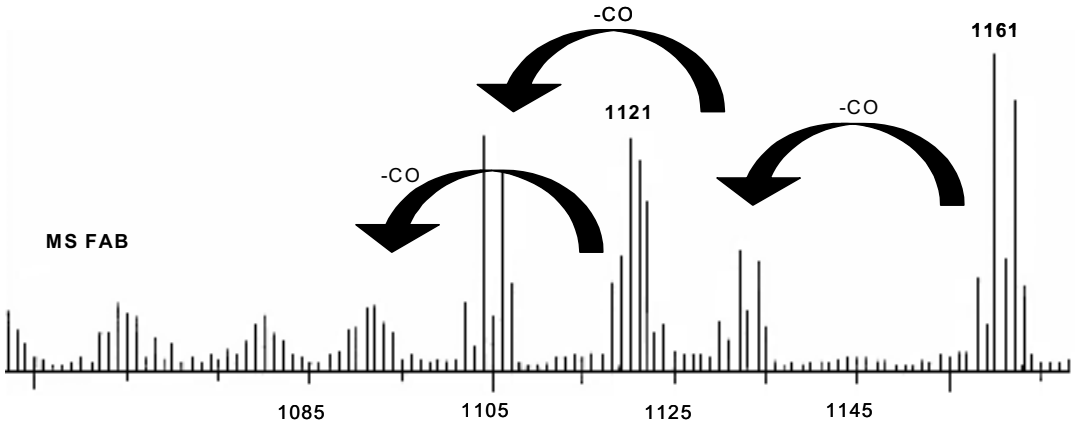

Figure 28 : Mass FAB spectrum on the product from the reaction between [PPN][$IrI_3(CH_3)(^{13}CO)_2$] 6 and 0.3 eq of $[PtI_2(CO)]_2$.

In order to get further information about these species, other experiments on the reaction between [PPN][$IrI_3(CH_3)(CO)_2$] 6 and $[PtI(CO)_2]_2$ 9 were performed varying the relative concentrations of the two complexes, and the resulting solutions were analyzed by ^{1}H NMR, FAB mass spectroscopy, and ^{13}C NMR. From these data, it was possible to characterize the two dimers $[IrI_2(CH_3)(CO)_2(\mu\text{-}I)PtI_2(CO)]^-$ and $[IrI_2(CH_3)(CO)_2(\mu\text{-}I)IrI_2(CH_3)(CO)_2]^-$ and to propose a catalytic cycle (Sc. 8). Under CO, the heterobimetallic complex seems to afford the neutral tricarbonyl complex $[IrI_2(CO)_3]$ within which the cis-migration occurs rapidly giving the acetyl iridium complex. All details of this study can be found in the PhD thesis of Dr. Gautron Samuel and in other papers[7, 8, 9].

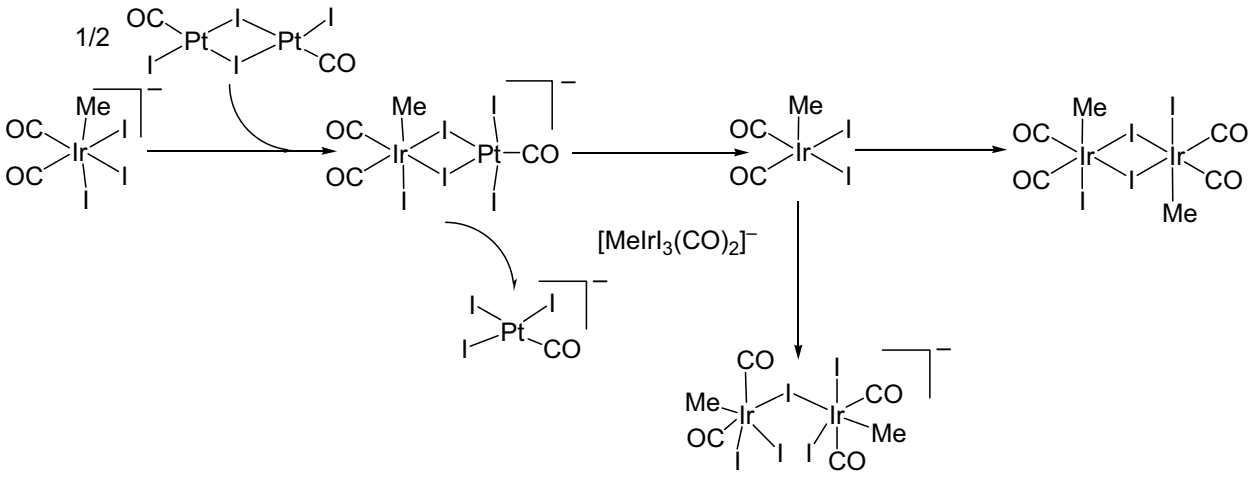

Scheme 7 : Proposed mechanistic pathway of the reaction between [PPN][$IrI_3(CH_3)(CO)_2$] 6 and $[PtI_2(CO)]_2$.

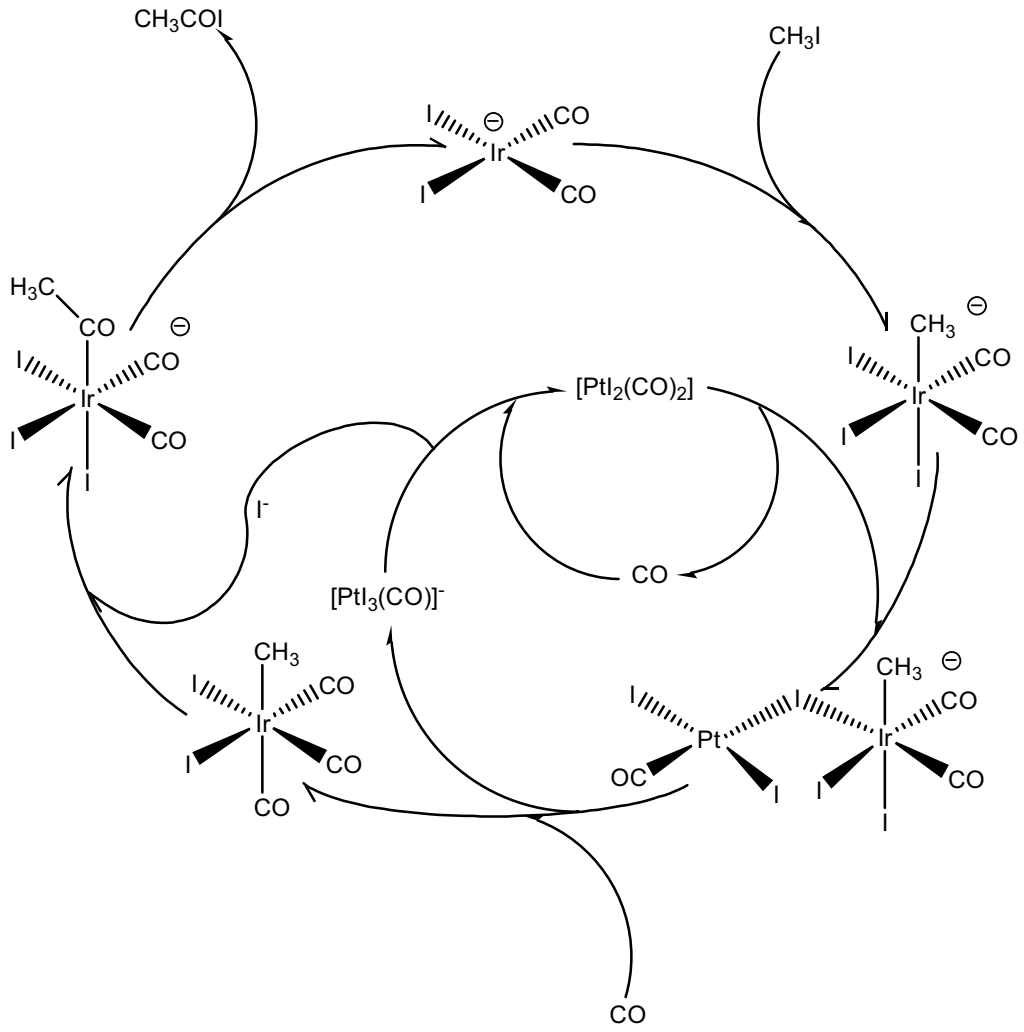

Scheme 8 : Proposed catalytic cycle for the iridium/platinum system.

II-3-3 The iridium-rhodium system.

Rhodium is known to have high activity for methanol carbonylation at high water content but shows low activity at low water concentration, where iridium catalytic system shows the best activity. The two catalytic cycles show similarities with respect to their intermediates, but their rate determining steps are different and the rhodium system shows high activity at low water content with high iodide salt concentration, whereas, in the iridium system, a iodide ligand must be removed from complex $[IrI_3(CH_3)(CO)_2]^-$ to accelerate the rate determining step. Hence, we tried to see if a synergistic effect could exist between iridium and rhodium. After Schenlk tube experiments on the relevant reaction and on the different intermediates in the two catalytic cycles, we have not observed any reaction. As $[PtI_2(CO)]_2$ can react with $[IrI_3(CH_3)(CO)_2]^-$ by abstracting an iodide ligand, we tried to see if the iodo-deficient complex $[Rh(\mu\text{-}I)(CO)_2]_2$ 10 is able to do the same.

We synthesized complex 10 by reaction of RhI_3 in a methyl acetate/ methanol solvent mixture with CO to obtain first $H[RhI_2(CO)_2]$ 1. By evaporation of the solvent under CO bubbling, complex 1 dimerizes to form $[Rh(\mu\text{-}I)(CO)_2]_2$ 10. Details on the synthetic procedure are given in the Experimental Section. Crystals of $[RhI(CO)_2]_2$ were obtained and analyzed by X-ray diffraction (Fig. 29).

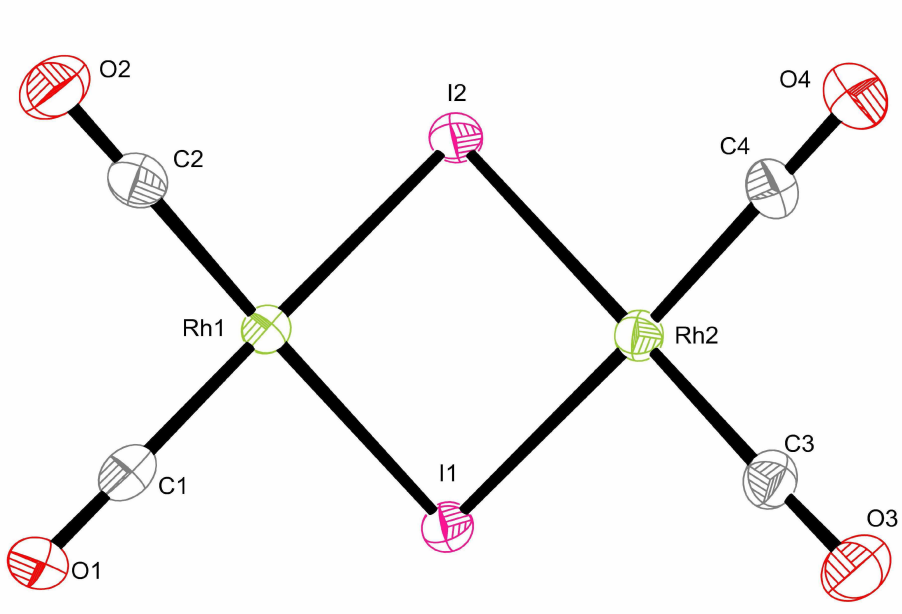

Figure 29 : X-ray crystal structure of $[RhI(CO)_2]_2$ 10

The crystal latice of 10 is monoclinic and the space group is P 1 $2_{1/n}$ 1. Data on the bond lengths (Á) and angles (deg) are given below:

Bond lengths: O(1)-C(1) = 1.131(8), O(2)-C(2) = 1.127(7), O(3)-C(3) = 1.127(7), O(4)-C(4) = 1.122(7), C(1)-Rh(1) = 1.861(7), C(2)-Rh(1) = 1.863(7), C(3)-Rh(2) = 1.861(6), C(4)-Rh(2) = 1.860(6), Rh(1)-I(1) = 2.6642(7), Rh(1)-I(2) = 2.6745(7), Rh(2)-I(2) = 2.6595(6), Rh(2)-I(1) = 2.6689(7).

Angles: O(1)-C(1)-Rh(1) = 178.6(6), O(2)-C(2)-Rh(1) = 178.7(6), O(3)-C(3)-Rh(2) = 177.2(6), O(4)-C(4)-Rh(2) = 179.2(6), C(1)-Rh(1)-C(2) = 90.0(3), C(1)-Rh(1)-I(1) = 90.55(19), C(2)-Rh(1)-I(1) = 176.3(2), C(1)-Rh(1)-I(2) = 179.2(2), C(2)-Rh(1)-I(2) = 90.37(19), I(1)-Rh(1)-I(2) = 89.04(2), C(4)-Rh(2)-C(3) = 89.5(3), C(4)-Rh(2)-I(2) = 88.84(19), C(3)-Rh(2)-I(2) = 173.86(19), C(4)-Rh(2)-I(1) = 176.34(19), C(3)-Rh(2)-I(1) = 92.0(2), I(2)-Rh(2)-I(1) = 89.25(2), Rh(1)-I(1)-Rh(2) = 78.77(2), Rh(2)-I(2)-Rh(1) = 78.76(2).

The infrared spectrum of complex 10 (Fig. 30), shows CO streching bands at 2095 cm^{-1}, 2080 cm^{-1} and 2028 cm^{-1}. The presence of these three bands shows that the atoms of the molecule are not in the same plan. The ^{13}C NMR spectrum of labeled 10 in CD_2Cl_2 (Fig. 31) shows a doublet at δ = 180.1, (d, $^1J_{C\text{-}Rh}$ = 74.96 Hz).

In order to get information on the effect exerted by $[RhI(CO)_2]_2$ 10 on [PPN][$IrI_3(CH_3)(CO)_2$] 6, we added 50 mg of 6 ($4.23.10^{-2}$ mmol) in 5 mL of dried dichloromethane to 0.5 equivalent of complex 10 ($2.11.10^{-2}$ mmol, 12 mg) in a Schlenk tube. Since the infrared spectra on this reaction mixture give further wide superposed CO stretching bands difficult to assign, we carried out this experiment in CD_2Cl_2 using labeled compounds 6 and 8 and analyze the resulting products by in ^{13}C NMR (Fig 32).

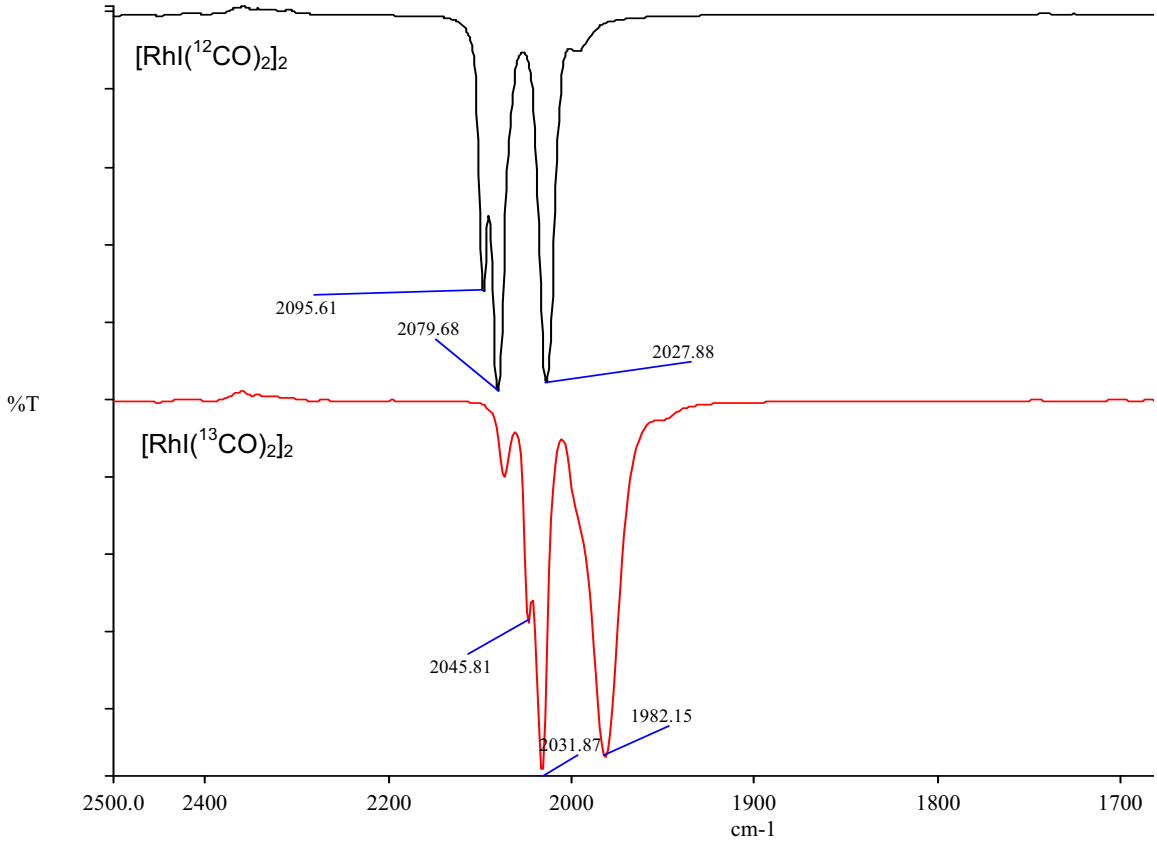

Figure 30 : Infrared spectra of $[RhI(CO)_2]_2$ and $[RhI(^{13}CO)_2]_2$ in CH_2Cl_2.

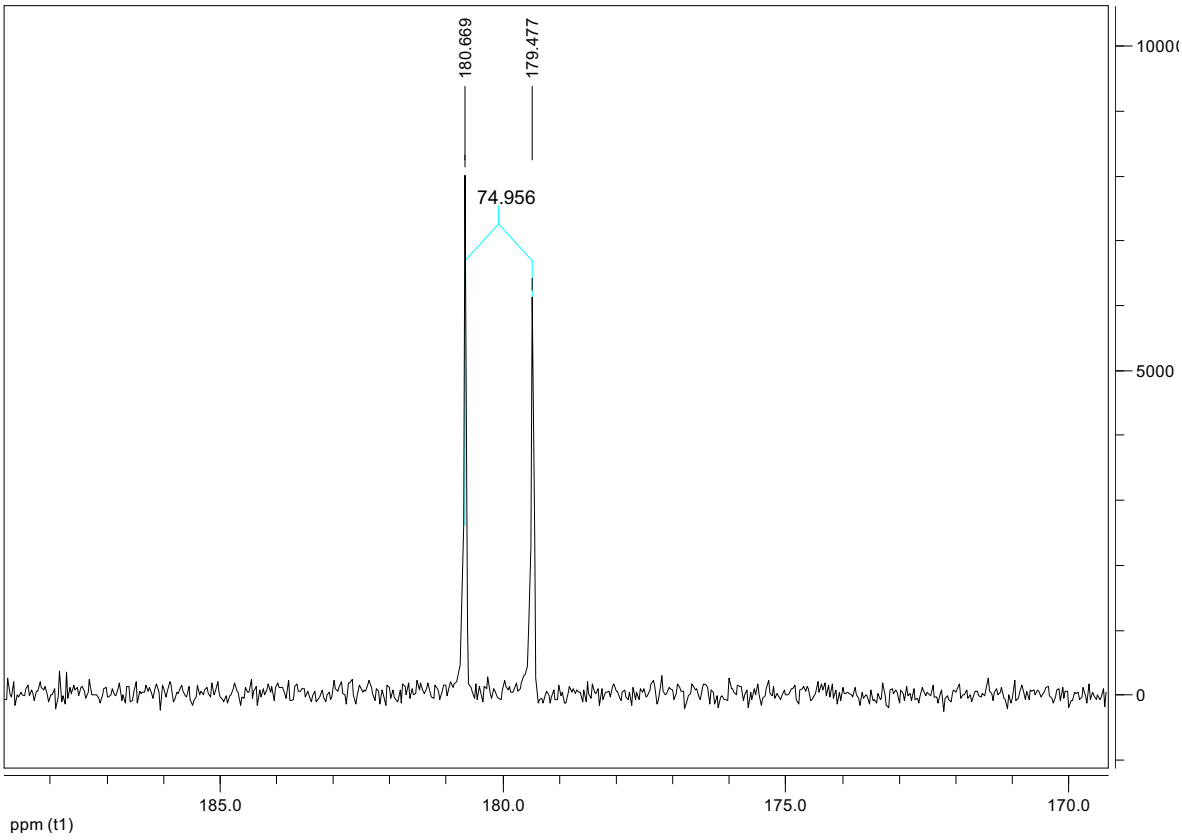

Figure 31 : ^{13}C NMR spectrum of $[RhI(^{13}CO)_2]_2$ in CD_2Cl_2, r.t.

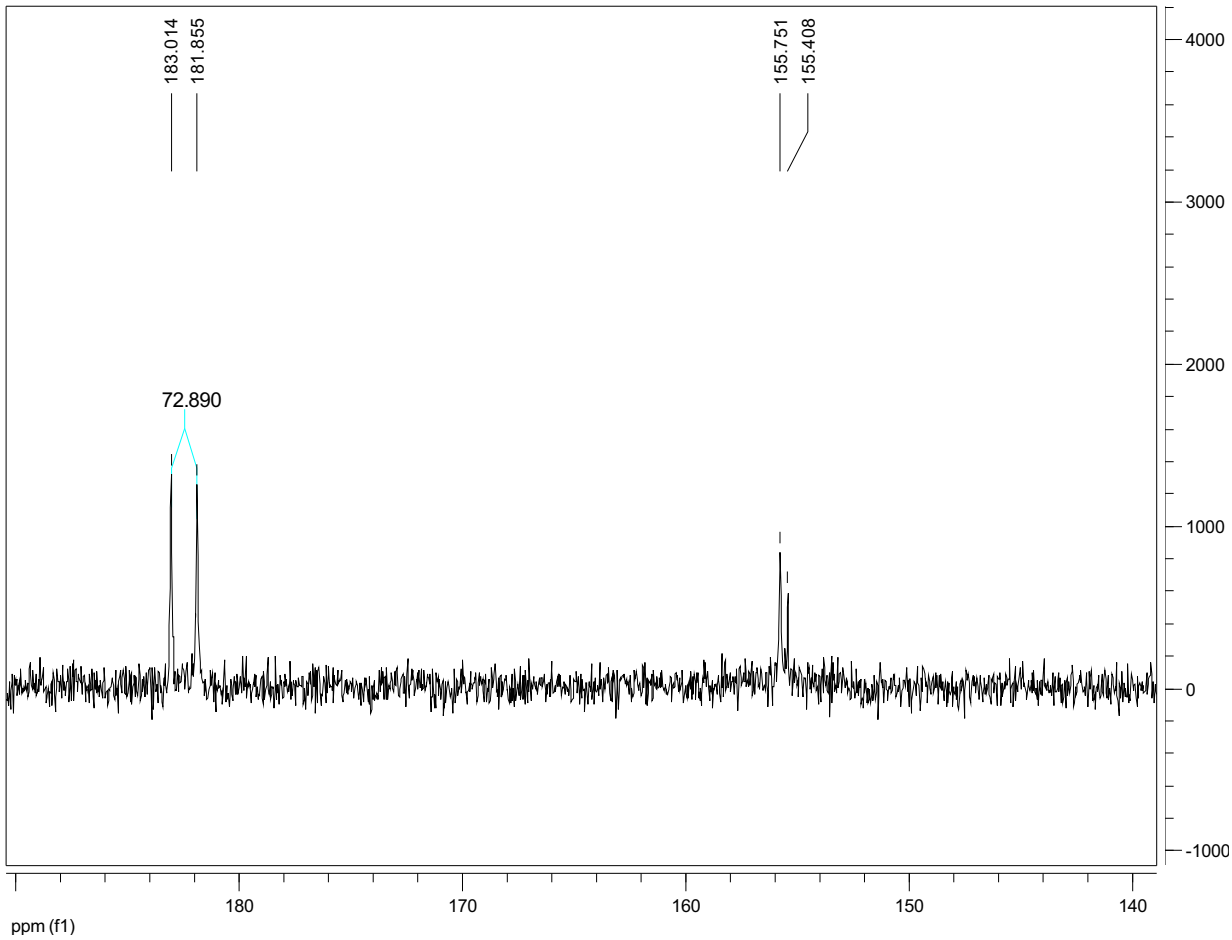

Figure 32 : ^{13}C NMR spectrum of the products from the reaction between $[RhI(^{13}CO)_2]_2$ 10 and $[PPN][IrI_3(CH_3)(^{13}CO)_2]$ 6 Rh/Ir = 1/1 in CD_2Cl_2, r.t.

We can observe the presence of three new signals at δ = 182.43 ppm (d, $^1J^{13}_{C-}{}^{103}_{Rh}$ = 72.89 Hz), at δ = 155.75 ppm and at δ = 155.41 ppm but we don't observe the signals corresponding to $[RhI(^{13}CO)_2]_2$ 10 at δ = 180.07 ppm (d, $^1J_{C\text{-}Rh}$ = 74.96 Hz), and to $[PPN][IrI_3(CH_3)(^{13}CO)_2]$ 6 at δ = 156.15 ppm. We can suppose that the neutral rhodium dimer 10 reacts with $[PPN][IrI_3(CH_3)(CO)_2]$ 6 abstracting an iodide ligand and giving complex $[PPN][RhI_2(CO)_2]$ 1 and a neutral unsaturated species as $[IrI_2(CH_3)(CO)_2]$ (Sc. 9) but the signals corresponding to $[PPN][RhI_2(CO)_2]$ 1 δ = 183.96 ppm (d, $^1J_{C\text{-}Rh}$ = 71.17 Hz) is not observed as well. Thus, the same reaction was analyzed by mass FAB spectroscopy in negative mode (Fig. 33).

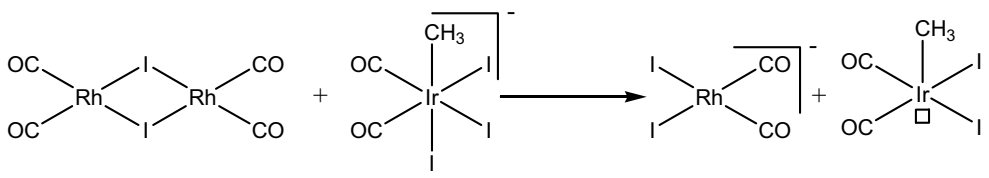

Scheme 9 : Proposed reaction between $[RhI(CO)_2]_2$ 10 and $[PPN][IrI_3(CH_3)(CO)_2]$ 6.

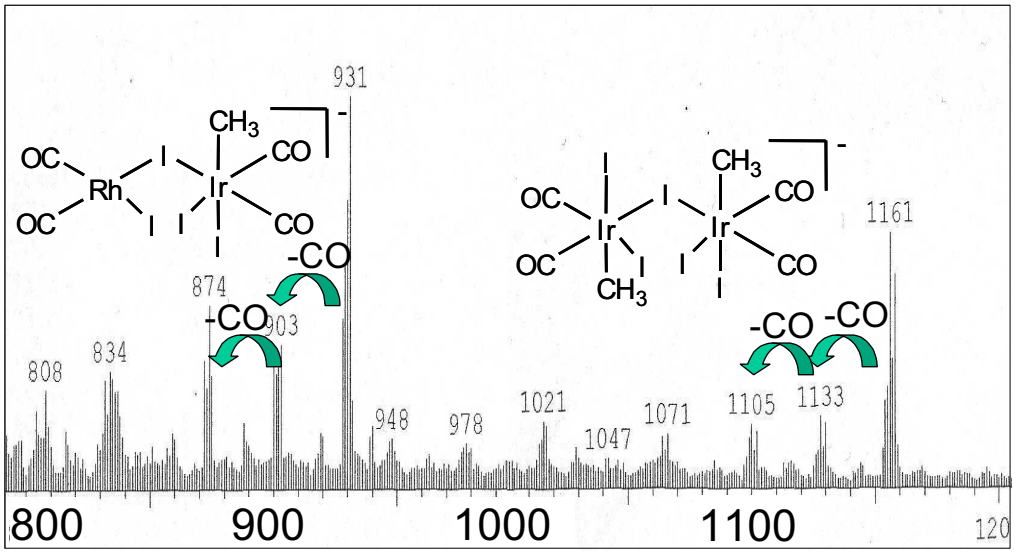

Figure 33 : MS FAB spectrum of the reaction between complex 6 and 10 in dried dichloromethane Rh/Ir = 1/1.

We can observe in this spectrum two mains peak at m/z = 1161 and m/z = 931 acconpagned by fragmentations corresponding to the loss of CO ligands (m/z = 28). The peak at m/z = 1161 was observed during the study of the iridium/platinum system in figure 28 (section II-3-2) and assigned to the dimeric complex $[IrI_2(CH_3)(CO)_2(\mu\text{-}I)IrI_2(CH_3)(CO)_2]^-$. We previously assigned[8] this species to a ^{13}C NMR signal at δ = 155 ppm, which could correspond to the signal observed at δ = 155.41 ppm in figure 32. The second peak in the mass spectrum at m/z = 931 is consistent with the formation of a heterobimetallic dimeric complex $[RhI(CO)_2(\mu\text{-}I)IrI_2(CH_3)(CO)_2]^-$, homologue of the [Ir-Ru] species in the Cativa system, and of the [Ir-Pt] species in the iridium/platinum system. We can envisage that the signal observed in figure 32 at δ = 182.43 ppm (d, $^1J_{C\text{-}Rh}$ = 72.89 Hz) may correspond to the carbon atoms of the CO ligands linked to the rhodium metal center and that the signal at δ = 155.75 ppm may correspond to the carbon atoms of the CO ligands linked to the iridium metal center. Hence, we believe that the neutral rhodium dimer 10 reacts with the methyl iridium complex 6 giving mainly the heterobimetallic complex $[RhI(CO)_2(\mu\text{-}I)IrI_2(CH_3)(CO)_2]^-$ and a small quantity of unsaturated neutral iridium species $[IrI_2(CH_3)(CO)_2]$ which could react with complex 6 giving a homobimetallic iridium compound $[IrI_2(CH_3)(CO)_2(\mu\text{-}I)IrI_2(CH_3)(CO)_2]^-$.

In a second set of experiments, we monitored this reaction by ^{13}C NMR varying the relative concentrations of the neutral rhodium dimer 10 and the methyl iridium complex 6. Figures 34, 32 and 35 show three representative ^{13}C NMR spectra for Rh/Ir = 1/2, Rh/Ir = 1 and Rh/Ir = 2, respectively.

For a molar ratio of Rh/Ir = 1/2 (figure 34), we can note the presence of a doublet at δ = 182.95 ppm, (d, $^{1}J_{C\text{-}Rh}$ = 72.4 Hz), and of a singlet at δ = 155.93 ppm that we assigned to the heterobimetallic complex $[RhI(CO)_2(\mu\text{-}I)IrI_2(CH_3)(CO)_2]^-$; we also observe a signal at δ = 155.26 ppm not well defined, which could correspond to the homo bimetallic complex $[IrI_2(CH_3)(CO)_2(\mu\text{-}I)IrI_2(CH_3)(CO)_2]^-$, and another signal at δ = 156.03 ppm very close to the chemical shift of $[IrI_3(CH_3)(CO)_2]^-$ 6 at δ = 156.15 ppm, meaning that complex 6 has not completaly reacted since it is in excess in the reaction mixture.

For a molar ratio of Rh/Ir = 1(figure 32), we observe, as previously described, a doublet at δ = 182.43 ppm (d, $^{1}J_{C\text{-}Rh}$ = 72.89 Hz) with a singlet at δ = 155.75 ppm assigned to the heterobimetallic intermediate, and a singlet at δ = 155.41 ppm assigned to the iridium dimer.

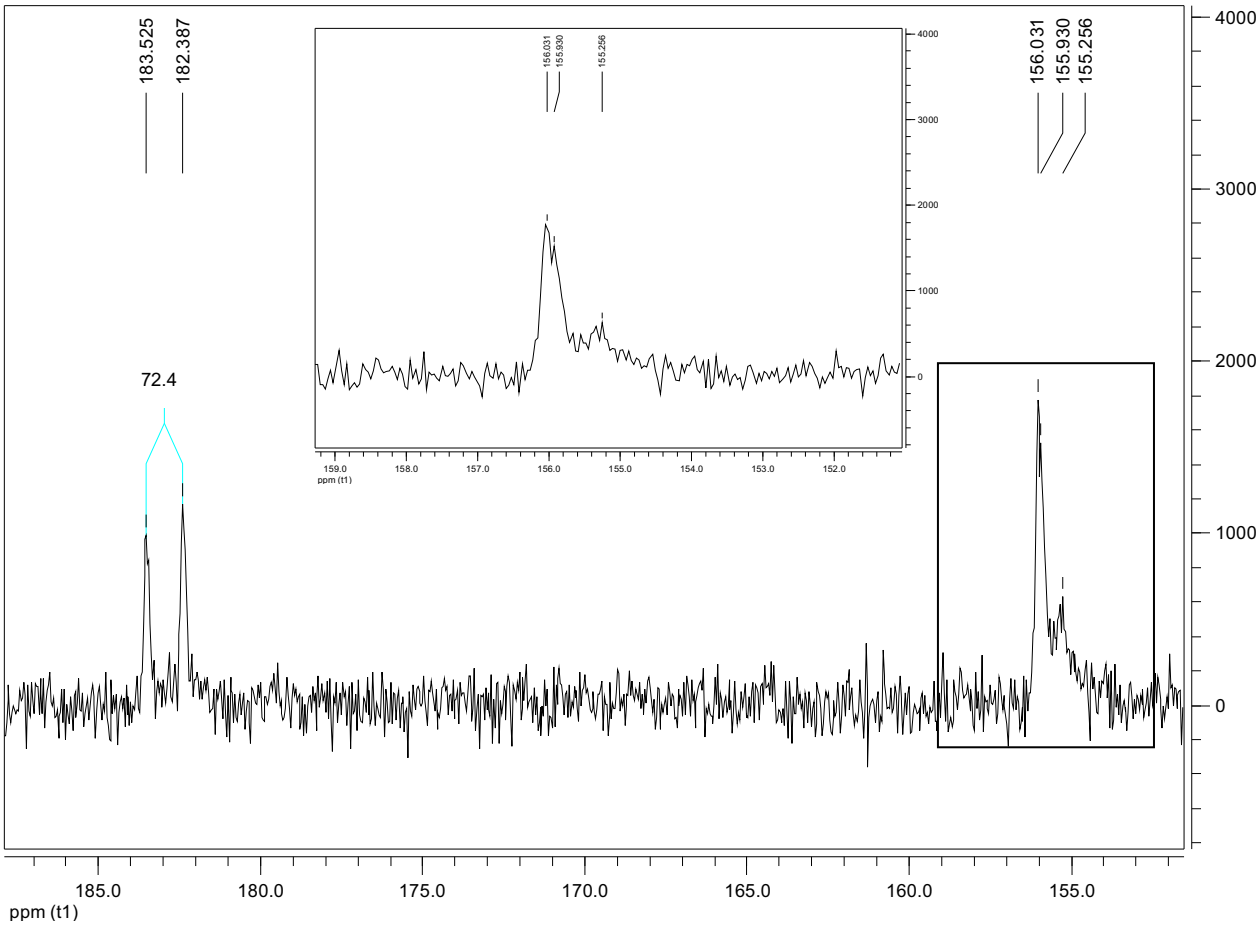

Figure 34 : ^{13}C NMR spectra of the mixture coming from reaction between 2 and 6, Rh/Ir = 1/2, in CD_2Cl_2, r.t.

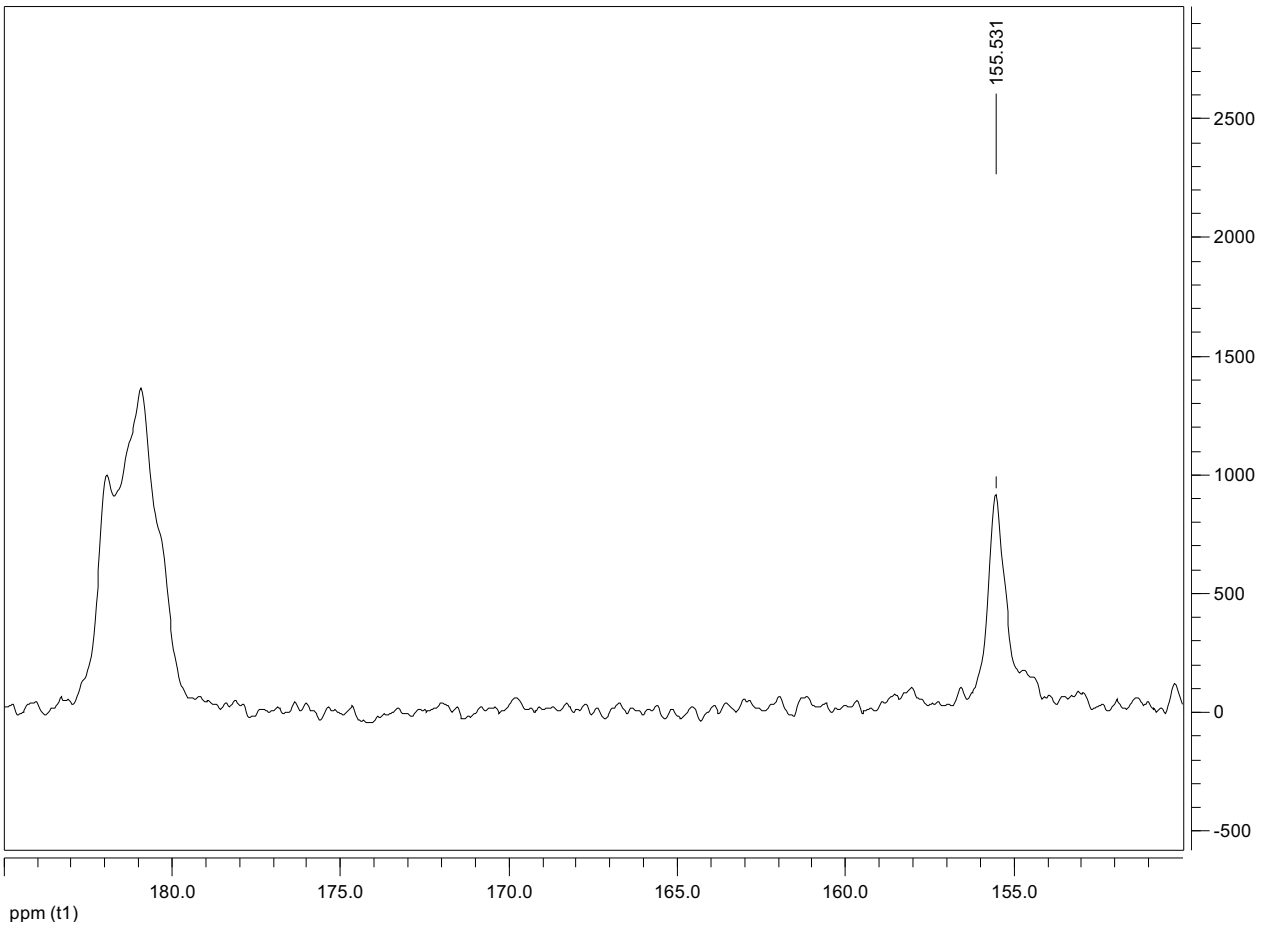

Figure 35 : ^{13}C NMR spectra of themixture coming from reaction between 2 and 6, Rh/Ir = 2, in CD_2Cl_2, r.t.

For the last case (Rh/Ir = 2, Fig.35), we observe a wide signal not well defined between δ = 180 ppm and δ = 183 ppm, pointing to a mixture of rhodium complexes, such as the heterobimetallic dimer and complex 10 still in solution since it is in excess, and also a wide signal not well at δ = 155.53 ppm that could hide the two signals that correspond to the carbon atoms of the CO ligands of the iridium moiety in the heterobimetallic compound and the carbon atoms of the CO ligands of the homobimetallic iridium dimer.

In order to investigate the above system and iys reactivity pattern, CO gas bubbled for 5 sec. through a solution of 25 mg of $[PPN][IrI_3(CH_3)(^{13}CO)_2]$ 6 ($2.11.10^{-2}$ mmol), with 0.5 equivalent of complex $[RhI(^{13}CO)_2]_2$ 10 ($1.05.10^{-2}$ mmol, 6 mg) in 2 mL of CD_2Cl_2 and analyzed the reaction mixture by ^{13}C NMR (Fig. 36).

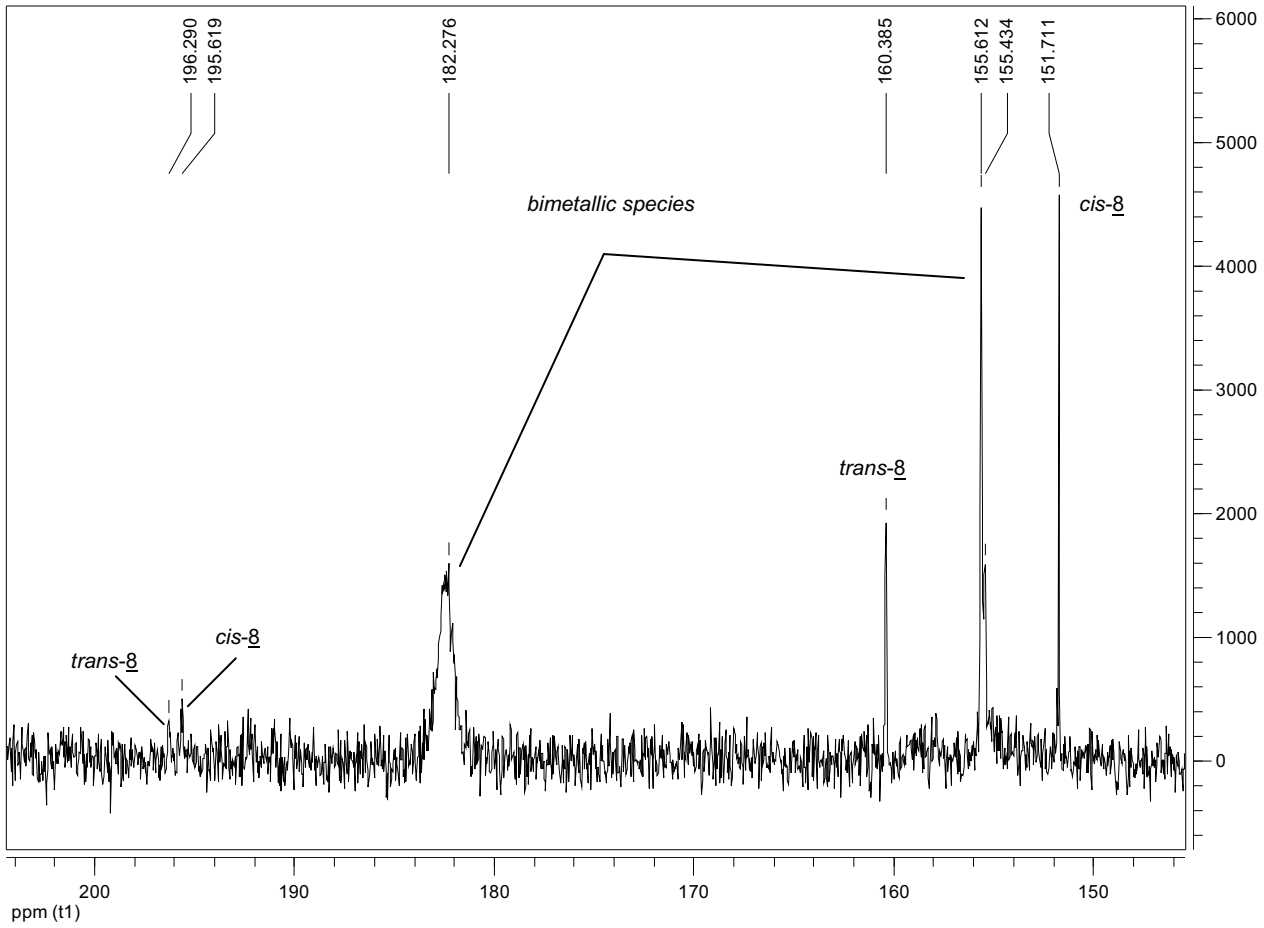

Figure 36 : ^{13}C NMR spectrum of the reaction between 6 and 10, Rh/Ir = 1, with CO bubbling in CD_2Cl_2

We can observe in this spectrum (Fig. 36) the appearance of different signals, not present in the spectrum shown in figure 32. This new signals at δ = 160.38 ppm, δ = 196.29 ppm and at δ = 151.71 ppm, δ = 195.62 ppm are consistent with the signals observed previously (Fig. 17 and Fig. 18) for the iridium acetyl complexes *trans*-[PPN][IrI_3(COMe)$(CO)_2$] *trans*-8 and *cis*-[PPN][IrI_3(COMe)$(CO)_2$] *cis*-8, respectively. We also note that the signals corresponding to the carbon atoms of the rhodium CO ligands in the heterobimetallic complex [$RhI(CO)_2(\mu\text{-}I)IrI_2(CH_3)(CO)_2]^-$ have changed to a wide peak meaning that other rhodium complexes may be present. The signals at δ = 155.61 ppm and at δ = 155.43 ppm show that the heterobimetallic complex and the iridium dimer [$IrI_2(CH_3)(CO)_2(\mu\text{-}I)IrI_2(CH_3)(CO)_2]^-$ are still present in solution. By bubbling CO through the same reaction solution for 5 min., we can observe the disappearance of the signal seen by 13C NMR because of the exchange between ^{13}CO and ^{12}CO. After CO bubbling, we extracted this solution with hexane and analyzed the

hydrcarbon phase by IR. We observed the three characteristic CO stretching bands at 2095 cm^{-1}, 2080 cm^{-1} and 2027 cm^{-1} of the neutral rhodium dimer $[RhI(CO)_2]_2$ 10, showing that it was formed by CO bubblingin solution: indeed, it was not detected by 13C NMR prior to CO bubbling.through the solution.

All these observations make us believe that the neutral rhodium dimer $[RhI(CO)_2]_2$ 10 reacts with the methyl iridium complex $[IrI_2(CH_3)(CO)_2]^-$ 6 mainly giving the heterobimetallic complex $[RhI(CO)_2(\mu\text{-}I)IrI_2(CH_3)(CO)_2]^-$ and a small quantity of homobimetallic dimer $[IrI_2(CH_3)(CO)_2(\mu\text{-}I)IrI_2(CH_3)(CO)_2]^-$ by the abstraction of an iodide ligand from the methyl iridium complex 6 (complex $[RhI_2(CO)_2]^-$ 1 has not been observed since it may be hidden by the spectrum noise). The formation of the heterobimetallic compound may reduce significantly the electron density on the iridium metal center so that under only one bar of CO, the cis-migration occurs rapidly giving the corresponding iridium acetyl complexes cis-8 and trans-8, and giving back the neutral rhodium dimer. In spite of all our attempts, we cannot explain why $[RhI(CO)_2(\mu\text{-}I)IrI_2(CH_3)(CO)_2]^-$ and $[IrI_2(CH_3)(CO)_2(\mu\text{-}I)IrI_2(CH_3)(CO)_2]^-$ remain in solution. May be the neutral rhodium dimer 10 formed by CO bubbling reacts with the homobimetallic iridium dimer forming again the heterobimetallic species. Unfortunately we didn't succeed in isolating or crystallizing the heterobimetallic species. A mechanistic pathway for the reaction between $[RhI\ (CO)_2]_2$ 10 and $[IrI_2(CH_3)(CO)_2]^-$ 6 is shown in scheme 10.

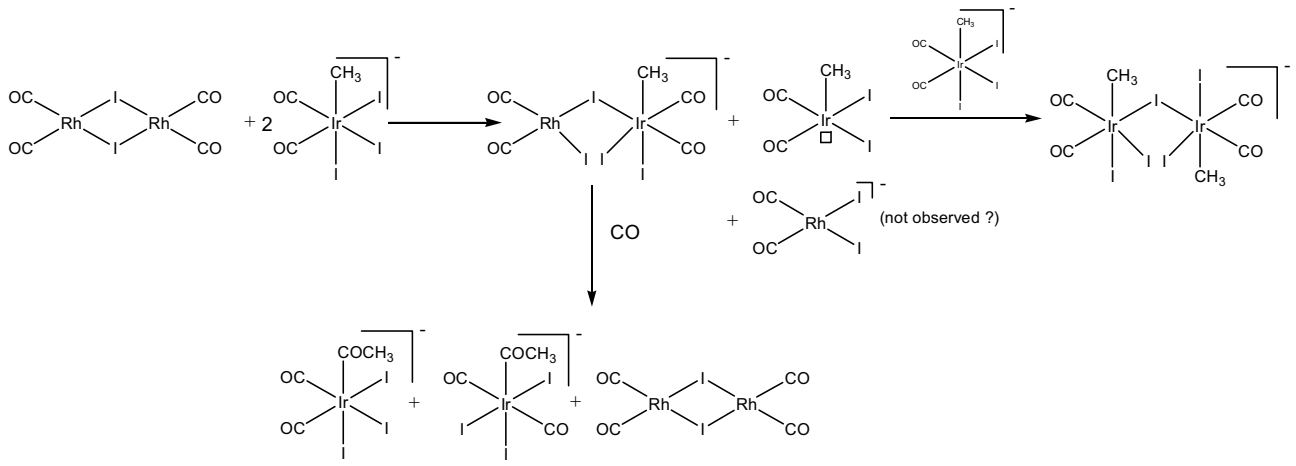

Scheme 10 : Proposed mechanistic pathway for the reaction between $[RhI(CO)_2]_2$ 10 and $[IrI_2(CH_3)(CO)_2]^-$ 6

Catalytic batch experiments starting from $IrI_{3,4}$ and RhI_3 were performed varying water concentration and the Rh/Ir molar ratio. Unfortunately, the observed carbonylation rates don't present significant enhancement in comparison with the iridium system alone. We know that the dimeric species $[RhI(CO)_2]_2$ 10 can be easily formed from complex $H[RhI_2(CO)_2]$ 1, even by evaporating a solution of 1, but we don't know if it can be formed under catalytic conditions. We can believe that this dimer might be produced in the flasher zone of a continuous plant. Thus, continuous catalytic experiments need to be made in order to know if the [Rh/Ir] system presents higher activities than those we have observed in batch experiments.

II-4. Conclusion

In this chapter, we describe the synthesis and characterization of the different intermediates in the rhodium and iridium catalytic cycle for methanol carbonylation into acetic acid and studied their reactivity, except for the methyl rhodium complex 2, which is a too short-lived species to be isolated.

At first, we investigated the rhodium catalytic cycle. In this case, the oxidative addition of methyl iodide to the starting complex 1 is the rate determining step. In comparison with the iridium cycle, only the *trans*-acetyl rhodium complex *trans*-4 has been observed under ambient conditions. Brunel *et al.*[6] have observed complex *cis*-4 by ^{13}C NMR at low temperature after oxidative addition of CH_3COI to the starting complex 1, but its presence under catalytic conditions is quite unlikely to occur. The rhodium catalytic cycle includes two acetyl intermediates, a mono-carbonyl species 3 and the di-carbonyl complex *trans*-4. We showed that insertion of CO into complex 3 giving complex 4 is reversible under ambient conditions, meaning that a CO ligand of complex 4 is very labile. The X-ray structure of mer-trans-4 has been solved.

As for the iridium system, in which the rate determining step is the *cis*-migration reaction, two acetyl isomers *cis*-8 and *trans*-8 were synthesized and isolated. The X-ray structure of *trans*-8 has been solved. The protic nature and the polarity of the solvent used for the *cis*-migration reaction play a prominent role on this reaction. Firstly, the increase in the concentration of a protic solvent, as methanol or water, increases the rate of the reaction. Secondly, the increase in the concentration of the protic solvent exerts an effect on the nature of the iridium acetyl isomer formed. At low protic solvent contents, the *cis*-8 isomer is preferentially formed, whereas at high protic solvent contents, the *trans*-8 isomer is formed. We checked by HP-IR and HP-NMR that a *cis*/*trans* isomerisation occurs. Thus, we believe that the *cis*-8 isomer is at first formed in the reaction mixture and then isomerises to the *trans*-8 isomer, the protic solvent allowing this isomerisation process.

In the second part, we observed that addition of co-catalyst as $[RhI(CO)_2]_2$ complex accelerates the CO migratory insertion reaction from complex 6 to complex 8. We showed that this accelerating effect is apparently due to the intermediate formation of a heterobimetallic species, not

yet isolated, in which the electron density on the iridium metal center is reduced thus facilitating the *cis*-migration reaction. But batch experiments using the [Ir/Rh] system do not show any significant acceleration of the carbonylation rate, and we cannot know if the dimer $[RhI(CO)_2]_2$ 10 forms under the catalytic conditions used. Further mechanistic experiments (H-P NMR) and continuous experiments are needed to know whether this system is based on bimetallic catalysis or the two metals do catalyze the reaction independently.

II-6 References

[1] B. L. Smith, G. P. Torrence, A. Aguilo, S. Alder, to Hoechst Celanese Corp., U.S Patent 5,001,259, **1991**.

[2] K. E. Clode, D. J. Watson, to BP chemicals, European Patent 616,997, **1994**.

[3] D. Forster, T. C. Singleton, *J. Mol. Cat.* **1982**, *17*, 299.

[4] P. M. Maitlis, A. Haynes, G. J. Sunley, M. Howard, J., *J. Chem. Soc., Dalton Trans.* **1996**, 2187.

[5] A. Haynes, P. M. Maitlis, G. E. Morris, G. J. Sunley, H. Adams, P. W. Badger, C. M. Bowers, D. B. Cook, P. I. P. Elliott, T. Ghaffar, H. Green, T. R. Griffin, M. Payne, J. M. Pearson, M. J. Taylor, P. W. Vickers, R. J. Watt, *J. Am. Chem. Soc.* **2004**, *126*, 2847.

[6] L. A. Howe, E. E. Brunel, *Polyhedron* **1995**, *14*, 167.

[7] S. Gautron, N. Lassauque, C. Le Berre, L. Azam, R. Giordano, P. Serp, G. Laurenczy, D. Thiébaut, P. Kalck, *Organometallics*, *in press*.

[8] S. Gautron, N. Lassauque, C. Le Berre, P. Serp, L. Azam, R. Giordano, G. Laurenczy, D. Thiebault, P. Kalck, *Eur. J. Inorg. Chem.* **2006**, *6*, 1121.

[9] S. Gautron, N. Lassauque, C. Le Berre, L. Azam, R. Giordano, P. Serp, G. Laurenczy, D. Thiébaut, P. Kalck, *Top. Cat.*, *in press*.

[10] F. E. Paulik, A. Hershman, W. R. Knox, J. F. Roth, to Monsanto compagny, US Patent 3,769,329, **1973**.

[11] D. Forster, *J. Am. Chem. Soc.* **1976**, *98*, 846.

[12] F. E. Paulik, J. F. Roth, *Chem. Commun.* **1968**, 1578.

[13] J. F. Roth, J. H. Craddock, A. Hershman, F. E. Paulik, *Chem. Tech.* **1971**, 600.

[14] D. Forster, *Adv. Organometal. Chem.* **1979**, *17*, 255.

[15] D. Forster, *J. Chem. Soc., Dalton Trans.* **1979**, 1639.

[16] S. Gautron, R. Giordano, C. Le Berre, J. Jaud, J.-C. Daran, P. Serp, P. Kalck, *Inorg. Chem.* **2003**, *42*, 5523.

[17] *Process Engineering* **1996**, *21*.

[18] A. Doppiu, U. Englert, A. Salzer, *Chem. Commun.* **2004**, 2166.

[19] T. Kinnunen, K. Laasonen, *J. Mol. Struct.* **2001**, *542*, 273.

[20] J. M. Pearson, A. Haynes, G. E. Morris, G. J. Sunley, P. M. Maitlis, *J. Chem. Soc., Chem Commun* **1995**, 1045.

[21] T. Kinnunen, K. Laasonen, *J. Organomet. Chem.* **2001**, *628*, 222.

[22] T. C. Singleton, L. J. Park, J. L. Price, D. Forster, *Preprints-ACS meeting. Division of Petroleum Chemistry* **1979**.

[23] M. Volpe, G. Wu, A. Iretskii, P. C. Ford, *Inorg. Chem.* **2006**, *45*, 1861.

[24] R. Whyman, A. P. Wright, J. A. Iggo, B. T. Heaton, *J. Chem. Soc., Dalton Trans.* **2002**, 771.

[25] C. Le Berre, P. Serp, P. Kalck, L. Layeillon, D. Thiebaut, to Acetex Chimie, French Patent 9813954, **1998**.

[26] T. R. Griffin, D. B. Cook, A. Haynes, J. M. Pearson, D. Monti, G. E. Morris, *J. Am. Chem. Soc.* **1996**, *118*, 3029.

[27] B. P. Andreini, D. B. Dell' Amico, M. G. Calderazzo, M. G. Venturi, *J. Organomet. Chem.* **1988**, *354*, 357.

CHAPTER III :

MECHANISTIC FEATURES OF THE LOW WATER CONTENT PROCESS USING RHODIUM CATALYST. STUDY OF THE REDUCTIVE ELIMINATION PROCESS.

CHAPTER III : MECHANISTIC FEATURES OF THE LOW WATER CONTENT PROCESS USING RHODIUM CATALYST. STUDY OF THE REDUCTIVE ELIMINATION PROCESS.

Methanol carbonylation to acetic acid using a rhodium catalyst was patented by Monsanto in 1973[1]. This process shows a selectivity of 99% with respect to methanol and 85% with respect to CO for high activity, but its major drawback is that it needs at least 14 %wt of water to achieve high carbonylation rates and good rhodium stability. This high water content leads to a high energy consumption and to high costs due to the distillation process needed to separate water from acetic acid. In 1991, Celanese patented an improved process[2] using rhodium catalyst and iodide salts such as LiI, NaI or KI as promoters. This new process shows a similar range of selectivities at only 4 %wt of water, and improved stability for similar activity. However, the role of iodide salt promoters in the catalytic cycle of rhodium remains not well understood.

In this chapter we will study the role of iodide salt promoters in the low water content process for methanol carbonylation to acetic acid using a rhodium catalyst. We will show the importance of the reductive elimination step at low water content, and the important role of water, as well of the iodide salt promoters on the reaction.

III-1. Effect of water and of the iodide salt promoter on the low water content process

Since Celanese patented its rhodium-based low water content process, research groups[3,4] have carried out studies in order to understand the role played by the iodide salt promoter, mainly LiI. They proposed that lithium iodide reacts with the starting complex $[RhI_2(CO)_2]^-$ 1 to form a dianionic species more nucleophilic than 1 that could react more rapidly with methyl iodide to give the methyl rhodium complex 2. Then, the acetyl complex 3 is formed by the rapid migratory CO insertion reaction. They also proposed that LiI may react with methyl acetate or acetic acid to give an acetate ion which might coordinate to the metal center giving a dianionic complex (Sc. 1).

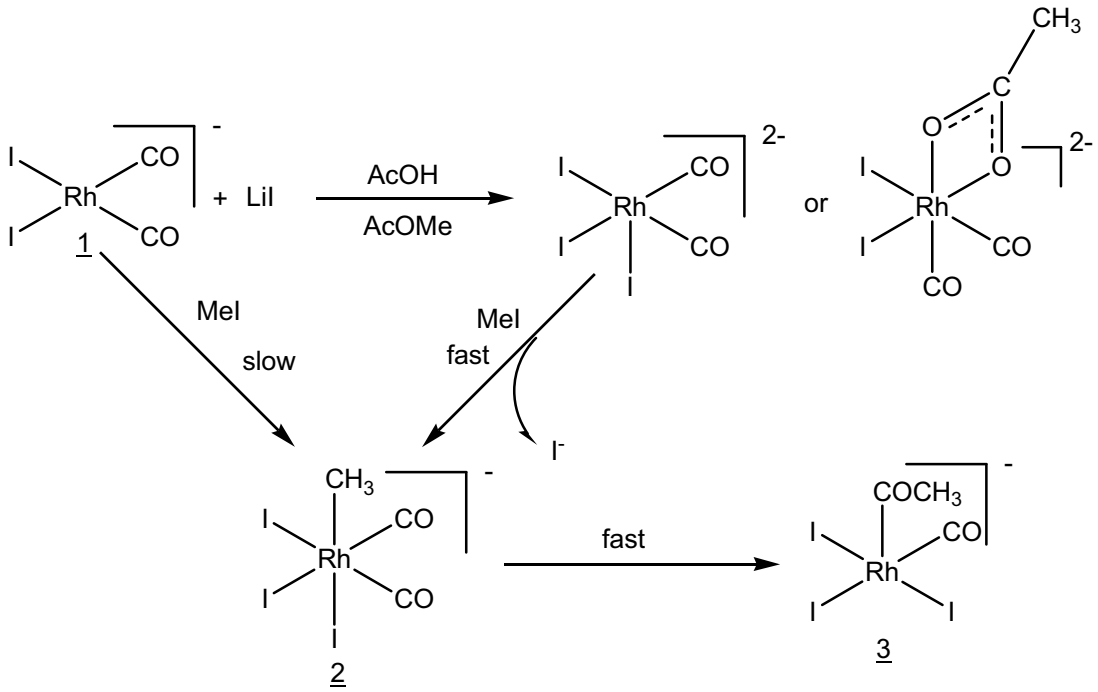

Scheme 1 : Proposed effect of LiI or acetate ions on $[RhI_2(CO)_2]^-$ 1

Many attempts were made at detecting such a dianionic compound, but up to now it has not been isolated yet, and not observed spectroscopically . On our part, we tried to synthesize and characterize such a species in different solvents (CH_2Cl_2, AcOH, AcOMe, MeOH…), by heating and freezing the reaction mixture but we never observed the formation of a new complex but only the formation of the rhodium acetyl complex $[PPN]_2[RhI_3(COCH_3)(CO)]_2$ 3 formed from the starting complex 1.

In order to get a deeper insight into the effect of iodide promoters, and especially of lithium iodide on the rhodium catalytic cycle, we performed two set of batch experiments, with and without LiI, and by varying the water content. In a 60 mL Hastelloy reactor we introduced RhI_3 (472 ppm) and a solvent mixture of AcOH/H_2O = 10/1 (wt%). The reactor was sealed, flushed three times with CO, pressurized to 6 bar of CO and heated at 190℃. Aft er a preformation step (25 min)., the reactor was fed via an additional tank to obtain the following reaction mixture (%wt): 27% methyl acetate, 14% CH_3I, 2%-14% water and acetic acid as balance. For the batch experiments with lithium iodide, we dissolved at first 17% (wt%) of LiI in methyl acetate. The carbonylation rates were calculated at 20% and 15% of methyl acetate remaining in the reactor, based on CO consumption corrected for the concentration of methyl acetate, acetic acid and water measured by gas-phase chromatography (see Context of the Present Work). The results are shown in figures 1 and figure 2. Each batch run was performed twice.

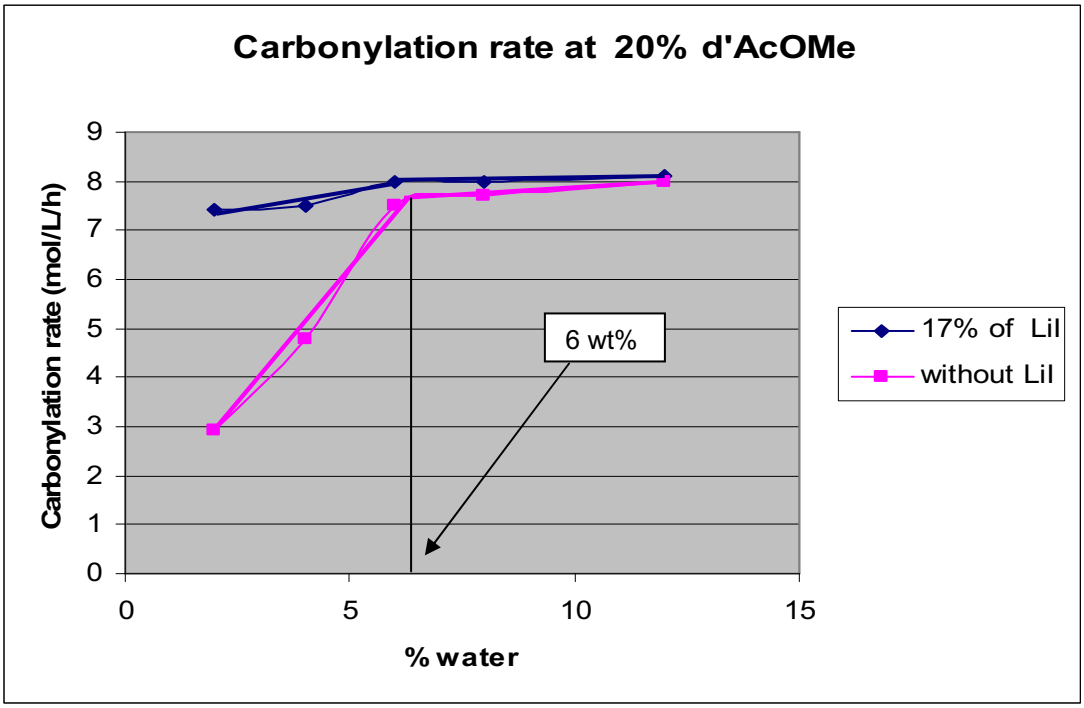

Figure 1 : Carbonylation rate at 20% methylacetate remaining

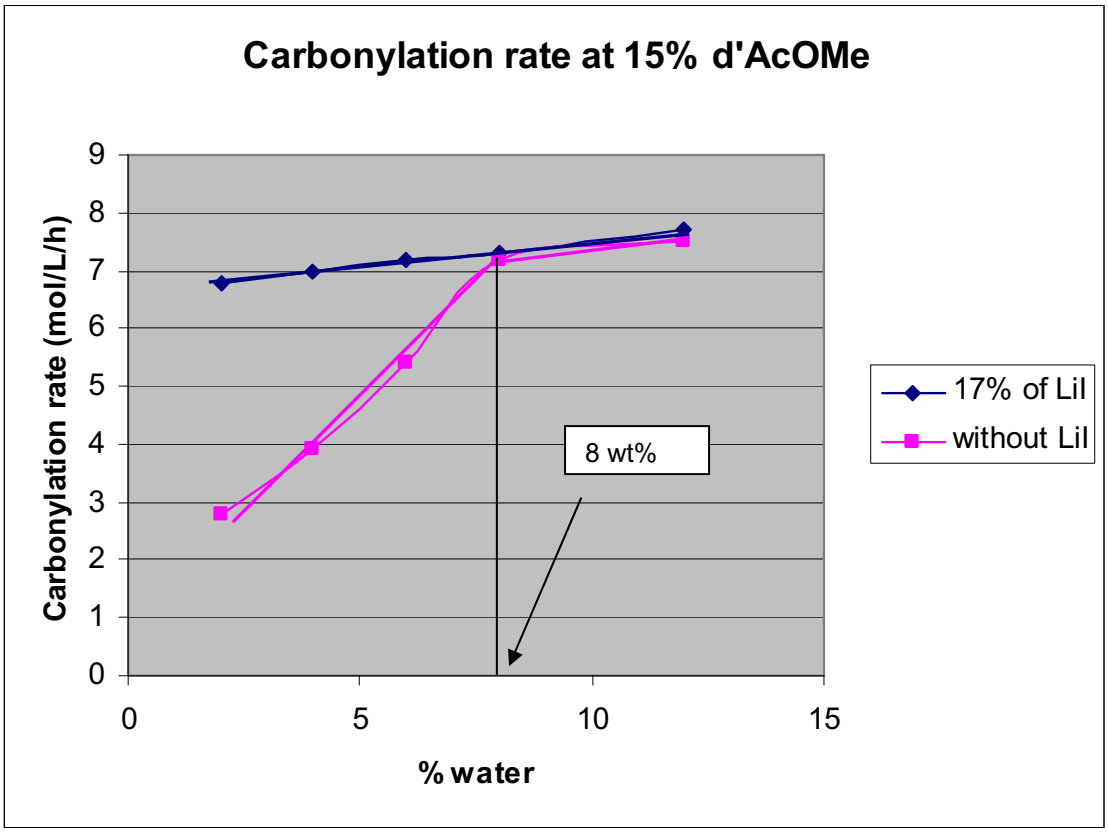

Figure 2 : Carbonylation rate at 15% methylacetate remaining

These two figures show indeed the same trend.

- For the curves showing the carbonylation rate measured in the absence of lithium iodide, we observe a break point at around 6 % of water for 20 % of methyl acetate remaining and at 8 % of water for 15% of methyl acetate remaining. The shift in the position of the break point observed in the two figures is due to water consumption between the two samplings, since no water is added during the batch experiment and the abscissa in the plot represents the water % introduced at the beginning of the experiment. We note that beyond these break point, the carbonylation rate is nearly constant while the water content increases. Before the break points, we can see that the carbonylation rates decrease dramatically and linearly. When we opened the reactor at the end of the experiment, we observed, for the run at 2% of water, a small quantity (not measured) of dark deposit on the walls of the reactor indicating that under these conditions some rhodium black is formed.

- As for the curves related to the carbonylation rate measured in the presence of lithium iodide, we don't observe a sharp breaking point. Indeed, the carbonylation rates decrease slowly and regularly while the water content is decreasing. For the curve at 20 % methyl acetate remaining, the carbonylation rates decrease equals only 0.5 mol/L/h when we reduce the water content from 14% to 2%. In each case, we never observed any dark deposit at the end of the experiments. It is also worth noting that above 6 % water content for the curves representing the calculated carbonylation rate at 20% of methyl acetate remaining, or above 8% water content for the curves at 15% of methyl acetate remaining, we observe only a slight difference between the two curves, with or without LiI, meaning that the carbonylation rates are quite similar.

Some questions arise from the analysis of these results:

- Firstly, why do we observe a sharp and dramatic decrease of the activity while the water content decreases below 6% (or 8%) without LiI? We don't believe that precipitation of rhodium black can fully explain this phenomenon since we observed a deposit only at 2% water, and in very small quantities. Thus, does water exert a role on the catalytic cycle and what is this role?

- Secondly, why the carbonylation rates remain quite constant whatever the water content when LiI is introduced in the reactor? The hypothesis of the formation of a dianionic complex increasing the methyl iodide oxidative addition rate is not convincing since the carbonylation rates above a water content of 6% (or 8%) are similar with or without lithium iodide. So, what is the role of lithium iodide in the rhodium catalytic cycle?

- Thirdly, if the carbonylation rates are quite the same beyond a water content of 6% (or 8%) with and without LiI and if these carbonylation rates are maintained below a water content of 6% (or 8%) with LiI and decrease dramatically without LiI, do lithium iodide and water play a similar role? Is LiI taking the place of water when the concentration of the latter is too low?

It is largely accepted that the main role of water in the catalytic cycle is to react with acetyl iodide produced from reductive elimination of $[RhI_3(COCH_3)(CO)_2]^-$ 4 to give acetic acid and HI (Sc. 2), but in fact this reactivity cannot explain the marked decrease in the carbonylation rates at low water content since, even at low water content, water is in large excess with respect rhodium concentration.

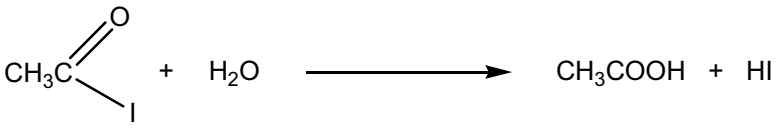

Scheme 2 : Reaction of water with acetyliodide

Lithium iodide can react with acetic acid to form lithium acetate and HI, the latter being able to react with methyl acetate producing acetic acid and methyl iodide (or LiI reacts directly with methyl acetate to give lithium acetate ion and methyl iodide)[5] (Sc. 3). These reactions could increase the methyl iodide concentration in the medium and, since the oxidative addition is first order in CH_3I, accelerate the rate determining step in the rhodium catalytic cycle. As for the higher concentration of methyl iodide when LiI is present in the reaction mixture, the carbonylation rate of the LiI promoted process should be faster than that of the high water content process, but this is not the case, the increase of methyl iodide concentration being to low to really promote the oxidative addition step[6].

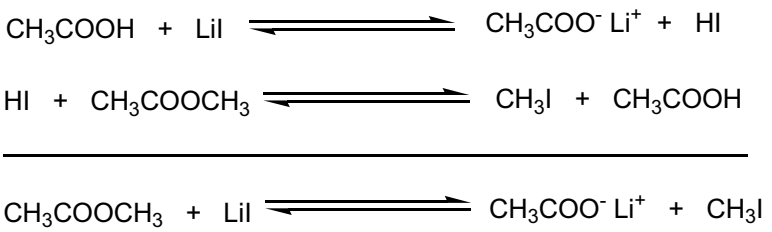

Scheme 3 : Reaction pathway leading CH_3I in the presence of LiI

In order to gain information about the role of water and lithium iodide in the reaction mixture, we performed a series of ^{13}C HP-NMR experiments. Firstly, we have synthesized [PPN][$RhI_4(CO)_2$] 11, which is an intermediate in the water gas shift reaction, in order to collect all IR and NMR data about the long-lived complexes that may be present in the catalytic reaction mixture. [PPN][$RhI_2(CO)_2$] 1 is dissolved in neat dichloromethane and 10 equivalents of HI are added. After 2 h, we only observed by IR (Fig 3) the presence of one CO stretching band at 2090 cm^{-1}, assigned to [PPN][$RhI_4(CO)_2$] 11. Complex 11 was labeled (Fig 3) and its ^{13}C NMR spectrum (Fig 4) shows a doublet at δ = 173.09 ppm (d, $^1J_{Rh-C}$ = 48.10 Hz).

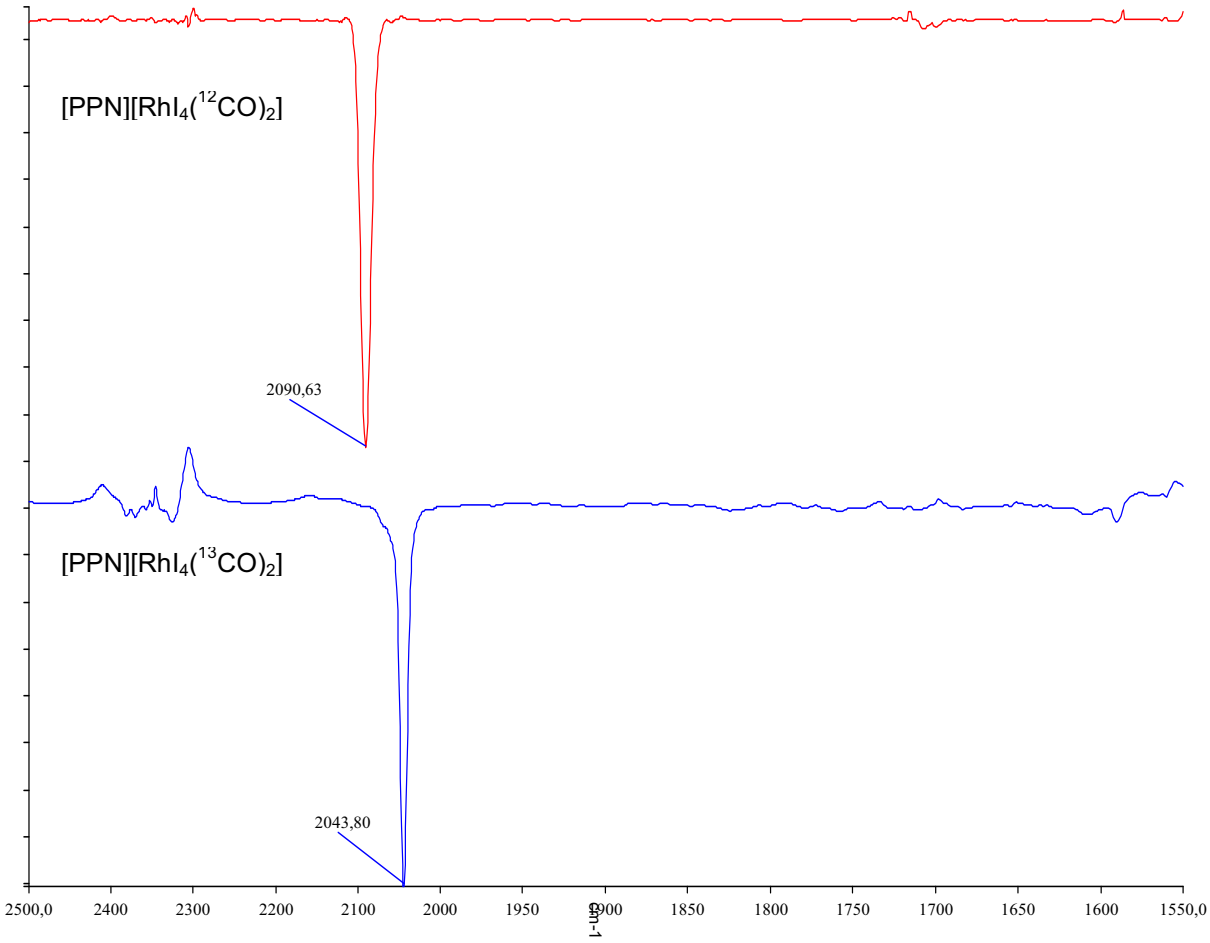

Figure 3 : IR spectra of [PPN][$RhI_4(CO)_2$] 11 and [PPN][$RhI_4(^{13}CO)_2$] 11

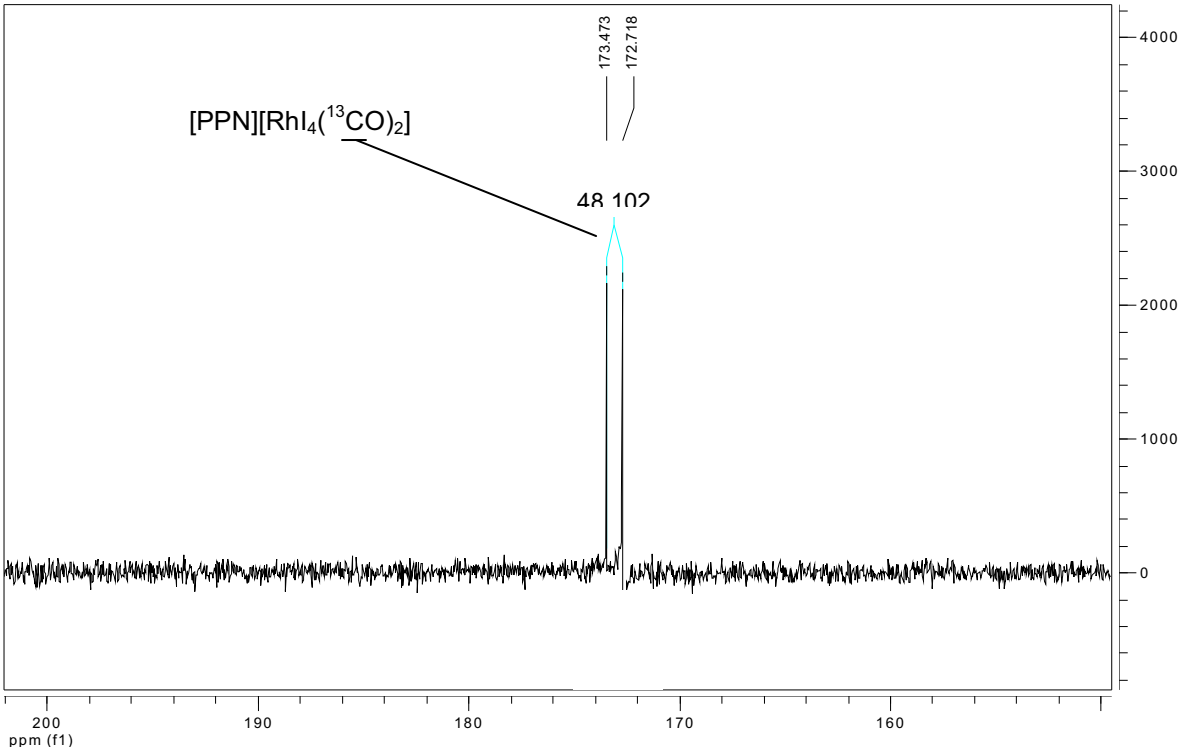

Figure 4 : ^{13}C NMR spectrum of [PPN][$RhI_4(^{13}CO)_2$] 11.

Then, ^{13}C HP-NMR experiments at different water contents were performed. The most representative spectra are shown in figure 5, 6, 7, 8 and 9. We have introduced to the sapphire tube 25 mg of [PPN][$RhI_2(^{13}CO)_2$] 1 (1000 ppm), 27% of methyl acetate, 14% of methyl iodide, water (5%, 10% or 20%) and deuterated acetic acid (balance). The sapphire tube is then sealed and filled with 15 bar of ^{13}CO. Before placing the tube into the NMR probe heated at 90°C, we have shaked it vigorously in order to dissolve the catalyst and ^{13}CO into the solvent. We have observed a significant decrease in the ^{13}CO signal (δ = 185 ppm) during the experiment due to its consumption or its going back to the gas phase at 90°C without stirring. Thus, we analyzed the reaction mixture during 10 min. in order to have the most representative medium comparing to batch experiments performed in an autoclave. We have also checked by gas phase chromatography, before and after the NMR experiments, that we have consumption of water and methyl acetate and formation of acetic acid but it was not possible to provide carbonylation rates since we have no information on the CO consumption and the real reaction time. Finally, we have repeated the same experiments by introducing 17% of LiI.

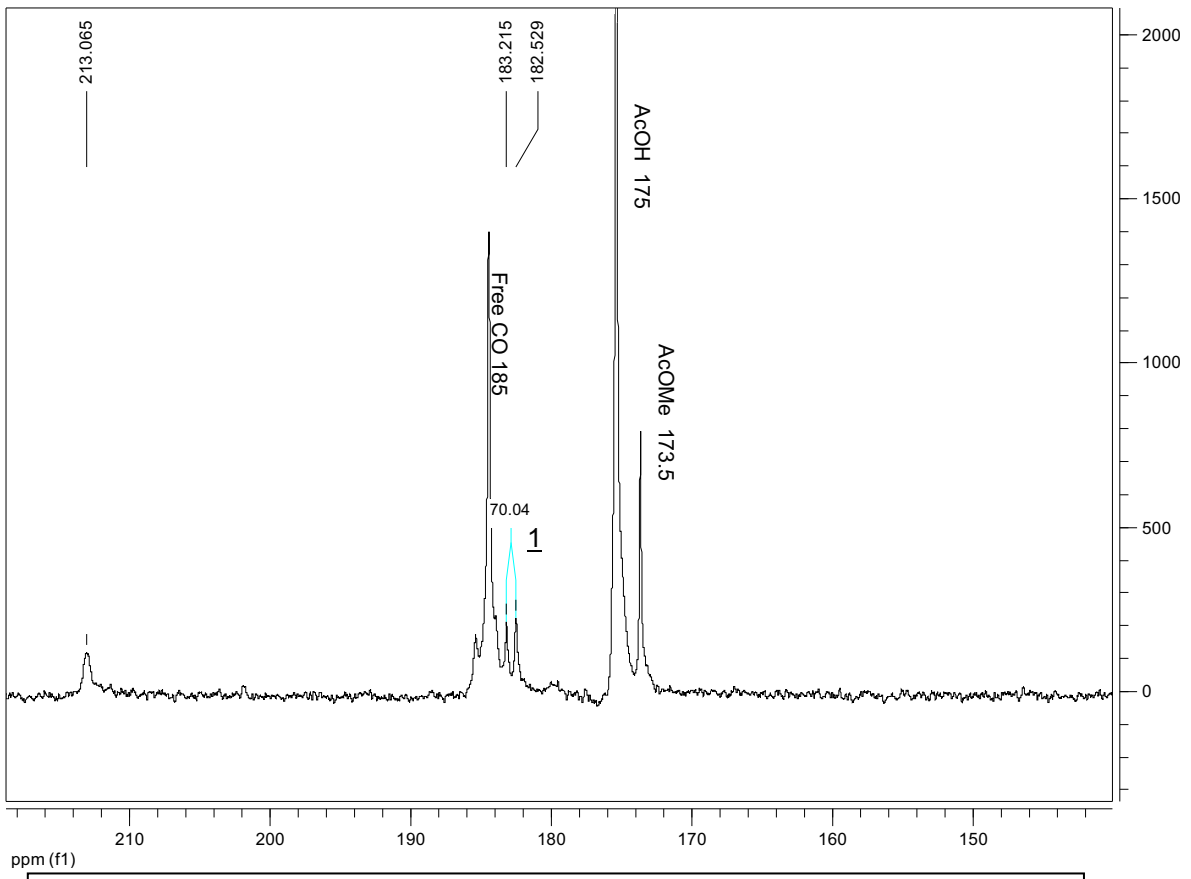

Figure 5 : ^{13}C HP-NMR spectrum of the carbonylation reaction mixture at 20% water.

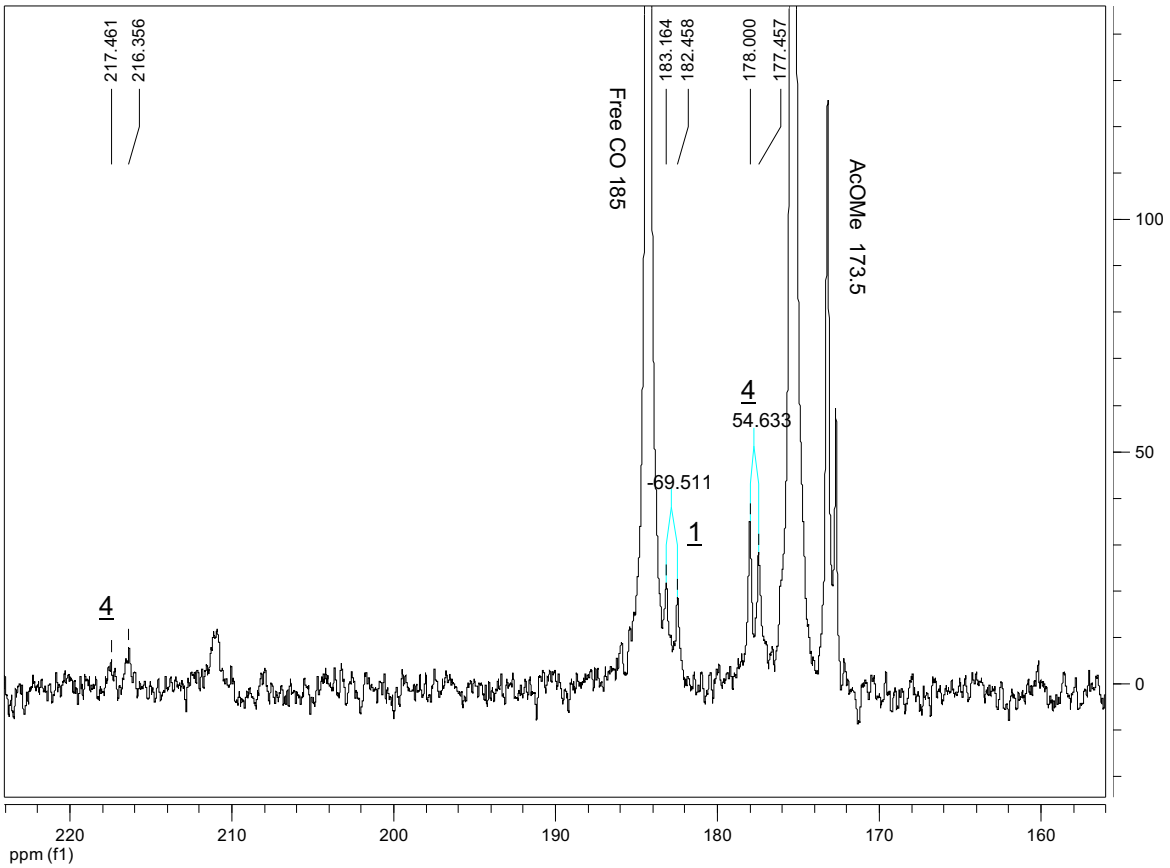

Figure 6 : ^{13}C HP-NMR spectrum of the carbonylation reaction mixture at 10% water.

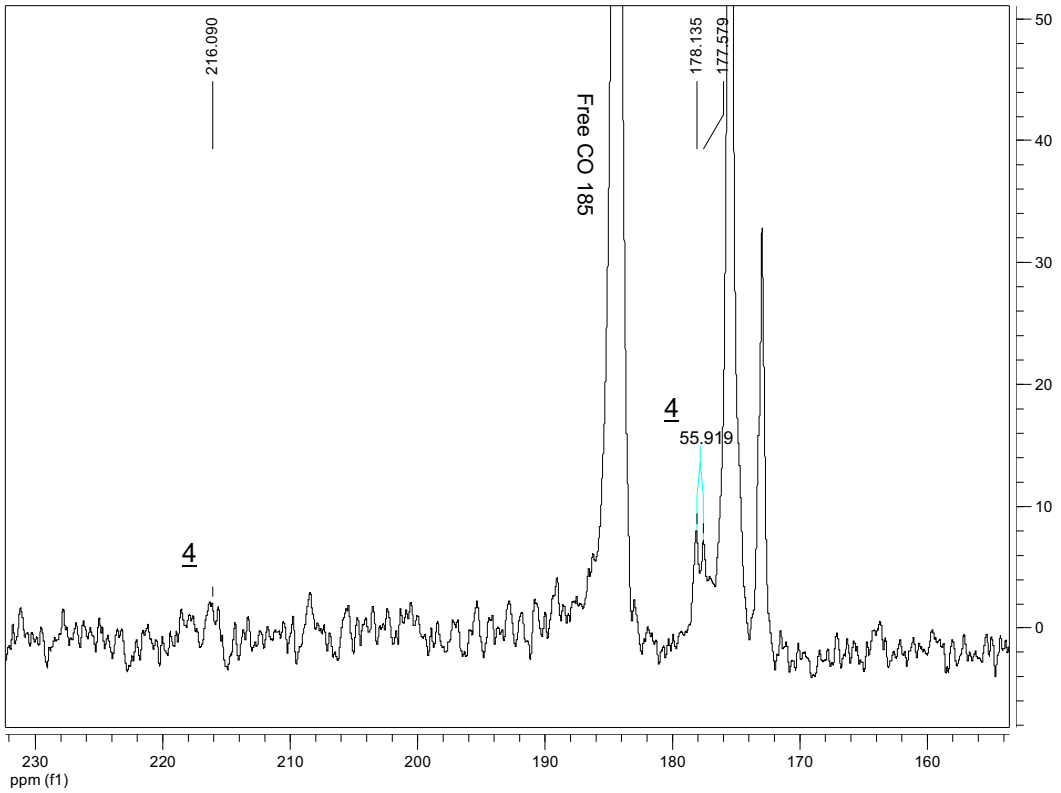

Figure 7 : ^{13}C HP-NMR spectrum of the carbonylation reaction mixture at 5% water.

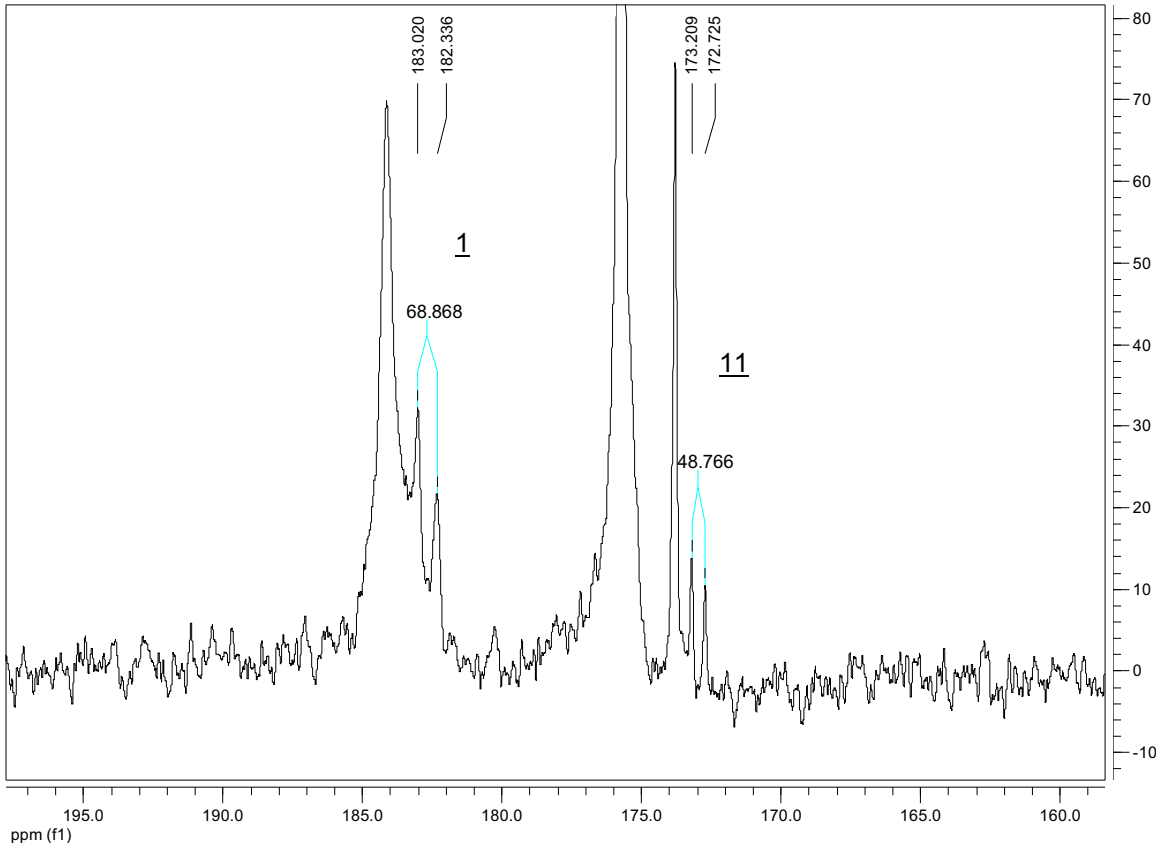

Figure 8 : ^{13}C HP-NMR spectrum of the carbonylation reaction mixture at 20% water with 17% of LiI.

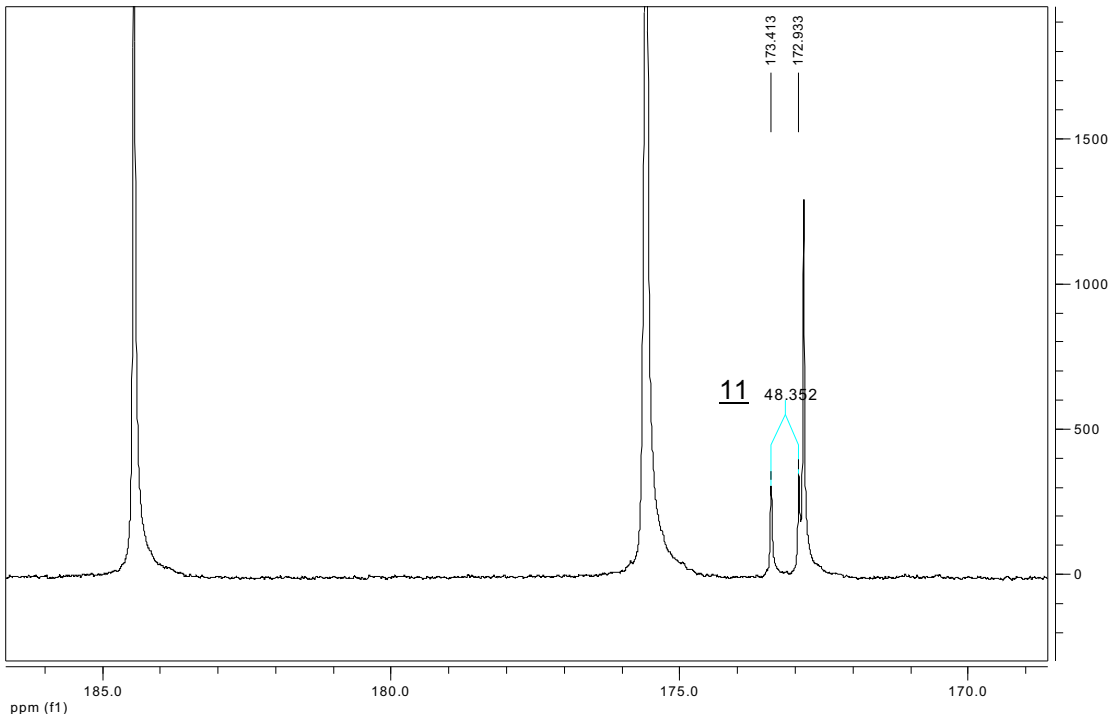

Figure 9 : ^{13}C HP-NMR spectrum of the carbonylation reaction mixture at 10% water with 17% of LiI.

In the above HP-NMR spectra we observe intense peaks: the signal at around δ = 185 ppm corresponds to free dissolved ^{13}CO, the signal at δ = 175 ppm corresponds to $CH_3\boldsymbol{C}OOH$ and the signal at arbout δ = 173.5 ppm to $CH_3\boldsymbol{C}OOCH_3$. We cannot explain the presence of a second signal in figure 6 and why this signal is shifted down in figure 9. Moreover, we observe carbon atoms in rhodium complexes. Since we have checked for every each experiment by gas chromatography that the carbonylation reaction occurs, the rhodium complexes observed are likely to be those with the longer life-times in the medium, that is to say those preceding the rate determining step(s). Results are summarized in table 1.

corresponding figure	water content (wt%)	LiI (wt%)	observed complex(es)
5	20	0	1
6	10	0	1, 4
7	5	0	4
8	20	17	1, 11
9	10	17	11

Table 1 : Summarized HP-NMR experiments.

In the spectrum shown in figure 5 corresponding to the reaction mixture containing 20% of water, we note the presence of a doublet at δ = 182.90 ppm (d, $^1J_{C\text{-}Rh}$ = 70.04 Hz). It's position and the relevant coupling constant are in good agreement with those observed for complex $[PPN][RhI_2(CO)_2]$ 1. Such signal could also correspond to the dimeric acetyl complex 3 but by running the reaction for 30 min. we observed the loss of the CO signal together with the appearance of a doublet at 179.52 ppm (d, $^1J_{Rh\text{-}C}$ = 68.04 Hz) and a signal at 209 ppm strongly suggested that the dimeric acetyl complex 3 is formed wia the loss of CO in the liquid phase

Therefore we can conclude that at high water content, the rate determining step is the oxidative addition reaction as expected.

We also observe a signal at δ = 213.06 ppm that has not been identified. Its position in the acetyl region could point to an acetyl species but no CO terminal corresponding to rhodium complexes of this kind are detected. It could correspond to acetate ions. Another small signal is present at 186 ppm, which we coul not identify.

When decreasing the water content to 10% (Fig. 6), we note some changes in the spectrum. Indeed, we observe the appearance of two novel signals at δ = 177.73 ppm (d, $^{1}J_{C\text{-}Rh}$ = 54.63 Hz) and at δ = 216.90 ppm, not well defined. The observed chemical shifts are good agreement with those obtained for complex [PPN][$RhI_3(COCH_3)(CO)_2$] 4. We observe also a signal at δ = 182.82 ppm (d, $^{1}J_{C\text{-}Rh}$ = 69.51 Hz) assigned to complex 1, and another unidentified signal at 173 ppm.

These pieces of observation mean that under these operating conditions two steps presents similar rates: oxidative addition as expected but also reductive elimination.

By decreasing the water content to 5% (Fig. 7), we only observe a doublet at δ = 177.86 ppm (d, $^{1}J_{C\text{-}Rh}$ = 55.92 Hz) assigned to complex 4, the signal corresponding to the acetyl group being presumably hidden by the spectrum noise.

At low water content, the reductive elimination reaction is slower than oxidative addition and becomes the rate determining step in the rhodium catalytic cycle.

It is worth noting that, at low water content, when we removed the sapphire tube from the NMR probe, we noted dark metallic deposit on the tube wall. This can explain the low definition of the spectrum.

We ran the same experiments again by introducing 17% of LiI. In figure 8, at 20% of water, we observe two doublets at δ = 182.68 ppm (d, $^{1}J_{C\text{-}Rh}$ = 68.87 Hz) corresponding to [PPN][$RhI_2(CO)_2$] 1, and at δ = 172.97 ppm (d, $^{1}J_{C\text{-}Rh}$ = 48.77 Hz) corresponding to [PPN][$RhI_4(CO)_2$] 11. Thus, addition of lithium iodide in the reaction mixture does affect the equilibrium between [PPN][$RhI_2(CO)_2$] 1 and [PPN][$RhI_4(CO)_2$] 11 without changing the carbonylation rate (Fig 1 and 2).

When we decrease the water content to 10% (Fig 7), we only observe a doublet at δ = 173.17 ppm (d, $^{1}J_{C\text{-}Rh}$ = 48.35 Hz) assigned to complex [PPN][$RhI_4(CO)_2$] 11. It is worth noting that no signal corresponding to the acetyl complex 4 is observed.

As far as these results are concerned, at low water content without LiI and at 10 wt% of methyl iodide the rate determining step in the rhodium catalytic cycle is reductive elimination. Addition of higher amounts of water changes the rate determining step to oxidative addition. Hence we can propose that one role of water in this process is to accelerate the reductive elimination rate.

Concerning the role of lithium iodide, we didn't observe acetyl rhodium species in the medium at low water content for the experiments using 17% of LiI. Hence, in the same way as water, LiI may accelerate the reductive elimination step. In these experiments we also observed the presence of [PPN][$RhI_4(CO)_2$] 11 and [PPN][$RhI_2(CO)_2$] 1 at high water content, but only complex 11 at low water content. This could mean, that high lithium iodide concentrations in the medium might favor the formation of HI by reaction with acetic acid or might accelerate the reductive elimination reaction that also produces HI thus favoring the formation of complex 11, and that water might cause formation of [PPN][$RhI_2(CO)_2$] 1 from [PPN][$RhI_4(CO)_2$] 11. We think that under the conditions used for HP-NMR experiments, the rhodium active species can also catalyze the water gas shift reaction, and that lithium iodide may reduce this side reaction since two iodide ligands must be removed from 11 to produce complex 1. The increase of iodide ions concentration in the medium should then limit this reaction, the resting state becoming complex [PPN][$RhI_4(CO)_2$] 11.

Jones proposed[6] that the reductive elimination reaction could be the rate determining step in the rhodium-catalyzed methanol carbonylation cycle under 8% water content, but no proofs were given for this hypothesis. Regarding the present ^{13}C HP-NMR experiments, we can conclude that water plays a major role, not only on the organic reaction with acetyl iodide to form acetic acid, but also on the final rate of the rhodium catalytic reaction, affecting the

reductive elimination step, as well as lithium iodide. We have summarized these conclusions in the catalytic cycle depicted in scheme 4.

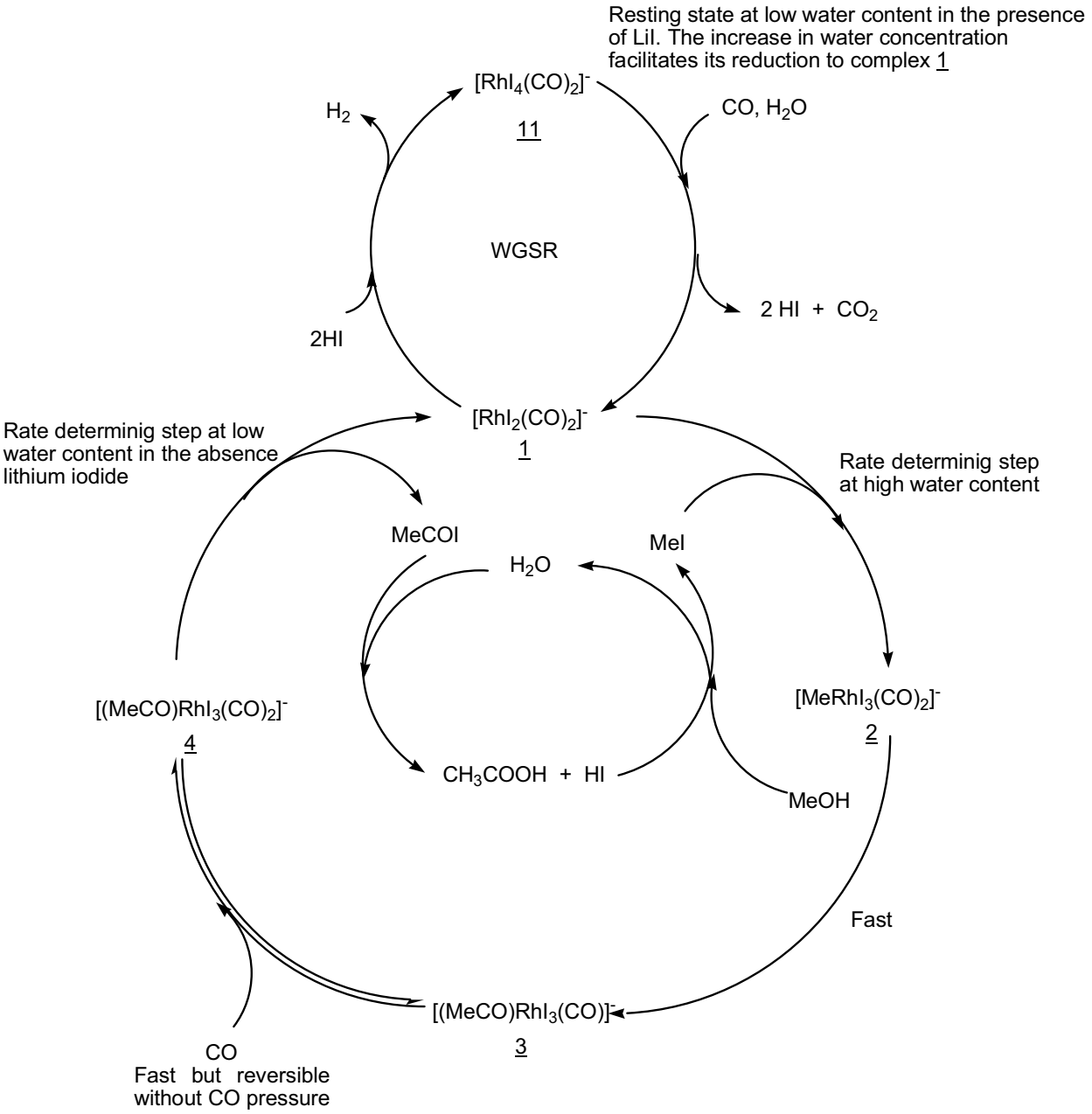

Scheme 4 : Proposed catalytic cycle depending on water and lithium iodide concentration.

III-2 Study of the reductive elimination reaction. Effect of acetate ions.

After careful study of the results obtained in section III-1, we have chosen to focus our attention on the reductive elimination step in the rhodium catalytic cycle. To the best of our knowledge, this reaction has not been examined in detail since it has been admitted thirty years ago it was to be a reductive elimination reaction of CH_3OI from complex 4[8] (Sc 5).

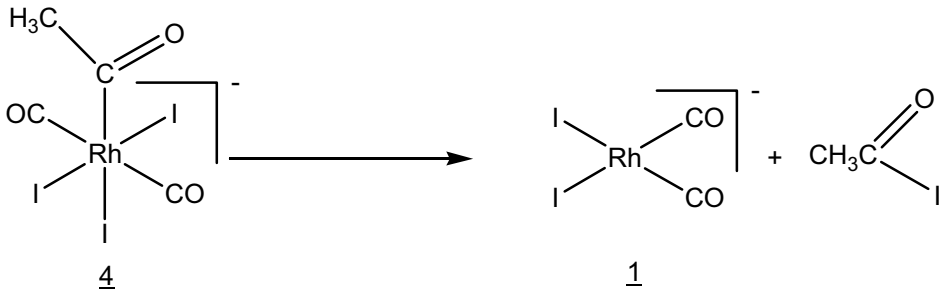

Scheme 5 : Classical reductive elimination reaction

Such reductive elimination pathway doesn't indeed explain the observed effect of water and LiI of on the previously HP-NMR experiments described in section III-1.

We monitored by IR the elimination reaction from $[PPN][RhI_3(COCH_3)(CO)_2]$ 4 and water (Fig. 10). In a Schlenk tube we introduced $[PPN]_2[RhI_3(COCH_3)(CO)]_2$ 3 (25 mg, $1.14.10^{-2}$ mmol) in 5mL of THF (we have chosen THF as solvent since water is not soluble in dichloromethane). After bubbling CO through the solution, we obtained the complex $[PPN][RhI_3(COCH_3)(CO)_2]$ 4 in solution (spectrum in red). Then, we added water (1 g, 55.55 mmol) to the solution and started to measure the reaction time. The reaction was performed under argon at room temperature. By introducing 1 g of water, we reach a molar ratio $[Rh]/[H_2O] = 4.12.10^{-4}$ in solution. If we compare this reaction to the batch experiments described in section III-1, we need to introduce in the reactor 12 g of water corresponding to a batch experiment at 20 wt% water.

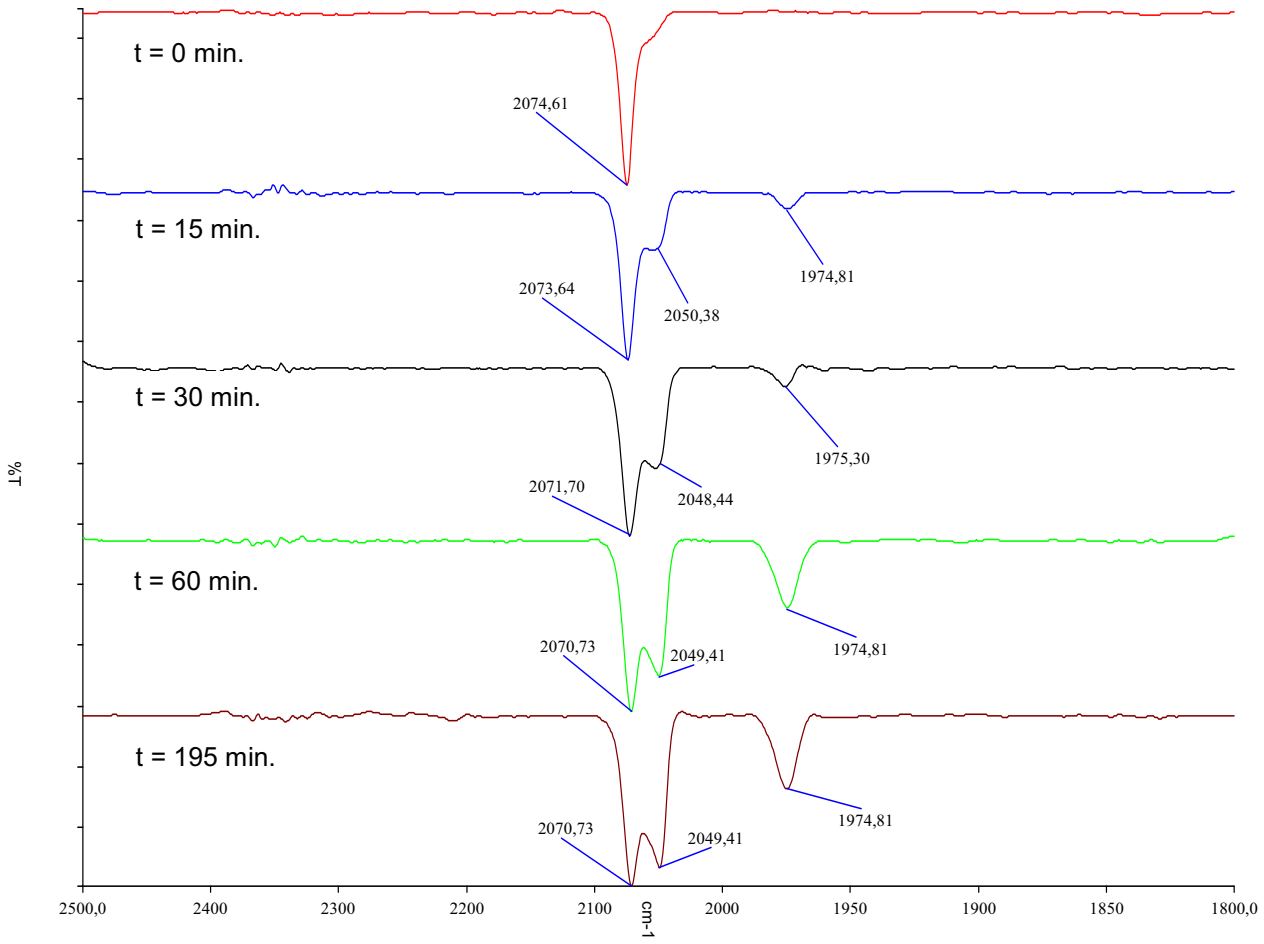

Figure 10 : IR-monitored elimination reaction in the presence of water.

From these spectra, we can note at first sight that the IR active CO stretching band corresponding to the terminal CO ligands of the rhodium complexes in THF is shifted to lower frequencies if compared to the bands observed in dichloromethane. Indeed, the CO band for complex 4 is at 2084 cm^{-1} in dichloromethane and 2074.6 cm^{-1} in THF.

In fact, the IR monitored reaction shows that the reductive elimination reaction occurs under these very conditions. The band at 2074.61 cm^{-1} (spectrum in red) corresponds to complex 4. The two bands at 2049 cm^{-1} and 1975 cm^{-1} correspond to the starting complex 1. During the reaction course, the intensity of the bands corresponding to complex 1 increaes, meaning that the concentration of 1 is increasing in the reaction mixture. After 195 min. reaction, we observed in solution (spectrum in

brown) that two complexes are present: complex 1 and an acetyl complex (band at 2070.7 cm^{-1}). It is worth noting that in the spectra at 60 min. (spectrum in green) and at 195 min (spectrum in blue), we observe no major differences in the intensities of the bands corresponding to complexes 1 and 4. Presumably, under these conditions, water induces reductive elimination which seems to be very slow so that an equilibrium is reached after a long reaction time.

Since water induces elimination, we thought that methanol could be able to induce this reaction too. Hence, we reacted 25 mg of complex 3 in 1mL of dichloromethane and 5 mL of freshly distilled methanol (see Experimental Section) and bubbled CO through the solution in order to obtain complex 4. This reaction was monitored by IR (Fig. 11). Surprisingly, we could not observe any elimination reaction but only the reformation of complex 3, meaning that methanol doesn't induce the expected reductive elimination reaction.

Thus, on one hand, water induces reductive elimination by reacting with acetyl iodide to give acetic acid, and in on the other, methanol does not induce any reductive elimination although it seems possible that methanol may react with acetyl iodide. To confirm this hypothesis, we independently synthesized acetyl iodide[9] starting from acetyl chloride and trimethylsilyliodide and studied its reactivity. The IR spectrum of acetyl iodide is shown in figure 12, and is in agreement with the calculated spectrum.

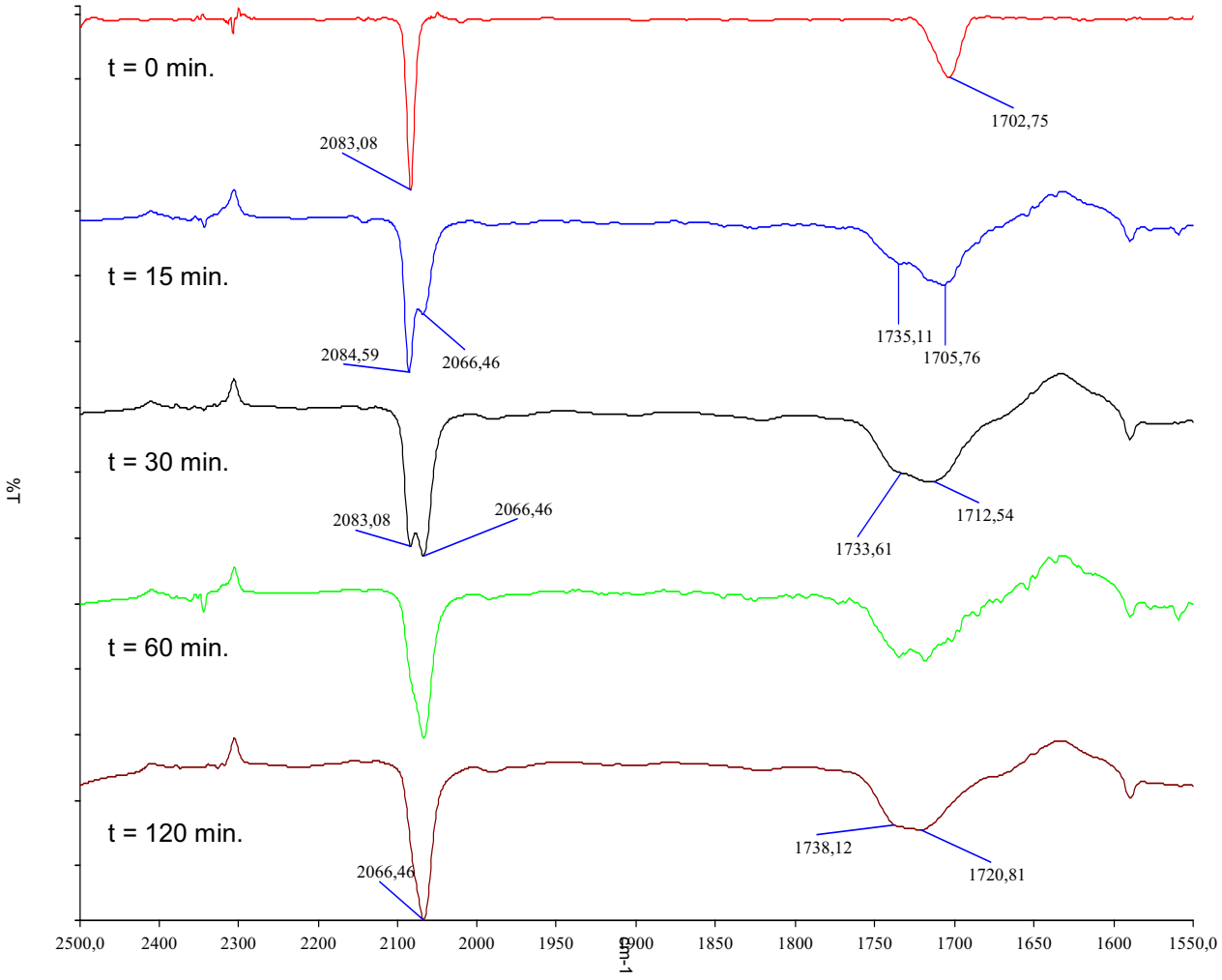

Figure 11 : IR monitored elimination reaction using methanol.

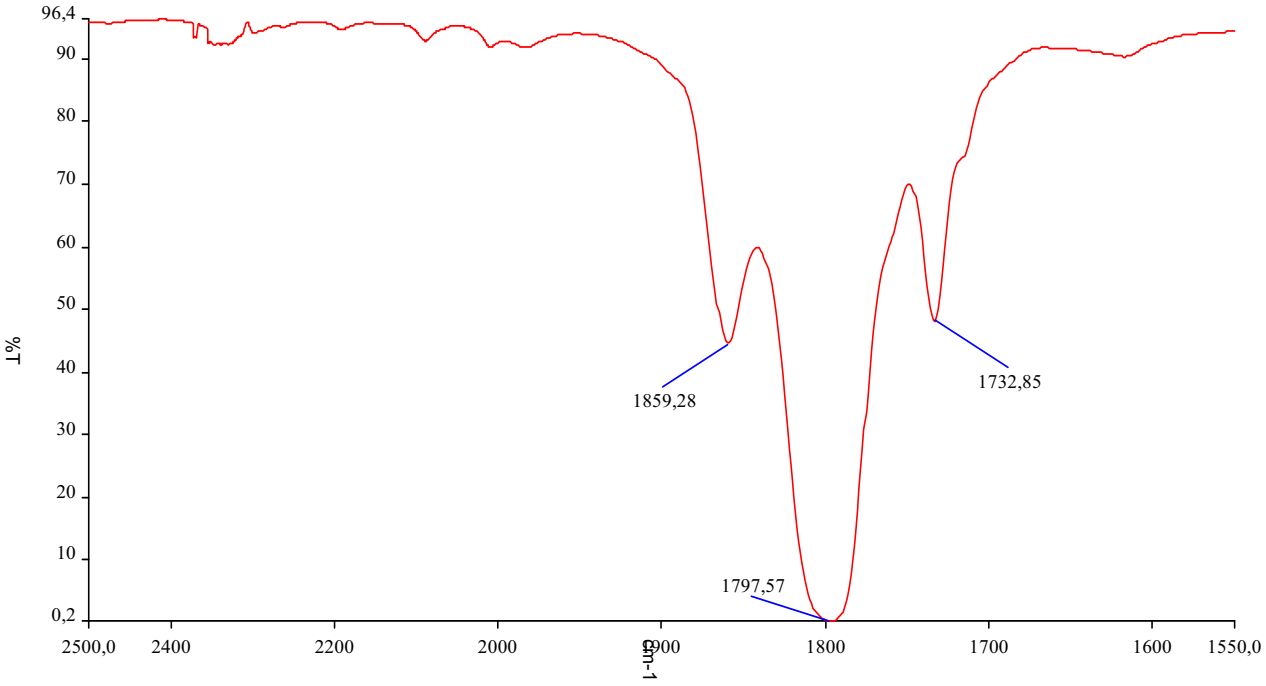

Figure 12 : IR spectrum of acetyliodide.

After this synthesis, we introduced acetyl iodide (2 g, 11.76 mmol) using a dry glass syringe into a dry Schlenk tube containing 5 mL of distilled dichloromethane and dry methanol (0.376 g, 11.76 mmol). Immediate IR analysis of the solution shows the CO stretching band of methyl acetate at 1738 cm^{-1} (Fig. 13).

As acetyl iodide reacts readily with methanol to form methyl acetate, we can believe that in the IR monitored experiment shown in figure 11 there is no formation of acetyliodide by elimination from complex [PPN][$RhI_3(COCH_3)(CO)_2$] 4. On the contrary, we observe a reductive elimination reaction in the IR monitored experiment using water (Fig 10). Thus, we have no proof of the formation of acetyl iodide from acetyl rhodium complex 4 under these conditions.

We believe that in the case of the reaction with water there is a direct interaction of water with the acetyl complex [PPN][$RhI_3(COCH_3)(CO)_2$] 4 whilst that is not the case with methanol, this latter being less reactive than water. In the same way as in the methanolysis

reactions of acetyl palladium complexes[10], we think that a nucleophilic attack of the oxygen atom of water at the electrophilic carbon atom of the acetyl group occurs (Sc 6).

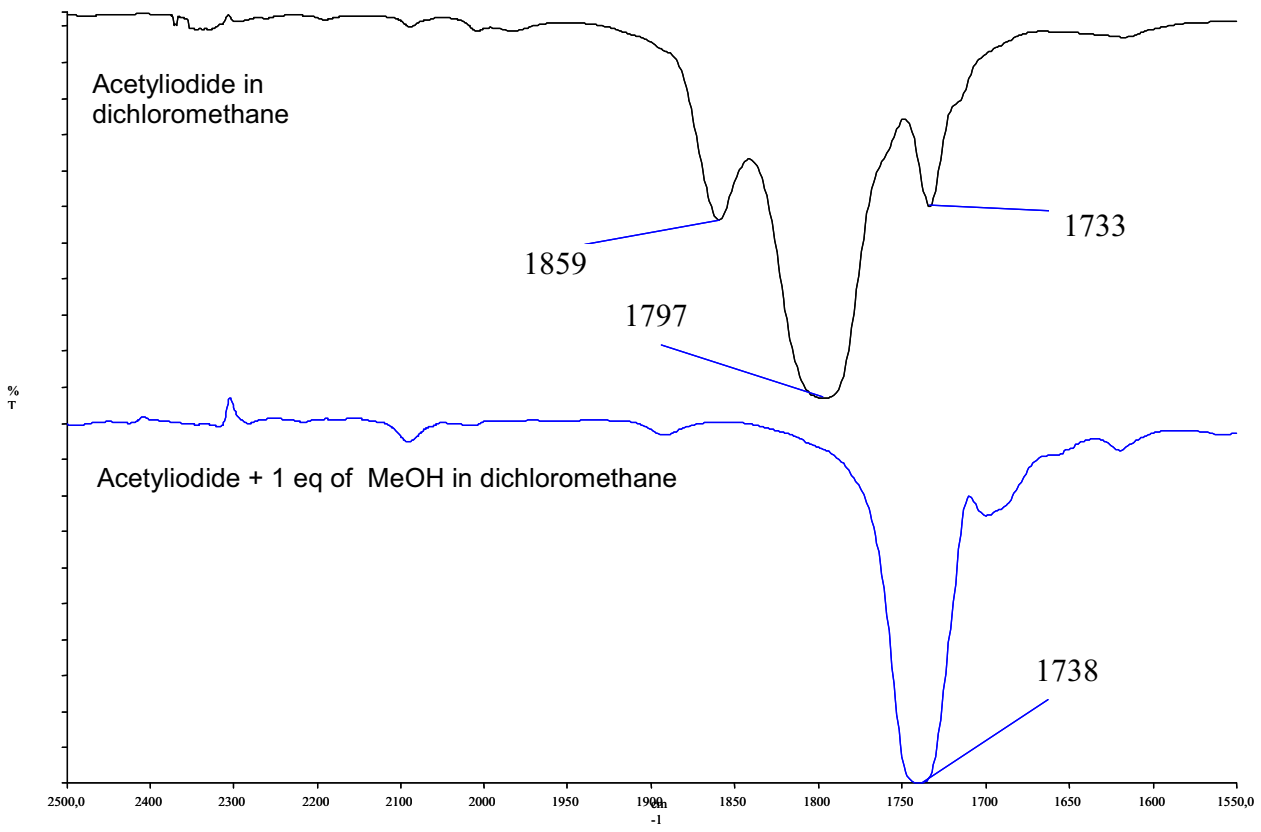

Figure 13 : Reaction of acetyliodide with methanol in dichloromethane.

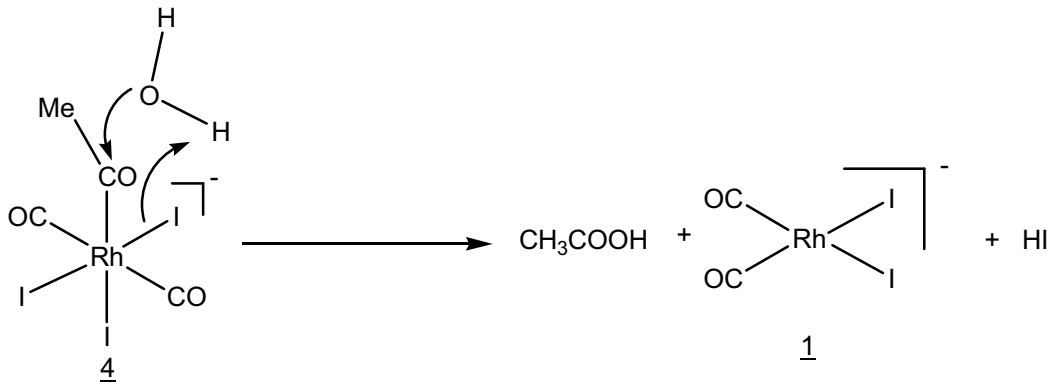

Scheme 6 : Proposed mechanistic pathway for the reaction between complex 4 and water.

Kilner *et al.* suggested such a mechanistic route for the elimination reaction occuring with rhodium[11] and observed that addition of acetic acid to the medium dramatically accelerates this reaction but this phenomenon is still unexplained. It is difficult to link their observations with the results obtained by the HP-NMR experiments (section III-1) since in the experiments in the absence of lithium iodide, the acetic acid content is high and the elimination step is slow at low water content. Moreover, such observations do not explain the LiI accelerating effect on the elimination reaction step.

An overview of all the experimental results, and observations from the literature, led us to the hypothesis that a relationship could exist between the reactivity of water, acetic acid, and lithium iodide. We can suppose that water with acetic acid and LiI with acetic acid are in equilibrium with acetate ions as shown in the two equations of scheme 7

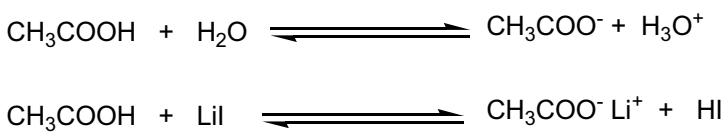

Scheme 7 : Formation of acetate ions from acetic acid, water and LiI

Then, we reacted the rhodium acetyl complex $[PPN][RhI_3(COCH_3)(CO)_2]$ 4 with anhydrous sodium acetate :

In a dried Schlenk tube, $[PPN]_2[RhI_3(COCH_3)(CO)]_2$ 3 (25 mg, $1.14.10^{-2}$ mmol) is dissolved in 5 mL of freshly distilled dichloromethane. CO is bubbled through the solution to obtain complex $[PPN][RhI_3(COCH_3)(CO)_2]$ 4 (25.67 mg, $2.29.10^{-2}$ mmol). Then, anhydrous sodium acetate (94 mg, 1.145 mmol) is added under argon. The reaction is monitored by IR every 5 min. (Fig. 14).

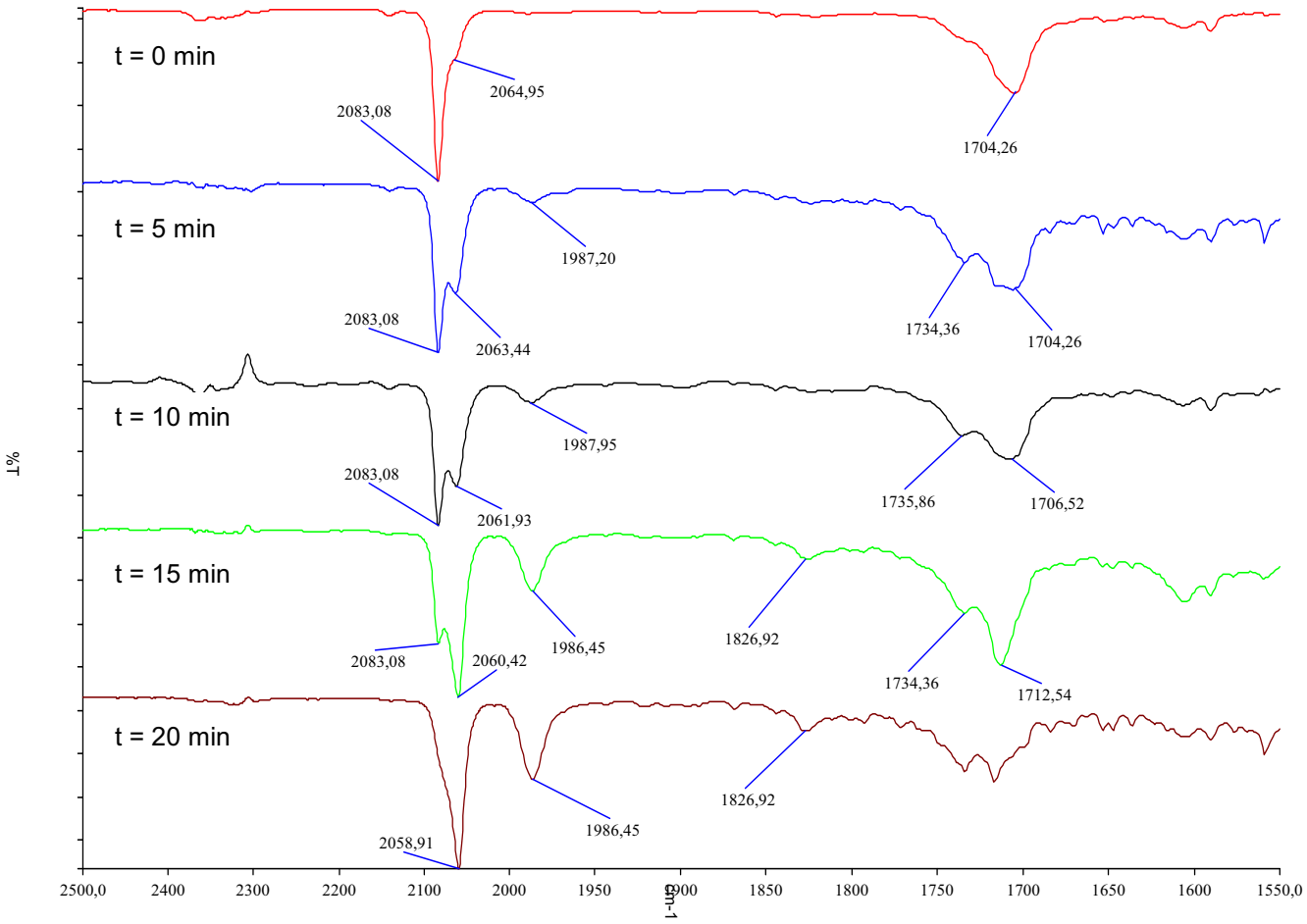

Figure 14 : IR monitored spectra of the mixture from reaction between complex 4 and sodium acetate.

These spectra show that sodium acetate induces elimination reaction from complex 4. Indeed, we observe the appearance of the CO stretching bands at 2058 cm^{-1} and 1986 cm^{-1} corresponding to the starting complex [PPN][$RhI_2(CO)_2$] 1 while the bands at 2084 cm^{-1} and 1704 cm^{-1} corresponding to complex 4 decrease. We can note the appearance of a ν_{CO} band at 1826 cm^{-1} that corresponds to acetic anhydride according to a calculated spectrum.

For this reaction the ratio Rh/AcO^- = 2.10^{-2} is about 100 times higher than the Rh/H_2O ratio used for the reaction shown in figure 10: in this case, we observe a nearly-complete elimination after only 20 min., whilst, for the reaction in presence of water, we still observe big bands of the acetyl complex after 195 min. Moreover, sodium acetate ions have a weak

solubility in dichloromethane. Indeed, addition of 1 mL of methanol to the reaction mixture induces a total and instantaneous elimination giving complex 1, acetic anhydride (1826 cm^{-1}), methyl acetate (1737 cm^{-1}) and acetic acid (1711 cm^{-1}) (Fig 15).

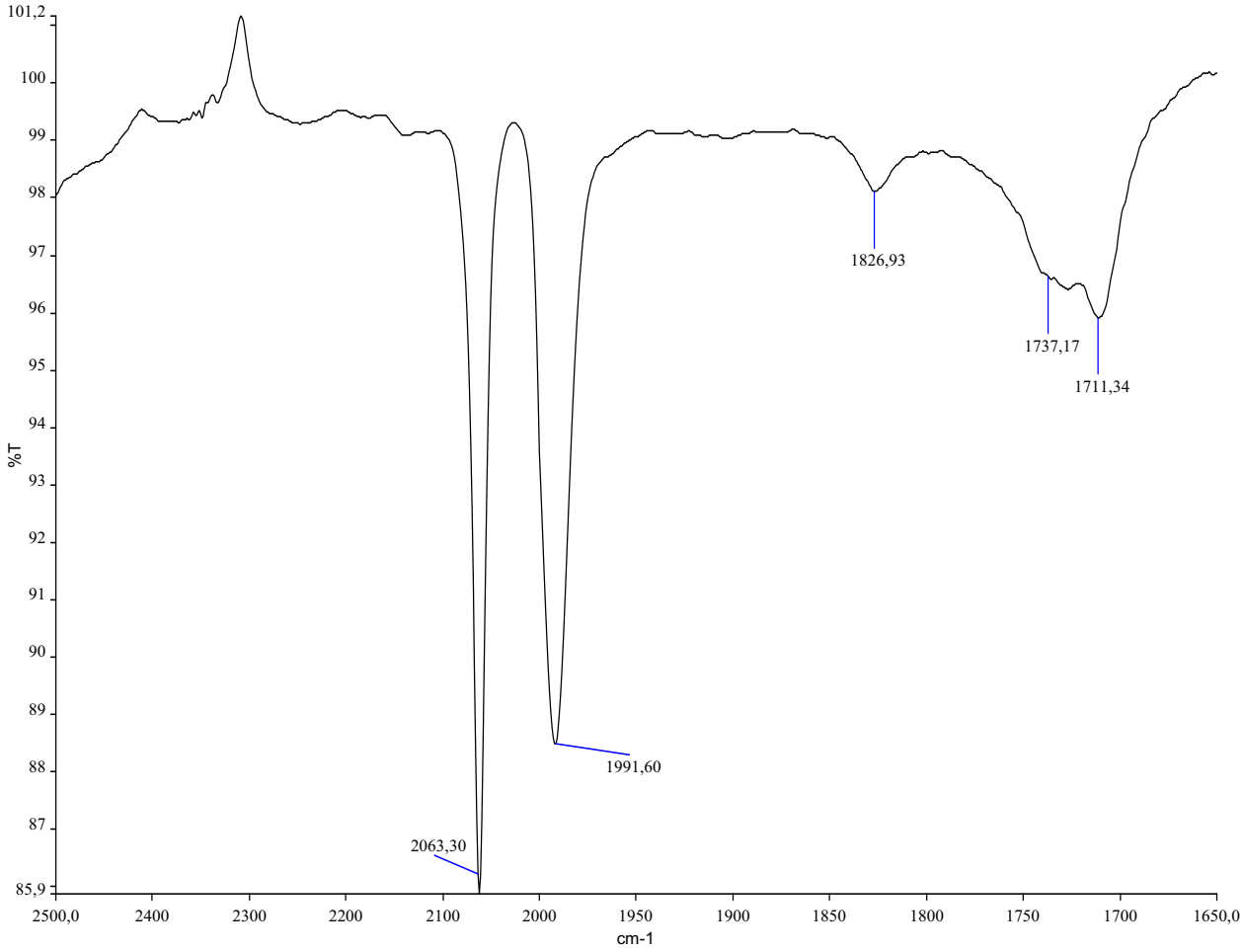

Figure 15 : IR spectrum of the reaction between complex 4 and sodium acetate ions in methanol/CH_2Cl_2 mixture

In addition, we performed the same reaction starting from 10 mg of [PPN][$RhI_3(^{13}COCH_3)(^{13}CO)_2$] 4, obtained after vigorous agitation under of 1 atm. of ^{13}CO of a solution of complex 3, in deuterated dichloromethane with more than 100 excess of sodium acetate. We analyzed the solution by ^{13}C NMR after 1 min. and 5 min of reaction, respectively (Fig 16 and 17). In figure 16, we can note after 1 min. a doublet at 177.73 ppm (d, $^1J_{C\text{-}Rh}$ = 54.27 Hz) together with a doublet at 215.69 ppm corresponding to the dicarbonyl acetyl rhodium complex 4. We can also

observe two doublets at 182.04 ppm and 182.38 ppm together with the signals at 204.108 ppm and 211 ppm corresponding to the mono-carbonyl acetyl rhodium complex 3 formed by the loss in a CO ligand in complex 4. We can note the presence of a singlet at 166.402 ppm that corresponds to the labeled carbon atom of acetic anhydride coming from the labeled acetyl group of complex 4. It is worth noting the presence of a weak signal at about 183 ppm that could correspond to complex 1. After a reaction time of 5 min. (Fig 17), we observe a doublet at 183.84 ppm (d, $^{1}J_{C\text{-}Rh}$ = 70.5 Hz) corresponding to the active complex [PPN][$RhI_2(^{13}CO)_2$] 1, and a signal at 166.53 ppm corresponding to acetic anhydride.

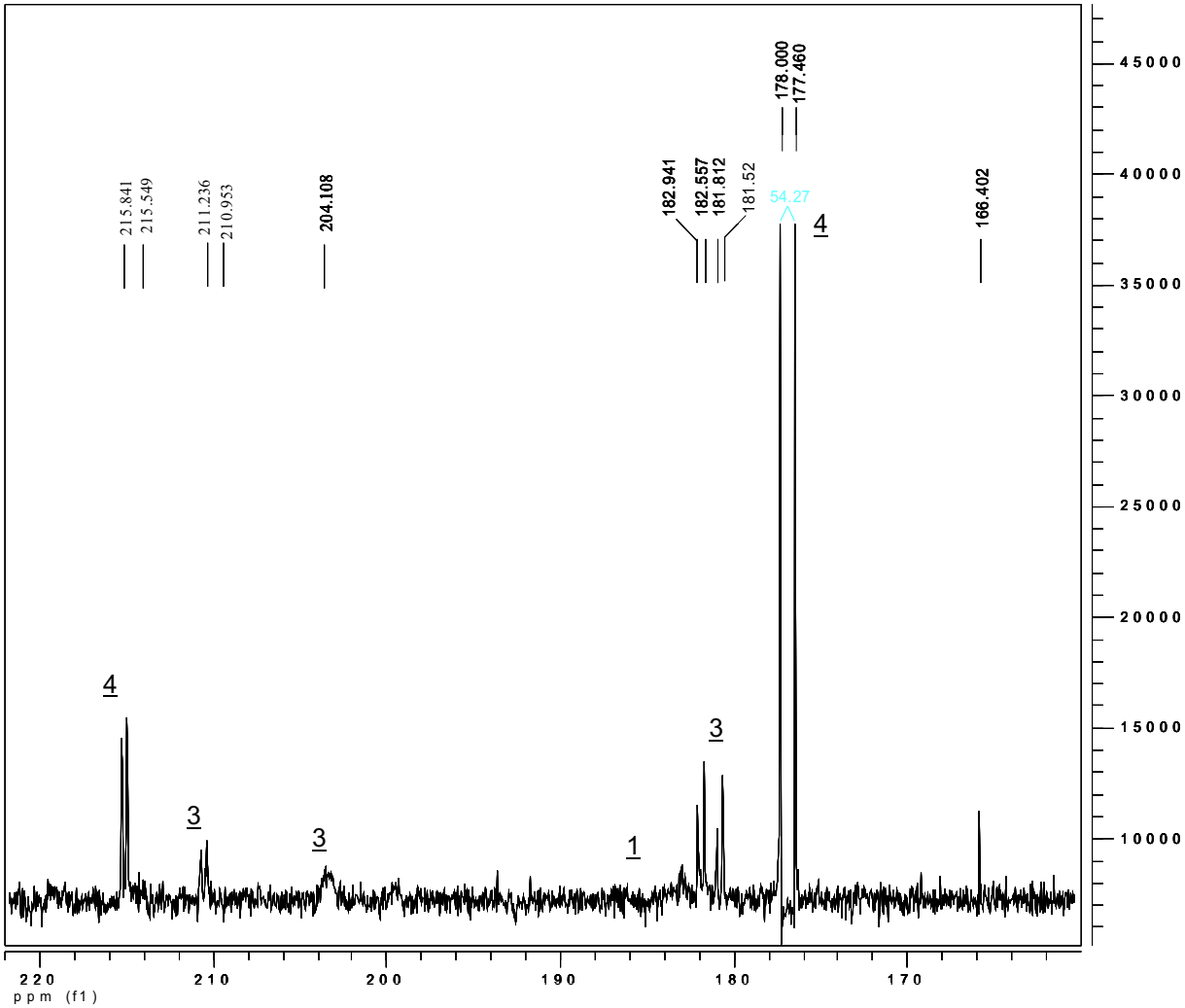

Figure 16 : ^{13}C NMR of the reaction between complex 4 and sodium acetate after 1 min.

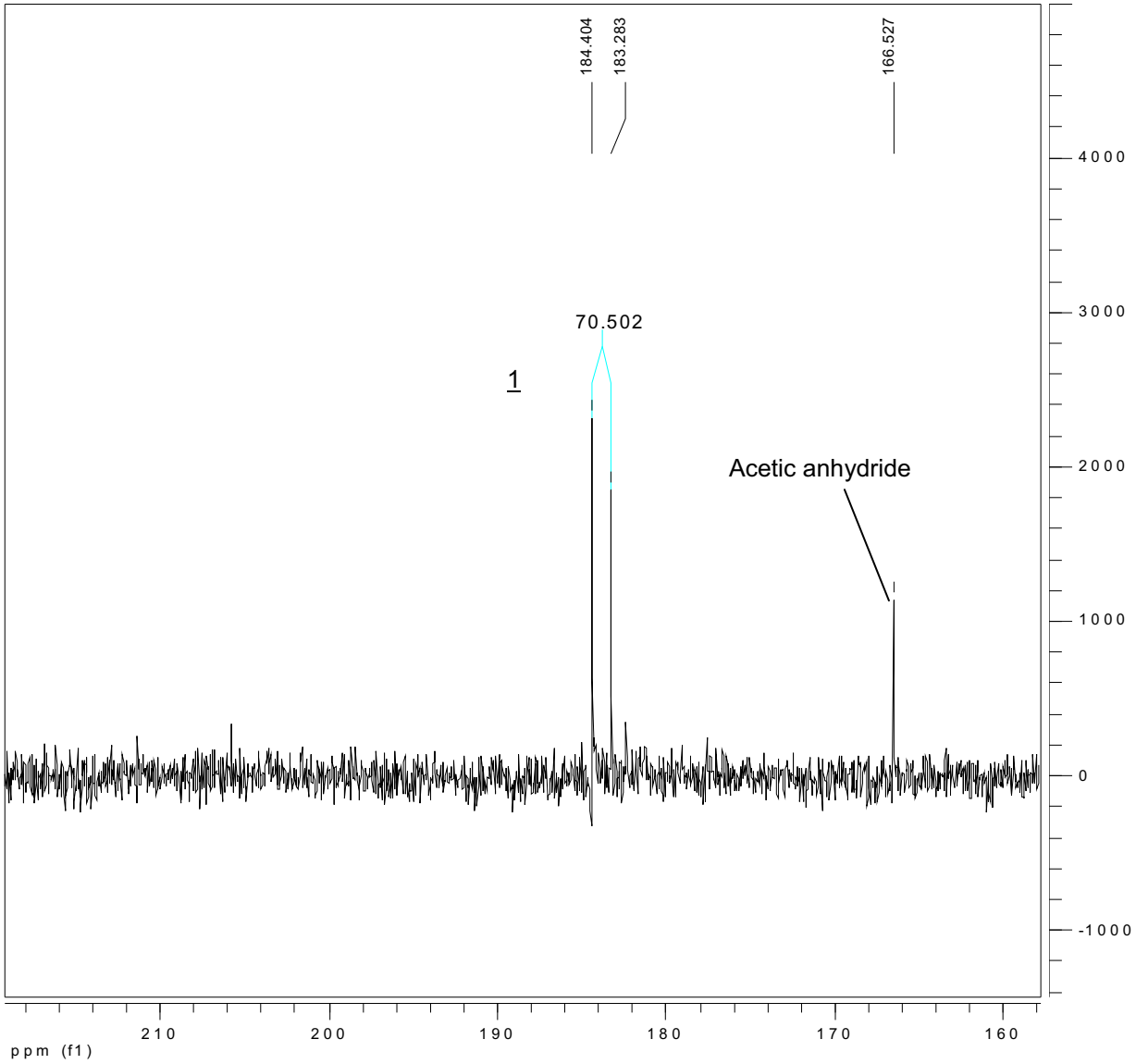

Figure 17 : ^{13}C NMR of the reaction between complex 4 and sodium acetate after 5 min.

The ^{1}H NMR spectrum at the end of the reaction is shown in figure 18. We note the presence of three signals that in fact consist in a singlet at 2.21 ppm and in a doublet (d, $^{2}J_{H-C}$ = 6.7 Hz). This is due to the asymmetric labeling of acetic anhydride: the acetyl group coming from the acetyl rhodium complex 4 is labeled whereas that is not the case for the acetyl group coming from the acetate ion. We can also note the presence of a singlet at 2.17 ppm corresponding to the methyl iodide that remains after the methylation reaction.

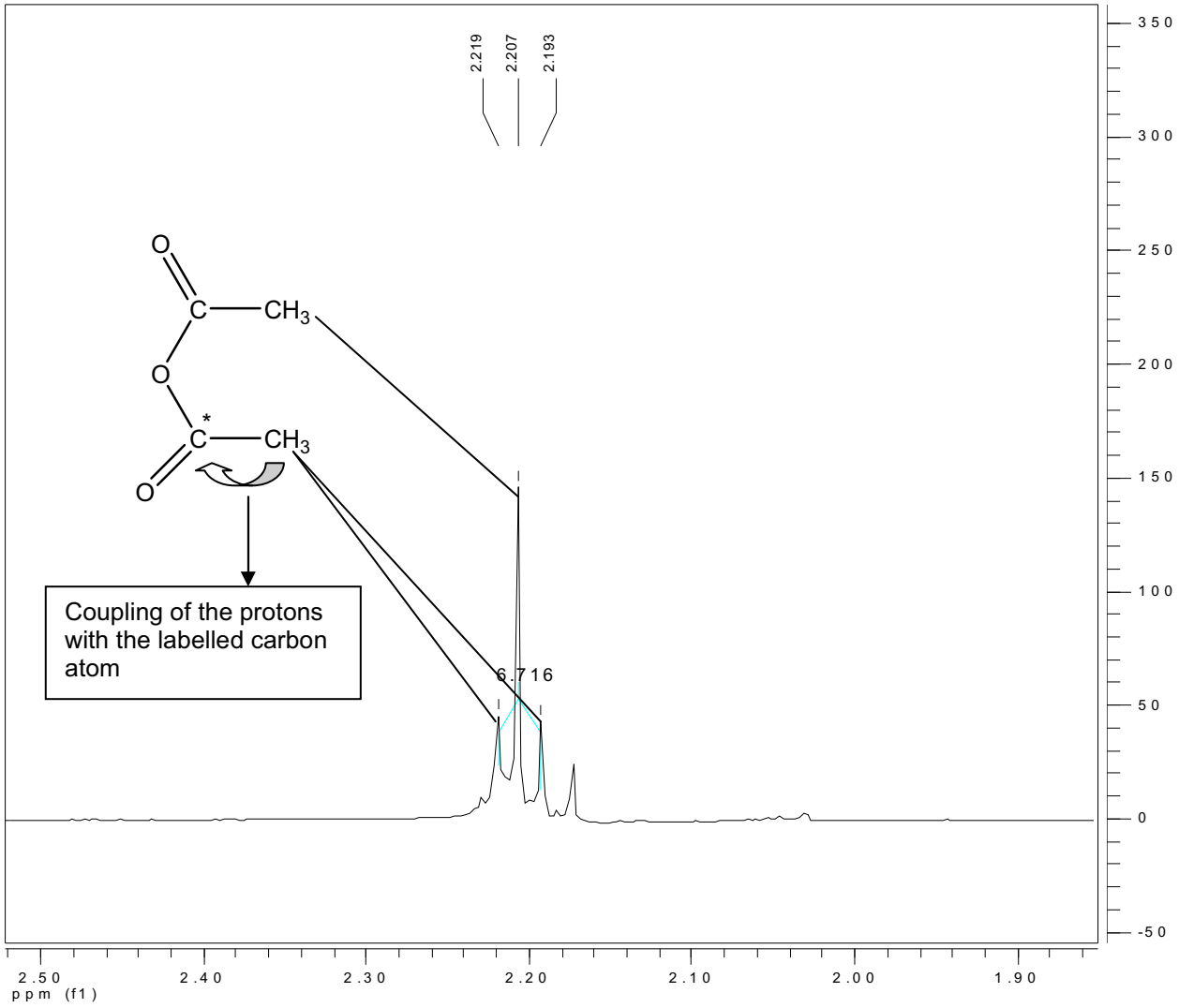

Figure 18 : ^{1}H NMR of the reaction between complex 4 and sodium acetate salt at a reaction time of 5 min.

All of these observations permit the confirmation that acetate ions react with the acetyl rhodium complex [PPN][RhI$_3$(COCH$_3$)(CO)$_2$] 4 affording the active complex [PPN][RhI$_2$(CO)$_2$] 1 and acetic anhydride, which in the reaction medium, reacts with water to form acetic acid. We can reasonably believe that this reaction consist in a nucleophilic attack of the oxygen atom of the acetate ion at the electrophilic acetyl carbon atom in complex 4 (Sc. 8). Under these conditions, the reductive elimination reaction occurs without formation of acetyl iodide.

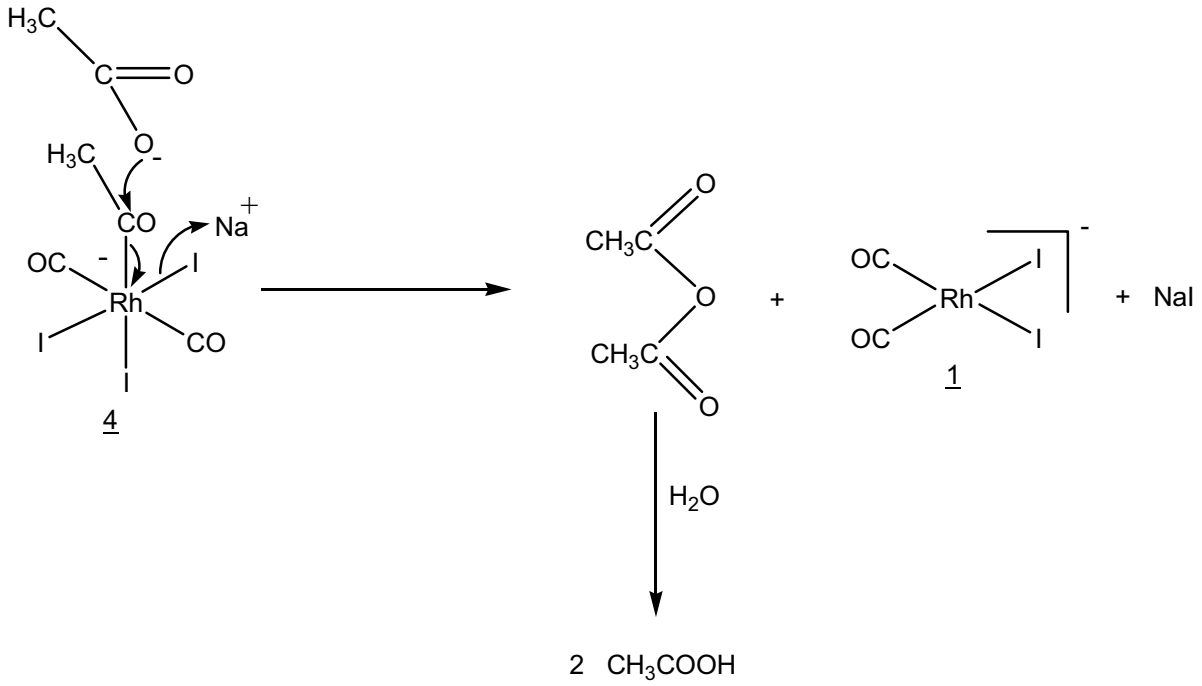

Scheme 8 : Proposed mechanistic pathway for the reaction between complex 4 and the acetate anions.

In summary, in one hand, at high water concentration (Monsanto process) acetate ions are formed in the medium by acetic acid dissociation. In another hand, at low water concentration (Celanese process), acetate ions are formed by the reaction of lithium iodide with acetic acid or methyl acetate. If no water is introduced in the medium, we should obtain only the formation of acetic anhydride. This corresponds to the process used today by Eastman compagny[11]. These conclusions are summarized in scheme 9.

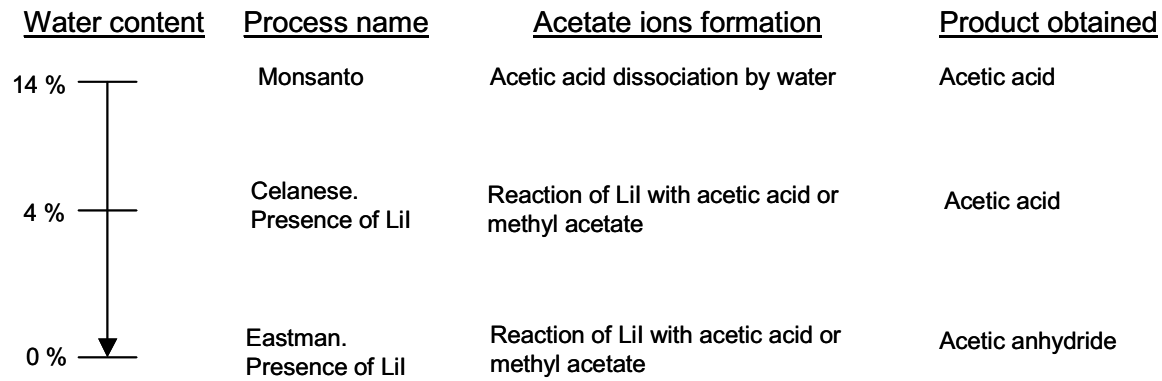

Scheme 9 : Summary of the differents processes depending on water content and the presence of LiI.

In order to confirm that the reaction of lithium iodide with acetic acid or methyl acetate can produce acetate ions together with HI or CH_3I, we have conducted further experiments, dissolving complex 3 in dichloromethane, bubbling CO through the solution so as to obtain complex 4, and adding a solution of acetic acid/LiI or methyl acetate/LiI with different LiI concentrations (50 to 200 equivalents with respect to rhodium concentration). Under these conditions, at room temperature and for reaction time of more than 3 hours, we have not observed the formation of the active complex 1 and acetic anhydride. According to the literature[5], these reactions seem very unlikely to occur under such operative conditions.

For this reason we performed a batch experiment introducing into a Hastelloy reactor the rhodium catalyst directly as $[PPN][RhI_2(CO)_2]$ 1 (800 ppm, 1.10 g) to avoid the preformation step and the use of water, and 25 g of methyl acetate. The reactor was sealed and flushed 3 times with CO. CO pressure was adjusted to 12 bar and the reactor was heated at 190℃ and the medium stirred at 1200 rpm. Once the temperature in the reactor reached 190℃, a solution of methyl acetate/LiI 75 g/50 g was added via an additional over-pressurized reservoir. The total pressure was then adjusted to 30 bar. During the first 30 min., we did not observe any CO consumption, but after this induction period a low CO consumption was noted (carbonylation rate < 1 mol/L/h). After a reaction time of 3 h, the reactor was cooled down to room temperature and depressurized. The analysis of the solution by gas chromatography showed the presence of large amounts of methyl acetate (about 80 wt%) but of also methyl iodide (about 5 wt%), acetic anhydride (about 13 wt%) and small amounts of acetic acid (less than 2 wt%) due to the presence of water in traces.

Thus, the presence of acetic anhydride and methyl iodide at the end of this experiment shows that the carbonylation reaction occurs (but at a very slow carbonylation rate ,since the catalytic medium employed is far from being the best and since the presence of PPN as counter ion may also reduce the activity of the catalyst) without any introduction of methyl iodide into the reactor. This result confirms that methyl iodide is formed from methyl acetate and lithium iodide and that acetate ions can indeed be formed under catalytic conditions (190℃, 30 bar) .

After having confirmed that acetate ions react with the acetyl rhodium complex $[RhI_3(COCH_3)(CO)_2]^-$ 4 and that acetate ions are formed in the catalytic medium in the presence of LiI, we investigated other nucleophilic compounds that could react with complex 4. In a first set of experiments we tested a non-ionic nucleophilic family of molecules such as para-methoxyphenol, triphenylmethanol or urea (Sc. 10). Using different solvent mixtures to dissolve complex 4 and the different nucleophilic compounds, we never observed any reaction, even by heating slightly the reaction mixture (50°C).

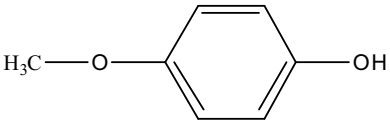

p-Metoxyphenol

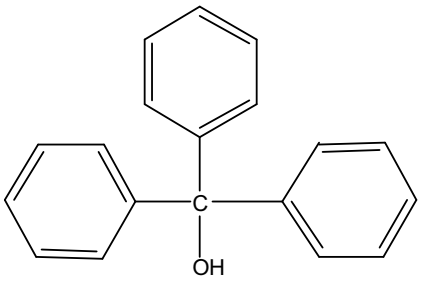

Triphenylmethanol

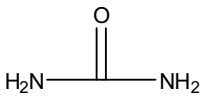

Urea

Scheme 10 : Example of non-ionic nucleophilic molecules tested in the reaction with complex 4.

In a second set of experiments, we tested some strong ionic nucleophilic/basic species as methanolate, obtained by the reaction of sodium with methanol, and sodium hydroxyde (Sc. 11). Introduction of methanolate or sodium hydroxyde into a solution of complex 4 leads instantaneously to the formation of rhodium black. No CO stretching band was observed by IR spectroscopy.

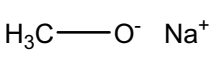

sodium methanolate

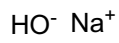

sodium hydroxyde

Scheme 11 : Example of strong ionic nucleophilic/basic species tested in the reaction with complex 4

In a third set of experiment, we checked other carboxylate anions than the acetate ions, such as sodium butyrate or sodium benzoate (Sc. 12)

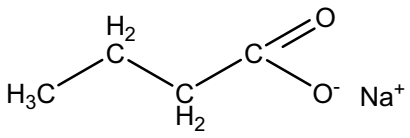

sodium butyrate

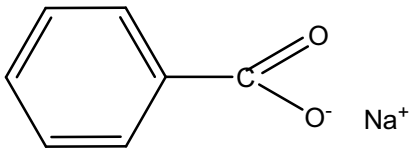

sodium benzoate

Scheme 12 : Example of carboxylate anions tested in the reaction with complex 4.

In each case we observed reaction between the carboxylate ion and the rhodium acetyl complex 4 giving the active complex 1 and mixed anhydride compounds. We monitored by IR (Fig. 19) the reaction of [PPN][$RhI_3(COCH_3)(CO)_2$] 4 (25.67 mg, $2.29.10^{-2}$ mmol) in 10 mL of anhydrous dichloromethane, obtained after bubbling CO through a solution of [PPN][$RhI_3(COCH_3)(CO)$] 3 (25 mg, $2.29.10^{-2}$ mmol), with sodium butyrate (0.126g, 1.14 mmol). We could observe the formation of complex [PPN][$RhI_2(CO)_2$] 1 , characterized by bands at 2057 cm^{-1} and 1986 cm^{-1}, together with a shouldered band at 1824 cm^{-1} assigned to the corresponding mixed anhydride. This result shows that sodium butyrate reacts readily with complex 4. This is maybe due to the higher solubility of sodium butyrate in dichloromethane.

We performed the same experiment using labeled [PPN][$RhI_3(^{13}COCH_3)(^{13}CO)_2$] 4 in deuterated dichloromethane. The corresponding ^{13}C NMR spectrum is shown in figure 20. In this spectrum we observe the doublet of the starting complex 1 at 184 ppm (d, $^1JC\text{-}Rh$ = 70.40 Hz), but also 2 signals at 166.72 ppm and 166.90 ppm corresponding to the carbonyl carbon atom of the anhydride. This observation is surprising since only the carbon atom of the rhodium acetyl carbonyl is labeled. We believe that a side reaction can occur, in that sodium butyrate reacts with the mixed anhydride giving an acetate ion that can react again with the mixed anhydride or with complex 10 giving acetic anhydride (Sc. 13)

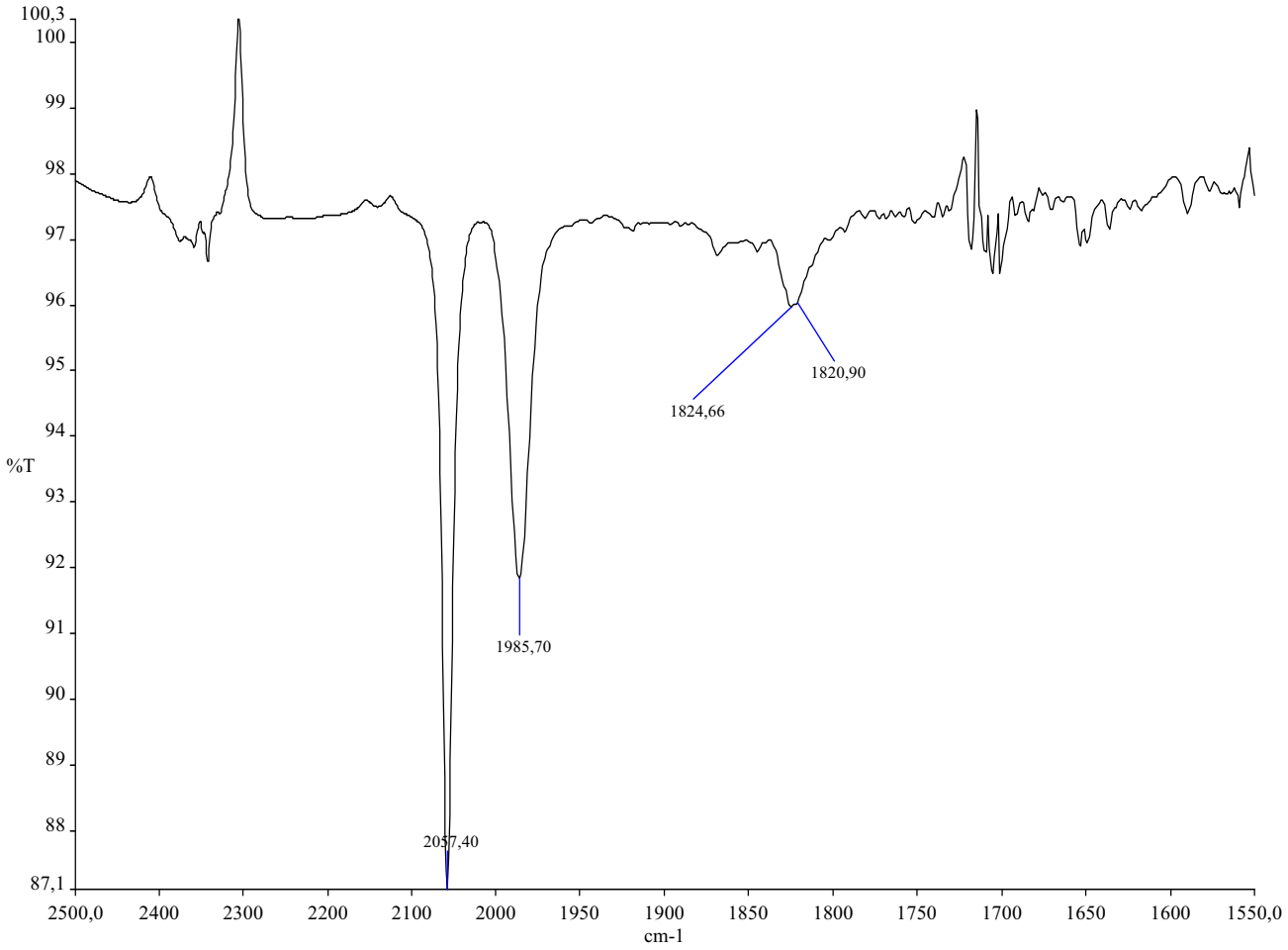

Figure 19 : IR spectrum of the reaction between sodium butyrate and complex 4.

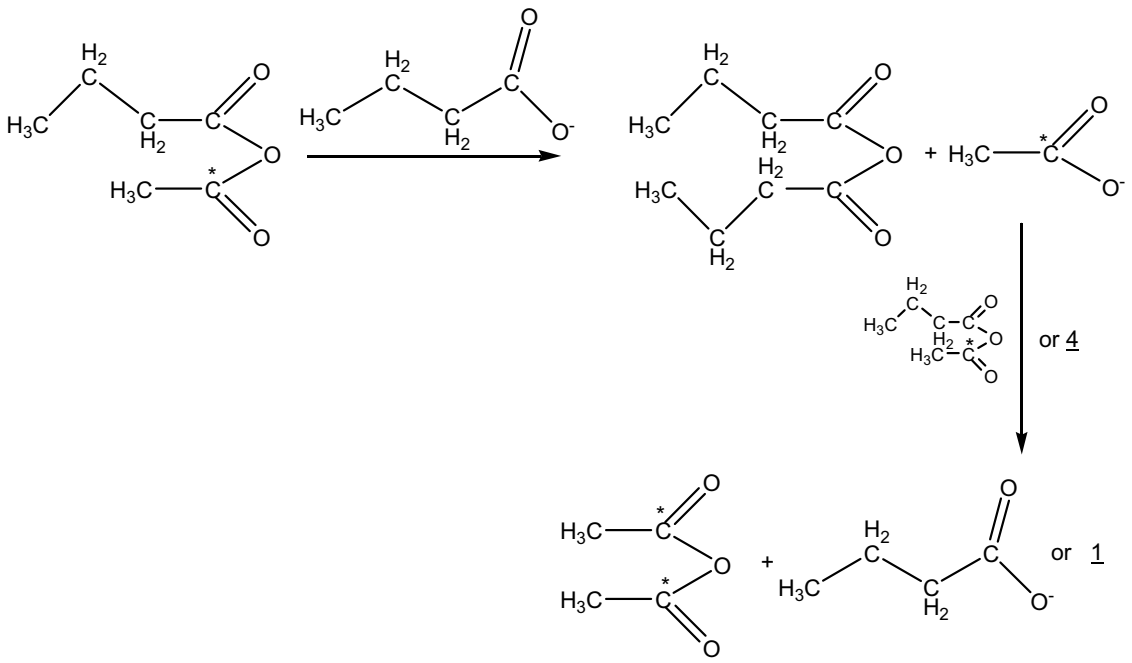

Scheme 13 : Proposed side reaction between sodium butyrate and mixed anhydride

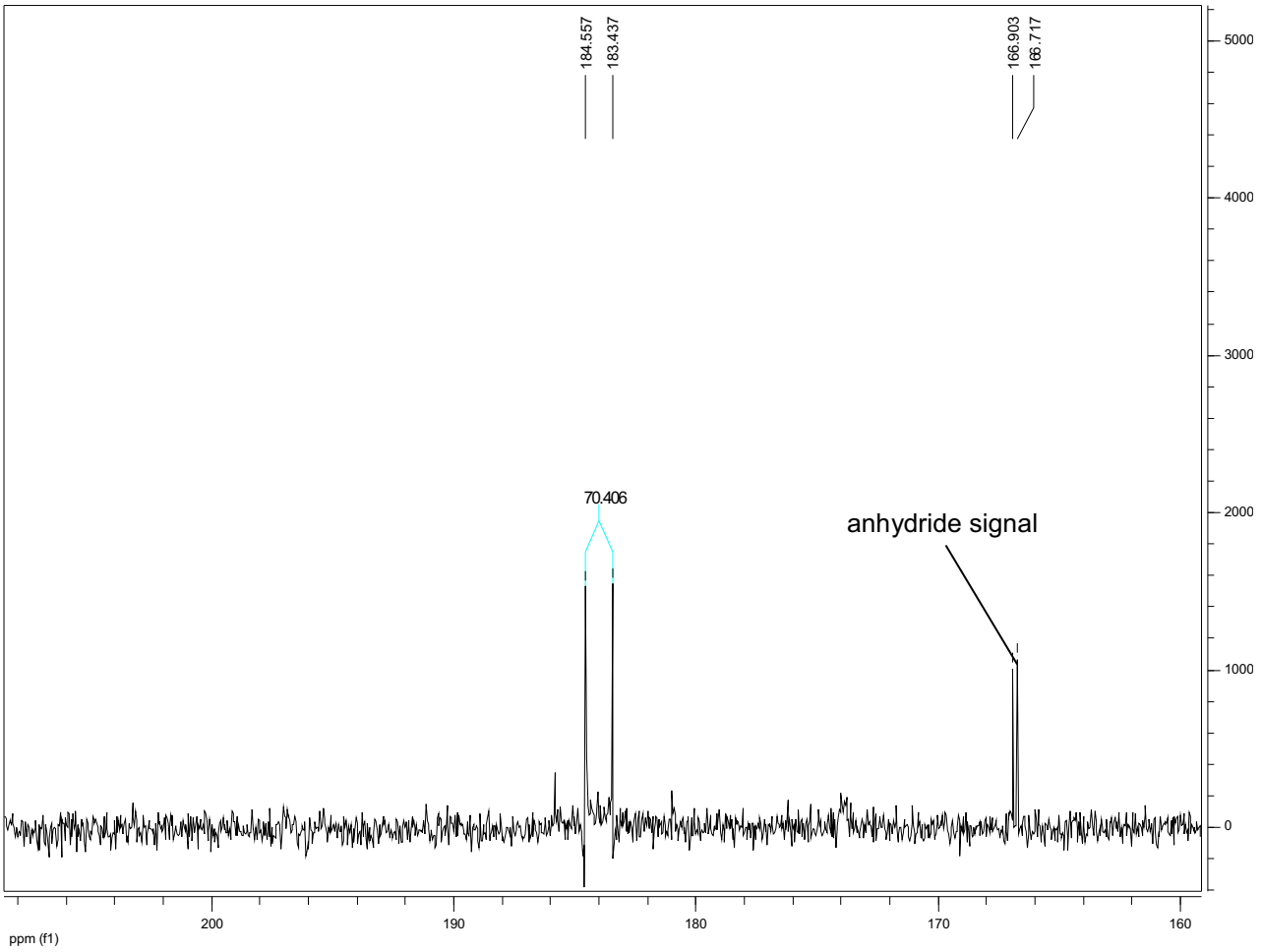

Figure 20 : ^{13}C NMR spectrum of the reaction between sodium butyrate and labelled complex 4.

The ^{1}H NMR spectrum of this reaction mixture is shown in figure 21. We observe several proton signals. The triplet at 0.98 ppm corresponds to the terminal CH_3 of the butyrate chain, a sextet at 1.68 ppm corresponds to the β-CH_2 of the butyrate group and a triplet at 2.44 ppm is related to the α-CH_2 group. For every each signal, we can observe a further smaller signal, respectively a triplet, a sextet and a triplet, meaning that another anhydride molecule containing a butyrate part is present. We observe also two doublets at 2.22 ppm (d, $^{2}J_{H-C}$ = 7.35 Hz) and 2.20 ppm (d, $^{2}J_{H-C}$ = 7.30 Hz), attributed to two CH_3 signals of the acetate in two different anhydride molecules. We note that each coupling constant is different from those observed in figure 18 for acetic anhydride, whereas the chemical shifts are in good agreement. We have no explanation for this phenomenon at this time, but these results obviously confirm that two different anhydride molecules are present. We should stress the presence of methyl iodide (2.17 ppm) in the medium.

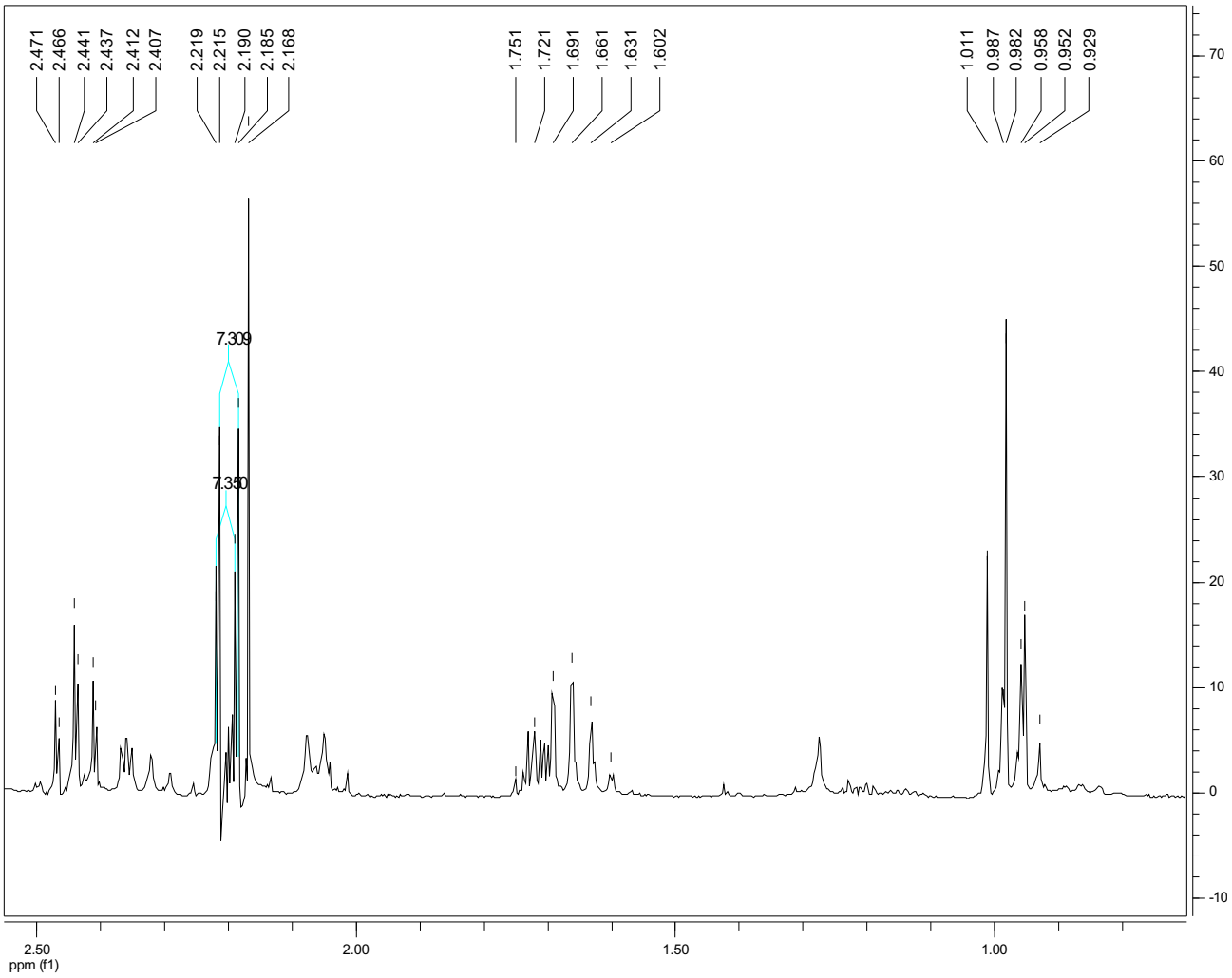

Figure 21 : ^{1}H NMR spectrum of the reaction between sodium butyrate and labelled complex 4.

Thus, almost all of the carboxylate salts we tested react with the rhodium acetyl complex 4 giving complex 1 and mixed anhydrides, their reactivity depending upon their solubility in the medium.

As a further step, we were also interested in investigating the reactivity of the monocarbonyl rhodium acetyl complex $[PPN]_2[RhI_3(COCH_3)(CO)]_2$ 3 with carboxylate ions and especially with acetate. Indeed, complex 3 contains a more electrophilic carbon in its acetyl group than 4. For this purpose, in a dried Schlenk tube we dissolved the complex $[PPN]_2[RhI_3(COCH_3)(CO)]_2$ 3 (25 mg,

2.29.10-2 mmol) in 5 mL of anhydrous dichloromethane. Then, sodium acetate (94 mg, 1.14 mmol) was added to the solution. The reaction was monitored by IR (Fig. 22).

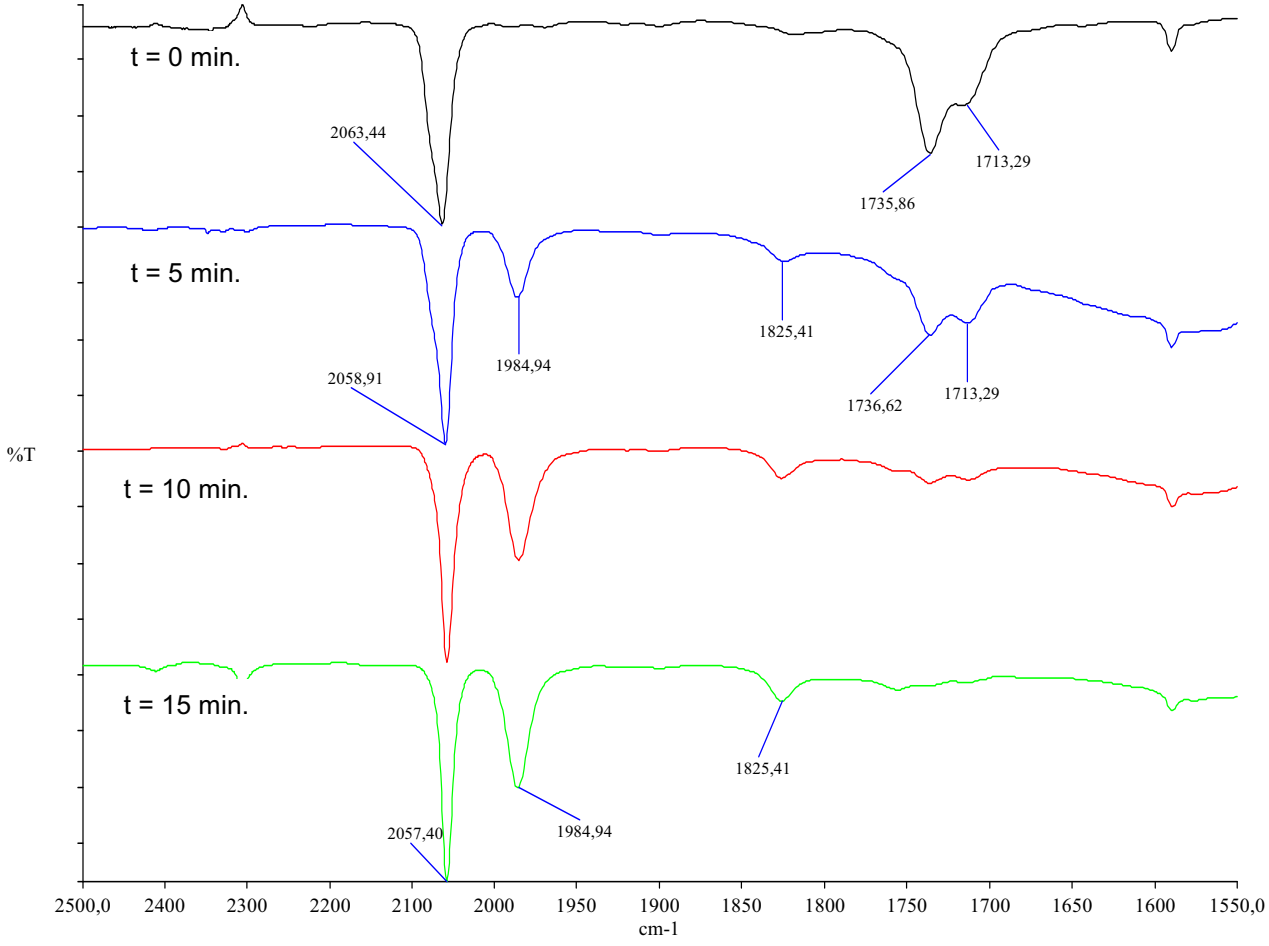

Figure 22 : IR spectra of the reaction between sodium acetate and complex 3 in dichloromethane.

In the first spectrum (black one) we observe at the very beginning of the reaction the bands at 2063 cm^{-1}, 1736 cm^{-1}, and 1713 cm^{-1} corresponding to complex 3. After 5 min. (spectrum in blue), we see clearly the presence of the bands at 2058 cm^{-1} and 1985 cm^{-1} corresponding to the active complex [PPN][$RhI_2(CO)_2$] 1, a band at 1825 cm^{-1} attributed to acetic anhydride and bands corresponding to

complex 3. After 15 min. (spectrum in green), we only observe the bands of complex 1 and acetic anhydride.

As for this result, we were really surprised that, starting from the monocarbonyl rhodium acetyl complex 3, we could obtain after reaction with acetate ions the dicarbonyl complex 1 and this, without no CO pressure and that, under the same reaction conditions employed in the experiment shown in figure 14 (same temperature, same materials, same solvent and same concentrations), the reaction involving complex 3 appears to be faster than that involving complex 4. We run the same experiments several times, starting from 4 and 3, and always obtained the same results.

With regard to CO exchange, we run the same experiment in 5 mL of dichloromethane while increasing by 5 times both the concentration of complex 3 and of sodium acetate. We observed the rapid formation of complex 1 together with acetic anhydride but the solution becomes green whereas it was red-yellow for the other experiments, with precipitation of rhodium black. By bubbling CO through the solution for 20 min., the latter became yellow and the precipitation disappeared. We have no clear explanation for this phenomenon but we can suppose that an intermolecular CO exchange occurs, which provides a black precipitation of RhI_3 or of colloidal Rh(0).

With regard to the rapidity of this reaction, we performed the same experiment as that described in figure 14, starting from the dicarbonyl rhodium acetyl complex 4 and bubbling CO through the solution. The reaction was monitored by IR (Fig. 23). We can observe in the two first spectra (spectra in blue and black, respectively) that the reaction between complex 4 and acetate ions starts quickly but spectra after a reaction time of 10 min (blue one) and 30 min (black one) are almost the same meaning that the reaction stops rapidly. After 30 min, bubbling of CO was stopped. The last spectrum (red one) was recorded 10 min after CO bubbling was stopped. We can see that the reaction has occurred rapidly and almost totally without any CO bubbling, affording the active species 1.

That means that first, CO decreases the rate of the reaction that leads to complex 1 and second, that very likely a CO ligand must be removed from complex 4 to provide the reaction. Indeed, with CO bubbling through the reaction mixture, we have observed a nearly complete reaction after more than 3 hours.

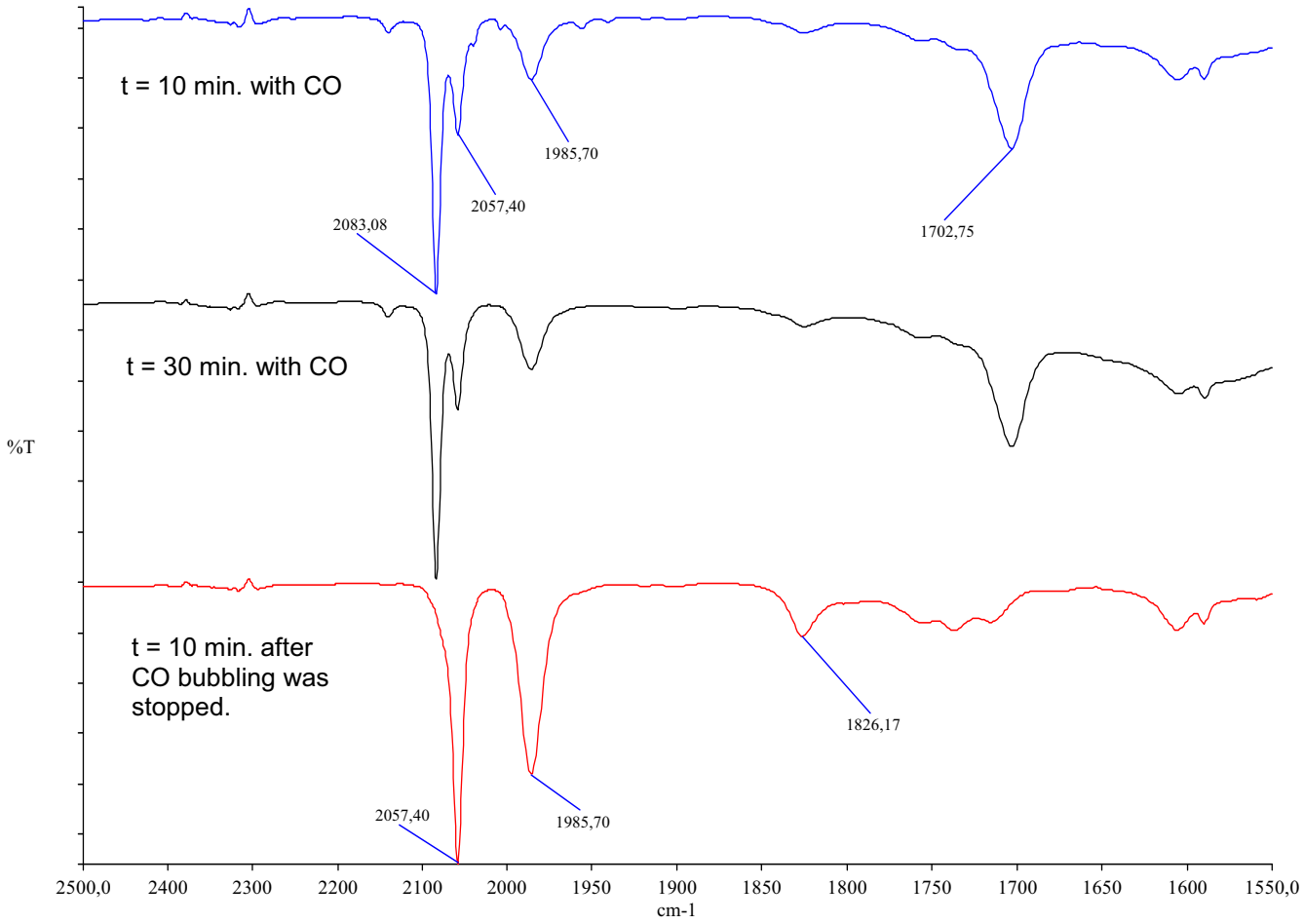

Figure 23 : IR spectra of the reaction between 4 and acetate ion under CO bubbling (blue and black spectra) and without CO bubbling (spectrum red)

As for these results, we cannot be sure that a nucleophilic attack of the acetate ions at the acetyl moiety in the rhodium acetyl complexes may occur since that does not explain why CO gas inhibits the reaction. As we believe that a CO ligand must be removed from complex 4 to afford the reaction, we could propose two reaction routes:

- Either a nucleophilic attack effectively occurs, but the hexacoordinated complex 4 is too crowded to provide this reaction, moreover, the presence of a second CO ligand increases the electron density on rhodium and thus reduces the electro-deficient character of the acetyl carbon atom.

- Or, an acetate anion must coordinate the metal center in the rhodium acetyl complex, taking the place of a CO ligand before a classical reductive elimination may occur (Sc. 14).

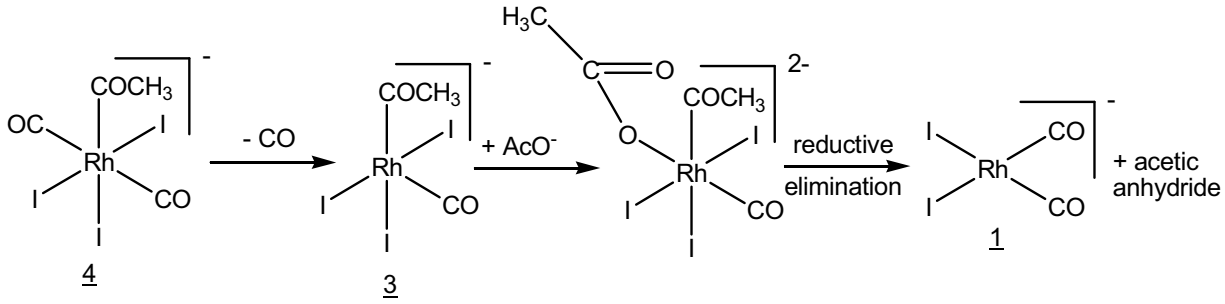

Scheme 14 : Proposed mechanistic pathway for the reaction of acetate with rhodium acetyl complex.

Despite all our efforts, our attempts at separating or observing spectroscopically the acetate rhodium complex were not successful. Indeed, we were not capable of proving the acetate coordination hypothesis but, as far as all our results are concerned, we can confirm that acetate ions react rapidly with the mono-carbonyl rhodium acetyl complex $[PPN]_2[RhI_3(COCH_3)(CO)]_2$ 3 giving the starting complex 1 and acetic anhydride, but react more slowly with the di-carbonyl acetyl rhodium complex $[PPN][RhI_3(COCH_3)(CO)_2]$ 4.

In order to determine if reductive elimination can occur from complex 4, we dissolved in 10 mL of anhydrous dichoromethane 100 mg of complex 3 in a glass reactor. The reactor was sealed and flushed three times with CO. The pressure was then adjusted to 5 bar and the reactor was heated at 50℃ and the solution stirred at 1000 rpm. After a reaction time of 2 hours, the stirring and the heating were stopped. After the solution was cooled down to room temperature, the reactor was depressurized and the solution analyzed by IR (Fig 24). By observing the spectrum of the solution coming from the reactor, large amounts of unreacted $[PPN][RhI_3(COCH_3)(CO)_2]$ 4, characterized by the bands at 2084 cm^{-1} and 1703 cm^{-1} are detected. We also note the presence of the bands at 2058 cm^{-1} and 1986 cm^{-1} corresponding to complex 1, which results from reductive elimination from the complex 4. Another band at 1733 cm^{-1} is also observed. It could correspond to the acetyl band of complex 3, other bands being hidden by the bands of complex 4 and 1. Or since acetyl iodide bands are not observed, it could even correspond to an organic compound formed by condensation of acetyl iodide.

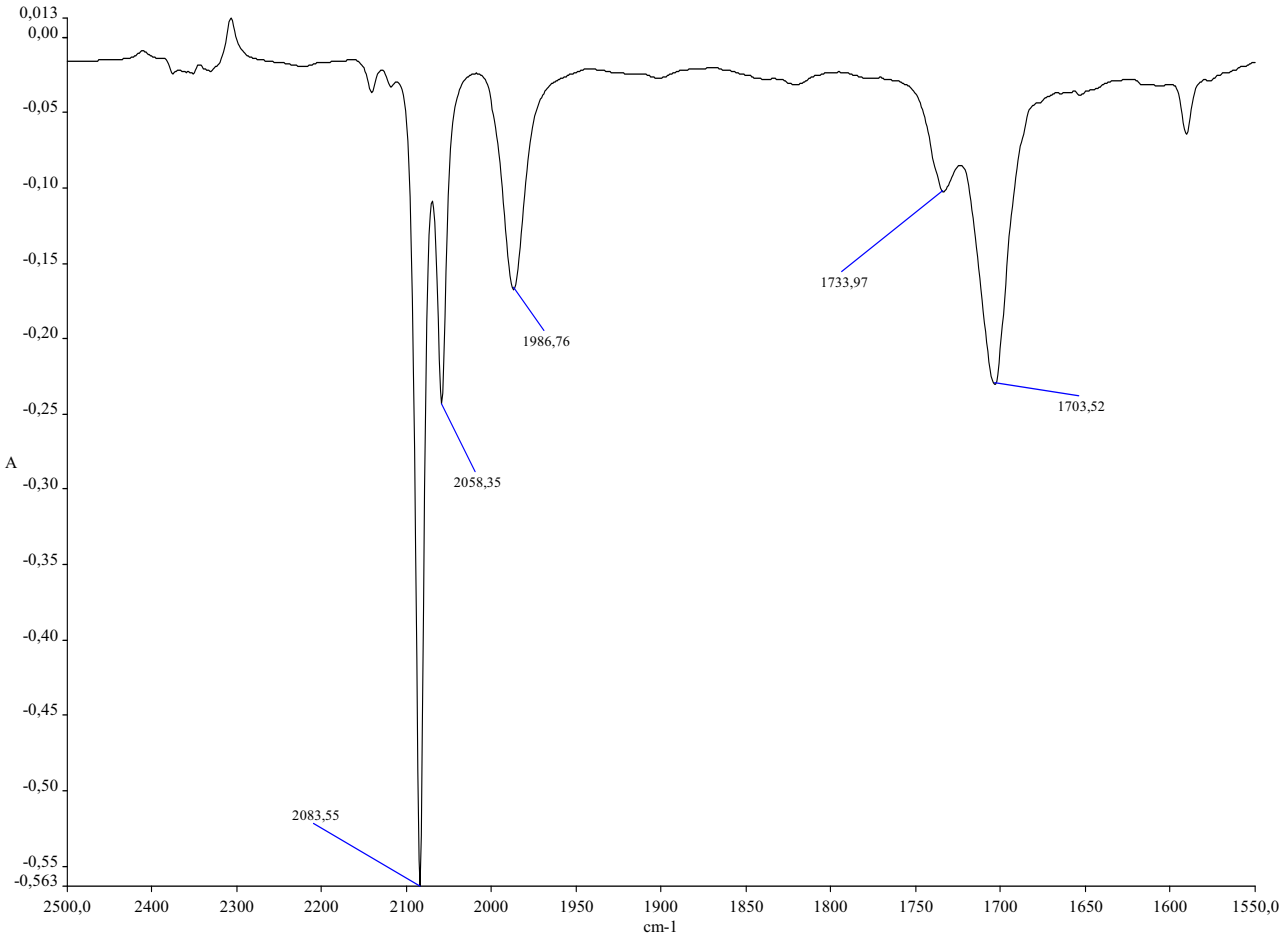

Figure 24 : IR spectrum of the reaction of complex 3 at 50℃ under 5 bar of CO for 2 h.

This experiment shows that classical reductive elimination can occur from complex 4 even if no water or acetate ions are present in the medium, but at a very slow rate. Thus, we propose that under catalytic conditions, two reductive elimination pathways are possible:

-A slow "classical reductive elimination" from complex 4 at low water content in the absence of lithium iodide.

-Or a rapid elimination reaction by nucleophilic attack or coordination of acetate ions onto complex 3 at high water content or in presence of lithium iodide.

On the basis of the observations in sections III-1 and III-2, the relevant catalytic cycle was modified and propose a new one is proposed (Sc. 15).

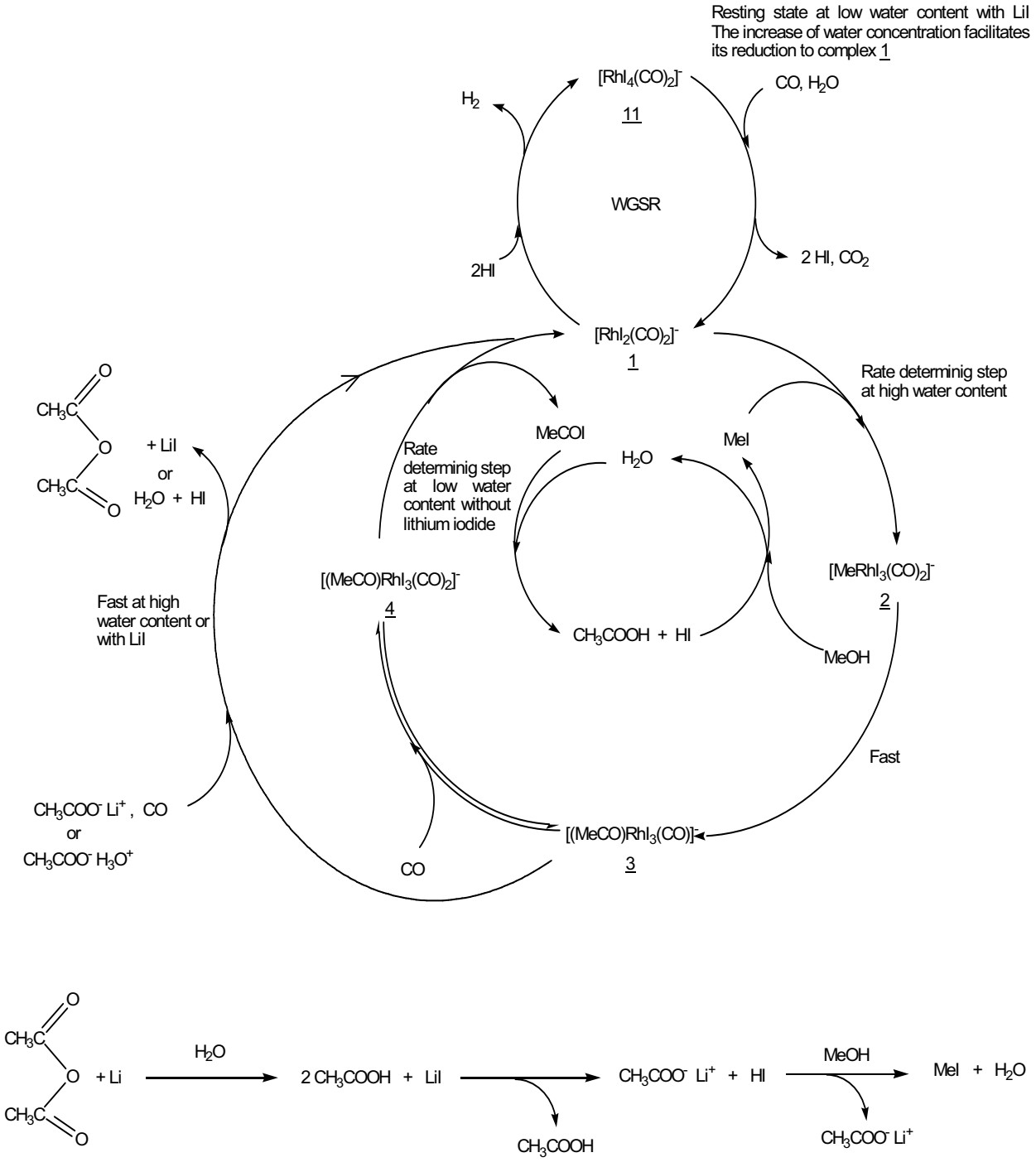

Scheme 15 : Proposed rhodium catalytic cycle for methanol carbonylation to acetic acid

III-3 Determination of reaction order.

In order to get a deeper insight into the effect of acetate ions on the elimination process, we performed a series of reactions with the dicarbonyl acetyl rhodium complex [PPN][$RhI_3(COCH_3)(CO)_2$] 4 at different concentrations of acetate ions and monitored them by infrared spectroscopy.

For each reaction, we introduced in a dry Schlenk tube containing stirring bar complex $[PPN]_2[RhI_3(COCH_3)(CO)]_2$ 3 (100 mg, $4.57.10^{-2}$ mmol) dissolved in 5 mL of dry dichloromethane. The Schlenk tube was placed in a water bath at 25℃. CO was bubbled through the solution for five seconds and 5 mL of a solution of sodium acetate in acetic acid were added with a glass syringe and a chronometer was started. The same reaction (same temperature, same Schlenk tube, same stirring magnet and same agitation) was run three times at different sodium acetate concentrations (5 eq/Rh, 2 eq/Rh, 1 eq/Rh, 0,5 eq/Rh). The IR spectrophotometer was initialized before each reaction and the period between two recorded spectra was as short as possible (usually 2 or 3 min.).

Spectra were recorded in transmittance mode. We chose to follow the appearance of the band at 1987 cm^{-1} of complex [PPN][$RhI_2(CO)_2$] 1 owing to the fact that it is far from the other bands. Thus, the reaction was monitored in transmittance mode by following the increase in intensity (calculated by the computer) of the aforementioned band. Then, we calculated the logarithm of each measured intensity, to transform the values into absorbance, directly related to the concentration of [PPN][$RhI_2(CO)_2$] 1 in the medium according to the Beer-Lambert law. An example of the recorded spectra is shown in figure 25.

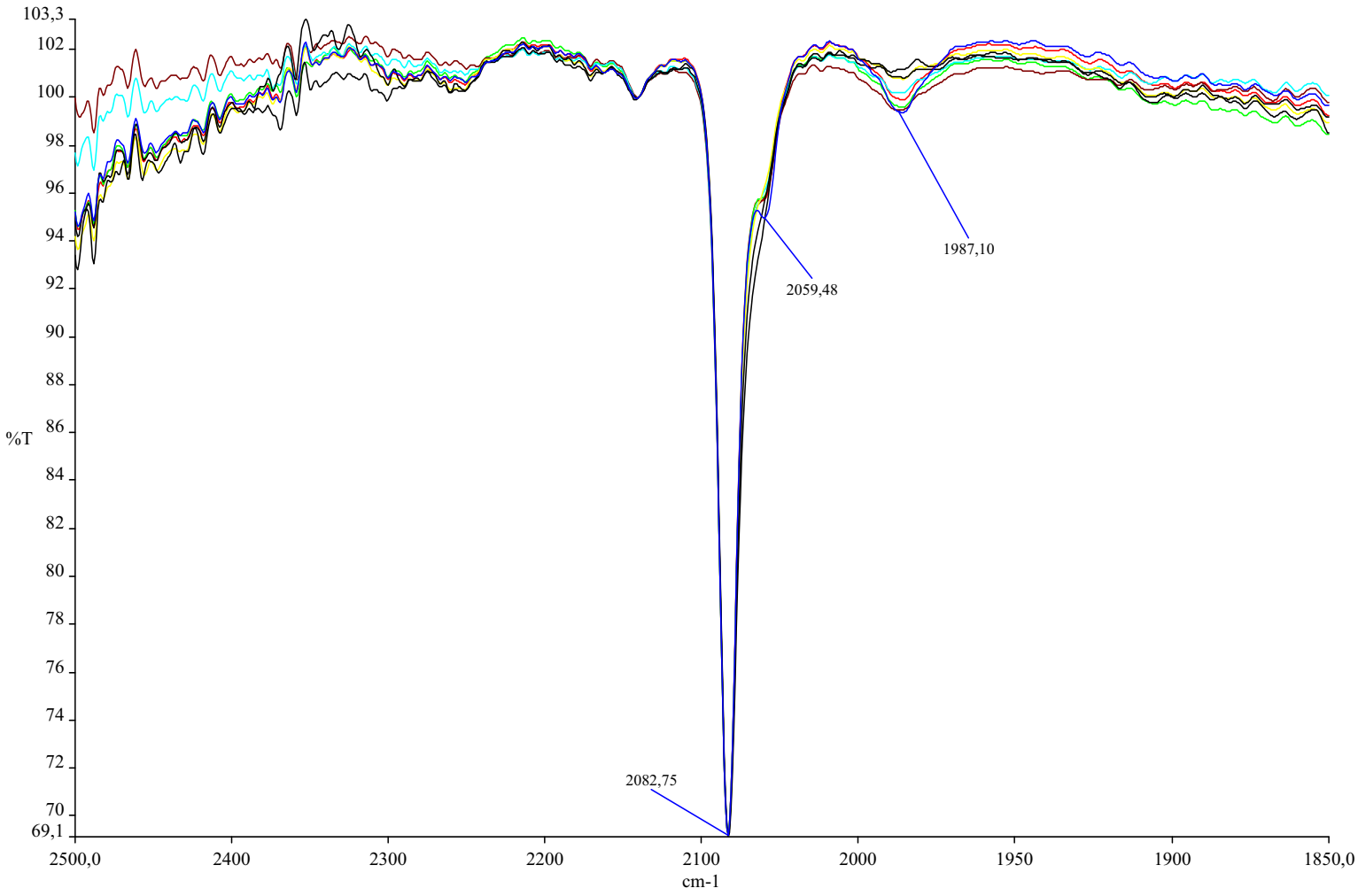

Figure 25 : IR spectra of the elimination reaction with 1 equivalent of sodium acetate.

If we measure the concentration of complex $[PPN][RhI_2(CO)_2]$ 1 formed very close to the initial time, we can make the approximation that the reactants concentration has not changed. Thus, we can write the following rate law regarding the reactants concentration at the initial time:

$$-(d[[PPN][RhI_3(COCH_3)(CO)_2]/dt) = k.[PPN][RhI_3(COCH_3)(CO)_2]^{\alpha}.[CH_3COO^-]^{\beta}$$

or $$d[[PPN][RhI_2(CO)_2]]/dt = k.[[PPN][RhI_3(COCH_3)(CO)_2]^{\alpha}.\ [CH_3COO^-]^{\beta}$$

thus $$\ln(d[[PPN][RhI_2(CO)_2]]/dt) = \ln k + \alpha.\ln([PPN][RhI_3(COCH_3)(CO)_2]) + \beta.\ln([CH_3COO^-])$$

We can consider that close to the initial time, the rate constant k and the concentration of $[PPN][RhI_3(COCH_3)(CO)_2]$ are constant, then we can replace $\ln k + \alpha.\ln([PPN][RhI_3(COCH_3)(CO)_2])$ with a constant K.

The rate equation becomes:

$$\ln(d[[PPN][RhI_2(CO)_2]]/dt) = \beta.\ln([CH_3COO^-]) + K$$

We first plotted the decimal logarithm of the calculated intensity as function of time, as shown in figure 26.

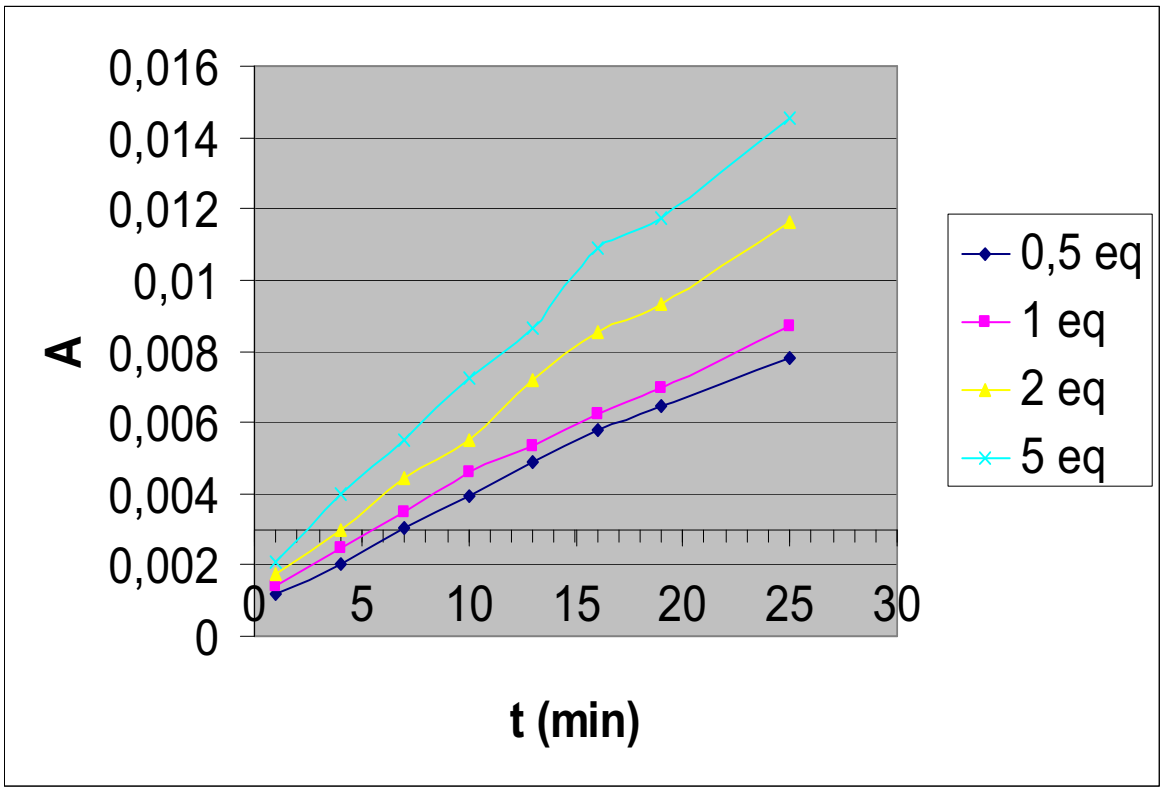

Figure 26 : Calculated absorbance of the band at 1987 cm^{-1} as function of time for the reaction between complex 4 and sodium acetate ions.

Second, we can assume that for the same absorbance value for each experiment, the concentration of complex $[PPN][RhI_2(CO)_2]$ 1 formed is the same, so, if we look at the time (t) for the same absorbance value close to the initial time for each experiment, (1/t) can be approximated to be

the pseudo-initial rate. As for the rate equation: $\ln(d[[PPN][RhI_2(CO)_2]]/dt) = \beta.\ln([CH_3COO^-]) + K$, if we plot the neperien logarithm of (1/t) as function of the neperien logarithm of the initial concentration of acetate ions in the medium we obtain a straight line in which the slope indeed is the reaction order toward acetate ions (Fig. 27). In this case, we have calculated the pseudo-initial rate for the same absorbance values equal to 0,003.

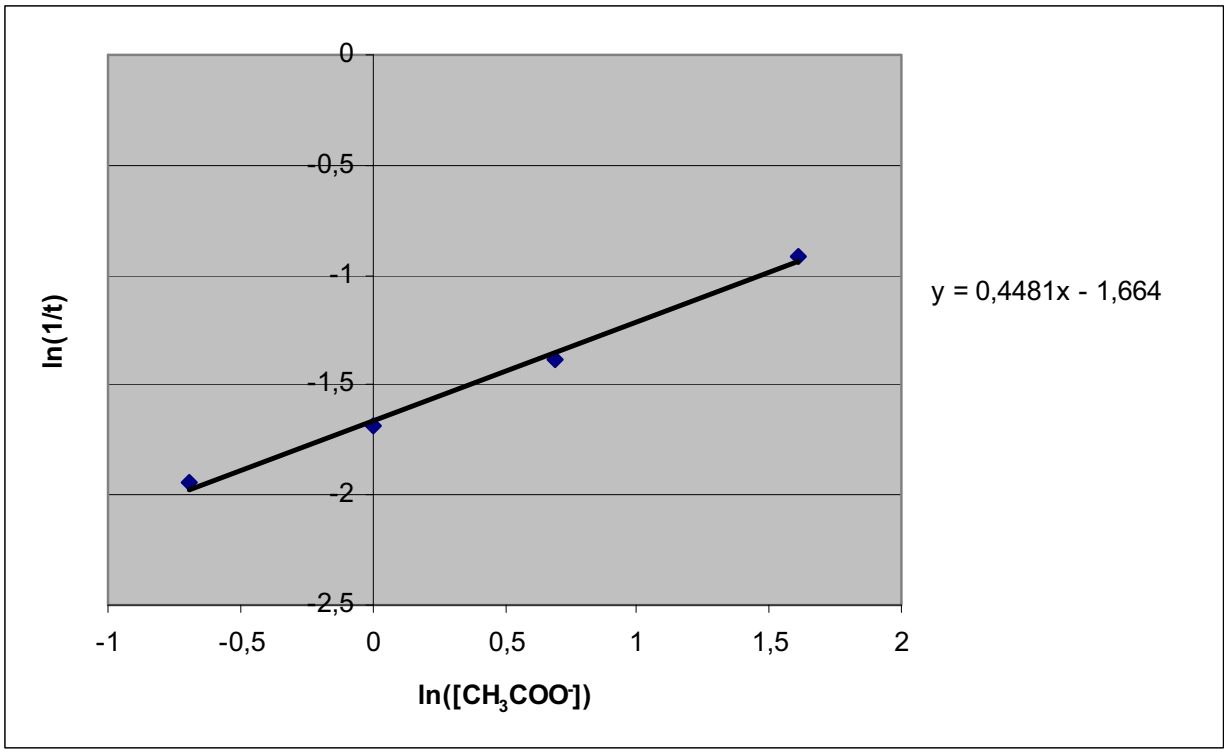

Figure 27 : Plot of $\ln(1/t)$ as function of $\ln([CH_3COO^-])$.

The coefficient slope of the straight line is close to 0,45. This value indicates that the reaction between complex $[PPN][RhI_3(COCH_3)(CO)_2]$ 4 and acetate ions does not consist of a single step, but may pass through a few slow steps, may be via the loss of a CO ligand.

In a second set of experiments, we have run the same experiments under the same conditions starting from the monocarbonyl acetyl complex $[PPN]_2[RhI_3(COCH_3)(CO)]_2$ 3 (100 mg, $4.57.10^{-2}$ mmol) and by varying the sodium acetate concentration (5 eq/Rh, 2 eq/Rh, 1 eq/Rh, 0,5 eq/Rh). The procedure is identical to that described above. The curves representing the absorbance as function of time are plotted in figure 28.

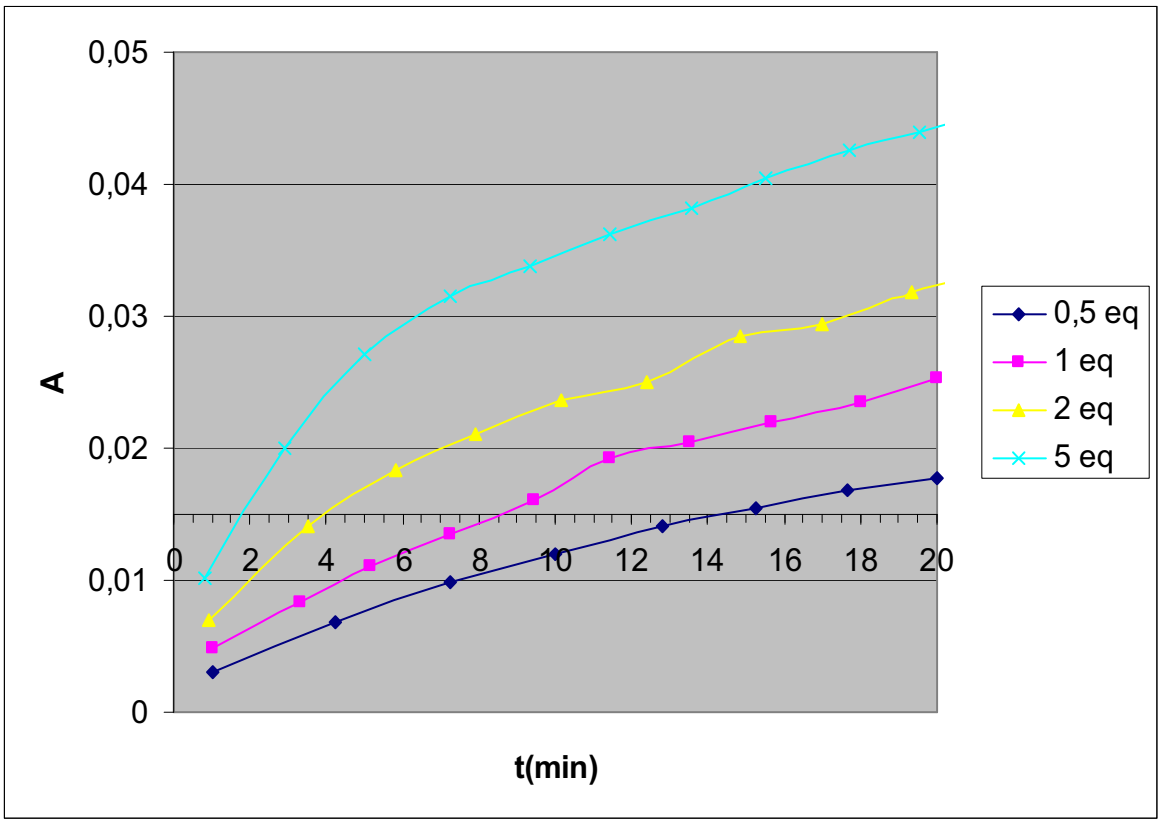

Figure 28 : Calculated absorbance of the band at 1987 cm^{-1} as function of time for the reaction between complex 3 and sodium acetate ions

By comparing figure 26 and figure 28 we can confirm that the reaction between acetate ions and complex 3 is more rapid than the same reaction with complex 4.

Then, we plotted the neperien logarithm of the pseudo-initial rate (calculated for the same absorbance equal to 0,015) as function of the neperien logarithm of the sodium acetate concentration and we obtained the straight line shown in figure 29.

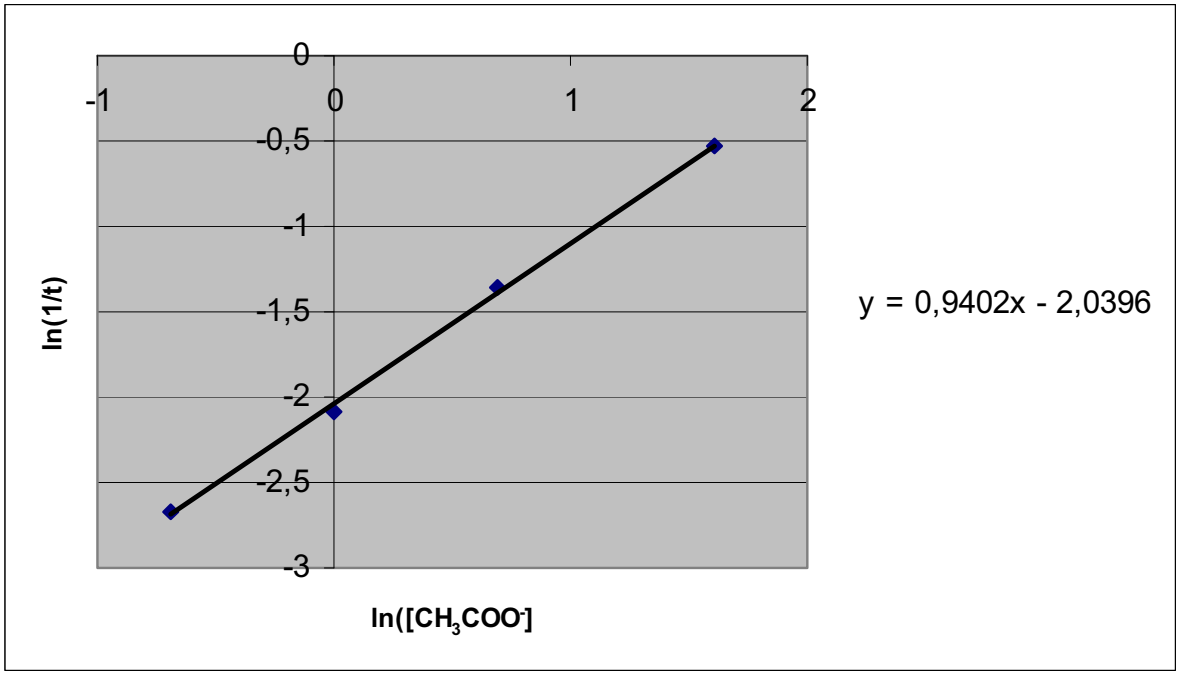

Figure 29 : Plot of ln(1/t) as function of ln([CH_3COO^-]).

The slope of the straight line is found to be close to 1, meaning that we have a direct reaction between the acetyl complex $[PPN]_2[RhI_3(COCH_3)(CO)]_2$ 3 and the acetate ions but on the basis of this result this result, it is not possible to determine whether the nucleophilic acetate ions attack the acetyl in complex 3 or acetate ions slowly coordinate onto complex 3 and then a rapid elimination occurs.

We also tried to determine the reaction order toward water for the elimination from complex 4. Hence we run the same reaction using the same procedure described above, but adding to the dichloromethane solution of 4; 5mL of a acetic acid/water mixture with water content of 12 wt%, 10 wt%, 8 wt% and 6 wt%. The plots of the calculated absorbance as function of time are shown in figure 30.

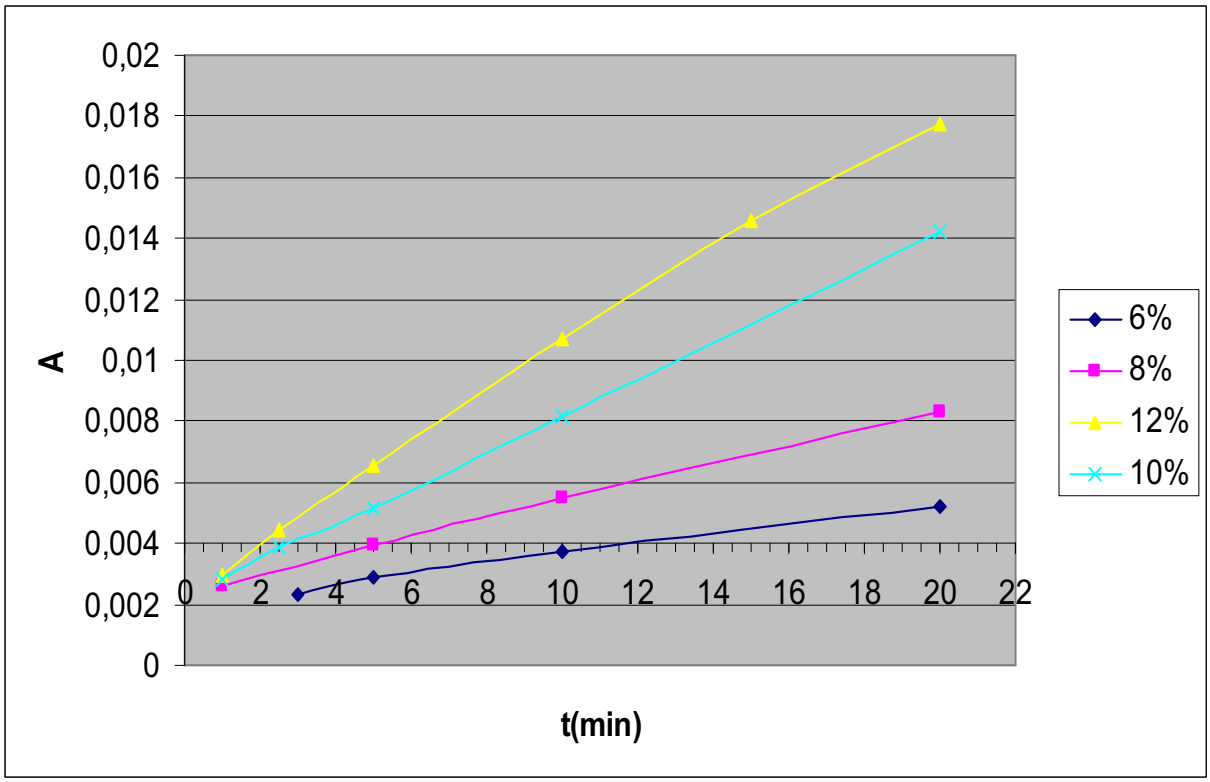

Figure 30 : Calculated absorbance of the band at 1987 cm^{-1} as function of time for the reaction between complex 4 and a solution of acetic acid/water.

This reaction seems to be rather fast for high water concentrations but becomes very slow for low water contents. By plotting the neperien logarithm of the pseudo-initial rate, calculated for an absorbance value equal to 0,004, as function of the neperien logarithm of water concentration, we obtained a straight line as shown in figure 31. The calculated slope is 2,8. This value is difficult to explain but we could imagine that further reactions may take place during the this elimination process and that water exerts a strong influence for this reaction.

We also tried to study the elimination reaction for higher water concentrations in the medium but we encountered some solubility problems by using water and dichloromethane.

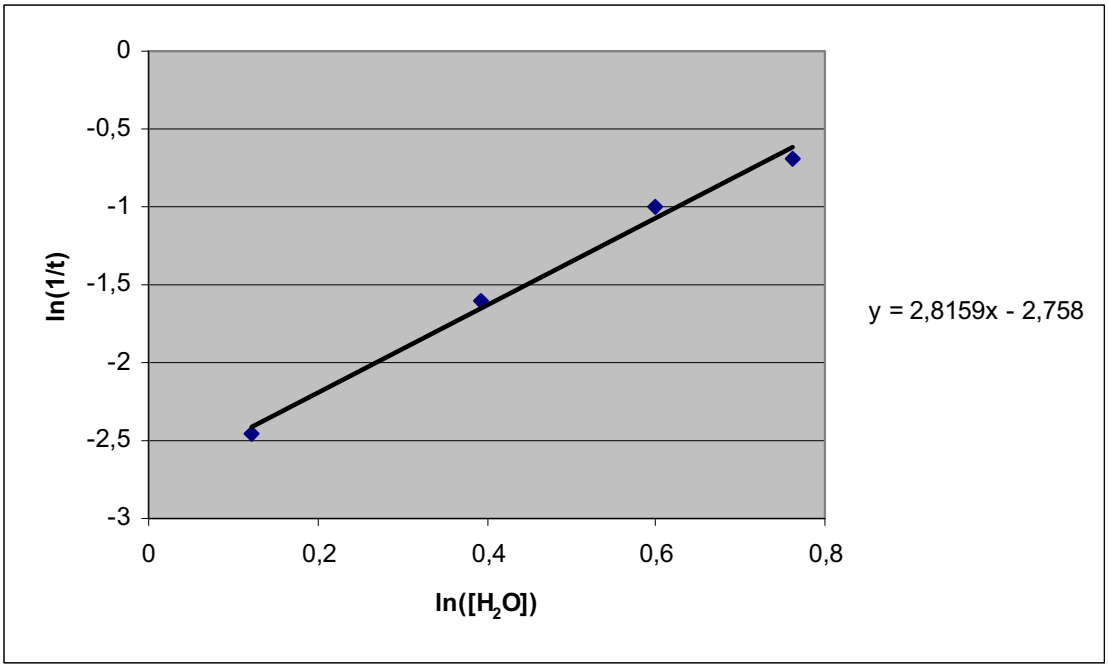

Figure 29 : Plot of ln(1/t) as function of ln([H_2O]).

Then, we run these experiments starting from complex 3 and using the same acetic acid/water mixture but surprisingly, we observed only a very slow rate of formation of complex [PPN][$RhI_2(CO)_2$] 1 even at 12 wt% water content and the data obtained cannot be use to determine the reaction order. We could propose that a molecule of water may be coordinated onto the unsaturated complex 3 inhibit the elimination reaction and that the concentration of acetate ions in the medium, formed by dissociation of acetic acid, is not high enough to induce the elimination process.

More kinetic measurements should be made, first to determine the reaction order toward the concentration of acetyl rhodium complexes and second, to study the effect of the temperature on the elimination reaction. It is worth noting that we performed these reaction with the acetyl iridium complex *cis*-[PPN][$IrI_3(COMe)(CO)_2$] *cis*-8 and with *trans*-[PPN][$IrI_3(COMe)(CO)_2$] *trans*-8 but no elimination reaction was observed.

III-4 Conclusion

In this chapter, we tried to explain the role of lithium iodide and water on the rhodium-catalyzed methanol carbonylation.

Firstly, batch experiments showed that the presence of lithium iodide in the catalytic medium was able to maintain high carbonylation activity even at low water content, whilst the carbonylation rate decreased rapidly below a water content about 6-8 wt% without lithium iodide in the medium. Thus, we focused our attention on the role played by lithium iodide and water on the catalytic process.

Secondly, we performed batch experiments in a sapphire NMR tube in order to get information on the rate determining step in the catalytic process under different water and lithium iodide concentrations. We observed that:

At low water content without lithium iodide the rate determining step in the catalytic cycle is the reductive elimination reaction whereas, at higher water content, oxidative addition of methyl iodide becomes the rate determining step, meaning that high water concentration accelerate the reductive elimination process.

By introducing lithium iodide into the medium, we observed that at low water content the only complex present was the tetra-iodo carbonyl complex [PPN][$RhI_4(CO)_2$] 11, but we didn't observe any acetyl species, meaning that, in the same way as water lithium iodide accelerates reductive elimination, the rate determining step becoming the formation of the active species 1 from complex 11.

Then, we tried to explain the accelerating effect of water and lithium iodide, and we found that acetate ions were able to dramatically increase the reductive elimination reaction rate. Hence, we proposed that acetates could be formed by reaction of lithium iodide with methyl acetate or acetic acid or by dissociation of acetic acid at high water content.

Thirdly, we determined order of the reductive elimination reaction toward acetate ions and water. As for acetate ions, we found a reaction order of 0.5 when starting from the dicarbonyl acetyl complex 4, meaning that the elimination process could include other slow reactions. But starting from the acetyl complex 3 we found a reaction order close to 1 indicating that the reaction between acetate ions and complex 3 involves no intermediates, or could include other rapid reaction(s). The reaction of acetyl complexes in a reaction mixture containing acetic acid and water seems to be more complicated. The reductive elimination process would pass through other routes maybe including the dissociation of acetic acid in water. More investigations ought to be made to explain this kind of reactivity.

III-5 References

[1] F. E. Paulik, A. Hershman, W. R. Knox, J. F. Roth, to Monsanto company, US Patent 3,769,329, **1973**.

[2] B. L. Smith, G. P. Torrence, A. Aguilo, S. Alder, for Hoechst Celanese Corp., U.S Patent 5,001,259, **1991**.

[3] M. A. Murphy, B. L. Smith, G. P. Torrence, A. Aguilo, *J. Organomet. Chem.* **1986**, *303*, 257.

[4] C. E. Hickey, P. M. Maitlis, *J. Chem. Soc., Chem Commun.* **1984**, 1609.

[5] A. Fulford, C. E. Hickey, P. M. Maitlis, *J. Organomet. Chem.* **1990**, *398*, 311.

[6] J. H. Jones, *Platinum Metals Rev.* **2000**, *44*, 94.

[7] D. Forster, *J. Am. Chem. Soc.* **1976**, *98*, 846.

[8] A. H. Schmidt, M. R. D. Grosse, *Synthesis* **1981**, 216.

[9] P. W. N. Van Leeuwen, M. A. Zuideveld, B. H. G. Swennenhuis, Z. Freixa, P. C. J. Kamer, K. Goubitz, J. Fraanje, M. Lutz, A. L. Spek, *J. Am. Chem. Soc.* **2003**, *125*, 5523.

[10] M. Kilner, N. J. Winter, *J. Mol. Catal.* **1996**, *112*, 327.

[11] T. H. Larkins, S. W. Polichnowski, G. Tustin, D. A. Young, to Eastman Chemical Compagny, U.S. Patent 4,374,070, **1983**.

GENERAL CONCLUSION

GENERAL CONCLUSION

In this PhD thesis, we studied iridium and rhodium catalyzed methanol carbonylation system for the production of acetic acid. We focused our attention on the acceleration of the rate determining step of the iridium catalytic cycle by addition of co-catalyst. We also studied the effect of water and iodide salt on the determining step of the rhodium catalytic cycle. For this study, we used different analytical tools such as high-pressure infrared spectroscopy and high-pressure NMR spectroscopy.

Concerning the iridium catalytic cycle study, we showed that protic and polar solvent played a major role on the rate determining step and on the nature of the obtained isomer from the methyl iridium species $[Ir(CH_3)I_3(CO)_2]^-$ to the acetyl iridium species $[Ir(COCH_3)I_3(CO)_2]^-$. First, two stable isomers of the acetyl species exist in solution, the *fac,cis*-$[Ir(COCH_3)I_3(CO)_2]^-$ and the *mer,trans*-$[Ir(COCH_3)I_3(CO)_2]^-$ and second, the increase of polar and protic solvent concentration in the medium, as methanol or water, increased the rate of the reaction rate but also the ratio of *mer,trans*-$[Ir(COCH_3)I_3(CO)_2]^-$/*fac,cis*-$[Ir(COCH_3)I_3(CO)_2]^-$ isomer. We observed by HP-IR and HP-NMR spectroscopy that with protic polar solvent, the complex *fac,cis*-$[Ir(COCH_3)I_3(CO)_2]^-$ isomerized to complex *mer,trans*-$[Ir(COCH_3)I_3(CO)_2]^-$ via further unidentified intermediates.

Preliminary studies first showed that introduction of a co-catalyst as $[PtI_2(CO)]_2$ in the iridium catalytic system increased the carbonylation rate. Mechanistic studies demonstrated that platinum co-catalyst was able to abstract an iodide ligand to the resting state complex $[Ir(CH_3)I_3(CO)_2]^-$ via an heterobimetallic species, leading under CO to the neutral species $[Ir(CH_3)I_2(CO)_3]$ where the CO insertion affording the acetyl complex occur more rapidly. By the addition of complex $[RhI(CO)_2]_2$ in a solution of $[Ir(CH_3)I_3(CO)_2]^-$, we observed by mass spectrometry and NMR spectroscopy the formation of a [Ir-Rh] heterobimetallic species. By bubbling CO through this solution, we observed the rapid formation of the acetyl iridium species indicating that rhodium co-catalyst was able to enhance the rate determining step of

the iridium catalytic species. Unfortunately, batch runs of the Iridium-rhodium system didn't showed any enhancement of the carbonylation rate in comparison with the iridium system under conditions used

.

Concerning the rhodium catalytic system, we observed by HP-NMR spectroscopy that both water and lithium iodide have an impact on the cabonylation rate and on the determining steps of the rhodium catalytic cycle. At low water content in the absence of lithium iodide, the carbonylation rate is low and the rate determining step is the reductive elimination from the acetyl rhodium complex $[Rh(COCH_3)I_3(CO)_2]^-$ to the active complex $[RhI_2(CO)_2]^-$. By increasing the water content, the carbonylation rate becomes faster and the rate determining step becomes the oxidative addition of methyl iodide on the complex $[RhI_2(CO)_2]^-$. By introducing lithium iodide, the carbonylation rate remains high even at low water content and the only observed complex in solution is $[RhI_4(CO)_2]^-$ at low water content whereas both $[RhI_4(CO)_2]^-$ and . $[RhI_2(CO)_2]^-$ complexes are observed at high water content Thus, we believe first that lithium iodide enhance the reductive elimination reaction since no acetyl rhodium complex was observed at low water content in comparison with the experiment performed without LiI, and second, lithium iodide reduces the water gas shift reaction rate since complex $[RhI_4(CO)_2]^-$ is observed in any cases, water enhancing the reduction of complex$[RhI_4(CO)_2]^-$ to complex $[RhI_2(CO)_2]^-$.

Then, we tentatively explained the effect of iodide salt or water by the formation of acetate ions either by the reaction of LiI with methyl acetate or by dissociation of acetic acid with water and we showed that acetate ions accelerate dramatically the reductive elimination reaction from acetyl complex to active complex $[RhI_2(CO)_2]^-$. It appears that acetate ions react more rapidly with the acetyl dimer $[Rh(COCH_3)I_3(CO)]_2^{2-}$ than with the dicarbonyl acetyl complex $[Rh(COCH_3)I_3(CO)_2]^-$.

Preliminary kinetic investigations showed an order around 0.5 in acetate ions for the reaction between acetate ions and the dicarbonyl acetyl complex $[Rh(COCH_3)I_3(CO)_2]^-$ but first order in acetate ions when the reaction is performed with the acetyl dimer $[Rh(COCH_3)I_3(CO)]_2^{2-}$. These results mean that in the case of the reaction between $[Rh(COCH_3)I_3(CO)_2]^-$ and acetate ions, other(s) slow reaction(s) may occur(s) before the formation of $[RhI_2(CO)_2]^-$, but for the reaction of $[Rh(COCH_3)I_3(CO)]_2^{2-}$ with acetate

ions, we believe that a direct interaction occurs between the two reactants or that other(s) rapid reaction(s) may occur(s) before the formation of the active complex $[RhI_2(CO)_2]^-$. Thus, we proposed two reactions pathways for this reaction: a nucleophilic attack of the acetate ions on the acetyl part of complex $[Rh(COCH_3)I_3(CO)]_2^{2-}$ or a coordination of an acetate ion on this complex followed by a rapid elimination.

Reaction of the rhodium acetyl species with an acetic acid/water mixture appears to be more complicated and the kinetic data obtained didn't allowed us to propose a mechanistic pathway.

Thus, looking at these results, we can believe that addition of a promoter which is able to form acetate ions, more efficiently than lithium iodide, in the catalytic medium from acetic acid or methyl acetate could be a good co-catalyst for the low water rhodium-catalyzed methanol carbonylation since a large amount of LiI is needed in the Celanese process. This promoter, which could be a salt or a metal, must not catalyze other side reaction and have to be stable in the reactor as well as in the flash tank.

EXPERIMENTAL SECTION

Experimental section

Materials:

All reactions and manipulations of Ir and Rh complexes were performed under argon or dinitrogen atmosphere using Schlenk tube technique. Dichloromethane was distilled using CaH_2. Methanol was distilled after reaction with Mg/I_2 and used immediatly. Other reagents were used as supplied: the salt IrI_3/IrI_4, named $IrI_{3,4}$ (Johnson-Matthey), RhI_3 salt from the Celanese plant at Pardies, bis-triphenylphosphoranylidene chloride [PPN]Cl, triphenylphosphine (Aldrich), acetyl chloride, methyl iodide, (Acros), acetone, acetic acid, chlorobenzene, chloroform, dichloromethane, dimethylformamide, n-hexane, n-heptane, methanol, pentane, toluene (Scharlau), chloroform-d_3, dichloromethane-d_2, methanol-d_4, toluene-d_8 (Eurisotop), argon, dinitrogen, carbon monoxide, ^{13}C-labeled carbon monoxide (Air Liquide), hydriodic acid (Merck). Labeling experiments were performed by stirring the relevant dissolved complex under a ^{13}CO atmosphere for some hours.

Instrumentation:

IR spectra were recorded on a Perkin-Elmer 1710 Fourier Transform spectrophotometer using either a solution cell with CaF_2 windows. ^{1}H, ^{13}C NMR spectra were recorded on a Bruker AC250, on a AMX400 or on a DPX300 spectrometer. Mass spectra were recorded by negative FAB method on a NERMAG R10-10 mass spectrometer.

X-ray crystallographic data were collected on a Stoe IPDS diffractometer for complex 1 and on an Oxford-Diffraction Xcalibur diffractometer for complexes 4, 10 and 8.

Batch experiments:

High pressure batch carbonylation experiments were performed in a Hastelloy® B2 100 mL autoclave (Top Industrie) equipped with a stirring axis. The reactor can be pressurised up to 90 bar from a gas reservoir and can be heated up to 200°C. A cons tant pressure can be maintained in the reactor during the batch experiment. We measured carbon monoxide consumption in the reservoir and then calculated

the carbonylation rate at 20 wt% and 15 wt% of unreacted methyl acetate calculated from CO consumption and corrected by gas-chromatography analyses. The reactor is equipped with a feed-line to introduce liquids under pressure. All batch experiments were started with the RhI_3 salt in a mixture of acetic acid and water (10 : 1). The reactor was closed and flushed several times with carbon monoxide, and then pressurized at 5 bar, heated at 190℃, and the mixture stirred at 1000 rpm to preform the iridium active species**.** After 30 minutes, the rest of the catalytic mixture is added through the liquid feed-line overpressurized with carbon monoxide. Pressure was then adjusted to 30 bar. It can be maintained constant by supplying gas from the reservoir during the experiments. A glassware reactor (Top Industrie) was used for some experiments. Technical features and working conditions were the same as those used for the Hastelloy® autoclave, except for the maximum operating pressure, which was 8 bar. With such a reactor it was possible to observe the reaction mixture during the experiments, and perform crystallizations afterwards.

High-pressure/high-temperature IR analyses:

Batch experiments were monitored *in situ* by high-pressure IR spectroscopy in an autoclave equipped with a Cylindrical Internal Reflectance (CIR) silicon rod. A “Cassegrain” lens system was used to focalize the IR beam onto the rod placed across a Hastelloy® B2 (Top Industrie) batch 100mL autoclave and to refocalize the IR beam onto the detector (Scheme 1). Spectra were recorded on a Perkin-Elmer GXII spectrophotometer. The reactor can be pressurized up to 50 bar with CO and heated up to 200℃. A solution can be added into the reactor under pressure using an additional tank. With this technique, it is possible to reproduce catalytic conditions and to observe the species present in the catalytic mixture by infrared analyses.

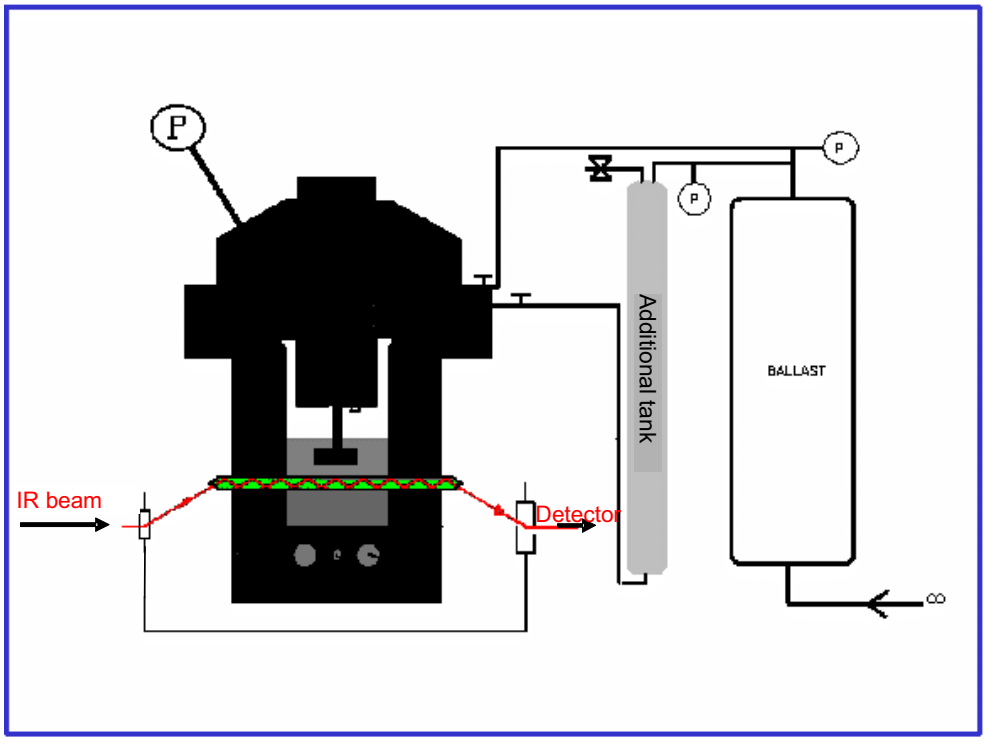

Scheme 1 : High-pressure infrared cell

High-pressure NMR analyses:

Batch carbonylation experiments were monitored *in situ* by high-pressure NMR spectroscopy using sapphire tubes (Universiteit van Amsterdam) (10 mm e.d.), pressure rated to 100 bar, fitted with a titanium valve. Reaction mixtures can be heated up to 100°C.

All high-pressure NMR experiments were performed on a Bruker DRX400 spectrometer. The NMR tube was charged with [PPN][$IrCH_3I_3(^{13}CO)_2$] 2 or with [PPN][$RhI_2(^{13}CO)_2$] 7 and the reaction mixture. Once the tube was sealed, the medium was flushed several times with ^{12}CO, then pressurized at at the desired pressure with ^{13}CO. Before to introduce the tube in the NMR probe, it was shaked vigorously to dissolve the complex and the ^{13}CO in the catalytic mixture.

Reaction order determination:

Reaction order in sodium acetate for the reaction of complex [PPN][$Rh(CH_3CO)I_3(CO)$] 9 and [PPN][$Rh(CH_3CO)I_3(CO)_2$] 10 with sodium acetate and order rate in water for the reaction of [PPN][$Rh(CH_3CO)I_3(CO)_2$] 10 with water were determined following the procedure described below:

In a dried 20 mL Schlenk tube under argon equiped with a stirring magnet and placed in a water bath at 25℃, complex 9 (100 mg, $9.15.10^{-2}$ mmol) is disolved in 5 mL of anhydrous dicloromethane. Complex 10 is obtained by bubbling CO through this solution for 5 secondes. Then, 5mL of a solution of acetic acid/sodium acetate or acetic acid/water is added through a septum seal with a 10 mL glass seringe and the chronometer is started. Infrared spetra were recorded with the same CaF_2 cell on a Fourrier Transform spectrophotometer Perkin-Elmer GXII. The instruments are aligned before each experiments and the time between each spectrum is as short as possible (usually of 2 or 3 minutes). The reaction has been monitored in transmitance by following the increase in intensity (calculated by the computer) of the 1987 cm^{-1} band characteristic of complex 7 formed in the medium. We have chosen to take into account the height of the band rather than the area to avoid errors due to the spectrum noise. The height of the band was calculated as shown in figure 1. The corrected height is the difference between the transmitance of the chosen limit of the band represented by base 1 and base 2 in figure 1, and the maximum transmitance of the band. In order to obtain absorbance values suitable for the determination of the reaction rate, according to the Beer's law, we have changed the Beer's law as follows.

$$A = -\log_{10}(T)$$

$$A = -\log10(1-(-\text{corr. height}/100))$$

Then, reaction order have been calculated as described in section III-3.

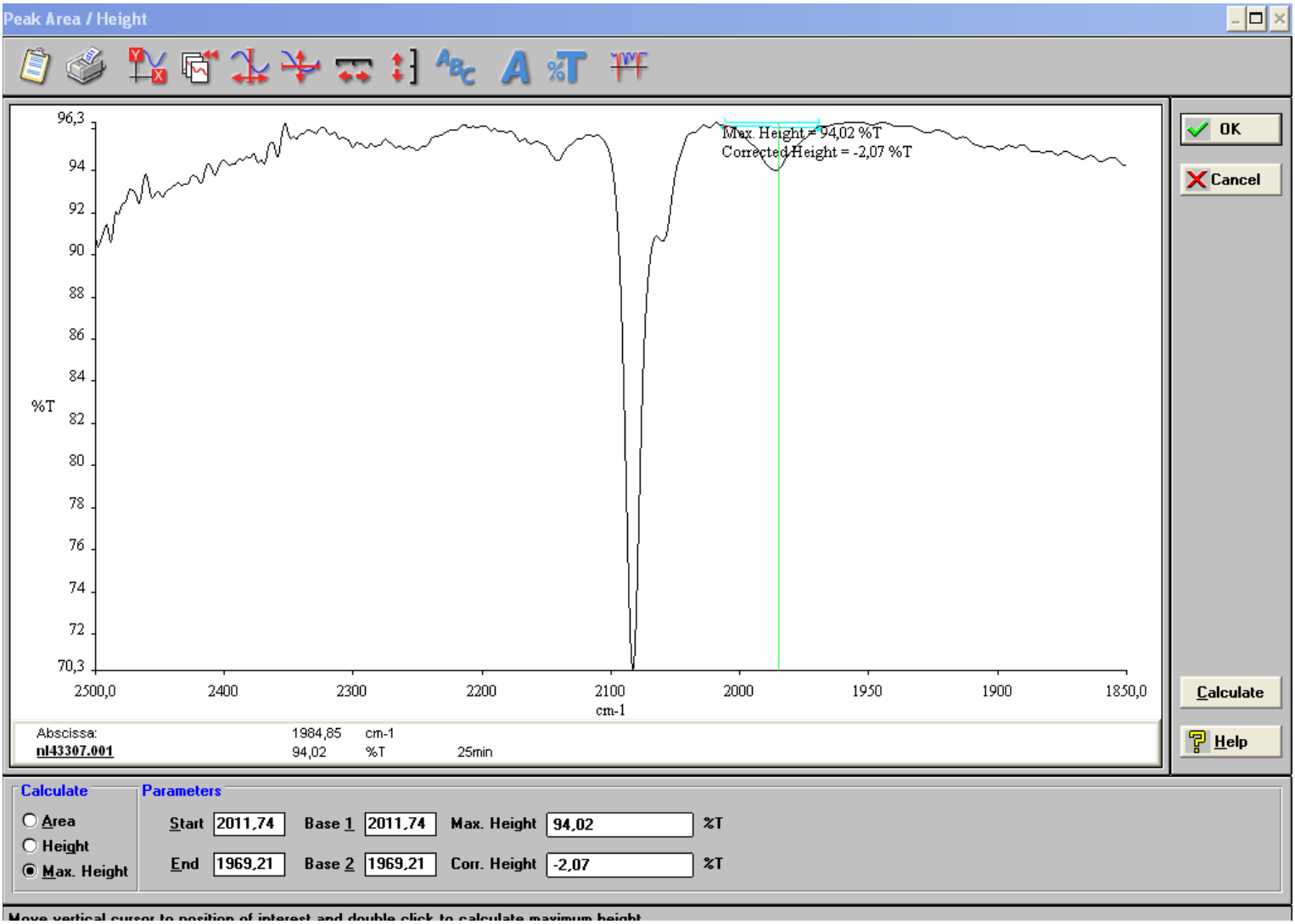

Figure 1 : Example of the maximum height calculation.

Synthesis of rhodium compounds

[PPN][$RhI_2(CO)_2$] 1:

3g of RhI_3 are added to 400mL of dimethylformamide (DMF) containing 2.5g of water. The mixture is stirred and heated at 160℃ under CO bubbling un til the solution becomes pale yellow. The solution is cooled at room temperature, 1 equivalent of PPNCl (3.34g) is added and then water is slowly added at 0℃ to precipitate **[PPN][$RhI_2(CO)_2$] 1** as a yellow powder. This product is filtered, washed with cold water and driedy under vacuum. By formation of a bilayer with CH_2Cl_2/hexane, we obtained yellow crystals suitable for X-ray analyses. Yield: 70%. IR (CH_2Cl_2): νCO= 2057, 1986 cm^{-1}. ^{13}C NMR (CD_2Cl_2): 183.3 ppm, CO, (d, J_{Rh-C}= 71 Hz). MS (FAB^-) m/z = 413. Calcd for $C_{38}H_{30}RhI_2NO_2P_2$: C: 47.94, H: 3.15, N: 1.51. Found: C: 47.93, H: 3.07, N: 1,51.

$$RhI_3 \xrightarrow[CO\ 1\ bar,\ 160℃]{DMF,\ H_2O} [NH_2(CH_3)_2][RhI_2(CO)_2] \xrightarrow[2)\ H_2O,\ -[NH_2(CH_3)_2Cl}{1)\ PPNCl} [PPN][RhI_2(CO)_2]$$

Scheme 9 : Preparation of [PPN][$RhI_2(CO)_2$] **1**.

Crystal data of 1.

Empirical formula	C38H30I2NO2P2Rh
Formula weight	951.28
Crystal system, space group	Triclinic, P1
Unit cell dimensions	a = 10.189 (5) Å, □ = 98.470 (5)
	b = 11.300 (5) Å, □ = 107.117 (5)
	c = 16.985 (5) Å, □= 95.685 (5)

Volume	1827.5 (13) Å^3
Z, Calculated density	2, 1.729 Mg m−3
Cell parameters from 7998 reflections	
Theta range for data collection	1.65 to 26.05 deg.
Absorption coefficient	2.277 mm−1
Temperature	180 (2) K
Color	Yellow
Crystal size	0.44 × 0.35 × 0.17 mm
diffractometer type	Stoe IPDS diffractometer
Absorption correction	refined from DF
Max. and min. transmission	Tmin = 0.5490, Tmax = 0.8610
18194 measured reflections, 6687 independent reflections, 5957 reflections with >2s(I)	
Rint = 0.0271	
Limiting indices	-12<=h<=12, -13<=k<=13, -20<=l<=20
Refinement	Refinement on F2
R indices (all data)	R(F) = 0.0277, wR(F2) = 0.0792
Extinction correction: none	

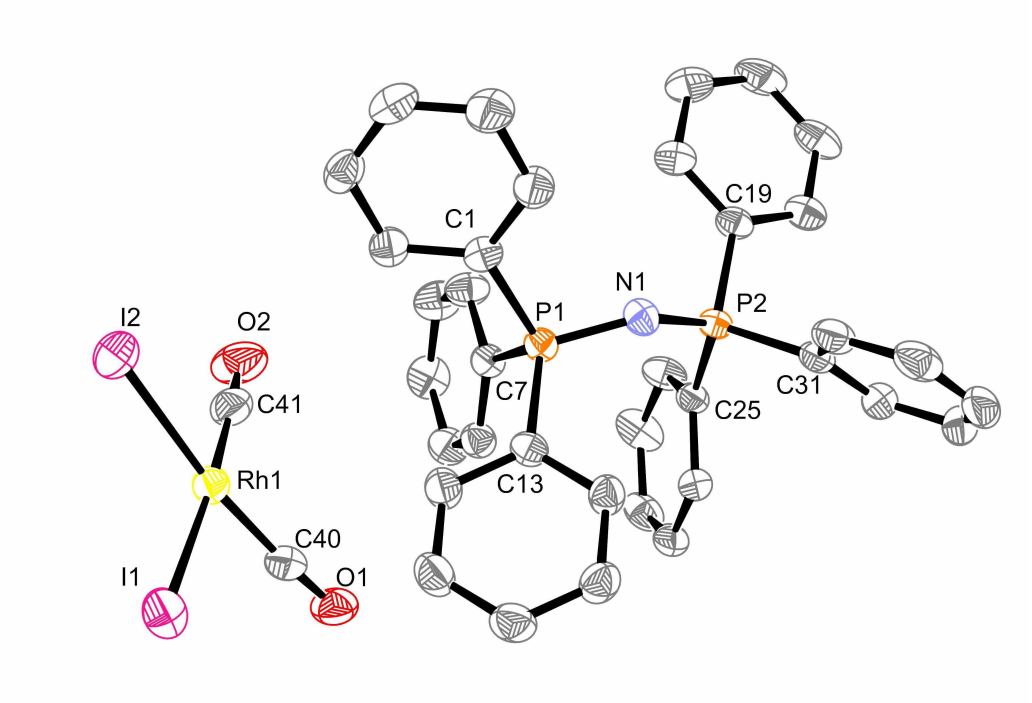

Scheme 10 : Crystal structure of [PPN][$RhI_2(CO)_2$] 1.

Bond length (Å):

C40—O1 = 1.140 (4), C40—Rh1 = 1.844 (4), C41—O2 = 1.140 (5), C41—Rh1 = 1.840 (4), Rh1—I2 = 2.6515 (11), Rh1—I1 = 2.6725 (7)

Angles (deg):

C35—C36—H36 = 120, O1—C40—Rh1 = 176.0 (3), O2—C41—Rh1 = 175.6 (4), C41—Rh1—C40 = 92.09 (16), C41—Rh1—I2 = 85.56 (12), C40—Rh1—I2 = 172.99 (11), C41—Rh1—I1 = 174.56 (13), C40—Rh1—I1 = 88.49 (10), I2—Rh1—I1 = 94.48 (3)

$[PPN]_2[RhI_3(COMe)(CO)]_2$ 3 :

A methyl iodide solution of $[PPN][RhI_2(CO)_2]$ **1** (1g) is stirred overnight at room temperature. Excess of MeI is removed under vacuum giving **$[PPN]_2[RhI_3(COMe)(CO)]_2$ 3** as a red powder; 2.30g. Yield: 100%. IR (CH_2Cl_2): νCO= 2055, 1735, 1720 cm^{-1}. ^{13}C NMR (CD_2Cl_2): 211.25 ppm, COMe, (d, J_{Rh-C}= 20.2 Hz); 204.10 ppm, COMe, (d, J_{Rh-C}= 20.5 Hz); 183.3 ppm, CO, (d, J_{Rh-C}= 71 Hz); 182 ppm, CO, (d, J_{Rh-C}= 67 Hz).^1H NMR (CD_2Cl_2): 3.15 ppm (s, CH_3); 3.13 (s, CH_3). Calcd for $C_{78}H_{66}Rh_2I_6N_2O_4P_4$: C: 42.81, H: 3.02, N: 1.28. Found: C: 42.62, H: 2.92, N: 1.33.

$$[PPN][RhI_2(CO)_2] \xrightarrow[r.\ t]{CH_3I} [PPN][Rh(CH_3CO)I_3(CO)]$$

Scheme 11 : Preparation of $[PPN]_2[RhI_3(COMe)(CO)]_2$ **3**

$[PPN][RhI_3(COMe)(CO)_2]$ 4:

$[PPN]_2[RhI_3(COMe)(CO)]_2$ **3** (1g, 0.915 mmol) is dissolved in CH_2Cl_2 and CO is bubbled through the solution at room temperature (Sc. 12). The reaction is fast but under nitrogen atmosphere, $[PPN][RhI_3(COMe)(CO)_2]$ **4** slowly gives back $[PPN]_2[RhI_3(COMe)(CO)]_2$ **3**. $[PPN][RhI_3(COMe)(CO)_2]$ **4** can be isolated as crystals suitable for X-ray analyses by adding hexane in the Schlenk under a CO atmosphere, making a bilayered mixture. (0.70g, 65 %) IR (CH_2Cl_2): νCO= 2083.5, 1704.2 cm^{-1}. ^{13}C NMR (CD_2Cl_2): 216.85 ppm, $COCH_3$, (d, J_{Rh-C}= 18.23 Hz); 177.7 ppm, CO, (d, J_{Rh-C}= 54 Hz). ^1H NMR 2.97 ppm (s, CH_3).

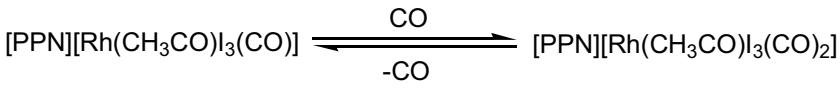

Scheme 12 : Preparation of [PPN][$RhI_3(COMe)(CO)_2$] **4**.

Crystal data for **4**.

Identification code	nl055
Empirical formula	C40 H33 I3 N O3 P2 Rh
Formula weight	1121.22
Temperature	180 (2) K
Wavelength	0.71073 A
Crystal system, space group	Monoclinic, P $2_{1/c}$
Unit cell dimensions	a = 14.601(5) A alpha = 90 deg.
	b = 18.580(5) A beta = 95.113(5) deg.
	c = 15.082(5) A gamma = 90 deg.
Volume	4075(2) A^3
Z, Calculated density	4, 1.828 Mg/m^3
Absorption coefficient	2.807 mm^-1
F(000)	2152
Crystal size	0.4 x 0.175 x 0.087 mm
Theta range for data collection	2.60 to 24.66 deg.
Limiting indices	-17<=h<=14, -21<=k<=21, -17<=l<=17
Reflections collected / unique	25289 / 6928 [R(int) = 0.0580]
Completeness to theta	24.66 99.8 %

Absorption correction	Semi-empirical from equivalents
Max. and min. transmission	0.6699 and 0.5249
Refinement method	Full-matrix least-squares on F^2
Data / restraints / parameters	6928 / 0 / 452
Goodness-of-fit on F^2	0.820
Final R indices [I>2sigma(I)]	R1 = 0.0353, wR2 = 0.0538
R indices (all data)	R1 = 0.0724, wR2 = 0.0607
Largest diff. peak and hole	0.764 and -0.672 e.A^-3

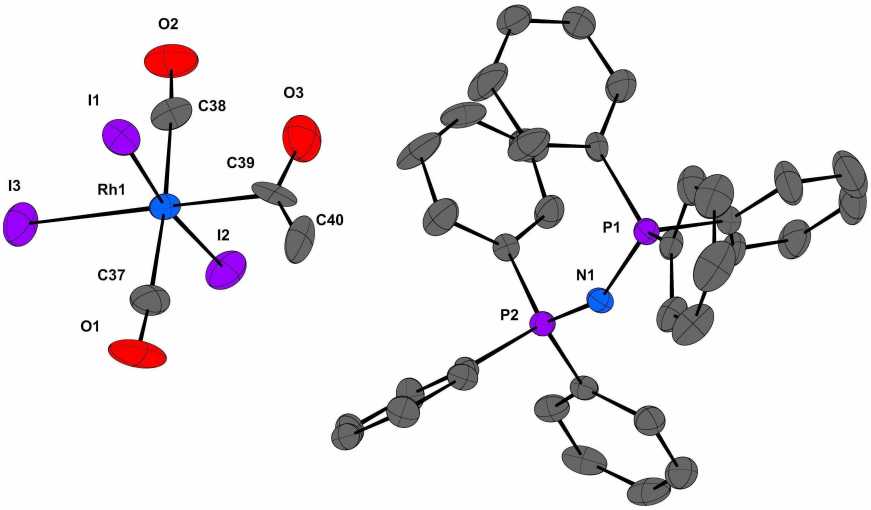

Scheme 13 : X-ray structure of [PPN][$RhI_3(COMe)(CO)_2$] **4**.

Bond lenghts:

C(37)-O(1) = 1.092(6), C(37)-Rh(1) = 1.945(7), C(38)-O(2) = 1.108(6), C(38)-Rh(1) = 1.926(7), C(39)-O(3) = 1.201(6), C(39)-C(40) = 1.234(8), C(39)-Rh(1) = 2.152(7), C(40)-H(40A) = 0.9600, C(40)-H(40B) = 0.9600, C(40)-H(40C) = 0.9600, Rh(1)-I(1) = 2.6602(9), Rh(1)-I(3) = 2.6702(9), Rh(1)-I(2) = 2.8137(11)

Angles

O(1)-C(37)-Rh(1) = 176.3(6), O(2)-C(38)-Rh(1) = 175.6(6), O(3)-C(39)-C(40) = 128.5(7), O(3)-C(39)-Rh(1) = 110.8(5), C(40)-C(39)-Rh(1) = 120.5(5), C(39)-C(40)-H(40A) = 109.5, C(39)-C(40)-H(40B) = 109.4, H(40A)-C(40)-H(40B) = 109.5, C(39)-C(40)-H(40C) = 109.5, H(40A)-C(40)-H(40C) = 109.5, H(40B)-C(40)-H(40C) = 109.5, C(38)-Rh(1)-C(37) = 174.7(2), C(38)-Rh(1)-C(39) = 93.6(3), C(37)-Rh(1)-C(39) = 91.5(3), C(38)-Rh(1)-I(1) = 91.28(19), C(37)-Rh(1)-I(1) = 90.08(16), C(39)-Rh(1)-I(1) = 86.52(15), C(38)-Rh(1)-I(3) = 91.02(19), C(37)-Rh(1)-I(3) = 88.25(16), C(39)-Rh(1)-I(3) = 86.38(15), I(1)-Rh(1)-I(3) = 172.66(2), C(38)-Rh(1)-I(2) = 84.94(17), C(37)-Rh(1)-I(2) = 89.90(18), C(39)-Rh(1)-I(2) = 178.31(19), I(1)-Rh(1)-I(2) = 92.59(2), I(3)-Rh(1)-I(2) = 94.56(2).

$[RhI(CO)_2]_2$ 10.

3g of RhI_3 are added to a solution of MeOH (200 mL) and $AcOCH_3$ (200 mL). The solution is stirred at reflux under a gentle CO bubbling until the solution becomes pale yellow conreponding to the formation of $H[RhI_2(CO)_2]$. The condenser is then removed and most of the solvent are evaporated at 70℃ under CO bubbling. When a small amount of sol vent remains in the flask, hexane is added to form a bilayered solution. After a few minutes, hexane (top layer) becomes red; it is taken out the flask and placed at –18℃. This extraction process can be rep eated to increase the yield. We can observe after 1h the formation of red crystals suitable for X-ray analyses: 0.9g. Yield: 25%. IR (CH_2Cl_2): νCO= 2096, 2080, 2027 cm^{-1}; ^{13}C NMR (CD_2Cl_2): 179.3 ppm, CO, (d, J_{Rh-C}= 75 Hz).

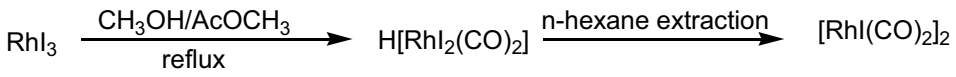

Scheme 7 : Preparation of $[RhI(CO)_2]_2$ **10**.

Crystal data of 10.

Empirical formula	C4 I2 O4 Rh2
Formula weight	571.66
Temperature	180(2) K
Wavelength	0.71073 A
Crystal system, space group	Monoclinic, P $2_{1/n}$
Unit cell dimensions	a = 9.4473(13) A alpha = 90 deg.

	b = 9.6107(14) A beta = 96.105(11) deg.
	c = 11.3419(16) A gamma = 90 deg.
	Volume1023.9(3) A^3
Z, Calculated density	4, 3.708 Mg/m^3
Absorption coefficient	9.225 mm^-1
F(000)	1008
Crystal size	0.4125 x 0.1 x 0.05 mm
Theta range for data collection	2.78 to 32.20 deg.
Limiting indices	-13<=h<=13, -13<=k<=14, -16<=l<=16
Reflections collected / unique	9898 / 3393 [R(int) = 0.0367]
Completeness to theta = 32.20	93.7 %
Absorption correction	Semi-empirical from equivalents
Max. and min. transmission	0.63 and 0.227
Refinement method	Full-matrix least-squares on F^2
Data / restraints / parameters	3393 / 0 / 109
Goodness-of-fit on F^2	1.057
Final R indices [I>2sigma(I)]	R1 = 0.0316, wR2 = 0.0843
R indices (all data)	R1 = 0.0469, wR2 = 0.1015
Largest diff. peak and hole	1.645 and -1.958 e.A^-3

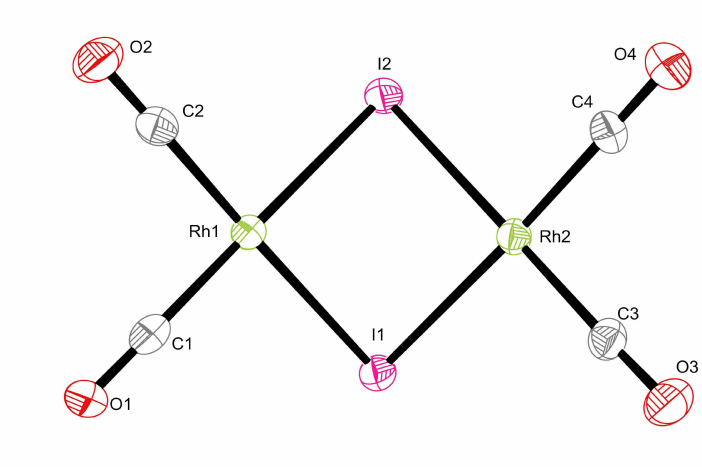

Scheme 8 : Structure of $[RhI(CO)_2]_2$ 10.

Bond length (Å): O(1)-C(1) = 1.131(8), O(2)-C(2) = 1.127(7), O(3)-C(3) = 1.127(7), O(4)-C(4) = 1.122(7), C(1)-Rh(1) = 1.861(7), C(2)-Rh(1) = 1.863(7), C(3)-Rh(2) = 1.861(6), C(4)-Rh(2) = 1.860(6), Rh(1)-I(1) = 2.6642(7), Rh(1)-I(2) = 2.6745(7), Rh(2)-I(2) = 2.6595(6), Rh(2)-I(1) = 2.6689(7).

Angle (deg.): O(1)-C(1)-Rh(1) = 178.6(6), O(2)-C(2)-Rh(1) = 178.7(6), O(3)-C(3)-Rh(2) = 177.2(6), O(4)-C(4)-Rh(2) = 179.2(6), C(1)-Rh(1)-C(2) = 90.0(3), C(1)-Rh(1)-I(1) = 90.55(19), C(2)-Rh(1)-I(1) = 176.3(2), C(1)-Rh(1)-I(2) = 179.2(2), C(2)-Rh(1)-I(2) = 90.37(19), I(1)-Rh(1)-I(2) = 89.04(2), C(4)-Rh(2)-C(3) = 89.5(3), C(4)-Rh(2)-I(2) = 88.84(19), C(3)-Rh(2)-I(2) = 173.86(19), C(4)-Rh(2)-I(1) = 176.34(19), C(3)-Rh(2)-I(1) = 92.0(2), I(2)-Rh(2)-I(1) = 89.25(2), Rh(1)-I(1)-Rh(2) = 78.77(2), Rh(2)-I(2)-Rh(1) = 78.76(2).

[PPN][RhI$_4$(CO)$_2$] 11:

[PPN][RhI$_2$(CO)$_2$] 1 (1g, 1.05 mmol) is dissolved in CH_2Cl_2 and an excess (10 equivalents, 2.36g of a HI solution in water at 57%) of HI is added. The solution is stirred for 2h at room temperature and the solvent and the excess of HI are removed under vacuum to obtain a red powder.

Yield: 100% (1.25 g). IR (CH_2Cl_2): νCO= 2090 cm^{-1}; ^{13}C NMR (CD_2Cl_2): 172.6 ppm, CO, d, J_{Rh-C}= 47.24 Hz

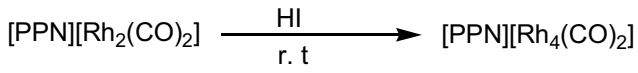

Scheme 14 : Preparation of [PPN][RhI$_4$(CO)$_2$] 11.

Synthesis of iridium compounds

[PPN][IrI$_2$(CO)$_2$] 5.

This compound was prepared from $IrI_{3,4}$ (2 g, 3.21 mmol) in a mixture of DMF (150 mL) and water (1.5 mL)(Sc. 2). The solution was stirred under a gentle CO bubbling at 160°C for three hours. The solution initially dark red turned to yellow due to the presence of [NH_2Me_2][IrI$_2$(CO)$_2$]. [PPN]Cl (1.84 g, 3.21 mmol) was then added and the solution was cooled to room temperature. Cold water (750 mL, 1-3°C) was then slowly added in order to precipitate [PPN][IrI$_2$(CO)$_2$] **5**. The yellow powder was filtered and washed three times with 50 mL of cold water. This product was dried under vacuum and crystallized at –18°C in a bilayered mixture of CH_2Cl_2/n-hexane (1:1). After a few hours yellow needle-shaped crystals were obtained (2.67 g, 80%). IR (CH_2Cl_2) ν(CO)/cm^{-1}: 2046, 1967. ^{13}C { ^{1}H} NMR (CD_2Cl_2): δ 169.9 (Ir-CO). MS (FAB$^-$): m/z = 503. Anal. Calcd for $C_{38}H_{30}IrI_2NO_2P_2$: C, 43.86; H, 2.91; N, 1.35. Found: C, 43.69; H, 2.81; N, 1.38.

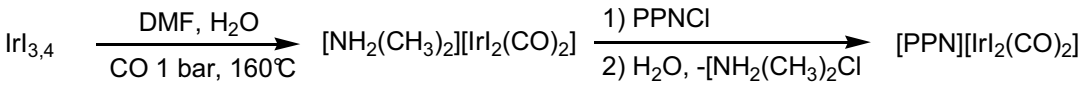

Scheme 2 : Preparation of $[PPN][IrI_2(CO)_2]$ **5**.

$[PPN][IrI_3(CH_3)(CO)_2]$ 6

This compound was prepared starting from $[PPN][IrI_2(CO)_2]$ **5** (1 g, 0.96 mmol) dissolved in 10 mL of dichloromethane. Methyl iodide (5.45 g, 38.4 mmol) was added to the medium and the solution was stirred at room temperature for 1 hour The solution is filtered. The solvent was removed under vacuum to obtain a the yellow-orange powder (1.08 g, 95%). IR (CH_2Cl_2) ν(CO)/cm^{-1}: 2100, 2048. ^1H NMR (CD_2Cl_2): δ 2.15 (s, CH_3). $^{13}C\ \{^1H\}$ NMR (CD_2Cl_2): δ 156 (s, Ir-CO), -16.6 (s, CH_3). MS (FAB^-): m/z = 646. Anal. Calcd for $C_{39}H_{33}IrI_3NO_2P_2$: C, 39.61; H, 2.81; N, 1.18. Found: C, 39.51; H, 2.72; N, 1.23.

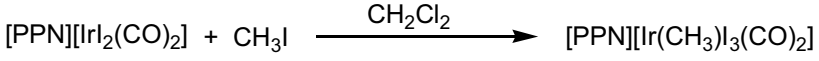

Scheme 3 : Preparation of $[PPN][IrI_3(CH_3)(CO)_2]$ 6.

***Mer,trans*-[PPN][Ir(COCH$_3$)I$_3$(CO)$_2$] 8.**

This complex was prepared by addition of H_2O (2 g, 0.11 mol) to a solution of [PPN][IrI$_3$(CH$_3$)(CO)$_2$] **6** (0.5 g, 0.42 mmol) in 30 mL of methanol. The solution was placed in a glass reactor and stirred for 1 hour under 5 bar of CO at room temperature. Then 20 mL of n-hexane were added by a liquid feed-line overpressurized with CO and the reactor was cooled to 0℃. After 2 hours we observed the formation of orange crystals (0.38 g, 75% yield) suitable for X-ray analysis (Sc.5), corresponding to *mer,trans*-[PPN][Ir(COCH$_3$)I$_3$(CO)$_2$]. IR (CH_2Cl_2) ν(CO)/cm^{-1}: 2114, 2070, 1655. ^{1}H NMR (CD_2Cl_2): δ 2.76 (s, CH_3). ^{13}C {^{1}H} NMR (CD_2Cl_2): δ 201.5 (*C*OCH_3), 162.7 (s, Ir-CO), 52.2 ppm (s, CH_3).

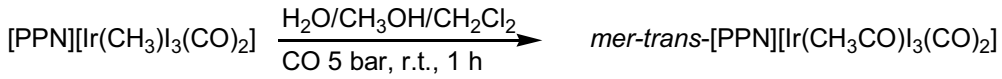

Scheme 4 : Preparation of *mer,trans*-[PPN][Ir(COCH$_3$)I$_3$(CO)$_2$] **8**.

Crystal data of complex *mer,trans*-[PPN][Ir(COCH$_3$)I$_3$(CO)$_2$] **8**:

Formula	C_{40} H_{33} I_3 Ir N O_3 P_2		
Crystal Class	Monoclinic		
Space Group	P 2_1/c		
a (Å)	14.605(1)	alpha	90
b (Å)	18.580(1)	beta	95.168(6)
c (Å)	15.176(1)	gamma	90
Volume (Å^3)	4101.4(5)		

Z	4
Radiation type	Mo K□
Wavelength (Å)	0.709300
Density	1.96
M ($g.mol^{-1}$)	1210.59
μ (mm^{-1})	5.628
Temperature (K)	180
Size (mm)	0.19x 0.23x 0.40
Colour	orange
Shape	block
Cell from	5785 Reflections
Theta range	3 to 32
Diffractometer type	X-Calibur
Scan type	Phi Omega
Absorption type	analytical
Transmission range	0.14 0.49
Reflections measured	39257
Independent reflections	13532
Rint	0.05
Hmin, Hmax	-21 21
Kmin, Kmax	-27 26
Lmin, Lmax	-22 19
Refinement	on F
R-factor	0.0397
Weighted R-factor	0.0436
Delta Rho min	-1.53
Delta Rho max	2.22

Reflections used	4885
sigma(I) limit	2.00
Number of parameters	452
Goodness of fit	1.129

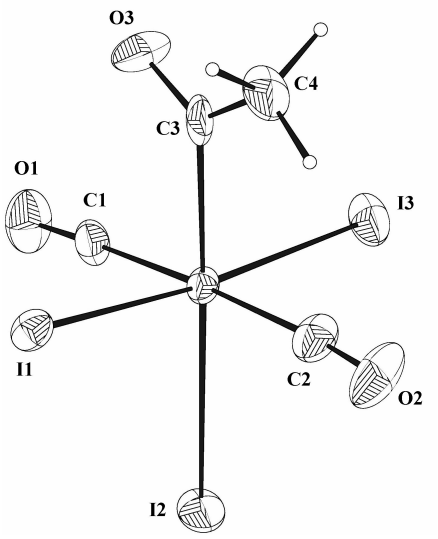

Scheme 5 : Structure of *mer,trans*-[PPN][Ir($COCH_3$)I_3($CO)_2$] **8**.

Bond length (Å): Ir(1) - I(1) = 2.6849(8), Ir(1) - I(2) = 2.8147(8), Ir(1) - I(3) = 2.6984(9), Ir(1) - C(1) = 1.929(11), Ir(1) - C(2) = 1.915(13), Ir(1) - C(3) = 2.058(12), C(1) - O(1) = 1.116(13), C(2) - O(2) = 1.104(14), C(3) - C(4) = 1.487(18), C(3) - O(3) = 1.183(14).

Angles (deg): I(1) - Ir(1) - I(2) = 91.85(3), I(1) - Ir(1) - I(3) = 174.65(3), I(2) - Ir(1) - I(3) = 93.07(3), I(1) - Ir(1) - C(1) = 89.8(3), I(2) - Ir(1) - C(1) = 89.8(3), I(3) - Ir(1) - C(1) = 88.1(3), I(1) - Ir(1) - C(2) = 91.6(4), I(2) - Ir(1) - C(2) = 86.1(3), I(3) - Ir(1) - C(2) = 90.8(4), C(1) - Ir(1) - C(2) = 175.7(5), I(1) - Ir(1) - C(3) = 87.4(3), I(2) - Ir(1) - C(3) = 178.3(3), I(3) - Ir(1) - C(3) = 87.7(3), C(1) - Ir(1) - C(3) = 88.7(5), C(2) - Ir(1) - C(3) = 95.5(5), Ir(1) - C(1) - O(1) = 177.8(11), Ir(1) - C(2) - O(2) = 175.4(12) Ir(1) - C(3) - C(4) = 117.9(9), Ir(1) - C(3) - O(3)= 119.9(9), C(4) - C(3) - O(3) = 122.0(12).

***Fac,cis*-[PPN][Ir(COCH$_3$)I$_3$(CO)$_2$] 8.**

The salt [PPN][IrI$_3$(CH$_3$)(CO)$_2$] **6** (0.5 g, 0.42 mmol) was dissolved in 40 mL of dichloromethane containing 5 mL of methanol. The solution was placed in a glass reactor and stirred for 90 minutes under 5 bar of CO at room temperature (Sc. 6). Then 20 mL of n-hexane were added by a liquid feed-line and the reactor was cooled to 0℃. After 2 hours we observe d the formation of yellow crystals (380 mg, 75% yield), corresponding to *fac,cis*-[PPN][Ir(COCH$_3$)I$_3$(CO)$_2$]. IR (CH_2Cl_2) ν(CO)/cm^{-1}: 2111, 2061, 1679, 1660. ^{1}H NMR (CD_2Cl_2): δ 3.13 (s, CH_3). ^{13}C {^{1}H} NMR (CD_2Cl_2): δ 196.2 (*C*OCH_3), 151.4 (s, Ir-CO), 49.5 (s, CH_3).

$$[PPN][Ir(CH_3)I_3(CO)_2] \xrightarrow[CO\ 5\ bar,\ r.t.,\ 1.5\ h]{CH_3OH/CH_2Cl_2} \textit{fac-cis}\text{-}[PPN][Ir(CH_3CO)I_3(CO)_2]$$

Scheme 6 : Preparation of *fac,cis*-[PPN][Ir(COCH$_3$)I$_3$(CO)$_2$] **8**.

Synthesis of CH_3COI:

We placed acetylchlorid (3.92 g, 0.05 mol) in a dry 100 mL three-necked, round-bottomed flask equipped with a pressure-equalizing dropping funnel, a thermometer and argon inlet and outlet. Then, trimethylsilyliodide (11.10 g, 0.055 mol) is added dropwise. The solution is stirred for 20 min. under argon. After that reaction time, a distillating column take the place of the pressure-equalizing dropping funel under argon flux equipped with a condenser and a Schlenck tube. The solution is heated at 100℃ for around 30 min. to remove trimethylsilylechlorid (b.p = 56-59℃). Then, we changed the Schenk tube and acetyliodide coumpound was distillated under reduced pressure. Due to the presence of iodine, the liquid was red. Thus copper powder was introduced under argon and the solution was stirred for 5 min before to be distillated again. By this procedur, we obtained a pale yellow liguid of acetyliodide (3.57 g, 42%). IR (CH_2Cl_2): 1859 cm^{-1}, 1797 cm^{-1}, 1733 cm^{-1}.